

Design and Optimisation of Elastic Gridshells

Vorgelegt von
Elisa Lafuente Hernández
aus Lleida (Spanien)

Hauptberichter: Prof. Dr.-Ing. Christoph Gengnagel
Mitberichter: Prof. Dr.-Ing. Olivier Baverel

Institut für Konstruktives Entwerfen und Tragwerkslehre der
Universität der Künste Berlin

2015

“This (Multihalle Mannheim) is not a case of a building creatively design, but based on a support system of additive known elements. This design is the result of a symposium of creative thoughts in the formation, the invention of building elements with the simultaneous integration of the theoretical, scientific contributions from mathematics, geodesy, model measuring, statics as well as control loading and - calculation. We are dealing with more than pure “teamwork”, we are dealing with team creation.”

“Honour must be given in the first place – from the point of view of the engineer to the builders who found themselves to be designers of this ingenious work. Also the sum of the details, the multiplicity of the most varying solutions for the supports, the assembly and erection methods, the actual building know-how and the constructive application of new and old buildings and working materials, such as wood, steel, wire-rope, steel-concrete, and plastic-coated film is an example of how free and open the engineer should be, how he has to see and to learn, to think and to work, if he wants to continue to exist in the work of tomorrow.”

Prof. Georg Lewenton, IL 13 Multihalle Mannheim (1976)

Preface

The present thesis on the subject of “Design and Optimisation of Elastic Gridshells” was developed between March 2010 and August 2014 at the Department of Architecture at the University of the Arts in Berlin.

I would like to express my most sincere gratitude to my supervisor Prof. Christoph Gengnagel for his support and trust during these more than four years – his multifaceted engagement and human values have been an important source of inspiration.

To my second supervisor Prof. Olivier Baverel I thank for his enriching advice and suggestions, particularly on the mathematical and numerical fields. His practical experience has been as well decisive, particularly during the construction of the prototypes.

I would also like to thank Thilo Rörig and Stefan Sechelmann from the Department of Mathematics at the TU Berlin who have provided the mathematical fundamentals of the variational method for the grid’s optimisation and facilitated the use of the modular Software Varylab, supported by the DFG Research Center MATHEON and the SFB/TR 109 Discretisation in Geometry and Dynamics.

The construction and testing of the prototypes would have not been possible without the financial support of the Fachagentur Nachwachsende Rohstoffe e.V. (FNR), the sponsoring of the company Ferrari for the tensile membrane, the collaboration of Prof. Mike Schlaich and Prof. Henning J. Meyer, who allowed the use of their installations, and the exceptional commitment of all the students and, particularly, of our student research assistants – Jil, Lisa, Noa and Philipp - who were involved on the preparation and erection of the gridshells.

For the structural analyses using finite element methods, the experience gained during my precedent years at Schlaich Bergermann und Partner in Berlin has been crucial. At this point, I would like to extend my absolute gratitude to my former colleague and present friend Uwe Burkhardt for all the fruitful discussions.

I genuinely appreciate the constructive and friendly support of all the members of the Institute for Structural Design and Technology at the UdK Berlin; a special thank to Holger Alpermann, with whom it was a real pleasure to work and collaborate.

I would also like to dedicate my gratitude to my mother and father, whose constancy, perseverance and optimism in life I deeply admire. Finally, I owe this work to my husband Julian, who has been providing me with confidence and conviction, and to my daughter NÚria and son Jendrik – the extraordinary happiness of having you brings everything in equilibrium.

Elisa Lafuente Hernández

Abstract

Design and Optimisation of Elastic Gridshells

Design Principles. Elastic gridshells are shell structures composed of a single- or multi-layer grid of continuous profiles, which are initially straight and will be progressively bent until achieving an architecturally and structurally satisfactory geometry. To provide the structure with in-plane shear stiffness, additional bracing members as diagonal profiles or cables are required. Usually used as medium to large span surface structures, elastic gridshells present a wide variety in their surface geometry, grid configuration and materiality. In this part of the work, the structural aspects to be considered on the design procedure of elastic gridshells have been summarised and identified on existing design approaches. One important structural criterion of elastic gridshells is the high residual stress to which they are subjected after the bending process. Using materials with high limit strain, the residual utilisation rate can be reduced. If initially timber was the material of preference, emerging fibre-reinforced plastics are becoming the more and more present in the construction of elastic gridshells because of their low ratio of flexural modulus to strength. The mechanical properties of available materials, suitable for elastic gridshells, have been compared and application examples have been presented and illustrated.

Grid finding and optimisation. Elastic gridshells offer significant cost and time advantages during the production, transport and construction processes. Nevertheless, the shaping of the initially flat grid also generates important bending stresses on the structures, reducing therewith their bearing capacity against external loads. In order to diminish the initial stresses, profiles with low sections and materials with low modulus of elasticity are usually chosen. However, this leads to a reduction of the global stiffness of the gridshell which can result in stability problems. With an optimisation of the grid pattern - orientation and arrangement of the grid profiles - a minimisation of the profiles' curvature can be obtained and the load-bearing capacity of the gridshells improved. In this section, an optimisation method based on variational principles for regular and irregular gridshells is proposed. The aim of using variational principles is to establish *extremal* functions which minimize the value of quantities related to particular grid properties. These properties are: the curvature of the profiles, the distance to a target surface geometry and the deviation of the edge lengths from a desired mesh size. The advantage of this method is that weighting factors can be applied to the grid parameters to be minimised, so that a variety of grid configurations can be established responding to different specific requirements: for example, grids with further optimized curvature when allowing a certain distance to the reference surface or variation of the edge lengths (*irregular gridshells*). Different case studies of double-curved gridshells show the advantages and capacity of this method.

Numerical analysis. The bending process and load-bearing behaviour of elastic gridshells can be modelled and analysed using three-dimensional finite element models. During the shaping of the profiles, internal forces are induced on the structure, so that the final equilibrium shape of the gridshell will be attained once its edges have been fixed, the bracing elements have been assembled and the external shaping forces have been removed. The goal of the numerical analysis is to quantitatively evaluate the geometry and material stresses resulting from the shaping process and the load-bearing capacity of the gridshell under external loading. The procedures of definition and calculation of the finite element models have been described in this part. Moreover, the influence of the orientation and arrangement of the grid profiles on the residual stresses after erection process and on the distribution of forces and deformability of the gridshell under external loading have been analysed comparing three regular anticlastic gridshells with varying grid pattern. At last, the potential and limitations of using tensile membranes as restraining and at the same time covering element of elastic gridshells has been studied on a hemispheric gridshell.

Experimental validation. Numerical techniques are commonly used for the calculation of stress distributions and displacements of complex indeterminate bearing structures. Nevertheless, to model the elements they are composed of and the connection properties between them, simplifications and approximations are done. The purpose of this part of the work is to analyse the influence of these simplifications on the results of the simulation and thereby recalibrate and benchmark the numerical models with physical prototypes. Two gridshells composed of GFRP profiles have been built: an irregular hemisphere of 10 m diameter, braced with a third layer of profiles, and a regular hemisphere of 5 m diameter, restraint with a tensile membrane. The prototypes have been loaded symmetrically and asymmetrically applying point loads at the grid nodes and the resulting nodal displacements have been compared to those calculated with the numerical models.

Table of Contents

1	Introduction	2
2	Design Principles	5
	2.1 On the Nomenclature	6
	2.2 Design Process	8
	2.2.1 Structural aspects	8
	2.2.2 Existing design approaches for regular gridshells	12
	2.2.3 Existing design approaches for irregular gridshells	19
	2.3 Construction Material	23
	2.3.1 Material selection criteria	23
	2.3.2 Available materials and application examples	29
	2.4 Summary	38
3	Grid Finding and Optimisation	40
	3.1 Methodology	41
	3.1.1 Discrete differential geometry	41
	3.1.2 Initialisation	42
	3.1.3 Optimisation with variational principles	43
	3.1.4 Implementation	47
	3.2 Optimisation Examples of Regular Grids	49
	3.2.1 Reference surface as geometric constant	50
	3.2.2 Influence of initialisation mesh	52
	3.2.3 Further optimisation by allowing distance to reference surface	53
	3.3 Optimisation Examples of Irregular Grids	54
	3.3.1 Reference surface as geometric constraint	55
	3.3.2 Further optimisation by allowing distance to reference surface	57
	3.4 Summary	59
	3.4.1 Influence of initialisation mesh and weighting factors on the optimisation	60

3.4.2	Reduction of mean vs. maximum curvature values	60
3.4.3	Construction of resulting geometry	60
3.4.4	Optimisation with irregular grids	61
4	Numerical Analysis	63
4.1	Definition and Calculation of the Finite Element Model	64
4.1.1	Initial Plane Configuration	64
4.1.2	Finite element model	66
4.2	Influence of the Grid Pattern on the Structural Behaviour	69
4.2.1	Bending process	70
4.2.2	External loading	74
4.2.3	Summary	84
4.3	Membrane as Bracing Element	85
4.3.1	Membrane braced 4-field grid	86
4.3.2	Membrane braced gridshell – Hybrid Hemisphere	90
4.3.3	Summary	95
5	Experimental Validation	97
5.1	Construction of a Developable Irregular Elastic Gridshell	98
5.1.1	Grid design	99
5.1.2	Numerical simulation	101
5.1.3	Construction	103
5.1.4	Comparison between numerical and physical models	106
5.2	Construction of a Membrane Braced Regular Elastic Gridshell	111
5.2.1	Grid design	111
5.2.2	Numerical simulation	112
5.2.3	Construction	113
5.2.4	Comparison between numerical and physical models	116
5.3	Summary	121
5.3.1	Developable irregular gridshell	121
5.3.2	Membrane braced regular gridshell	122

6	Conclusion and perspectives	124
	Bibliography	132
	APPENDIX	
	Construction Plans of Developable Irregular Elastic Gridshell	137

1. Introduction

1 Introduction

Lightweight structures in civil engineering are the responsible answer to a world moved by global ecological, economic and social challenges (Schlaich, [1]). Shell structures are surface structures whose curvature allows the bearing of distributed loads through membrane (axial) forces and, consequently, the minimisation of their thickness and material per covered surface. Shell structures can be built as continuum surfaces (*continuum shells*) or as triangulated grids (*gridshells*). Distinguished examples of continuum shells are the prestressed and reinforced concrete shells, impressively performed along the 20th century by *Nervi*, *Candela* or *Isler*. Considering gridshells, two main groups can be identified according to their form-giving process: gridshells shaped by inducing elastic bending on the continuous (from edge to edge) grid profiles (Figure 1-1 - *left*) and gridshells formed by addition and connection of discrete (from grid node to grid node) grid segments (Figure 1-1 - *right*).

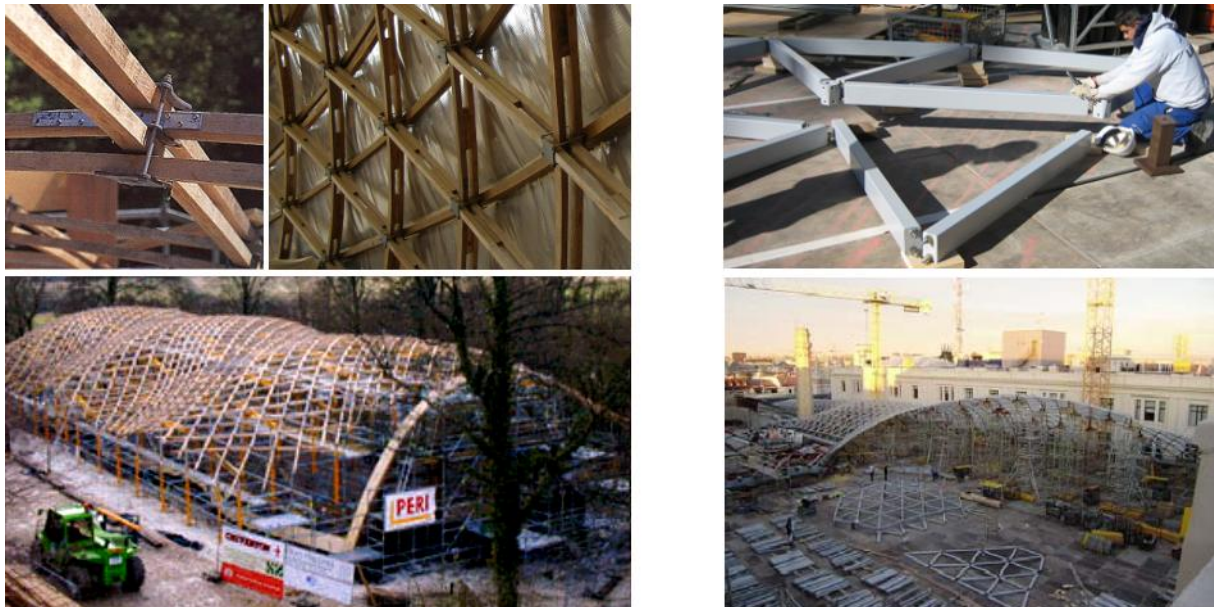


Figure 1-1: (*left*) Example of gridshell shaped by inducing elastic bending on the continuous grid profiles – Weald & Downland Museum, Sussex, England –; (*right*) Example of gridshell formed by addition and connection of discrete grid segments – Palacio de Comunicaciones, Madrid, Spain.

Gridshells of the first group are named in this thesis *elastic gridshells*. They have their origins in the vernacular architecture, in the construction of permanent or temporary wooden huts and tents, for example the Yurts of the pastoral nomads in Turkestan, Kasakstan and Mongolia [2]. In the early 1970s, the principles and form-finding methods of elastic gridshells were extensively researched by *Frei Otto* and the Institute für Leichte Flächentragwerke [3]. In 1975, these principles could be applied on the construction of the pioneering large-span timber gridshell: Multihalle Mannheim [2]. The main advantage of elastic gridshells resides on their economic and time-efficient production and construction methods.

The second group of gridshells is mainly constituted by steel-glass gridshells. The origins of these gridshells lie on the steel-glass constructions for greenhouses, which were built in England at the end of the 18th century. The revolution of steel-glass gridshells starts at the end of the

1980s and beginning of the 1990s, when *Jörg Schlaich* and *Hans Schober* apply the fundamentals of elastic gridshells, which were studied by Frei Otto in the early 1970s, to the design of cable-braced steel-glass gridshells. The construction of the dome of the AQUAtoll in Neckarsulm in 1989 represents the first application example. Since then, several design and form-finding procedures for steel-glass gridshells have been further developed according to new calculation and manufacture possibilities (*Schlaich, Knippers*). Steel-glass gridshells are highly appreciated by their luminosity and structural efficiency.

Contrary to steel-glass gridshells, elastic gridshells are subjected to high inner forces after being shaped, which have to be considered and integrated on their design procedure and structural analysis. On the one hand, these residual forces affect the equilibrium shape adopted by the grid, once it has been bent and fixed at its edges. On the other hand, the induced material stresses on the profiles are generally higher than those proceeding exclusively from external loads. In order to reduce these residual stresses as well as the magnitude of the shaping and support forces, low profiles and materials with low modulus of elasticity are usually used. In contrast, the stiffness of the grid profiles should be high enough to provide the gridshell with sufficient out-of-plane stiffness and avoid stability problems. The final design of elastic gridshells results from an iterative process, where the surface geometry, grid pattern and boundary conditions are modified and adapted until obtaining a structurally efficient and architecturally satisfactory construction.



Figure 1-2: Research about bent geometry and structural behaviour of elastic gridshells with physical prototypes: (left) protective roof on a playground in Wandsworth Common executed by students of the North London Polytechnic in 1976 and (right) research structure constructed by students of the University of Stuttgart at the IL in 1976 [2]

The aim of the present thesis is to explore the structural criteria to be considered on the design and construction of elastic gridshells. Besides a review and classification of existing design procedures and construction materials for elastic gridshells, this work proposes an optimisation method to determine grids with reduced profiles' curvature on or near a reference surface. Furthermore, investigations of the influence of the grid's definition on the load-bearing behaviour of elastic gridshells by means of finite element methods are provided. The numerical simulations have been as well compared with physical prototypes.

The thesis has been divided in four parts:

- *Design Principles*. The first part of the work is initially dedicated to the nomenclature used to characterise and describe the composition and structural behaviour of elastic gridshells.

Moreover, the structural aspects, which should be integrated on their design process, are determined and identified on existing design approaches. Finally, the selection criteria for the choice of the construction material are defined and several application examples of built structures are presented.

- *Grid finding and optimisation.* On the second part of the thesis, a method based on variational principles to establish grid patterns with constant and variable mesh size and reduced profiles' curvature is proposed. After describing the fundamentals of the methodology, examples of optimised double-curved grids are presented and the results are discussed.
- *Numerical analysis.* The objective of this part of the work is to analyse the structural behaviour of elastic gridshells using finite element methods. A detailed description of the used numerical model and the simulation of the bending process is provided. The structural analyses firstly focus on the influence of the grid pattern on the shaping process and the load-bearing capacity of elastic gridshells. An anticlastic surface has been taken as example. Secondly, the potential of tensile membrane as restraining element for elastic gridshells is studied on a hemispheric gridshell.
- *Experimental validation.* The last part of the thesis consists in evaluating the results of the numerical simulation, comparing them with those obtained with physical prototypes. Two GFRP gridshells have been built and loaded symmetrically and asymmetrically applying point loads at the grid nodes. The resulting nodal displacements of the numerical and physical models have been analysed and compared. The influence of the connection properties at the grid nodes has been studied.



Figure 1-3: Loading test on a hemispheric irregular gridshell of 10 m diameter (Chapter 5)

2. Design Principles

2 Design Principles

2.1 On the Nomenclature

In this thesis, the definition of *elastic gridshell* corresponds to a shell structure composed of a single- or multi-layer grid of continuous profiles, which are initially straight and will be progressively bent until achieving an architecturally and structurally satisfactory geometry. This form-giving bending process induces important residual stresses on the grid profiles; reason why these structures are also known as *strained gridshells* [4]. To provide the structure with in-plane shear strength, additional *bracing members* as profiles or cables, which diagonalise or triangulate the grid, are required. The objective of introducing shear strength on the grid is to reduce its deformations, on the one hand, after removing the shaping forces – when a predefined geometry is to be maintained – and, on the other hand, under external loading. Usually used as medium to large span surface structures, elastic gridshells present a wide variety in their surface geometry, grid pattern and materiality.

The continuous profiles of elastic gridshells in one grid direction are always *superposed* to those of the second direction. The *number of layers* characterising elastic gridshells refers only to one grid direction: in this way, single- and a double-layer grids are composed, respectively, of two and four superposed profiles in total.

As *shell structure*, the shape of elastic gridshells describes surfaces with single or double curvature, so that they can resist out-of-plane loads basically through membrane forces. A same target surface can be reproduced by multiple *grid patterns*. Nevertheless, due to structural and constructive limitations, not all patterns are buildable. The grid patterns basically differ from another in the orientation of the profiles and in their density (profiles' length per surface unit). The orientation and density of the grid has an influence on the bending process of the structure and its load-bearing capacity.

The process of applying large deformations on initially straight profiles or surfaces to obtain curved structures is known since the 2010s as *active-bending* [5]. The main motivation for using *active-bending* in gridshell structures relies in the fact that, by bending continuous profiles, the number of connections at the grid nodes can be reduced - compared, for example, to steel-glass gridshells. Only connections between superposed profiles and at prolongation points, in case of existing length limitations on the fabrication or transport of the profiles, are needed. The use of continuous profiles simplifies thus the construction process: fewer elements have to be handled on site and fewer connections have to be assembled, which allows time and cost savings. Moreover, in the case of *developable gridshells*, the grid can be comfortably assembled on its flat position and afterwards bent as a whole. Another advantage of building the structure through bending is the reduction of the employment of large lifting and scaffolding systems.

Depending if the grid pattern has constant edge length (mesh size) or not, elastic gridshells can be classified as *regular* and *irregular* gridshells. By the construction process of regular gridshells, the grid is usually bent as a whole from a flat position. Distortion and scissoring of the grid is possible by using hinged joints at the grid nodes. Elastic gridshells using this erection

process are known as **developable gridshells**. By irregular gridshells, the grid profiles are usually individually bent in an incremental process and subsequently connected to each other. This process is generally more time-consuming than that of regular gridshells. Recent examples of regular and irregular timber gridshells are the 12 m long and 5 m wide gridshell in the Chiddingstone Castle Orangery, England 2007, and the 10 m high Kupla Helsinki Zoo Lookout Tower, Finland 2002 (Figure 2-1).

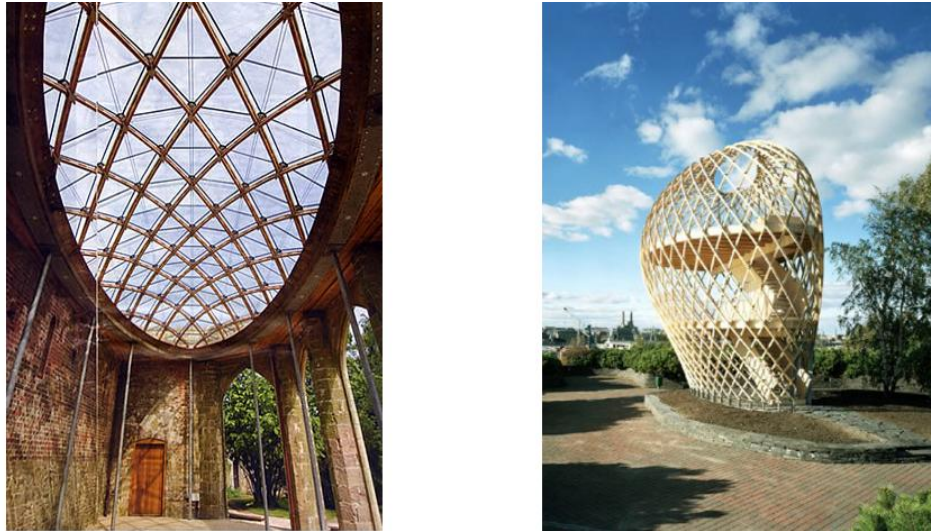


Figure 2-1: Examples of regular and irregular gridshells: the Chiddingstone Castle Orangery, England 2007, and the Kupla Helsinki Zoo Lookout Tower, Finland 2002.

By both regular and irregular gridshells, the calculation of the static equilibrium through physical or numerical models is required to determine the **released geometry** of the grid: the geometry that it acquires once it has been bent and fixed at its edges, and the shaping forces have been removed. This geometry is strongly influenced by the inner forces and moments induced through bending on the grid profiles. At this point, it is important to remark that there are two building techniques which affect in different manner the released geometry of the grid. If the geometry imposed by the external shaping forces is to be maintained, the grid has to be braced before removing the applied shaping or restraining devices. In this case, the grid can adopt a geometry which can respond to more specific structural or architectural requirements. The second technique consists in letting the grid adopt the released geometry: the bracing elements are introduced after removing the shaping forces. The advantage of this technique is that the number of devices, used to manipulate the shape of the gridshell, and, consequently, time and costs during the erection process can be reduced.

The **design procedure** of elastic gridshells must include the structural and constructive consequences of the shaping process. Since the early 2000s, diverse design approaches for elastic gridshells have been developed. Two main groups of design approaches can be distinguished, which mainly differ from each other in the use or not of a static equilibrium [6]: the approaches of the first group consist in determining a grid pattern through geometric or mathematical principles on a predefined surface geometry; by the approaches of the second group, the grid pattern results from the calculation of a static equilibrium under a design shaping load (*form-finding*). On this calculation, the inner forces induced on the profiles by bending the grid are generally taken into account.

The following sections have the aim to present the main structural and constructive aspects to be considered on the design of elastic gridshells, concerning their bending process, material and grid configuration. Furthermore, the core steps of existing design approaches for regular and irregular gridshells have been identified and compared.

2.2 Design Process

2.2.1 Structural aspects

To explore the design process of elastic gridshells, let us compare it to that of tensile membrane structures. In the European Design Guide for Tensile Surface Structures [7], three main structural aspects are mentioned to be considered when designing tensile membranes: choice of the surface geometry, levels of prestress and membrane's deformability. The *surface geometry* is generally determined through form-finding: here, the static equilibrium of the membrane is calculated under predefined prestress and boundary conditions. The choice of the *level of prestress* results from a compromise between constructive and structural requirements: on the one hand, it should be sufficient high to avoid a lack of stress and wrinkles on the membrane, under all possible load combinations, and to provide the structure with enough stiffness; on the other hand, it should be low enough to be able to be technically applied. Finally, it should be proved that, when the *membrane deforms* under external loading, positive gradients are always maintained.

Elastic gridshells deal with different physical effects than tensile membranes. Nevertheless, following the design strategy of tensile membranes, three principal structural aspects can be identified on the design process of elastic gridshells:

a) Gridshell's geometry:

The first step on the design of elastic gridshells consists in defining a ***target or reference surface geometry*** - or ***boundary conditions*** – which respond to the required building's function, aesthetics and surrounding situation. The geometry, and specially the curvature, of the gridshell play an important role on its structural performance and behaviour as shell structure. Physical or computational modelling is usually employed to define the surface geometry.

Afterwards, an adequate fitting ***grid pattern*** has to be determined. There exist different design procedures to establish the grid's geometry of a elastic gridshell. Generally, they can be classified into two main groups:

a.1) Design approaches not considering a static equilibrium:

In these approaches the grid pattern is established by using geometric and mathematical principles (e.g. genetic algorithms, variational principles). No equilibrium of forces is calculated.

a.2) Design procedures considering a static equilibrium or form-finding:

Here, the grid pattern results from the calculation of the static equilibrium of the grid under a designed shaping load. The inner forces induced through bending, and therewith the material and sectional properties of the grid profiles, are considered. The design approaches of this group mainly differ on the definition of the shaping loads.

b) Level of residual stresses:

Due to the shaping process, profiles are subjected to residual stresses, usually much higher than those exclusively resulting from external loads. The level of the residual stresses is directly proportional to the curvature values to which the profiles are bent. According to the Euler-Bernoulli beam theory, the uniaxial bending moment M_y and stress σ_x of slender beams with linear elastic material behaviour can be expressed by the equations given in Figure 2-2; where E is the Young's modulus, I is the second moment of inertia and ρ is the radius of curvature of the grid profiles:

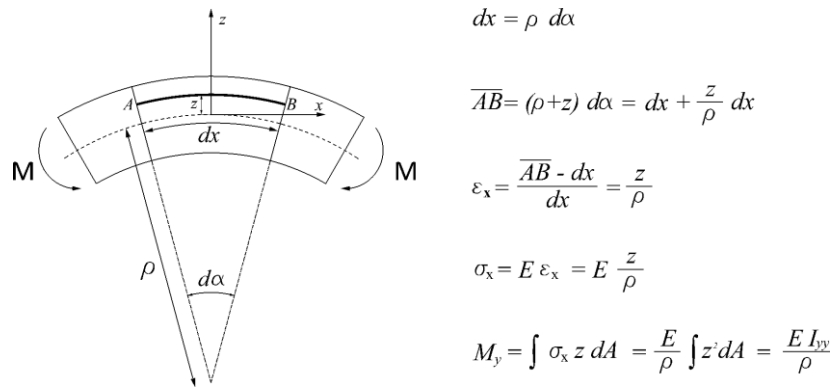


Figure 2-2: Bending moment and stresses of a slender beam according to the Euler-Bernoulli beam theory

The choice of the level of residual stresses, or admissible curvature, should assure that the profiles own enough stress reserves so that allowable stresses are not exceeded under any design load combination. At this point, it is important to remark that effects due to long-term behaviour, as relaxation and creep, should be also considered on the calculation of the final residual stresses and deformations (s. Section 2.3.1).

c) Gridshell's stiffness:

The stiffness of the gridshell depends on its spatial curvature and the material's and cross-section's properties of the grid profiles. The choice of the profiles' stiffness should result from a compromise between constructive and structural requirements: on the one hand, it should be low enough to be technically able to bend the grid and to avoid excessive support and shaping forces; on the other hand, it should be high enough to provide the gridshell with sufficient out-of-plane stiffness and avoid stability problems.

In the following Figure 2-3, the three precedent aspects – gridshell's geometry, residual stresses and gridshell's stiffness - to be considered during the design of elastic gridshells are illustrated as thirds of a circle. The circle is surrounded by architectural, structural or constructive criteria by

which the three aspects are affected. The design process of elastic gridshells usually starts with the definition of the gridshell's surface geometry which is influenced by the building's function, aesthetic purpose and the surrounding conditions. Afterwards, a grid pattern reproducing this surface geometry has to be determined. The choice of the grid pattern, involving the profiles' curvature, material and sectional properties, is initially restricted by the allowable residual stresses on the structure. Once the grid pattern has been selected, the bracing system and the support conditions of the gridshell are defined and its load-bearing behaviour, particularly its stiffness, is analysed. On the case the structural requirements are not achieved, e.g. due to stability problems or exceeding of allowable deformations or stresses, the grid's properties (geometry, material and cross-section) should be adapted and modified under consideration of the structural and constructive limitations imposed by the grid's shaping process. The final design of elastic gridshells results from an iterative process where the geometric, material and sectional properties of the grid evolve until obtaining an architecturally, structural and constructive efficient gridshell.

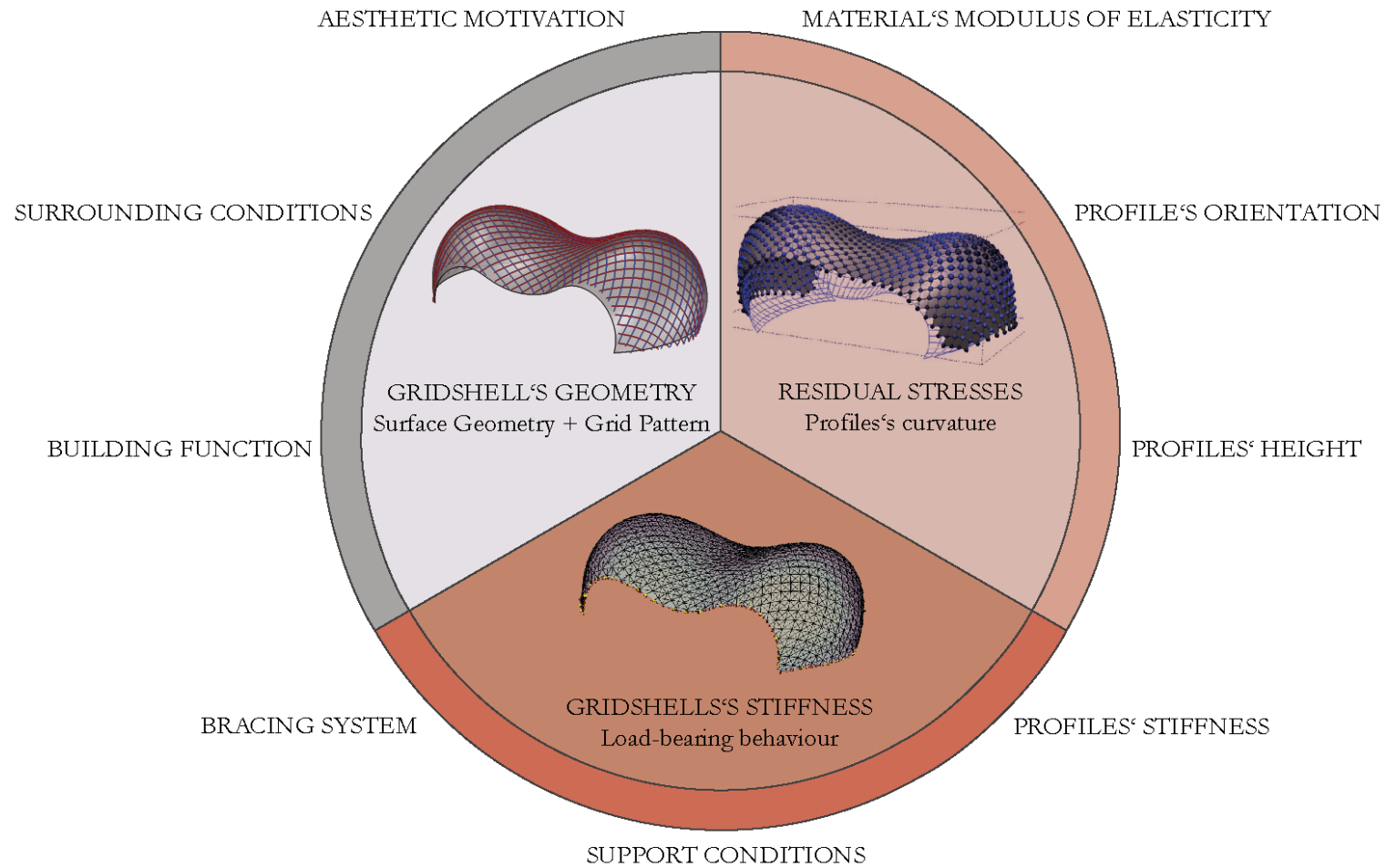


Figure 2-3: Design criteria for elastic gridsells

2.2.2 Existing design approaches for regular gridshells

Design approaches for regular gridshells have the objective to find grids with constant edge length reproducing the geometry of, mostly predefined, target surfaces. Grids with constant edge length are systems with one degree of freedom in their flat position. “*If they were formed of rigid members with frictionless joints, movement of one lath parallel to another would evoke a sympathetic movement of the whole frame causing all the squares to become similar parallelograms. This movement causes changes in length of diagonal lines through the nodes*” [2]. It is this property which allows the grid to acquire specified double-curved surface geometries. Once the grid is braced after the shaping process, the lengths of the grid’s diagonals are constrained and the grid is provided with shear stiffness.

For the design of the pioneering Multihalle gridshell in Mannheim, Germany 1975, a funicular surface shape was chosen which was determined by a combination of physical modelling and computational calculation [2]. Firstly, a suspended net model (scale 1:100) with equilateral mesh was employed. The geometry of the suspended net model was based on the wire model of a preliminary design (scale 1:500). Corrections of the net were carried out manually. A direct geometric transfer of the model into the real structure was not done to avoid very probable transfer errors which could have significant structural impacts on the gridshell (e.g. by building or measuring the model) as well as due to simplifications done on the model (only each third mesh was modelled). Therefore, the grid was additionally computationally modelled, taking the existing physical model as reference through photogrammetry. Its suspended shape was calculated using force density methods and applying dead weight as point loads on the grid’s nodes. The pattern data for the production was extracted from this computational model. In this procedure the residual internal forces after the shaping process were not considered on the determination of the grid’s bent geometry. In Henniecke and Matsushita’s manuscript about gridshells [8], investigations were performed to study the difference between the catenary and elastica curves adopted by single-span beams: the results showed that the geometries of the catenary and elastica curves are practically equivalent for ratios of arch rise to span length up to 0.3.

Since the construction of Multihalle Mannheim numerous methods have been developed to determine developable regular gridshells. As proposed in 2011 [6], the existing design procedures can be classified in two groups, according to the ***use or not of a static equilibrium*** for the determination of the bent geometry of the grid pattern: the first group employs geometric and mathematic principles (e.g. genetic algorithms, variational principles) to generate a mesh over a usually predefined reference surface; by the second group, the definition of the grid pattern results from a static equilibrium under design shaping loads and boundary conditions (*form-finding*). The design shaping loads can correspond to weight loads generating a suspended shape or virtual forces pushing the grid towards a target surface geometry. In contrast to the first group, the inner forces induced by bending the grid are considered, so that the *released geometry* of the grid - the geometry that it acquires after bending it, fixing the edges and removing the shaping forces – can be calculated with the same approach.

In a similar way, in 2013 Du Peloux et al. [9] distinguished also two different design procedures, according to the choice of the ***initial input data***: those where the grid pattern derives from a

given surface geometry (*grid-finding*) and those where the bent grid's geometry is a consequence of a form-finding process (*form-finding*), driven by given support and grid's properties.

According to the first classification, the first group of design approaches generally uses geometric and mathematical principles to generate meshes on predefined reference surfaces. The mathematical principles can be employed to establish and optimise grid's properties, especially the angles between consecutive edges which have an influence on the profiles' curvature and residual stresses. Design approaches included on this group are:

The “compass” method

In 1974 Frei Otto's Institute for Lightweight Surface Structures [8] proposed one geometric method consisting in tracing a grid with equilateral meshes on a target surface, at that time with only the help of a compass. One should start by defining on the surface two guide curves, the main profile directions, having a common intersection point. The guide curves divide the surface in four parts. Each part can be meshed as follows: two half-curves are subdivided into equal segments (desired edge length or mesh size); the first segments of both half-curves, both containing the intersection point, are the sides of the first equilateral face; its fourth corner can be then determined by intersecting circles traced on the surface at the ends of the segments with a radius equal to the fixed edge length. The rest of the surface can be meshed by using the same principle. Depending on the surface, the choice of the guide curves can become complicated, as overlapping of mesh faces or singularities points can occur.

Genetic algorithm method

In 2011 Bouhaya et al. [10] from the Navier Laboratory, Université Paris-Est of the École des Ponts ParisTech, presented a method to determine regular grids on target surface geometries with optimised profiles' curvature. This method consists in mapping a population of potential grids on a target surface, using the previously described *compass method*, then comparing them in terms of profile's curvature and selecting the best grid configuration by means of stochastic genetic algorithms.

Variational principles method

In 2011 Lafuente Hernández et al. [6][11][12] from the Department of Architecture at the UdK Berlin and from the Department of Mathematics at the TU Berlin proposed the use of variational principles to determine grids with optimised curvature on reference surface geometries. The aim of using variational principles is to establish *extremal* functions which minimize the value of quantities related to selected grid properties. These properties are: the curvature of the profiles, the distance to a reference surface geometry and the deviation of the edge lengths from a desired mesh size. The advantage of this method is that weighting factors can be applied to the grid parameters to be minimised, so that a variety of grid configurations can be established responding to different structural requirements. For example, grids with further optimized

curvature can be generated by allowing a higher distance to the reference surface or variation of the edge lengths (*irregular gridsbells*). Details to the algorithm and case studies of optimisations of double-curved grids are given in Chapter 3.

In the following Table 2-1, the three presented approaches for regular gridshells are compared. In contrast to the two first methods, the surface geometry on the variational principles method is a geometric reference and not constraint. In contrast to the compass method, the genetic algorithm and variational principles methods offer an optimisation of the profiles' curvature.

By this group of design approaches, after defining the grid pattern, an additional method is needed to determine the static equilibrium of the bent grid and to evaluate the structural behaviour of the gridshell under external loading. Here, the real material and sectional properties of the structural elements are to be considered and the internal forces induced during the bending process are to be taken into account. The most common numerical techniques used for these calculations are based on Dynamic Relaxation methods and Finite Element methods.

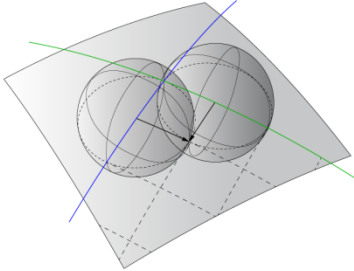
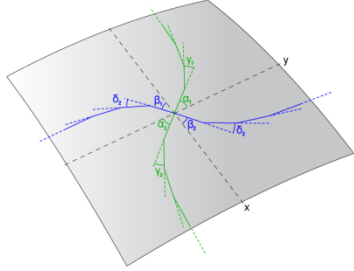
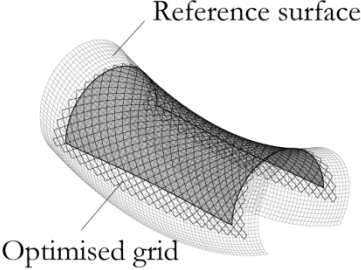
	<p>COMPASS METHOD</p> <p><i>Otto F. et al. (1974)</i></p> 	<p>GENETIC ALGORITHMS</p> <p><i>Bouhaya L. et al. (2011)</i></p> 	<p>VARIATIONAL PRINCIPLES</p> <p><i>Lafuente Hernández E. et al. (2011)</i></p>  <p>Reference surface</p> <p>Optimised grid</p>
SURFACE GEOMETRY	TARGET SURFACE AS GEOMETRIC CONSTRAINT	TARGET SURFACE AS GEOMETRIC CONSTRAINT	TARGET SURFACE AS GEOMETRIC REFERENCE
GRID PATTERN	PROGRESSIVE INTERSECTION OF CRICLES TRACED ON THE TARGET SURFACE	GENETIC ALGORITHMS: OPTIMISATION OF PROFILES' CURVATURE	VARIATIONAL PRINCIPLES: OPTIMISATION OF PROFILES' CURVATURE
STATIC EQUILIBRIUM	<p><i>not specified</i></p> <p><i>(Du Peloux L. et al. 2013)</i></p> <p>NON LINEAR ANALYSIS BASED ON DYNAMIC RELAXATION</p>	<i>not specified</i>	<p><i>(Lafuente Hernandez E. et al. 2011, 2013)</i></p> <p>NON LINEAR ANALYSIS WITH FINITE ELEMENT METHODS</p>

Table 2-1: Design approaches for regular gridshells based on geometric or mathematical principles

On the second family of design approaches, the grid pattern results from the calculation of the static equilibrium of the grid, under design shaping forces. The definition of these shaping forces is the main difference between the approaches belonging to this group. For the calculation of the static equilibrium, algorithms based on Dynamic Relaxation are mostly used. In contrast to the first group, the same algorithm can calculate the equilibrium geometry of the grid, after being bent, when the real material and sectional properties of the profiles are taken into account.

Form-finding with predefined flat grid pattern

This approach was considered for the design of the Weald and Downland Museum in Sussex, England 2002 [13], and the first GFRP gridshell of the Navier Laboratory, Université Paris-Est of the École des Ponts ParisTech, France 2005 [14]. Here, the static equilibrium of forces is calculated with Dynamic Relaxation methods, which were introduced by A. S. Day in 1965 in [15] and further developed by Prof. M. Barnes in [16][17]. In both approaches, the flat pattern of the grid is predefined: squared and elliptic shapes were respectively used for the timber and GFRP gridshells. In the former case, external springs were introduced to induce the shaping of the grid, while in the latter case upward loads at the grid nodes were applied as shaping forces. The final grid geometry is conditioned by the initial definition of the flat pattern; a specific surface geometry is thus difficult to be achieved.

Form-finding with application of vertical shaping forces

In the design approach proposed in 2009 by Kuijvenhoven et al. from the Delft University of Technology [18][19], the grid pattern results from an iterative process, where an initially flat grid with free-boundary conditions is vertically pushed towards a reference surface, as far as no stresses in the profiles exceed the allowable ones, by a system of *vertical shaping springs*. The approaching process of the grid to the reference surface is controlled and manipulated through the stiffness coefficients of the shaping springs: if somewhere the maximum permissible curvature of the profiles is exceeded, the stiffness coefficient of the spring at this point will be reduced. The process ends when the grid attains a shape in equilibrium between internal and shaping forces and the stress conditions are fulfilled everywhere. A second static equilibrium is afterwards established without shaping forces. Algorithms based on Dynamic Relaxation methods are used for the calculations.

In 2009 Bouhaya et al. [20] from the Navier Laboratory, Université Paris-Est of the École des Ponts ParisTech, proposed a similar design method where the initially flat grid with free-boundary conditions is set up over a reference surface through a system of vertical shaping forces. Friction between grid and reference surface is allowed. The shape in static equilibrium of forces is calculated using explicit Dynamic Finite Element methods.

“Least Strain Energy” Method

In the design approach presented by Li et al. in 2013 [21], an initially flat grid is set up over a reference surface applying constraint forces at the grid nodes. The constraint forces are defined by vectors pointing from the grid nodes towards the respective closest points on the reference surface and proportional to the distance between them. The distance between grid and reference surface during the approaching process is controlled and manipulated through the magnitude of the constraint forces. Tangential movement of the grid on the reference surface is allowed. Irregular gridshells can also be determined with this method by applying fictitious stiffness values to the profiles. In contrast to the previous approaches, torsion on the profiles is considered as Dynamic Relaxation with six, instead three, degrees of freedom per node is used.

The following Table 2-2 compares the presented design approaches for regular gridshells based on form-finding. Except of the approach with predefined flat grid pattern, the other three approaches make use of a reference surface geometry. The shaping forces applied on the first approach are *external springs* or *upward loads*, while for the rest of approaches, the shaping forces are defined between the grid and the reference surface in form of *vertical springs*, *vertical forces* or *constraint forces*, which makes the grid nodes approach vertically or straight to the target geometry. Algorithms based on Dynamic Relaxation and Dynamic Finite Element Methods are used in all the approaches. Regarding the profiles' curvature, the particle-spring method and the least strain energy method afford grids whose bending stresses do not exceed predefined values.

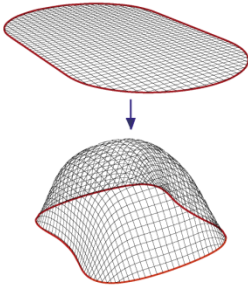
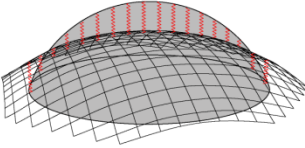
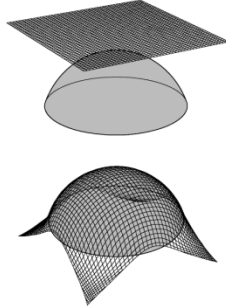
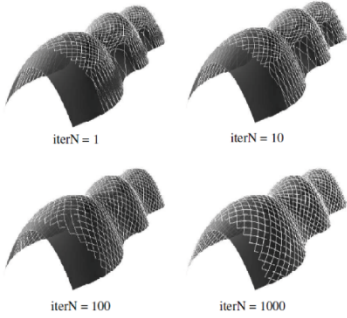
	<p>FORM-FINDING WITH PREDEFINED FLAT GRID</p> <p><i>Harris R. et al. (2003), Doutbe C. et al. (2006)</i></p> 	<p>FORM-FINDING WITH VERTICAL SHAPING SPRINGS</p> <p><i>Kuijvenhoven M. et al. (2009, 2012)</i></p> 	<p>FORM-FINDING WITH VERTICAL SHAPING FORCES</p> <p><i>Bouhaya L. et al. (2009)</i></p> 	<p>LEAST STRAIN ENERGY METHOD</p> <p><i>Li J. et al. (2013)</i></p> 
SURFACE GEOMETRY	No target surface is provided THE GRID'S PATTERN IS DEFINED IN ITS FLAT POSITION	TARGET SURFACE AS GEOMETRIC REFERENCE	TARGET SURFACE AS GEOMETRIC REFERENCE	TARGET SURFACE AS GEOMETRIC REFERENCE
GRID PATTERN	SHAPING FORCES: „External springs“ (<i>Harris R. et al.</i>), „upward loads“ (<i>Doutbe C. et al.</i>)	SHAPING FORCES: „Vertical springs“ between grid and surface The grid pattern fulfills predefined stress conditions	SHAPING FORCES: „Vertical forces“ between grid and surface Friction between grid and surface is allowed	SHAPING FORCES: „Constraint forces“ between grid and surface The grid's curvature is manipulated through the magnitude of the constraint forces
results from a STATIC EQUILIBRIUM	ALGORITHM: DYNAMIC RELAXATION	ALGORITHM: DYNAMIC RELAXATION	ALGORITHM: EXPLICIT DYNAMIC FINITE ELEMENT METHODS	ALGORITHM: DYNAMIC RELAXATION WITH 6 DEGREES OF FREEDOM

Table 2-2: Design approaches for regular gridshells based on form-finding

2.2.3 Existing design approaches for irregular gridshells

The choice of a non-constant mesh by irregular gridshells is motivated by diverse structural, constructive or architectural reasons. As the edge length varies, the mesh edges are not parallel to another anymore and distortion and deployment of the whole grid is restricted. Therefore irregular gridshells are generally not shaped as a whole grid but built in a progressive construction process, where the profiles are incrementally bent, independently from each other. As by the design approaches for regular gridshells, the design procedures can integrate or not a form-finding calculation. The design approaches mainly differ on the aspects according to which the grid pattern is defined. Two of the design approaches for regular gridshells presented in the previous section are suitable for irregular gridshells: the variational principles and the least strain energy methods. In both of them, the profiles' curvature is optimised or controlled. Next, different examples of irregular gridshells are shown.

Helsinki Zoo Lookout Tower, Finland 2002 – Example of architectural purpose

The irregular timber gridshell of the 10 m high Helsinki Zoo Lookout Tower was designed by Ville Hara, who was principally motivated by the natural surroundings of the tower. The grid's geometry and pattern were developed at the HUT Wood Studio workshop, experimenting with 1:5 physical models. Figure 2-4 shows, on the left, a moment of the design process and, on the right, an image of the built structure. The single-layer profiles were bent and twisted on site from seven pre-formed guide types by steaming: traditional method used in boatbuilding [22].

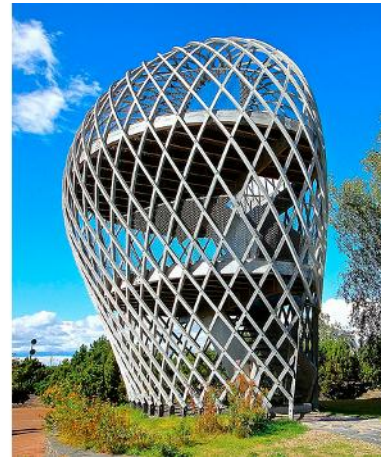


Figure 2-4: Helsinki Zoo Lookout Tower gridshell, Finland 2002

"Geodesic Lines on Free-Form", Switzerland 2006 – Example of structural purpose

By the designed approach proposed by Pirazzi et al. [23] in 2006, the grid pattern results from the determination of geodesic curves on a predefined target surface. The objective of this method is to obtain profiles which are subjected to bending, only about their weak axis: then, efficient low cross-sections, for example in multi-layer systems, can be used. A prototype of dimensions 8 m x

3 m x 2.06 m made of timber was built and its bearing behaviour compared with a simulation model at the École Polytechnique Fédérale of Lausanne. In the computational model, residual internal forces due to bending were not considered. Figure 2-5 shows, on the left, the mono-patched free-form surface and the corresponding grid composed of geodesic curves and, on the right, the built prototype.

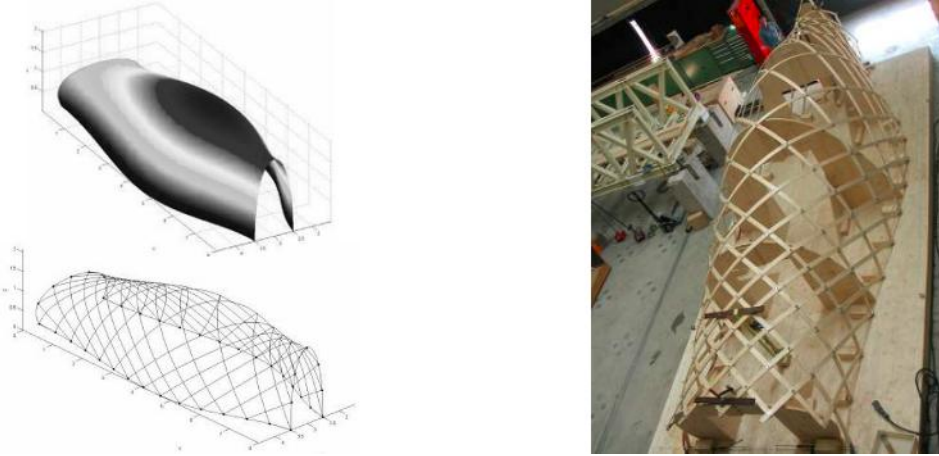


Figure 2-5: Timber gridshell with grid pattern composed of geodesic curves, Switzerland 2006

Irregular gridshell with optimised curvature, Germany 2012 – Example of structural purpose

In 2012 Lafuente Hernandez et al. [12] presented a design approach for regular and irregular gridshells based on variational principles. With this method, grids with optimised profiles' curvature can be determined on a specific reference, but not constraint, surface. A prototype of a 10 m diameter hemisphere composed of GFRP tubes was built. Figure 2-6 illustrates the built prototype. The static equilibrium of forces and the structural behaviour of the grid during the bending process and under external loading were analysed by means of finite element methods. In contrast to other built irregular gridshells, the most of the grid was bent as a whole and not in a successive process in order to accelerate its construction. The detailed design procedure and the results of the structural analyses are given in Chapter 5.



Figure 2-6: GFRP irregular gridshell with optimised curvature, Germany 2012

Faraday Pavilion, Roskilde 2012 - Example of architectural and structural purpose

In 2012 Nicholas et al. [24] proposed a design approach based on a simulation model in which the bending of the profiles can be partially controlled and manipulated by the designer. In the simulation, the paths of the profiles are constraint to target local surfaces and cannot exceed predefined curvature values. The static equilibrium of the structure is calculated using algorithms based on Dynamic Relaxation. The Faraday Pavilion, an ensemble of three half-toroidal GFRP gridshells of about 4 m height and 10 m span, was design and built at the Roskilde Festival by means of this design approach. The grids are composed of radial and transverse elements, which are bent and assembled in a rapid erection process: the radial profiles are firstly bent, independently from each other, by just approximating their ends and then temporary fixed; the transverse profiles are afterwards set up over or under the radial ones and connected to them. Figure 2-7 illustrates, on the left, the bending simulation of the radial profiles and, on the right, the built structure. The bearing behaviour of the structure was additionally analysed using Finite Element methods.



Figure 2-7: Faraday Pavilion at the Roskilde Festival, Denmark 2012

The following Table 2-3 shows the diversity of the presented design approaches for irregular gridshells. The design approaches vary on the definition of the surface geometry, which is applied as geometric reference on Lafuente's and Li's approaches, as local or partial geometric constraint on the approach proposed by Nicholas, as geometric constraint on Pirazzi's approach and as experimental output on Hara's gridshell. The approaches also differ on the method with which the grid pattern is defined: Li's and Nicholas' approaches apply form-finding methods, Lafuente's approach makes use of variational principles, Pirazzi's approach is based on the calculation of geodesic curves on the predefined surface geometry while Hara's design results from a physical modelling process. Concerning the calculation of the static equilibrium, Finite Element Methods have been used on the variation principles approach and Dynamic Relaxation on Li's and Nicholas' approaches.

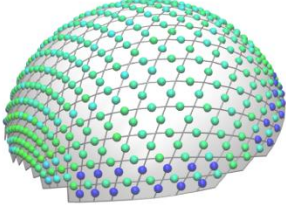
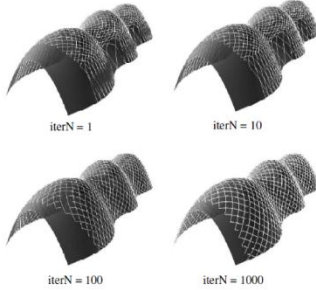

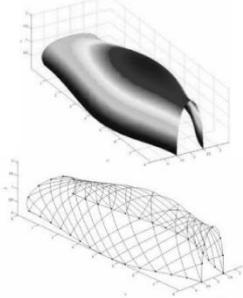
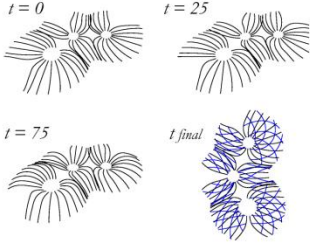
	<p>VARIATIONAL PRINCIPLES</p> <p><i>Lafuente Hernández E. et al. (2011, 2013)</i></p> 	<p>LEAST STRAIN ENERGY METHOD</p> <p><i>Li J. et al. (2013)</i></p> 	<p>PHYSICAL MODELLING</p> <p><i>V. Hara, HUT Wood Studio Workshop Finland 2002</i></p> 	<p>OPTIMISATION THROUGH GEODESIC LINES</p> <p><i>Pirazzoli C. et al. (2006)</i></p> 	<p>FORM-FINDING INTEGRATING DESIGN, BENDING BEHAVIOUR AND ASSEMBLY PROCESS</p> <p><i>Nicholas P. et al. (2012-13)</i></p> 
SURFACE GEOMETRY	TARGET SURFACE AS GEOMETRIC REFERENCE	TARGET SURFACE AS GEOMETRIC REFERENCE	Experimentation with 1:5 physical models	TARGET SURFACES AS GEOMETRIC CONSTRAINT	TARGET LOCAL SURFACES AS GEOMETRIC CONSTRAINTS
GRID PATTERN	VARIATIONAL PRINCIPLES: OPTIMISATION OF PROFILES' CURVATURE	SHAPING FORCES: „Constraint forces“ between grid and surface The grid's curvature is manipulated through the magnitude of the constraint forces		Grid pattern results from the determination of geodesic curves on a predefined target surface	SHAPING FORCES: Induction of profiles' bending by simulated displacement of supports. Constraint forces for local surface constraints. Their magnitude is limited by the allowable bending radius.
STATIC EQUILIBRIUM	NON LINEAR ANALYSIS WITH FINITE ELEMENT METHODS	ALGORITHM: DYNAMIC RELAXATION WITH 6 DEGREES OF FREEDOM	<i>not specified</i>	<i>not specified</i>	ALGORITHM: DYNAMIC RELAXATION

Table 2-3: Design approaches for irregular grids

2.3 Construction Material

To make the grid profiles acquire the curvature of the desired surface geometries, materials with high limit strain are necessary. If initially timber was the material of preference, emerging fibre-reinforced plastics are becoming more and more present in the construction of elastic gridshells because of their low ratio of flexural modulus to strength. A study of materials suitable for actively-bent structures has been presented by Kotelnikova-Weiler et al. in [25]. The following section focuses on three structural selection criteria which are essential for the choice of the gridshell's material. Application examples are also given and illustrated.

2.3.1 Material selection criteria

When choosing the material for a elastic gridshell, the following mechanical properties are to be taken into account:

1. Ratio of modulus of elasticity to strength

According to the Euler-Bernoulli beam theory given in Figure 2-2, the minimum radius of curvature ρ_{min} (2-1) that can be achieved with a profile subjected to uniaxial bending moment and its material utilisation factor (2-2) can be written as:

$$\rho_{min} = \frac{E}{\sigma_d} \cdot z \quad (2-1)$$

$$\frac{\sigma_x}{\sigma_d} = \frac{E}{\sigma_d} \cdot \frac{z}{\rho} \quad (2-2)$$

The terms E and σ_d represent respectively the flexural modulus of elasticity and the design strength of the profiles' material. The lower the ratio Young's modulus to strength is, the further the profiles can be bent before achieving the allowable maximum stresses and the higher the remaining stress reserve will be.

Consider for example three 15 m long profiles with the same sectional height ($h = 40$ mm) but different ratios of Young's modulus to strength ($E/\sigma_d = 200, 150$ and 100 – comparable to timber, natural-fibre reinforced polymers and glass-fibre reinforced polymers, respectively). The profiles are progressively bent by applying increasing opposite horizontal displacements at their ends, which are vertically restrained, as illustrated in Figure 2-8. A small upward force at the middle-point of the profiles has been initially applied to induce buckling and the consecutive bending. Horizontal displacements are restrained at the middle of the profile. The simulation and analysis of the bending process have been done with Finite Element methods.

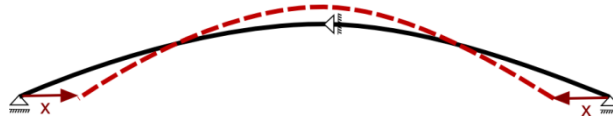


Figure 2-8: Bending of a beam by applying horizontal displacements at its extremities

Figure 2-9 shows the increment of the utilisation factor as a function of the horizontal displacements. On the top of the graphic, the corresponding elastica curves acquired by the profiles are illustrated. One can observe how the ratio of Young's modulus to strength influences the increment of stress utilisation and the maximum curvature reached by the profiles.

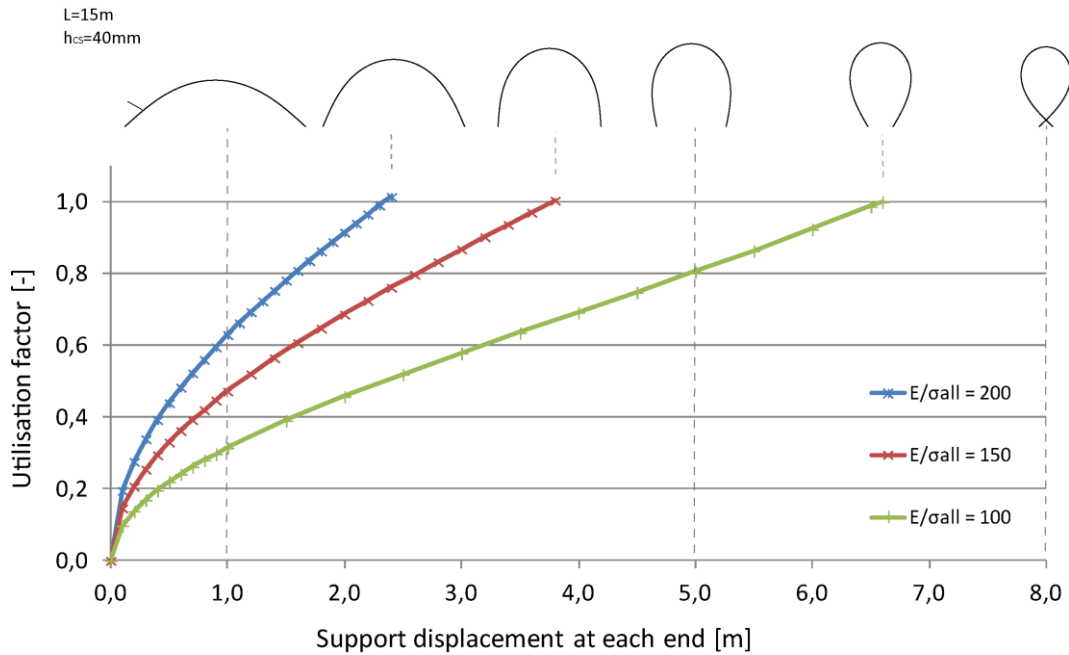


Figure 2-9: Increment of utilisation factor in function of the horizontal displacement applied at the extremities of a 15 m-long profile with 40 mm sectional height, for ratios of Young's modulus to strength of 100, 150 and 200

2. Axial and bending stiffness of the profiles

The axial and bending stiffness of the profiles, EA and EI , are given by the Young's modulus E multiplied by the area A and the moment of inertia I of the profiles' cross-section. The stability behaviour of compression-loaded light-weight shell structures is usually a decisive aspect for their structural design. Generally, it can be said that failure loads are directly proportional to the bending stiffness of a shell. Nevertheless, the stability analysis that J. Graf [26] performed for single-layer steel-glass gridshells showed that the axial stiffness of the profiles has a higher influence on the bearing behaviour of the steel-glass gridshells than the bending stiffness: the loading capacity of the gridshell increases approximately quadratically with the value of the profiles' axial stiffness.

The choice of the sectional properties of the profiles should result from a compromise between structural and constructive requirements. On the one hand, the profiles' stiffness should be high enough to provide the gridshell with sufficient out-of-plane bending stiffness and avoid stability

problems. On the other hand, higher bending stiffness implies more resistance to shape the grid, which results on an increment of the needed external shaping forces during the erection process and reaction forces on the gridshell's supports.

The choice of the material has as well an influence on the designation of the profiles' cross-section according to its manufacture possibilities. While timber profiles are generally restricted to full sections, the production technique of *pultrusion* for composites offers a great variety of hollow-sections. *Pultrusion* is a cost-effective manufacturing process for long-fibre unidirectionally reinforced profiles with constant cross-section. The fibres are pulled continuously firstly through an impregnating resin bath (*open* impregnation method) or resin injection die (*closed* impregnation method), afterwards through heated dies used to shape the composite into the desired cross-section. A wide range of profile lengths and sections can be processed using this technique, which means that weaknesses otherwise caused by prolonging connections can be reduced and the sectional properties of the profiles can be optimised in terms of weight and structural efficiency.

Let us compare the properties of four different grid configurations, which have been used for the construction and research of elastic gridshells:

1. The first grid configuration corresponds to a **single-layer of timber laths**, as used on the gridshells of the Earth Center, England 1998, or Helsinki Zoo Lookout Tower, Finland 2002. The chosen ratio between sectional width and height is the same as the one selected for the Helsinki Tower: 60 to 60.
2. The second configuration consists in a **double-layer of timber laths**, used for example at the Multihalle Mannheim, Germany 1975 [2], and Weald and Downland Museum [13], England 2002. The chosen ratio between width and height is the same as that of the profiles of the second structure: 50 to 35.
3. The third configuration represents a **quadruple-layer of GFRP laths**, proposed by Darby et al. in [27]. The ratio between width and height corresponds to 80 to 20.
4. To directly compare the different multi-layer systems independently of the material, a **quadruple-layer of timber laths** has been also considered. The width and height of the profiles are the same as on the configuration 3.
5. The fifth configuration is a **single-layer of GFRP tubes** with a wall thickness equivalent to 8% its outer diameter, similar to the GFRP tubes (D=41.7 mm, t=3.5 mm) used for the Soliday's Festival gridshell, France 2011 [9].

The material properties of timber and GFRP used for the calculations are summarised in the following Table 2-4:

	Allowable stress [N/mm²]	Modulus of elasticity [N/mm²]	Density [kg/m³]
Timber	50	10.000	500
GFRP	250	25.000	2.000

Table 2-4: Properties of timber and GFRP, considered in Figure 2-10 and Figure 2-11

The main advantage of a multi-layer configuration with low profiles is that, during the bending process, each layer can slide respect to the other – by using slotted connections and clamping plates - so that the bending stiffness of only one layer had to be overcome. Once the grid is shaped, shear blocks are added between layers, in order to transfer shear forces between them. The low profiles can be bent to lower radii of curvature while the structure will be provided with the aggregate stiffness of the connected layers. Therefore, on the following analyses, the utilisation factor due to the profiles' bending has been calculated considering only one layer, while the stiffness properties and weight have been determined taking into account all the layers.

The aim of the calculations presented in Figure 2-10 is to compare the quantity of material, in terms of sectional area and weight, that are needed for a required moment of inertia or bending stiffness. On the left, one can observe that, with the same amount of material or sectional surface, slightly higher moments of inertia can be reached with hollow tubular sections than with multi-layer laths. The double-layer with rectangular section is a bit more efficient than the quadruple-layer with lower laths; the single-layer with square section is the more material-consuming. Nevertheless, that changes when not only the sectional but also the material properties are considered. On the right of Figure 2-10, the weight of the profiles in function of their bending stiffness is shown. One can observe that the high density of GFRP, which is approximately four times that of timber, dominates against the previously obtained efficiency of the tubular section. Here, plastics reinforced with natural fibres (NFRP), which are almost two times lighter than glass fibres and offer the same manufacture possibilities for hollow-sections, represent a potential alternative. Compared to the graphic on the left, the order of the configurations of the same material remains the same: the double-layer with rectangular section is slightly lighter than the quadruple-layer with lower laths and the single-layer with square section is the heaviest.

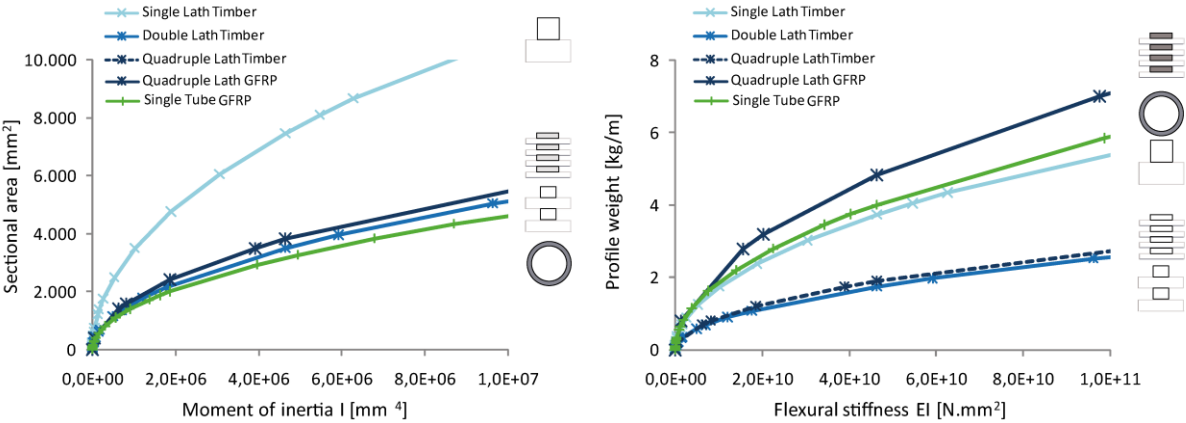


Figure 2-10: Comparison of the increment of the moment of inertia in function of the sectional area (left) and of the flexural stiffness in function of the profile weight (right) for different grid configurations

The objective of the calculations on Figure 2-11 is to compare the stress reserve of the grid configurations, under a bending radius of 5 m - lowest radius of curvature on the Weald and Downland gridshell -, in function of their axial and bending stiffness. One can see that, for a given required axial or bending stiffness value, the utilisation factor of multi-layer configurations will be lower than that of single-layer ones. The same can be said for GFRP compared to timber, due to the higher limit strain and modulus of elasticity of the former material. For example, to

dispose of an axial stiffness equivalent to that of the Weald and Downland gridshell ($EA=3.5 \cdot 10^7$ N), the required profiles will be subjected to an utilisation factor of 118% with a single-layer of squared timber laths, 78% with a single-layer of GFRP tubes, 70% with a double-layer of rectangular timber laths, 30% with a quadruple-layer of slender timber laths and 9% with a quadruple-layer of slender GFRP laths. In the same way, to dispose of the bending stiffness of the same section ($EI = 4.6 \cdot 10^{10}$ N.mm²), the corresponding profiles will be subjected to an utilisation factor of 173% with a single-layer of squared timber laths, 93% with a single-layer of GFRP tubes, 70% with a double-layer of rectangular timber laths, 31% with a quadruple-layer of slender timber laths and 12% with a quadruple-layer of slender GFRP laths. Given a required out-of-plane stiffness of a gridshell, this comparison shows that multi-layer sections and composite materials allow the highest stress reserves on the profiles after the shaping process. Nevertheless, it is important to remark that the assembling process of multi-layer grids is usually more time and cost-intensive than that of single-layers.

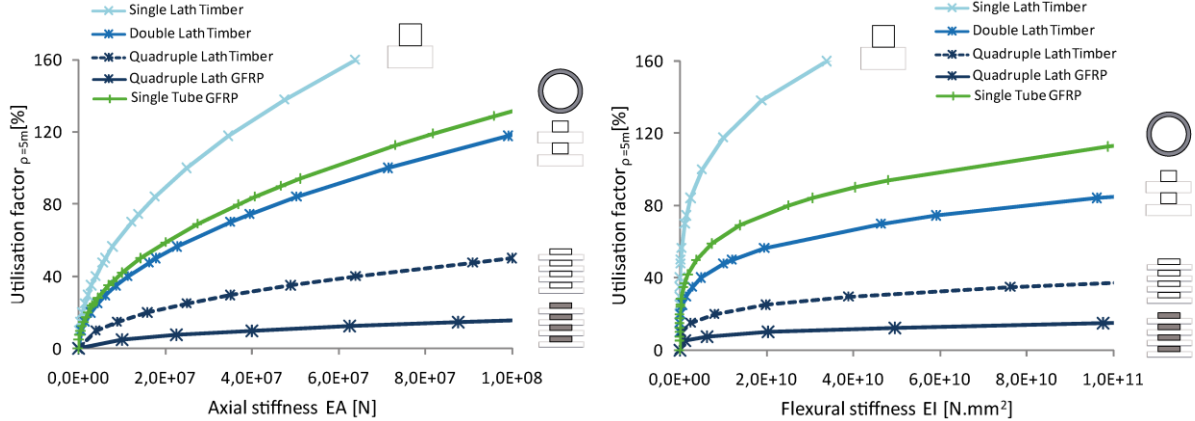


Figure 2-11: Comparison of the increment of the utilisation factor in function of the axial (left) and flexural (right) stiffness for different grid configurations.

3. Long-term behaviour

Material creep and relaxation are important aspects for the design of timber and composite gridshells and have a relevant influence on their long-term residual stresses and geometry. As a result of the shaping process, the grid profiles are subjected to residual bending stresses and, with it, to a time-depending increment of the gridshell’s deformation, which can partially become irreversible (*creep*). On the other hand, under constant bending deflection, material stresses tend to relax and decrease in the course of time (*relaxation*). Creep factors are important to deduce the long-term deflection on the gridshell’s geometry, while relaxation factors are needed to calculate the long-term residual stress level on the profiles and the subsequent stress reserve for external loading. Creep and relaxation factors depend on the material but also on the duration, intensity and nature of the applied loads.

In Figure 2-12, the results of creep tests performed with spruce timber in [28] are shown. One can observe the influence of the nature – tension, bending, compression and torsion – and intensity of the loads on the time-depending creep factors: ratio of strain at time t to elastic strain

at $t=0$. After 8000 h, the spruce timber exhibited creep factors between 1.40 and 1.85 under bending loads by stress levels of 22 to 67% of the limit stress.

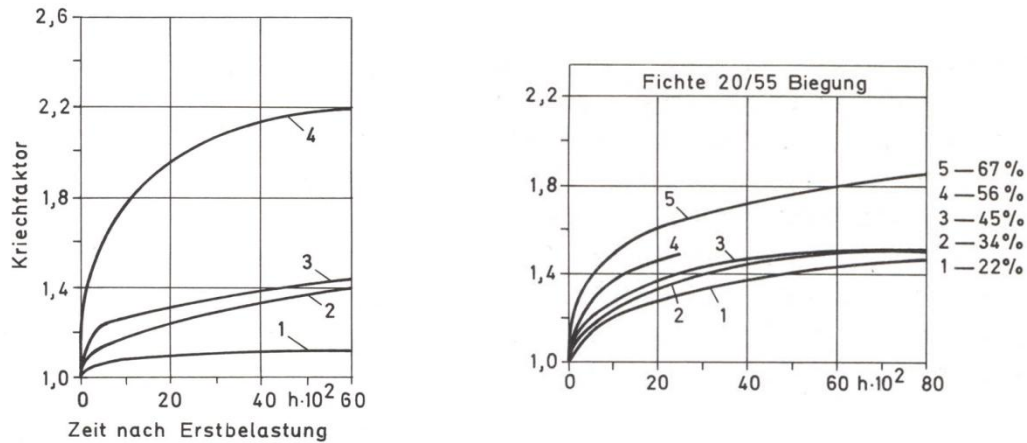


Figure 2-12: Time-dependent creep factors of spruce timber by varying loading nature (1=Tension, 2=Bending, 3=Compression, 4=Torsion; by load factors of 20-30%) at the left and by varying loading intensity, under bending, at the right by constant humidity and temperature conditions (55% / 20°C) [28]

Tests of creep-relaxation behaviour are important to anticipate structural failures; they are usually performed under stress levels, to which the gridshell is planned to be subjected. For a first very approximate estimation, the engineers in charge of the construction of the timber Multihalle Mannheim gridshell applied the reciprocal rule: “If it takes x days for deflection to increase by a factor of y , for constant load-deflection testing, then in the same x days at constant deflection, the stress will reduce by the factor y ($=1/y$ times the original stress)” [2]. The advantage of this creep-relaxation effect is that the high residual stresses resulting from the shaping process gradually decrease, so that the gridshell is provided with higher stress reserves by the time it is subjected to external loads.

To further analyse the creep-relaxation behaviour of the timber laths, the engineers of the Multihalle Mannheim performed stress relaxation tests with laths of different lengths, which were bent approaching their ends and connecting them with a calibrated spring dynamometer, as illustrated in Figure 2-13. The radii of curvature, to which the profiles were bent, were kept constant and the decreasing spring forces were registered. The results of the tests, done in indoor climate conditions, showed a significant reduction of the spring force, and consequently of the initial bending stresses on the profile, of about 30% after 40 days.

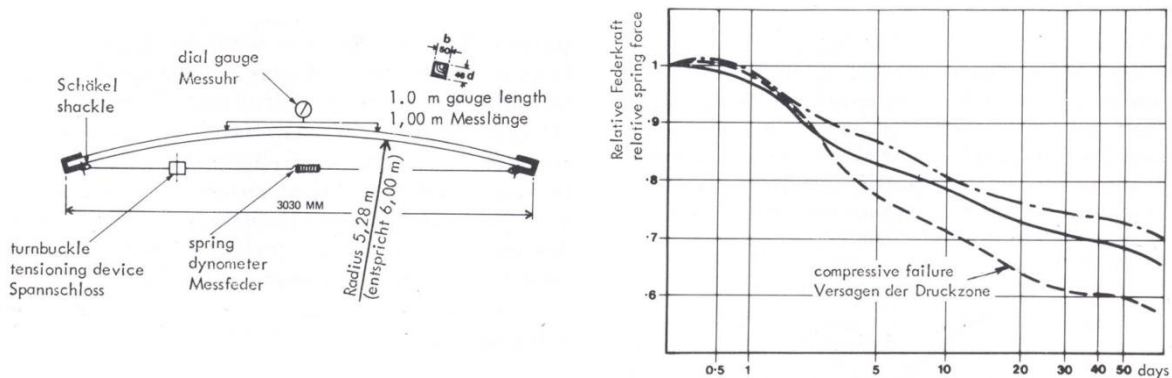


Figure 2-13: Stress relaxation test performed by the construction of the Multihalle Mannheim gridshell [2]

Concerning the long-term behaviour of GFRP, Douthe et al. referred, on the report about the construction of the first GFRP gridshell of the Navier Laboratory, Université Paris-Est of the École des Ponts ParisTech [14], the creep tests performed by Caron et al. [29] with pipes under permanent bending. Here, the creep strain (strain at time t minus elastic strain at $t=0$) resulted to be roughly 8% of the total strain (a creep factor of about 1.08), independently of the load intensity. It could also be observed that under a load factor of 30% of the limit strain, non-linear effects could be neglected. That would mean that the creep-relaxation behaviour of gridshells, subjected to stresses up to 30% of the limit strain, can be deduced from Caron's creep tests. On the tests presented by Kotelnikova-Weiler et al. in [30], rectangular pultruded GFRP profiles with vinylester matrix were subjected to bending load factors of 35%. After 140 h, creep factors of around 1.03 were attained. It is important to remark that by reinforced composites not only the nature, intensity and duration of the load, but also the composition (nature of fibres and matrix) and cross-section of the profiles have an influence on their long-term behaviour.

Also in [30], results of creep tests of tubular sections made of pultruded NFRP (natural fibre reinforced plastics) are given. The NFRP samples exhibited much higher creep factors than GFRP: 1.50 after 140 h. That could be partially due to the cellulose contained on the natural fibres but also to flaws, twisting and material heterogeneities generated during the manufacture process of the pultruded NFRP tubes. Further research on the creep behaviour of NFRP for longer loading duration and under varying humidity and temperature conditions are necessary.

2.3.2 Available materials and application examples

The first part of this section intends to compare the mechanical properties of existing materials, used for the construction of elastic gridshells, and introduce built application examples. Some of the research data has been already published on [31]. The mechanical properties of the materials are summarised at the end of the section.

Timber

The pioneering gridshells of the Multihalle in Mannheim, Germany (1975) [2] and Weald and Downland Museum in Sussex, Great Britain (2002) [13], with maximum span lengths of 60 and 16 m, are respectively made of hemlock and oak. In Figure 2-14 both timber gridshells are illustrated. With a Young's modulus of about **11 – 17 GPa** and a characteristic flexural strength of about **24 – 60 MPa** according to Eurocode 5 [32], the allowable minimum radius of curvature of timber corresponds to **280 – 480·z**, where z is equal to the half-height of the cross-section. Because of manufacture reasons, timber profiles generally possess full-sections. Single- and double-layer grid configurations of quadratic or low rectangular profiles are usually used.



Figure 2-14: Examples of timber gridshells: Mulithalle Mannheim, Germany (1975) at the left and Weald & Downland Museum, Great Britain (2002) at the right

Bamboo

Bamboo is of great interest not only because of its environmentally-friendly and economic advantages but also due to its excellent flexural properties. Nevertheless, as natural material, the mechanical properties and section of the bamboo canes can strongly vary: depending on its class, origin, age, moisture content and cane's diameter, the flexural strength and stiffness of bamboo can reach values about **119 – 185 MPa** and **8.7 – 13.4 GPa** [33] [34], corresponding to minimum radii of curvature between **66 - 85·z**, with z as half-height of the profiles' section.

Research on constructions, using bamboo as structural material, was published by the Institute of Light Surface Structures (IL) of the Stuttgart University in [2][35]. In the books, some prototypes and experimental gridshells are presented and different solutions for the connection of the bars are proposed. Figure 2-15 shows two of these prototypes: the one on the left was performed by students of the Architectural Association (AA), under the direction of Jonathan Park and Bernd Oleiko, in London (England) on 1976; the one on the right, by students of the School of Architecture, under the direction of Eda Schaur (IL), in Ahmedabad (India) on 1977. Since then, the use of bamboo in elastic gridshells has been being further practised.

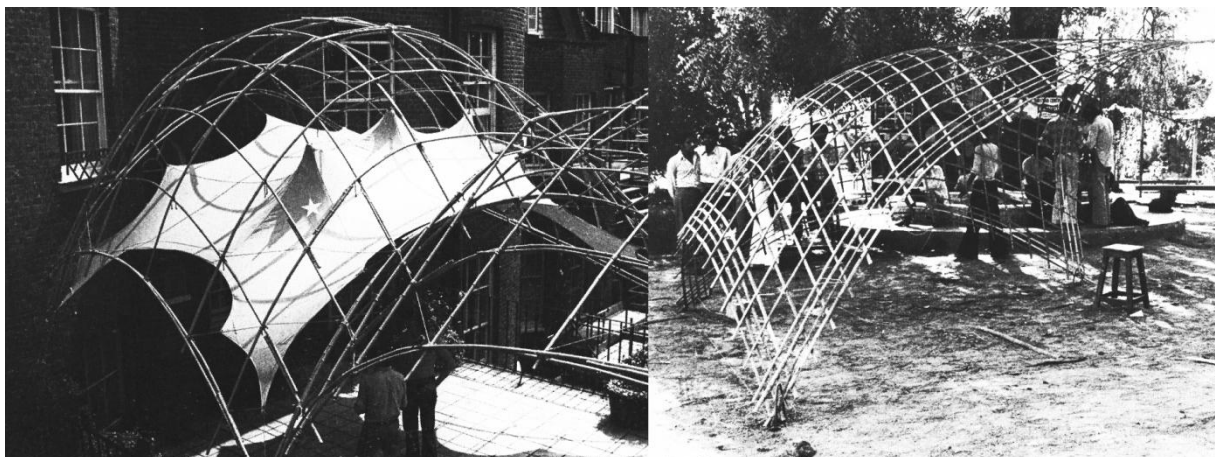


Figure 2-15: Research examples of bamboo gridshells in London (England, 1976) at the left and Ahmedabad (India, 1977) at the right [2]

Paper

Sustainable and low-tech recycled paper tubes were used for the construction of Shigeru Ban's Japan Pavilion at the Expo 2002 in Hannover, Germany: a elastic gridshell spanning 35 m with a maximum height of 15 m, illustrated in Figure 2-16. The manufacture process of these tubes starts with rolls of recycled paper cut into strips, saturated with glue and wound spirally around a short metal rod that creates the hollow core of the tube [34]. Relative low radii of curvature, of about $100 \cdot z$ – with z as half-height of the profiles' section - are possible with paper tubes due to the small ratio of bending stiffness to strength: **1.4 GPa / 14.5 MPa**. Nevertheless, due to their low modulus of elasticity, the out-of-plane stiffness of paper gridshells are often limited and additional reinforcement is needed: on the Japan Pavilion, a timber frame of ladder arches and longitudinal rafters were employed.

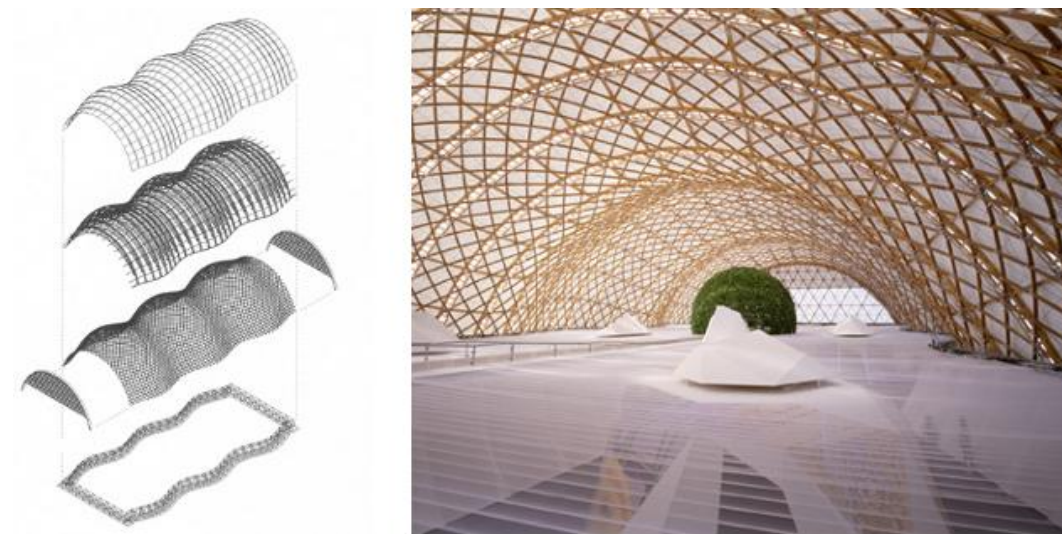


Figure 2-16: Japan Pavilion gridshell at the EXPO 2000, Hannover (Germany), made of paper tubes and bracing timber frame [34]

Fibre reinforced polymers - FRP

Emerging composite materials such as glass, natural and carbon fibre-reinforced polymers, with higher modulus of elasticity and limit stresses but lower ratio of stiffness to strength than timber, allow lower radii of curvature, providing at the same time more rigidity to the gridshell. FRP can be used for the industrially scaled manufacture of unidirectionally fibre-reinforced profiles by means of the pultrusion technique. Profiles with unidirectional orientation of fibres offer ideal mechanical properties for a variety of structural applications. Furthermore, arbitrary profiles' lengths and sections can be manufactured with pultrusion so that weaknesses otherwise caused by nodal connections can be reduced and sectional properties can be optimised.

Glass fibre-reinforced polymers - GFRP

Depending on the content of reinforcing fibres and the nature of the matrix, the flexural modulus of elasticity and strength of GFRP oscillate between about **12 - 41 GPa** and **200 - 700 MPa**, allowing radii of curvature of **46 – 86·z**, with z as half-height of the profiles' section. The first examples of GFRP gridshells have been carried out by the Navier Laboratory, Université Paris-Est of the École des Ponts ParisTech, France. In 2005 Douthe et al. [14] presented the first prototype: a 13 m wide and 5.80 m high synclastic gridshell. In 2011 six students from the École des Points ParisTech, supported by the Navier Laboratory, built the first GFRP gridshell in use: a 15 m wide and 7 m high peanut-shaped pavilion to house the visitors of the Solidays' Festival in Longchamps, Paris [9] (see Figure 2-17 – left). Based on the experience with these pioneering composite gridshells, in 2013 the largest GFRP gridshell was built: a 550 m² cathedral in Créteil, France [36] (see Figure 2-17 – right). The grid of the three structures consists of two superposed single-layers of GFRP tubes, braced with a third layer of the same profiles. Further grid configurations with GFRP full-laths in multi-layer systems have been also proposed by Darby et al. in [27].



Figure 2-17: Examples of GFRP gridshells: Solidays' Festival (2011) at the left and Créteil Cathedral (2013) at the right

Natural fibre-reinforced polymers - NFRP

Despite the great mechanical properties of GFRP, the environmental impact of the glass fibre production and the difficulties in their recycling and reuse are generally considered as critical aspects. Natural-fibre reinforced polymers NFRP are likely to be a more environmentally friendly and lightweight alternative to GFRP due to the lower environmental impact of the natural fibres and their end of life incineration as well as the good specific properties of the composite (strength per unit weight) [37][38][39]. However, it is important to note that not only the production of the natural fibres but also the origin and biodegradability of the polymer matrix are decisive aspects concerning the sustainability of the whole composite.

A great variety of natural fibres can be used on NFRP – the most common are flax, hemp, jute, sisal, ramie, coir and cotton fibres. Unlike industrially produced continuous synthetic fibres, the properties of natural fibres can vary significantly, thus attributing a high diversity of mechanical properties to NFRP.

The main current industrial applications of NFRP can be found in the automotive industry, particularly for interior trim. Only few studies investigate structural applications of NFRP; in most of them, processes far from industrially-scaled production are used. In 2003 and 2004 Dweib and O'Donnell et al. [40] [41] manufactured NFRP sandwich beams by means of vacuum assisted resin transfer moulding, made of varying natural fibres (flax, cellulose, pulp and hemp), soy oil-based resin and structural foam. Depending on the nature and content of the fibres (10 - 50 W%), the beams exhibited by three-point bending tests flexural moduli between **1-6 GPa** and strengths between **30-60 MPa**. Similar values were obtained by Burgueño et al. [42] in 2004 with cellular beams and plates made of industrial hemp and flax fibres and unsaturated polyester resin. The manufacture process of the samples began with a manually impregnation of the fibres with the resin; then, the impregnated fibres were placed in a compression mould, where the composite was cured for a total of 4h. Moduli of elasticity between **3 - 8 GPa** and tensile strengths between **10 – 20 MPa** were obtained, depending on the nature and content of the fibres (13 - 33 W%).

With the manufacture technique of pultrusion, unidirectional composites, with higher strength and stiffness values on the reinforced direction, can be produced. Compared to glass and carbon fibres, natural fibres possess far lower thermal stability, resistance to moisture and strong hydrophilicity. For this reason, standard pultrusion parameters must be investigated and adapted according to the properties of NFRP. In 1999, Riedel et al. [43] succeeded in creating pultruded profiles from flax fibres and bio-based resin which achieved the 91% and 40% of the bending stiffness and strength of equivalent GFRP profiles by 0% relative humidity. However, these values were reduced to 55% and 24% by 50% relative humidity. Instead of thermosetting resins, K. Van de Velde et al. made use in [44] of thermoplastic polymers as matrix. The *thermoplastic* pultrusion of the profiles was done with hybrid flax/PP yarns (50/50 W% - 38/62 V%). Bending stiffness and strength of **14 GPa** and **101 MPa** (corresponding to a minimum radius of curvature of **142·z**) were reached. In 2007 I. Angelov et al. analysed in [45] the influence of pultrusion parameters, in particular the preheating and die temperatures and the pulling speed, on the mechanical properties of flax/PP samples with 30 and 50% weight fibre fraction. The pultruded samples reached, respectively, stiffness values of **7.5** and **9 GPa** and strengths of **95** and **125 MPa** (corresponding to a minimum radius of curvature of **72·z**). Higher values were obtained by Xi Peng et al. in [46] with rods made of polyurethane, vinylester and polyester reinforced with hemp and wool: bending stiffness values between **11.5 - 13 GPa** and flexural strength values between **145 – 180 MPa** (corresponding to minimum radii of curvature of **63-89·z**). A compilation of recent research studies on NFRP between 2000 and 2010 is given in [47].

The samples of the previously mentioned studies had rectangular and circular full-sections. In 2012, tests with hollow tubular sections were carried out at the Faserinstitut Bremen e.V. (FIBRE) in cooperation with the Department of Architecture of the UdK Berlin [48]. Sisal yarns of Nm 0.45 and 0.8 and partially bio-based resin (13% soybean oil and 12% bioethanol / Envirez 70302 co. Ashland) were used for the manufacture of the tubes of 20 mm diameter, 2 mm thickness and 5 m length. Figure 2-18 illustrates the impregnation of the sisal fibres on the resin bath, the heated die where the profiles are hardened and the bending tests of the tubes.

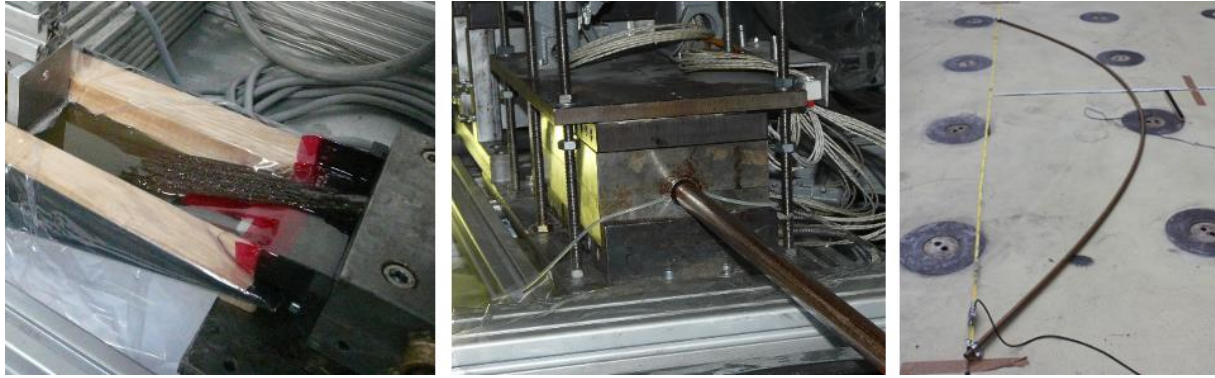


Figure 2-18: Impregnation of the sisal fibres in a resin bath at the left, hardening of the profiles in the heated die on the middle and bending tests of the tubes of 20mm diameter at the right

Some deficits could be observed in the pultruded NFRP tubes, mostly concerning the strong twisting of the natural fibres' yarn. Natural fibres need to be spun and twisted into yarns to be able to be used for pultrusion – which, additionally, should be also considered in the energy and economic cost of the final product. The compact twisting of the yarn does not allow the optimal wetting of the fibres, which results on resinous zones, consequent local reduction of fibre content and torsion on the pultruded profiles. This irregularity of the fibre distribution, together with the thermal deformations taking place during the hardening phase, can be reasons for the longitudinal flaws that appeared in some of the profiles. Despite of these imperfections, the NFRP tubes exhibited good bending properties: a bending stiffness and strength of **21.6 GPa** and **153 MPa** (corresponding to minimum radii of curvature of **89-141·z**).

Despite the numerous research studies about NFRP, their use in construction is practically inexistent. To be able to be used as structural elements, further analysis should be done concerning their long-term behaviour (creep), non-linear behaviour, fibre processing and fibre-matrix adhesion [47].

Carbon fibre-reinforced polymers - CFRP

Pultruded CFRPs are well-known because of their great strength and stiffness. In [49], the mechanical properties of carbon fibre reinforced epoxy bars and strips are given. With fibres volume contents between 50 and 65%, tensile strenghts of **2255 – 2800 MPa** and moduli of elasticity of **145 – 165 GPa** are reached; allowing radii of curvature of **58 – 64·z**, with z as half-height of the profiles' section. Nevertheless, due to their expensive production, their application on the civil engineering is generally limited.

Aluminium

Compared to other metals, aluminium posses a relative low modulus of elasticity (**70 GPa**) and density (**2700 kg/m³**). Depending on the alloy and sectional properties, strength values of about **120 – 280 MPa** and radii of curvature of **250 - 583·z** can be attained.

In Figure 2-19, two examples of gridshells made of continuous aluminium rods and some constructive details between superposed layers and at the edge beams, presented in [2], are

illustrated. The structure on the left consists in a 10 m x 10 m square grid performed by Seibu Construction Co., Tokyo, in cooperation with IL Stuttgart on 1973, while the structure on the right represents a 3.7 m high and 7.3 m wide grid designed by students of the Universidad La Salle, under the direction of Francisco Montero, in Mexico City on 1977.

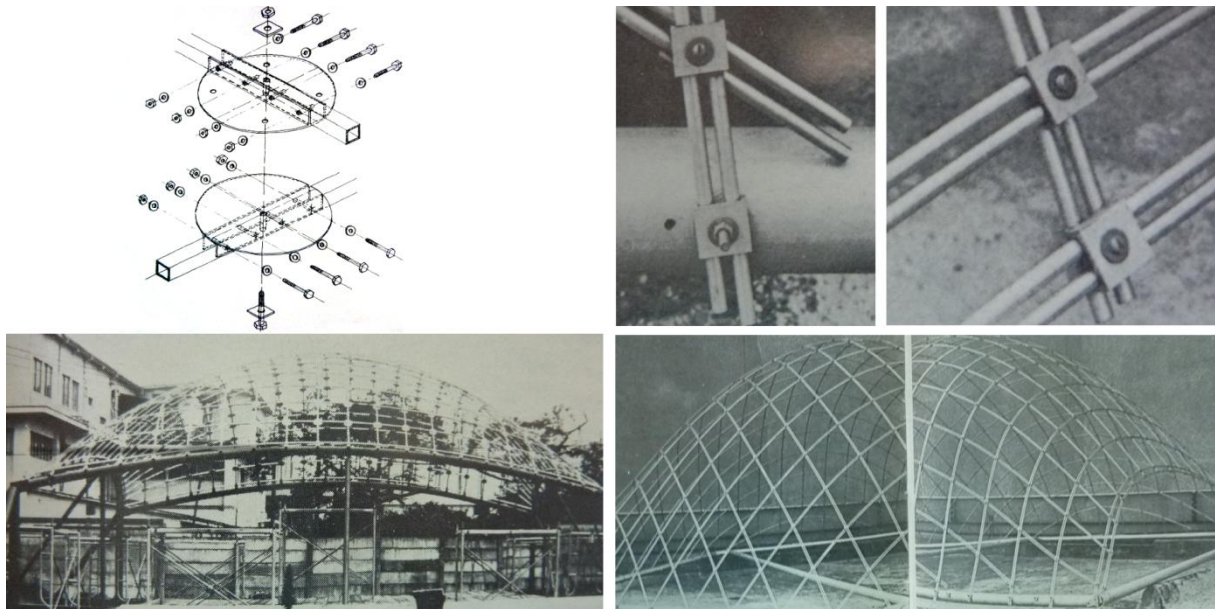


Figure 2-19: Examples of aluminium gridsbells built in Tokyo, Japan, on 1973 (left) and in Mexico City, Mexico, on 1977 (right) and corresponding constructive details

Another metal suitable for the construction of elastic gridshells is titanium. Depending on the alloy and sectional properties, a modulus of elasticity of about **110 GPa**, strength values of about **1000 – 2000 MPa** and with it radii of curvature of **55 - 110·z** can be attained. However, its cost-intensive production limits their application on the construction of elastic gridshells.

On Table 2-5, the mechanical properties - flexural strength, modulus of elasticity, allowable minimum radius of curvature in function of the sectional half-height z and specific strength - of the previous materials have been summarised.

Remarks on the table - Natural materials as timber or bamboo exhibit a wide range of values as they depend on numerous biological aspects. On the table, the characteristic strength values of timber, according to Eurocode 5 [32], and experimental values, obtained on the tests performed for the construction of the Multihalle gridshell [2], are given. Bamboo's properties depend on the plant nature, age, moisture content and cane diameter. Properties of laminated bamboo lumber, consisting of long bamboo strips cut in fibre's longitudinal direction and laminated in flat layers [34] are also included. Composites' strength and stiffness strongly vary, depending on the nature of the fibres and matrix, their percentage and cross-section. Also the mechanical properties of aluminium significantly depend on the alloy category and section thickness; values for extruded profiles, tubes, bars and drawn tubes of standard codes have been selected. Furthermore, it is important to note that the found values do not always refer to same strength levels: characteristic and ultimate strength values are defined for timber, yield strength for aluminium and ultimate strength for composites and bamboo.

		Charact. flexural strength [N/mm²]	Modulus of elasticity [N/mm²]	All. radius of curvature [m]	Density [kg/m³]	Strength to weight ratio [N.m/g]	
Timber	GL 24 [32]	24	11600	483*z	380	63	
	D 60 [32]	60	17000	283*z	700	86	
		Ultimate flexural strength [N/mm²]	Modulus of elasticity [N/mm²]	All. radius of curvature [m]	Density [kg/m³]	Strength to weight ratio [N.m/g]	
Timber	Hemlock (51% m.c.) [2]	49	8700	177*z	380	129	
	Hemlock (12.8% m.c.) [2]	83	10400	125*z	700	119	
Bamboo	Phyllostachys pubescens (1 year old) [33]	119	8680	72*z	330	362	
	Phyllostachys pubescens (3 years old) [33]	152	10122	66*z	610	249	
	Phyllostachys pubescens (5 years old) [33]	185	13410	72*z	660	280	
	Moso bamboo [34]	141	12115	85*z	600*	235	
	Laminated bamboo [34]	125	10899	87*z	600*	208	
Paper	Durolen paper / glue PVA (10.1% m.c.) - tubes [34]	15	1464	100*z	800*	18	
NFRP	Flax/PP 50/50 W% - rods [44]	101	14380	142*z	800	126	
	Flax/PP 50/50 W% - strip [45]	125	9000	72*z	1190	105	
	Hemp+wool/Polyurethane 30+5/65 W% - rods [46]	145	12250	84*z	996	146	
	Hemp+wool/Vinylester 30+5/65 W% - rods [46]	145	13000	89*z	1087	133	
	Hemp+wool/Polyester 30+5/65 W% - rods [46]	180	11500	63*z	1221	147	
	Flax / biobased polyester (65-75 V _f %) – strip [48]	153	14943	97*z	1320	116	
	Sisal / biobased polyester (65-75 V _f %) – strip [48]	132	11764	89*z	1260	104	
	Sisal / biobased polyester (68 V _f %) – tubes [48]	153	21600	141*z	1260	121	
	GFRP	Glass/PP 50/50 V% - strip [44]	335	28800	85*z	1480	226
		GRP (20-35 V _f %) Vinylester – sheet [49]	224	14000	62*z	1800	124
GRP (25-40 V _f %) Vinylester – shapes [49]		273	12500	45*z	1800	151	
GRP (50-60 V _f %) Vinylester – rods [49]		690	41000	59*z	2050	337	
		Ultimate tensile strength [N/mm²]	Modulus of elasticity [N/mm²]	All. radius of curvature [m]	Density [kg/m³]	Strength to weight ratio [N.m/g]	
CFRP	CRP (50-60 V _f %) Epoxy – bar [49]	2.255	145000	64*z	1600	1409	
	CRP (65 V _f %) Epoxy – strip [49]	2.800	165000	58*z	1600*	1750	
		Yield strength [N/mm²]	Modulus of elasticity [N/mm²]	All. radius of curvature [m]	Density [kg/m³]	Strength to weight ratio [N.m/g]	
Aluminium	EN AW-6060 - T5 - bars, tubes [50]	120	70000	583*z	2700	44	
	EN AW-7020 [50]	280	70000	250*z	2700	104	

m.c.= moisture content, V% = volume percentage, V_f% = volume percentage of fibre, W% = weight percentage, * = estimated

Table 2-5: Properties of materials suitable for elastic gridshells

Considering the allowable radii of curvature, fibre-reinforced composites - CFRP, GFRP and NFRP - and bamboo can reach the highest curvature values before exceeding the materials' strengths, followed by paper, timber and aluminium. According to their specific strength, CFRP exhibits by far the highest values, followed by bamboo and the composites GFRP and NFRP; less efficient are timber and aluminium followed by paper.

As mentioned in the previous chapters, not only the structural behaviour of the grid during the bending process but also under external loading is crucial for the design of the gridshells. Materials with high modulus of elasticity provide the structures with more out-of-plane stiffness, thus decreasing stability problems. On the following Figure 2-20, the previously presented materials have been arranged in the horizontal axis, according to their modulus of elasticity and, in the vertical axis, according to their allowable radius of curvature. One can observe that CFRP allow small radii of curvature while offering much higher stiffness values than the rest of materials. GFRP offer similar allowable curvature values than CFRP but lower stiffness. The next smallest radii of curvature belong to bamboo and NFRP, both owning lower stiffness than CFRP and GFRP. The modulus of elasticity of timber is comparable to NFRP and bamboo, but its allowable radius of curvature is higher. Finally, paper owns low radii of curvature but extreme low stiffness while aluminium exhibits high stiffness but higher allowable radii of curvature. On the left of the graphic, in order to visualise the values of the allowable radii of curvature, some elastica curves of a 10 m long profile with a 10 mm high cross-section have been illustrated and their corresponding minimum radii of curvature, on the middle of the profile, have been indicated.

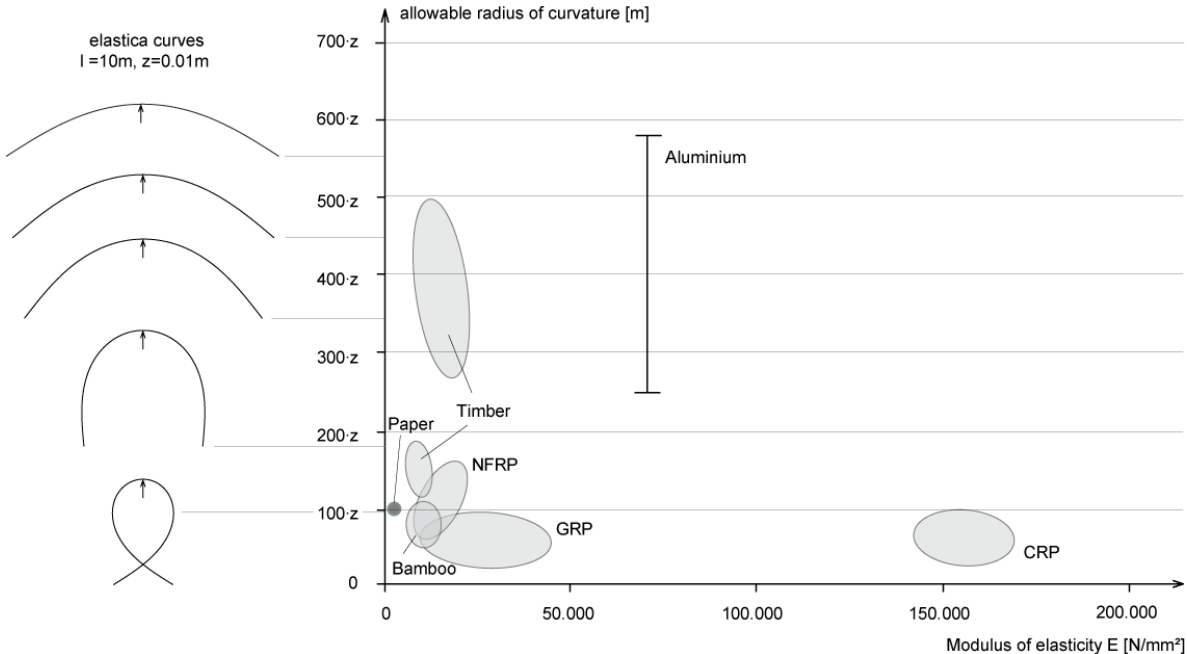


Figure 2-20: Distribution of materials, suitable for the construction of elastic gridshells, according to their modulus of elasticity and allowable radius of curvature

2.4 Summary

The aim of this chapter has been to present and discuss the main structural and constructive aspects to be considered on the design of elastic gridshells. Generally, the main motivation for using elastically-bent continuous profiles relies in the reduction of the number of connections and the consequent time and cost savings on the construction process: fewer elements have to be handled on site and fewer connections have to be assembled. Moreover, in the case of developable gridshells, the grid can be comfortably assembled on its flat position and bent afterwards as a whole. Nevertheless, the bending process induces important material stresses on the profiles, which are usually much higher than those resulting exclusively from live loads and which have to be taken into account when defining the gridshells' geometry and grid pattern.

Concerning the structural performance of the gridshells, three design criteria have been identified: gridshell's geometry, post-bending residual stress and gridshell's stiffness. Firstly, the gridshell's geometry should fulfil, besides the required building's function, specific surrounding conditions and aesthetic expectations. Moreover, the geometry, and specially the curvature, of the gridshell plays an important role on its structural performance and behaviour as shell structure. Different design approaches to determine grid patterns reproducing predefined surface geometries have been presented and classified according to the use or not of form-finding methods. The profiles reproducing the intended curved patterns are subjected to bending stresses which have to be compensated with appropriate material and sectional properties. At this point, by the choice of the profiles' properties, two contradictory constructive and structural aspects have to be respected: the stiffness of the grid should be low enough to be technically able to be bent and to prevent extreme shaping and support forces; at the same time, it should be high enough to provide the grid with enough out-of-plane stiffness and avoid stability problems. The final design results from an iterative process where the surface geometry and the grid's pattern and stiffness are modified and adapted until obtaining a structurally efficient and architecturally satisfactory gridshell.

The higher the post-bending residual stresses are, the lower the stress reserve for external loading will be. For this reason, materials with high limit strain are optimal for the construction of elastic gridshells: a low ratio of modulus of elasticity to strength allows high curvature on the profiles and provides them with more stress reserves after bending. In addition, materials with high moduli of elasticity can better supply the gridshell with the needed stiffness. Here, it is important to remark that the stiffness of the profiles do not only depend on the materials' mechanical properties but also on their manufacture possibilities and, with it, the cross-sectional properties of the profiles. The profiles properties of different built elastic gridshells have been compared in this chapter and it has been shown that, given a required out-of-plane stiffness of a gridshell, tubular sections and timber are respectively the most efficient in terms of material quantity and weight of the structure and that multi-layer sections and composite materials allow the highest stress reserves on the profiles after the shaping process. Moreover, the creep-relaxation behaviour of the materials is crucial to anticipate the long-term deflection of the gridshell and its actual stress reserve by the time live loads are applied. Recent creep tests, performed with glass fibre reinforced composites under bending loads, show that the creep factors of GFRP are lower than those of timber or NFRP.

The mechanical properties - flexural strength, modulus of elasticity, allowable minimum radius of curvature and specific strength - of materials suitable for elastic gridshells have been specified and compared. Considering the minimum radii of curvature and the modulus of elasticity of the materials, CFRP allow the smallest radii of curvature (together with GFRP) while offering much higher stiffness than the rest of materials. Nevertheless, due to their high production costs, the use of CFRP in construction engineering is relatively reduced. GFRP offer similar allowable curvature values than CFRP but relatively lower stiffness. The next smallest radii of curvature are provided by bamboo and NFRP, both owning lower stiffness values than CFRP and GFRP. The elasticity modulus of timber is comparable to that of NFRP and bamboo; however, their allowable radii of curvature are higher. At last, paper exhibits low radii of curvature but extreme low stiffness while aluminium exhibits high stiffness but higher allowable radii of curvature. Examples of their application on the construction of elastic gridshells have been presented and illustrated.

3. Grid Finding and Optimisation

3 Grid Finding and Optimisation

In order to diminish the residual stresses on elastic gridshells, induced during the erection process, profiles with low sections and materials with low modulus of elasticity are usually chosen. However, this leads to a reduction of the global stiffness of the gridshell which can result in stability problems. With an optimisation of the grid pattern - orientation and arrangement of the grid profiles - a minimisation of the profiles' curvature can be obtained as well as the load-bearing capacity of the gridshells improved [6].

In this chapter an optimisation method based on variational principles for regular and irregular gridshells is proposed. The aim of using variational principles is to establish *extremal* functions which minimize the value of quantities related to particular grid properties. These properties are: the curvature of the profiles, the distance to a reference surface geometry and the deviation of the edge lengths from a desired mesh size. The advantage of this optimisation method is that weighting factors can be applied to the grid properties to be minimised, so that a variety of grid configurations can be established responding to different specific structural and constructive requirements [11][12]. Different case studies of double-curved gridshells show the advantages and capacity of this method in the following chapters.

3.1 Methodology

3.1.1 Discrete differential geometry

In architecture, especially in the design of surface structures, the use of geometric and mathematical concepts to solve constructive and structural problems has been increasing in the last decade. For the discretisation of predefined smooth surfaces, a great variety of approaches can be developed with *discrete differential geometry* by using fundamental discretisation principles and applying them to particular constraint conditions [51]. The parameterisation of these discrete surfaces is the base for the generation of optimised meshes according to selected properties by means of variational principles. A selection of existing applications of variational principles in architecture has been recently done by Sechelmann et al. in [52]: a well-known application example is to be found on the determination of grids which are composed of planar or single curved panels [53][54].

In our case, the mesh optimisation focuses on three structural and constructive aspects: angle between consecutive edges, edges' length and distance to a predefined surface - corresponding respectively to the profiles' curvature, mesh size and distance to a reference surface geometry. These three parameters are expressed in form of functions or *sub-energies*, which are affected by weighting factors and linearly added as global energy. It is the minimiser of this global energy that provides the resulting optimised grid configuration. The modular software for discrete surfaces VaryLab, developed by the team of DFG SFB/TR 109 Discretization in Geometry and Dynamics with Thilo Rörig and Stefan Sechelmann [55], allowed the implementation of the

proposed approach. In the next sections, the steps of the optimisation methodology are introduced.

3.1.2 Initialisation

The global energy to be minimised with the variational principles is in general non-convex: many local optima solutions are possible, which are strongly influenced by the initialisation mesh. In the proposed approach, the initialisation mesh consists in a conformal mesh, generated with the conformal mapping technique presented by Springborn et al. in [56]. The reason for using conformal meshes resides in their property of owning almost constant angle between edges, so that kink points are usually avoided and homogeneous curvature distributions are generally provided. Further research could focus on the use of alternative mapping techniques, e.g. the Wire Mesh Design approach with which regular meshes can be obtained.

Let us consider the example of an anticlastic surface, with parallel longitudinal and transverse edges, to describe the definition process of the reference surface and initialisation mesh. The **target surface** is 5 and 7.5 m high, 14 and 15 m wide and 30 m long and the desired mesh size is 1 m. First of all, the target surface is modelled as NURBS-surface with the 3D-modeling software Rhinoceros, then enlarged at its four edges by about 5 m and finally converted into a polyhedral mesh. This enlarged polyhedral mesh is going to be used as **reference surface** during the optimisation in VaryLab and as input surface to generate the **initialisation mesh**. In order to obtain an optimised mesh that completely covers the planned gridshell's surface, it is important to define an enough wide initialisation mesh which, after optimisation and relocation of its vertices, still encloses the whole target surface. The reference surface should as well enclose the initialisation mesh, so that the distance between mesh and reference surface can be controlled at each mesh vertex. Figure 3-1 illustrates the target anticlastic surface as NURBS and the corresponding enlarged reference surface as NURBS and as polyhedral mesh, modelled in Rhino.

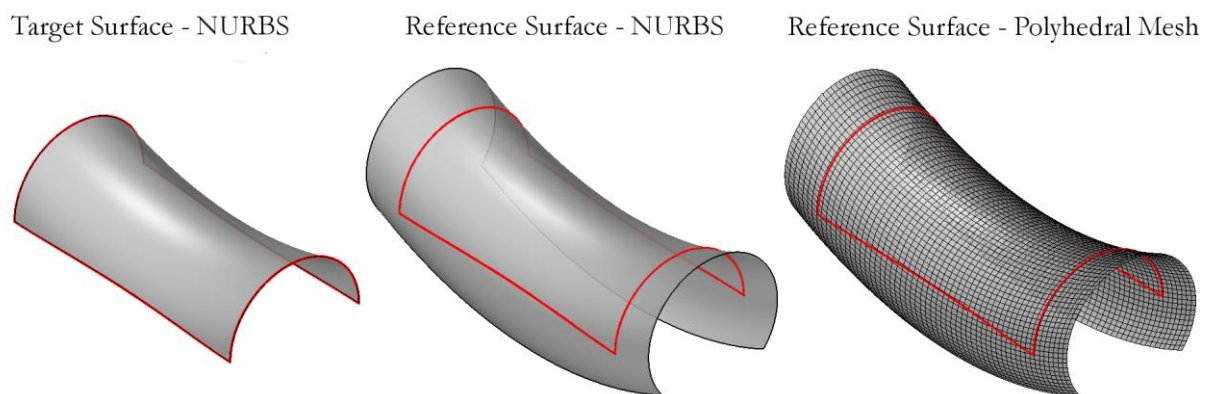


Figure 3-1: Modelling of target surface as NURBS (left), enlarged reference surface as NURBS (middle) and as polyhedral mesh (right) in Rhino

Once the enlarged polyhedral mesh has been defined in Rhino, it is imported twice in VaryLab: once as reference surface and once to be remeshed as initialisation mesh. Afterwards, the second mesh is conformally parameterised and converted to a new mesh, with almost constant angles

between edges. The mesh density (mesh size) and orientation as well as the angle between the mesh edges (shear angle) of the new conformal mesh can be controlled and selected. By remeshing the initial polyhedral mesh, some triangles and pentagons are generated at the mesh borders. These have to be deleted, so that the initialisation mesh only contains quadrangles. In Figure 3-2, the conformally parameterised initialisation mesh is shown, before and after removing the border triangles and pentagons.

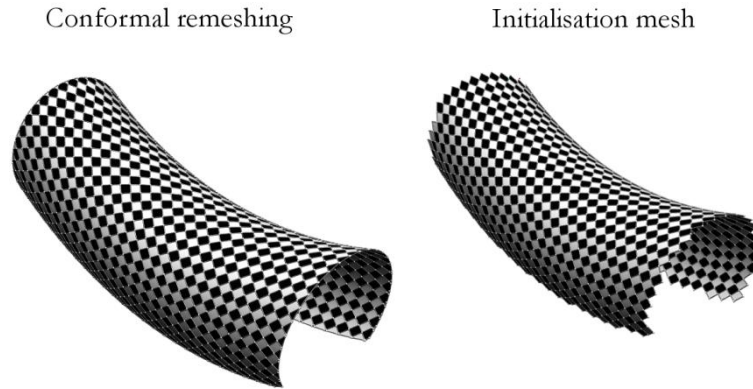


Figure 3-2: Conformal initialisation mesh before and after removing border triangles and pentagons in VaryLab

To accelerate the optimisation process, it is important to choose start values of the mesh density and shear angle that approximate the desired ones. Figure 3-3 illustrates three different conformal meshes for the anticlastic surface, with varying shear angle.

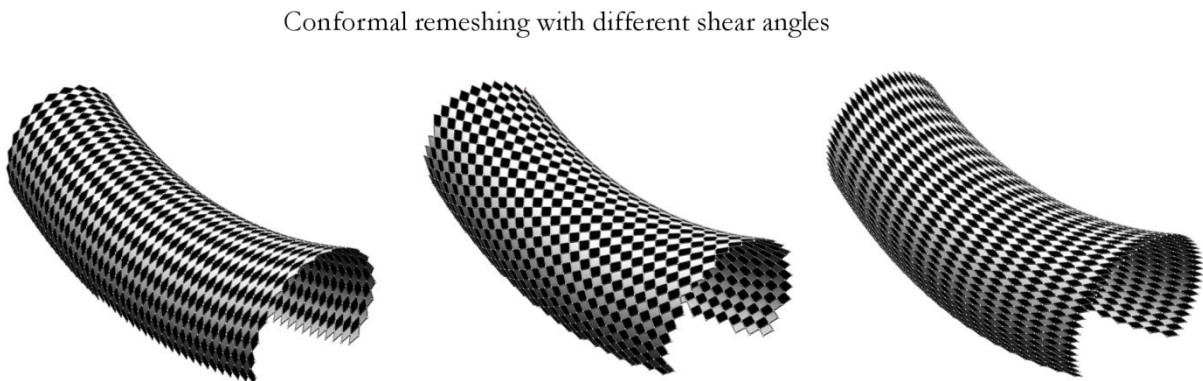


Figure 3-3: Initialisation meshes of anticlastic surface with varying shear angle

3.1.3 Optimisation with variational principles

The optimisation of the initialisation mesh is performed by defining a global energy E (3-1), as the linear combination of three sub-energies - E_{ref} , E_{len} and E_{cur} - related to the three optimisation parameters - distance to a reference surface, edges' length and angle between consecutive edges - and searching its minimisers.

$$E = \lambda_1 E_{ref} + \lambda_2 E_{len} + \lambda_3 E_{cur} \quad (3-1)$$

The three sub-energies are influenced by weighting factors λ_i and are defined as penalising energies: the difference between actual and desired values is considered.

E_{ref} - Reference surface energy

Being $M = (V, E, F)$ a quadrilateral mesh, whose vertices are denoted by $v_i \in V$, edges by $e_{ij} \in E$ and quadrilaterals by $f_{ijkl} \in F$, the first energy E_{ref} (3-2) considers the distance between the mesh to be optimised and a given reference surface. As reference surface, a polyhedral mesh created for example using 3D-modelling softwares can be used.

$$E_{ref}(M) = \sum_{v_i \in V} \langle v_i - cp_i, v_i - cp_i \rangle \quad (3-2)$$

The distance to the reference surface is calculated between the mesh vertices v_i and their respective closest points cp_i on the reference surface. To rapidly find the closest point cp_i on the reference surface of a mesh vertex v_i , a *k-d-tree* is used: a space-partitioning data structure which allows the preselection of points on the reference surface that are located in the vicinity of the vertex v_i . Then, the triangular mesh faces adjacent to the preselected points are chosen to calculate the distance between them and the considered vertex through projection, as illustrated in Figure 3-4. The minimum distance is then taken to determine the reference surface energy.

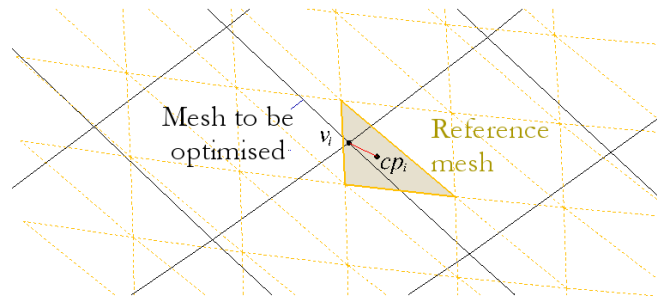


Figure 3-4: Distance between the mesh to be optimised and the reference mesh, calculated as the projection of the vertex v_i to the nearest mesh face

E_{len} - Edge length energy

The second energy E_{len} is used to obtain a predefined mesh size or edge length. The meshes can be optimised as regular and irregular grids - with constant or variable edge length -, depending on the selected energy definition. The energy E_{len} can be calculated as the difference between the edge lengths and a target value expressed as a constant length L (3-3), an average length L_{aver} (3-4) or a range of length values between L_{min} and L_{max} (3-5).

$$E_{len}(M) = \sum_{e_{ij} \in E} (\|v_i - v_j\| - L)^2 \quad (3-3)$$

$$E_{len}(M) = \sum_{e_{ij} \in E} (\|v_i - v_j\| - L_{aver})^2 \quad \text{with } L_{aver} = \frac{\sum_{e_{ij} \in E} \|v_i - v_j\|}{n_{Edges}} \quad (3-4)$$

$$E_{len}(M) = \sum_{e_{ij} \in E_{min}} (\|v_i - v_j\| - L_{min})^2 + \sum_{e_{ij} \in E_{max}} (\|v_i - v_j\| - L_{max})^2 \quad (3-5)$$

where E_{min} and E_{max} represent,

$$E_{min} = \{e_{ij} \in E \mid \|v_i - v_j\| < L_{min}\} \quad (3-6)$$

$$E_{max} = \{e_{ij} \in E \mid \|v_i - v_j\| > L_{max}\} \quad (3-7)$$

and,

$$E_{in} = \{e_{ij} \in E \mid L_{min} < \|v_i - v_j\| < L_{max}\} \quad (3-8)$$

$$E = E_{min} \cup E_{in} \cup E_{max} \quad (3-9)$$

The edge length $\|v_i - v_j\|$ is defined as the magnitude of the vector pointing from the vertex v_i to its adjacent v_j . Figure 3-5 illustrates two adjacent vertices and the corresponding vector e_{ij} .

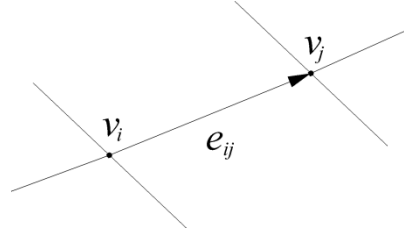


Figure 3-5: Edge length defined as the magnitude of the vector e_{ij}

E_{cur} and E_{CirCur} – Curvature energies

The third energy has the aim to optimise the curvature of the grid profiles. In this thesis, two notions of curvature have been considered: the *opposite edges curvature* E_{cur} and the *circumcircle curvature* E_{CirCur} . Given a vertex v_i and its adjacent vertices v_1, v_2, v_3 and v_4 , the energy of the opposite edges curvature E_{cur} is calculated from the deviation of the angles spanned by opposite edges $\angle(e_{ij}, e_{ik})$ from the straight angle π (3-10):

$$E_{cur}(M) = \sum_{v_i \in V} (\pi - \angle(e_{i1}, e_{i3}))^2 + (\pi - \angle(e_{i2}, e_{i4}))^2 \quad (3-10)$$

The edges e_{ij} represent vectors pointing from the vertex v_i to the adjacent vertices v_{1-4} . In Figure 3-6 the edges $e_{i1} - e_{i3}$ and $e_{i2} - e_{i4}$ and the angles spanned between them are illustrated:

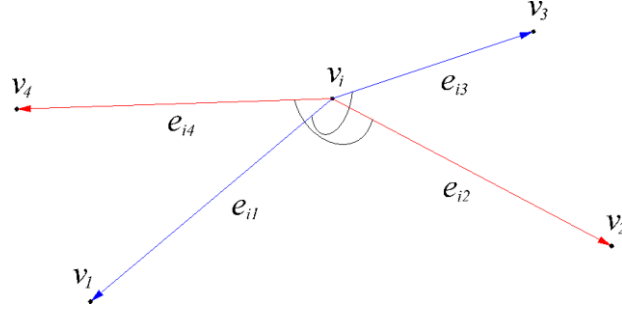


Figure 3-6: Angle spanned by opposite edges $e_{i1} - e_{i3}$ and $e_{i2} - e_{i4}$

This notion of curvature allows efficient and rapid calculation. Nevertheless, when applied to grids with variable edge length, this definition can supply inaccurate values. Indeed, by calculating the angle between opposite edges, the edges' length - straight distance between two adjacent vertices - is considered and the actual curvature of the profiles passing through these adjacent vertices is neglected, which becomes important by irregular meshes. The higher the variation on the edges' length is, the higher the actual curvature of the profiles comprised into these edges can vary. In this case, more reliable values are provided with the definition of the circle passing through three consecutive vertices, given that the arch approximates more to the resulting profiles' curvature. This circle definition, which has been previously used in approaches proposed by Adriaenssens et al. in [57] and Douthe et al. in [58], has been considered for the calculation of the circumcircle curvature energy E_{CirCur} and employed for the optimisation of irregular grids. The considered curvature corresponds to the inverse of the radius of the arch defined by three consecutive vertices and can be described as a function of the sinus of the angle between opposite edges ($\sin \alpha_{13}$ and $\sin \alpha_{24}$) and the distance between the opposite vertices (magnitude of e_{13} and e_{24}):

$$E_{CirCur}(M) = \sum_{v_i \in V} \kappa_{13}^2 + \kappa_{24}^2 = \sum_{v_i \in V} \left(\left(\frac{2 \cdot \sin \alpha_{13}}{\|e_{13}\|} \right)^2 + \left(\frac{2 \cdot \sin \alpha_{24}}{\|e_{24}\|} \right)^2 \right) \quad (3-11)$$

Figure 3-7 compares both definitions. On the left, two edges with variable length (e_{i1} and e_{i3}) and the circle passing through their vertices have been illustrated. On the right, the opposite edges and circumcircle curvatures by meshes with equal (e_{i1} and e_{i3}) and variable (e_{i1} and e_{i3}) edge length are compared. According to the definition of the opposite edges curvature, the profiles comprising the vertices $v_1 - v_i - v_3$ and $v_1 - v_i - v_3$ own the same curvature in v_i , as the angle between opposite edges is the same. In contrast, according to the circumcircle definition, the curvature of the profile comprising $v_1 - v_i - v_3$ is lower than that of the profile comprising $v_1 - v_i - v_3$, as the radius of the circle passing through the first vertices r_1 is higher than that of the circle passing through the second vertices r_2 .

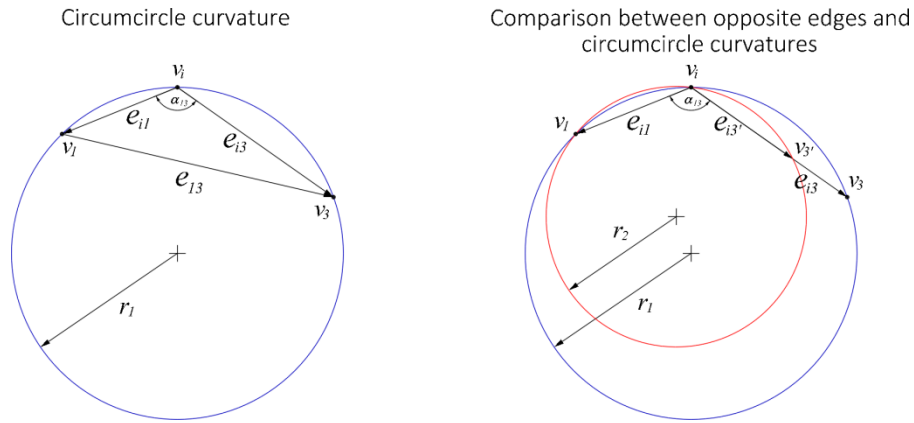


Figure 3-7: Arch passing through three consecutive vertices, considered on the definition of circumcircle curvature (left); Difference between opposite edges and circumcircle curvature, when considering regular and irregular meshes (right)

The following Figure 3-8 compares the curvature distributions according to the opposite edges (left) and the circumcircle curvatures (right) of a calotte gridshell, which has been optimised as irregular mesh in VaryLab. The optimisation according to the opposite edges energy shows maximum curvature values (red nodes) at the crown of the calotte, while the optimisation according to the circumcircle curvature exhibits maximum values on the base of the calotte, at the two sides with smaller edge lengths.

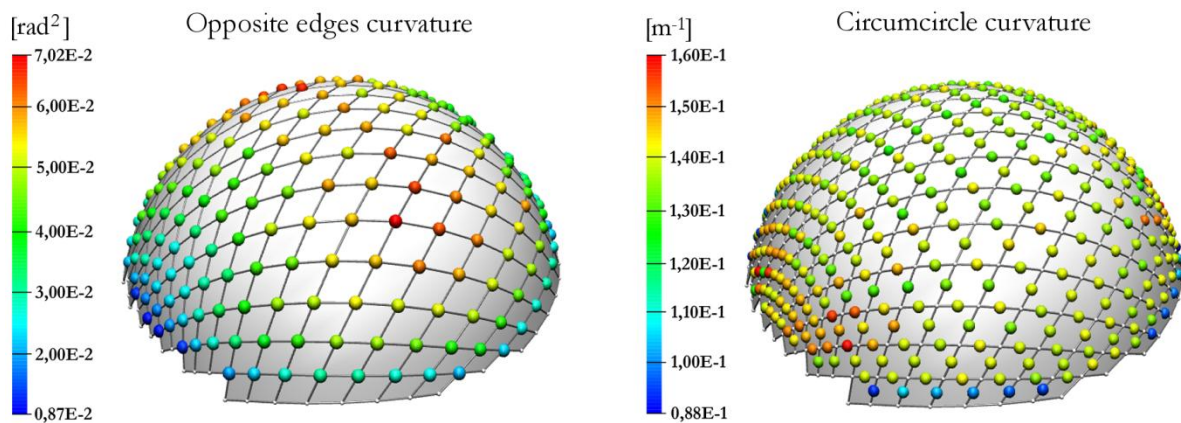


Figure 3-8: Comparison of curvature energies of an irregular calotte gridshell, optimised according to the opposite edges (left) and circumcircle curvatures (right)

3.1.4 Implementation

The software VaryLab uses the non-linear optimization package PETSc/TAO [59][60] and its java binding [61] to minimise iteratively the global energy E . Before optimisation, the energies can be normalised to have gradient length one, which usually supplies more efficient results. The weighting factors of the three penalising sub-energies are defined according to the existing structural, constructive and architectural requirements: allowed profiles' curvature, regular or irregular grid configuration or predefined target geometries.

Each iteration of the optimisation provides a new grid configuration. The values of the weighting factors can be maintained or modified depending on the resulting solutions. When, with a further iteration, a new configuration cannot be calculated or the properties of the mesh cannot be further optimised, one can try to deactivate one of the energies (not consider it on the calculation) or change drastically the values of its weighting factors for a few iterations. In order to obtain a good minimiser, different combinations of weighting factors and different initial meshes with varying shear angle should be explored. The energy minimisation can be solved with diverse numerical methods; in the following application examples, the conjugate gradient method was used. The iterative calculation ends when the predefined requirements are fulfilled.

On the following Table 3-1, an optimisation example using the anticlastic gridshell, presented at the beginning of the chapter, is shown. The values of the weighting factors and those of the distance to the reference surface and opposite edges curvature are given for each iteration. The edge length of the initialisation mesh varies from 0.927 to 1.098 m. The first optimisation requirements are: a maximum distance to the target surface of 0.2% of the span length (0.025 m, about 0.130 m to the enlarged reference surface), a constant edge length of 1 m (with $\pm 1\%$ tolerance) and an optimal reduction of the edges curvature. Once the optimised grid fulfils these requirements, a further optimisation is done by allowing a higher distance to the reference surface (0.20 m to the target surface, about 0.40 m to the enlarged reference surface). The resulting circumcircle profiles' curvature and the distance from the optimised mesh to the target geometry have been determined, using scripts, with the 3D-modeling software Rhino.

Iter. no.	λ_{ref}	λ_{len}	λ_{cur}	Min / Mean / Max		
				Distance to reference surface [m]	Edge length [m]	Opposite edges curvature [rad ²]
Initialisation				0.000/0.010/0.117	0.927/1.007/1.098	0.04E-2/0.87E-2/2.17E-2
<i>Requirements</i>				Max Distance < 0.13 m, Edge length tolerance ± 0.01 m		
1	2	4	4	0.000/0.007/0.094	0.932/0.994/1.108	0.30E-2/0.76E-2/2.29E-2
2	2	4	4	0.000/0.010/0.156	0.964/0.990/1.020	0.18E-2/0.72E-2/1.36E-2
3	2	4	4	0.000/0.018/0.140	0.967/0.991/1.015	0.10E-2/0.70E-2/1.28E-2
4	2	4	4	0.000/0.019/0.132	0.992/0.998/1.008	0.09E-2/0.70E-2/1.02E-2
<i>Observation</i>				Edge Length tolerance achieved		
5	2	4	6	0.000/0.029/0.166	0.991/0.998/1.009	0.09E-2/0.67E-2/1.03E-2
6	2	6	6	0.000/0.048/0.211	0.994/1.001/1.010	0.07E-2/0.60E-2/0.99E-2
<i>Observation</i>				Distance to surface should be reduced		
7	6	6	6	0.000/0.021/0.171	0.993/0.999/1.011	0.08E-2/0.62E-2/0.93E-2
8	6	6	6	0.000/0.016/0.135	0.994/0.999/1.012	0.09E-2/0.63E-2/1.00E-2
9	6	6	2	0.000/0.011/0.125	0.993/0.999/1.009	0.14E-2/0.65E-2/1.05E-2
<i>Observation</i>				Requirements fulfilled, curvature optimised		
				Allowing more distance to reference surface:		
<i>Requirements</i>				Max Distance < 0.40 m, Edge length tolerance ± 0.01 m		
10	2	10	16	0.000/0.030/0.169	0.997/0.999/1.004	0.10E-2/0.59E-2/0.86E-2
11	2	10	16	0.000/0.058/0.314	0.996/0.999/1.006	0.06E-2/0.54E-2/0.83E-2
12	2	6	16	0.000/0.106/0.553	0.992/0.999/1.010	0.05E-2/0.47E-2/1.02E-2
13	2	10	6	0.000/0.060/0.341	0.993/0.999/1.007	0.06E-2/0.50E-2/0.79E-2
<i>Observation</i>				Requirements fulfilled, curvature optimised		

Table 3-1: Example of optimisation steps for an anticlastic surface

After each iteration, the values of the weighting factors have been modified according to the evolution of the mesh's parameters: e.g. at the 5th iteration, the factor for the curvature energy has been increased, from 4 to 6, to obtain a stronger reduction of the curvature values or, at the 7th and 8th iterations, the factor of the distance to reference surface, from 2 to 6, to approach the mesh to the target surface. After 9 iterations, a grid configuration that fulfils the predefined requirements and with an optimised curvature has been attained. The maximum circumcircle profiles' curvature of the optimised mesh, calculated in Rhino, corresponds to 0.073 m⁻¹, approximately 71% of the initial maximum circumcircle curvature. On the next steps of the optimisation, the higher distance to the target surface is allowed: 0.20 m (about 0.40 m to the enlarged reference surface). After 4 additional iterations, a grid configuration that fulfils the second requirements and with a maximum circumcircle curvature of 0.064 m⁻¹ (about 62% of the initial maximum circumcircle curvature) is achieved. Each iteration takes approximately 1 minute. The mesh could be further optimised in terms of curvature by exploring other combinations of weighting factors. Nevertheless, it is important by the optimisation to always control that other relevant constructive and structural needs are satisfied.

The next chapters present examples of optimisations using variational principles for gridshells with anticlastic, synclastic and a combination of anticlastic and synclastic surfaces, for regular and irregular grid configurations.

3.2 Optimisation Examples of Regular Grids

In *discrete differential geometry* a mesh with constant edge length is called a discrete Chebyshev net. Thus, the optimisation of regular elastic gridshells implies the determination of discrete Chebyshev meshes with minimised curvature between opposite edges and close to a given reference surface [11]. In the optimised examples, the opposite edges curvature energy E_{cur} has been considered and initialisation meshes with a shear angle of 90° have been used. The length energy has been applied as constant value of 1 m ± 1% tolerance. Furthermore, the distance between optimised mesh and target surface cannot exceed 1/500 of the span length.

Three double-curved target surfaces have been optimised:

- an anticlastic surface between 5 and 7.5 m high, 14 and 15 m wide and 30 m long;
- a synclastic surface between 7.5 and 10 m high, 14 and 15 m wide and 30 m long;
- a surface with anticlastic and synclastic curvature, analogue to the Downland Museum gridshell in Sussex, Great Britain (2002), between 7.35 and 9.50 m high, 12.5 and 16 m wide and 50 m long.

The resulting circumcircle curvatures of the profiles of the optimised meshes have been calculated in Rhino and compared to those of meshes obtained using the classic compass method with an angle between guide curves of 90° [8].

3.2.1 Reference surface as geometric constraint

In the following examples, the distance between the optimised mesh and the target surface cannot exceed 1/500 of the span length of the structure: about 0.03 m. The curvature distributions, calculated with the variational method in terms of E_{cur} , have been illustrated in the next figures through coloured points. The maximum and minimum curvatures correspond to red and blue, respectively. The colour scales of the compass and variational method are the same for an easier comparison. The size of the points is also proportional to the curvature values. During optimisation, the weighting λ -factors of the sub-energies in (3-1) were modified and adapted, taking values between 2 and 10 for the reference surface energy, between 4 and 20 for the edge length energy and between 4 and 10 for the curvature energy.

On the left of Figure 3-9, one can observe that, by the anticlastic surface, the mesh obtained with the compass method (red) mostly differs from the mesh optimised with variational principles (blue) at the corners, at the intersection between longitudinal and transverse edges. Also here, the highest curvature values (red/yellow) of both meshes are to be found. The variational principles provide a grid pattern with a more homogeneous curvature distribution and reduced maximum and mean curvature values: respectively, 87% (0.082 m^{-1}) and 92% (0.060 m^{-1}) of those obtained with the compass method (0.094 and 0.065 m^{-1}).

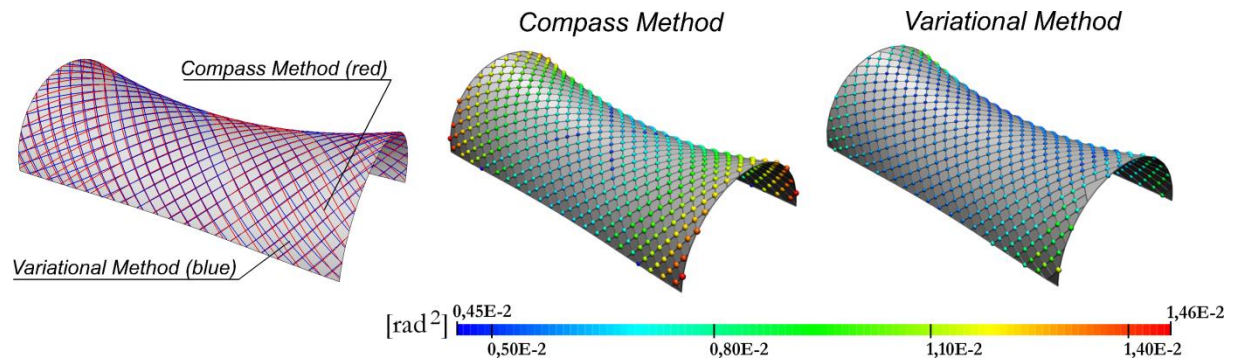


Figure 3-9: Comparison between grid patterns obtained with the compass and variational methods and their opposite edges curvature distributions for an anticlastic surface

On the case of the synclastic surface, Figure 3-10 shows that the pattern obtained with the variational method (blue) is slightly more stretched in longitudinal direction than that resulting from the compass method (red). The grid pattern determined with the compass method presents higher curvature values at the corners of the surface and on its crown. The variational method provides a grid configuration with lower curvature values on the top and higher in the middle of the longitudinal edges of the surface: the maximum and mean values could be reduced to 88% (from 0.106 m^{-1} to 0.093 m^{-1}) and 97% (from 0.073 m^{-1} to 0.071 m^{-1}), respectively.

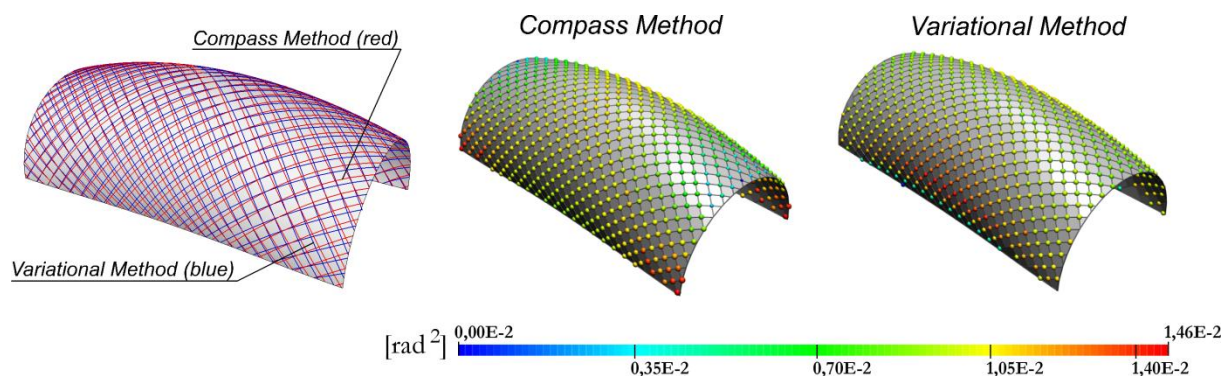


Figure 3-10: Comparison between grid patterns obtained with the compass and variational methods and their opposite edges curvature distributions for a synclastic surface

On the case of the surface with anticlastic and synclastic curvature, Figure 3-11 shows that differences between the resulting patterns increase when approaching from the middle to the transversal edges of the surface. In both methods, higher curvature values are to be found on the crowns and lower curvature values on the valleys. In the pattern resulting from the variational method, extreme curvature values are less concentrated than in the pattern determined with the compass method. The maximum and mean curvature values could be respectively minimised to 88% (from 0.160 m^{-1} to 0.140 m^{-1}) and 93% (from 0.074 m^{-1} to 0.069 m^{-1}).

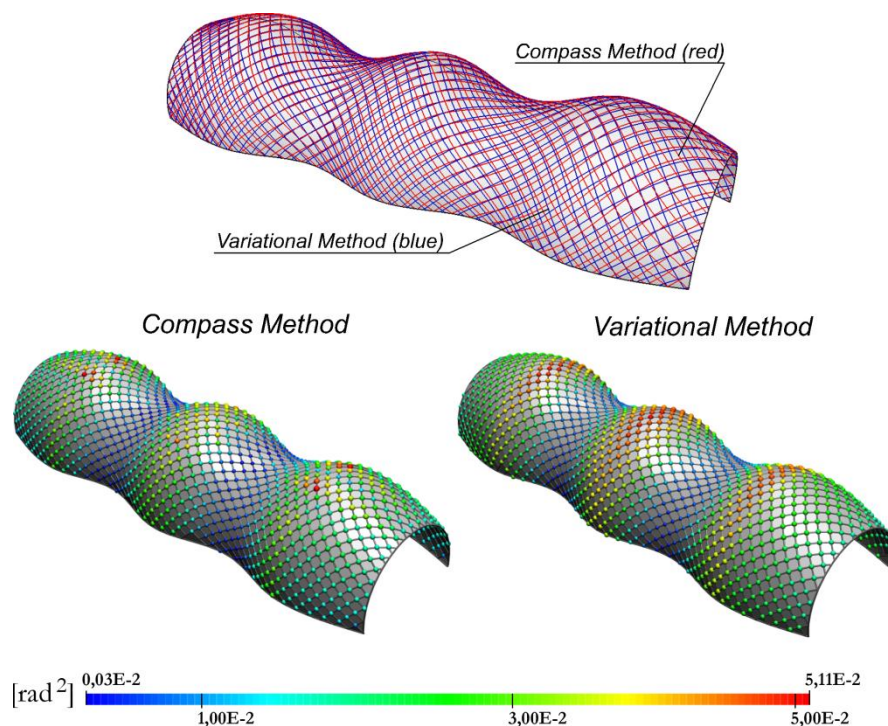


Figure 3-11: Comparison between grid patterns obtained with the compass and variational methods and their opposite edges curvature distributions for a surface with combined anticlastic and synclastic curvatures

3.2.2 Influence of initialisation mesh

The influence of the shear angle of the initialisation mesh on the optimised curvature has been tested on a 5 m high section of a sphere of 15 m diameter. The calotte has been chosen to avoid the singularity points that are characteristic of optimised spherical meshes. Three initial conformal meshes with shear angles of 45°, 67.5° and 90° have been chosen. In the optimisation, the opposite edges curvature energy E_{cur} has been considered and the length energy has been applied as constant value of 1 m. The distance between optimised meshes and target surface does not exceed 1/500 of the span length. The weighting λ -factors of the sub-energies in (3-1) take values between 0 and 12 for the reference surface energy, between 2 and 10 for the edge length energy and between 2 and 4 for the curvature energy.

The maximum and mean resulting circumcircle curvature values are resumed in the following Table 3-2. The optimisation with the initialisation shear angle of 45° provides the lowest curvature values, followed by those obtained with the shear angle of 67.5°. The highest curvature values are obtained with the 90° angle.

Curvature [m^{-1}]	45°	67.5°	90°
Maximum	0.159	0.197	0.215
Mean	0.141	0.150	0.151

Table 3-2: Comparison of maximum and mean circumcircle curvature values, resulting from optimisations with initialisation meshes with varying shear angles - 45°, 67.5°, 90° - for a calotte surface

Figure 3-12 illustrates the distribution of the opposite edges curvature for the three optimised meshes. The maximum and minimum curvature values correspond respectively to red and blue; the colour scales are equivalent. One can observe that the three meshes exhibit higher curvatures at their base, concentrated in two (by the 45° and 67.5° meshes) or four (by the 90° mesh) opposite sides.

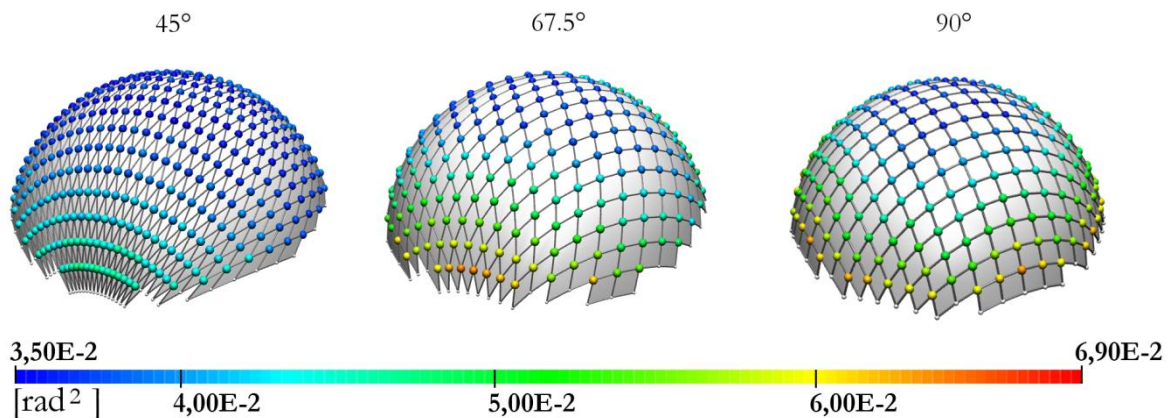


Figure 3-12: Comparison of opposite edges curvature distributions, resulting from optimisations with initialisation meshes with varying shear angles (45°, 67.5°, 90°) for a calotte surface

3.2.3 Further optimisation by allowing distance to reference surface

A further optimisation can be achieved by tolerating a higher distance to the reference surface. In this section, the three previous double-curved surfaces have been further optimised reducing the weighting factor λ_{ref} of the reference surface energy, by allowing a maximum distance between optimised mesh and target surface of 0.60 m, in order to achieve a higher reduction of the profiles' curvature. The range of values for the weighting factors goes from 2 to 3 for the reference surface energy, 4 to 12 for the edge length energy and 4 to 16 for the curvature energy.

Generally, when allowing more distance to the reference surface, the optimised grids mostly deform there, where the highest curvature values exist. On the case of the anticlastic surface, the corners of the longitudinal edges move outwards, reducing here the maximum curvature values to 45% - from 0.094 m^{-1} to 0.042 m^{-1} - and obtaining a more homogeneous curvature distribution, compared to the mesh resulting from the compass method. The mean curvature could be reduced to 51% - from 0.065 m^{-1} to 0.033 m^{-1} . By the synclastic surface, the mesh tends to distort outwards on the middle of the longitudinal edges and slightly upwards on the crown. The maximum and mean curvature values could be reduced to 79% - from 0.106 m^{-1} to 0.084 m^{-1} - and 78% - from 0.073 m^{-1} to 0.057 m^{-1} , respectively. By the gridshell with anticlastic and synclastic curvatures, the crowns deform inwards and the valleys outwards. The maximum and mean curvatures values could be reduced to 76% - from 0.160 m^{-1} to 0.122 m^{-1} - and 64% - from 0.074 m^{-1} to 0.047 m^{-1} , respectively. In Figure 3-13, the optimised meshes of the three double-curved surfaces and their respective target surfaces have been illustrated.

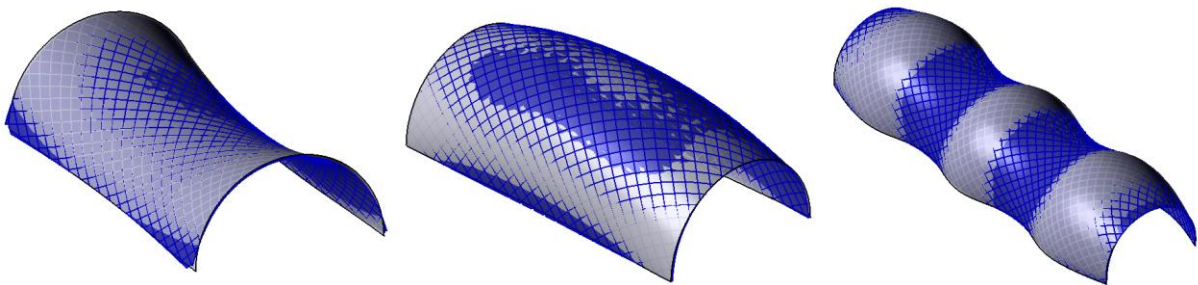


Figure 3-13: Geometry of optimised meshes (blue) by allowing a distance up to 0.60m to the target surface (grey)

The diagrams on Figure 3-14 outlines the optimisation results achieved with the variational method in comparison to the compass method for the three double-curved surfaces. The maximum and mean curvature values are given. The colour of the bars represents the maximum distance between mesh and target surface. On the mesh with synclastic curvature and the one combining synclastic and anticlastic curvatures, the mean values could be more strongly reduced than the maximum ones. That is mainly due to the applied minimisation of the curvature energy E_{cur} , which affects the sum and not directly the maximum curvature values.

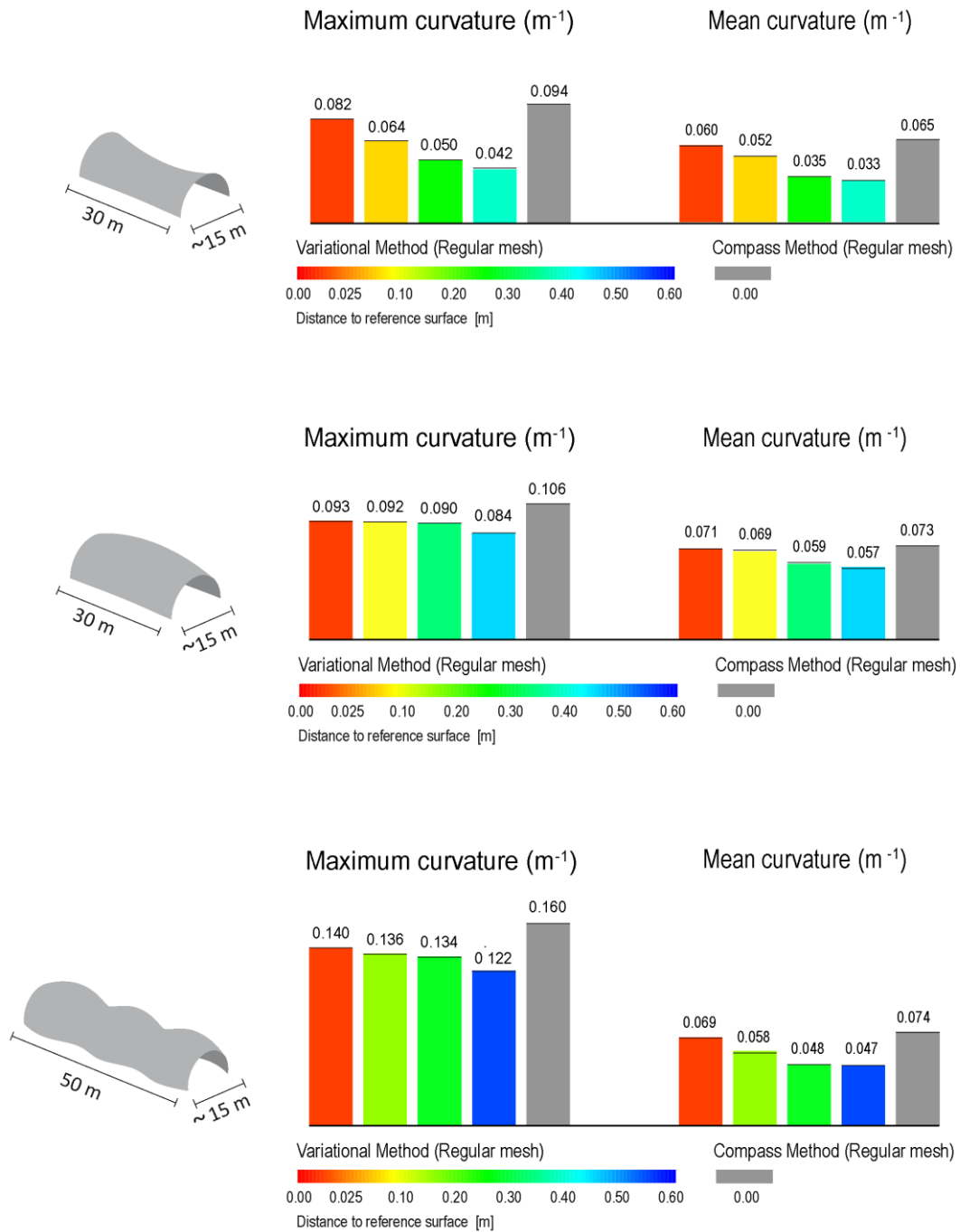


Figure 3-14: Comparison of the maximum and mean circumcircle curvature values for three double-curved grids, optimised as regular meshes, obtained with the variational (coloured) and compass (grey) methods

3.3 Optimisation examples of irregular grids

A further optimisation can also be achieved by allowing the edge lengths to vary (*irregular grids*), reducing thus locally and globally the curvature of the profiles. For the optimisation of irregular grids the circumcircle curvature energy E_{CirCur} has been considered. On the following sections, a calotte and the three double-curved surfaces, which have been optimised as regular grids in the

precedent chapter, have been optimised allowing variation on the mesh size between 0.5 m and 1.5 m. By the edge length energy E_{len} , two length definitions have been considered: the average value L_{aver} of 1 m and the range values 0.5 and 1.5 m for L_{min} and L_{max} . The distance between optimised mesh and target surface cannot exceed 1/500 of the span length. The resulting curvature values of the regular and irregular configurations have been compared.

3.3.1 Reference surface as geometric constraint

The objective of the following optimisations is to obtain meshes with lower curvature values than the optimised regular meshes, by allowing variation of the edge length but remaining as near as possible to the reference surface. Firstly, the calotte surface, which has been optimised as regular mesh with an initialisation angle of 67.5° in Figure 3-12, has been considered. The weighting λ -factors of the sub-energies in (3-1) took values between 0 and 8 for the reference surface energy, between 1 and 8 for the edge length energy and between 3 and 4 for the curvature energy.

Figure 3-15 compares the grid patterns, edges' length and circumcircle curvature values of the optimised regular and irregular calottes. On the case of the regular configuration, due to the characteristic polar singularities of spherical surfaces, higher local concentrations of curvature can be observed at the base of the mesh, at the two opposite singularity points and in their vicinity. By letting the mesh size vary, the edge lengths become shorter on these poles and the grid arrangement in S tends to disappear.

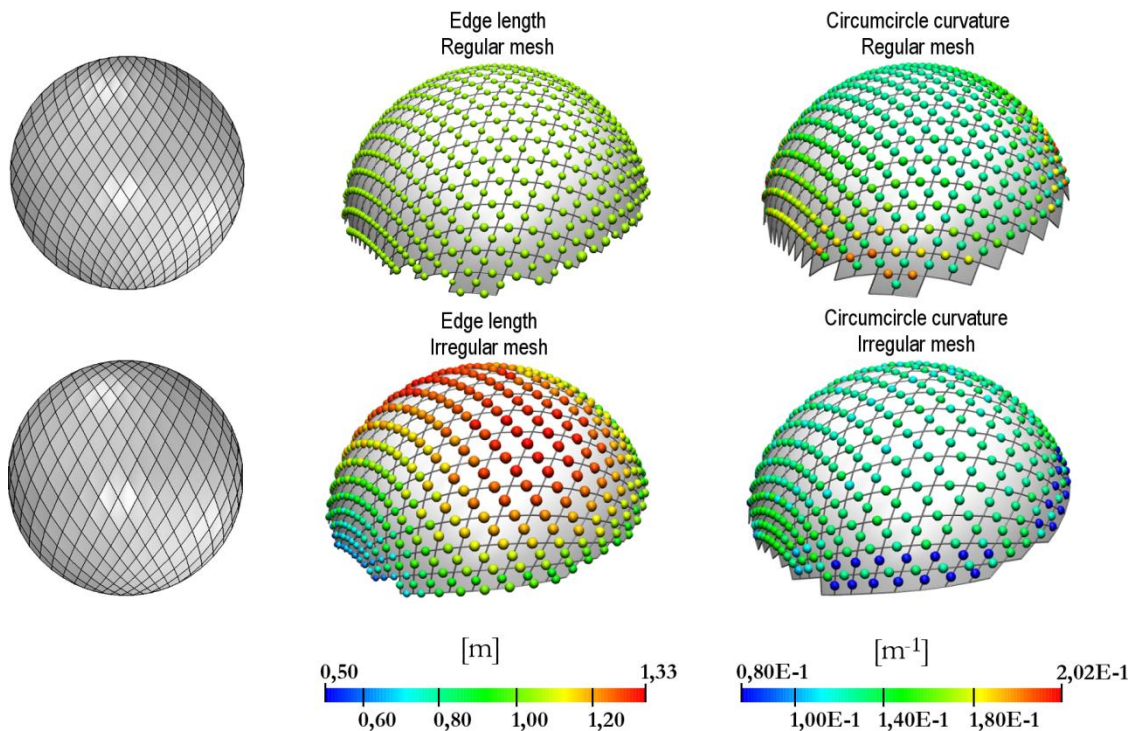


Figure 3-15: Comparison of grid patterns (left), edges' length (middle) and circumcircle curvature (right) of a calotte, optimised with regular and irregular grids.

The edges' length of the optimised irregular mesh varies from 0.504 m to 1.329 m. The resulting circumcircle curvature values of the optimised regular and irregular patterns are given in Table 3-3.

Curvature [m^{-1}]	67.5° - Regular	67.5° - Irregular
Maximum	0.197	0.160
Mean	0.150	0.134

Table 3-3: Curvature values of the optimised regular and irregular meshes for a calotte surface

The following examples are the three double-curved surfaces with anticlastic, synclastic and a combination of anti- and synclastic curvatures, already optimised as regular grids in Chapter 3.2. During optimisation, the values of the weighting λ -factors of the sub-energies in (3-1) were modified in a similar way for the three surfaces and ranged between 4 and 10 for the reference surface energy, between 0 and 1 for the length energy and between 4 and 10 for the curvature energy.

In the following figures, the circumcircle curvature of the meshes, optimised as regular and irregular grids, are illustrated by means of coloured nodes: blue/smaller and red/larger nodes represent respectively the lowest and highest values. The colour scales of the regular and irregular grids are equivalent, which makes easier to identify the corresponding reduction of the curvature values. The mesh size of the irregular configuration is also illustrated with the same colour rule: blue/smaller and red/larger nodes give respectively the lowest and highest edge length values.

On the case of the anticlastic surface, Figure 3-16 shows that the curvature values on the centre span could be optimised (green to blue nodes), reducing the mean value of the profiles' curvature to 85% - from 0.060 m^{-1} to 0.051 m^{-1} . Nevertheless, the highest curvature values (red nodes) located at the grid corners could be hardly minimised. Concerning the mesh size of the irregular grid, the segment length increases from the centre span to the transversal edges of the surface, varying from 0.862 m to 1.124 m.

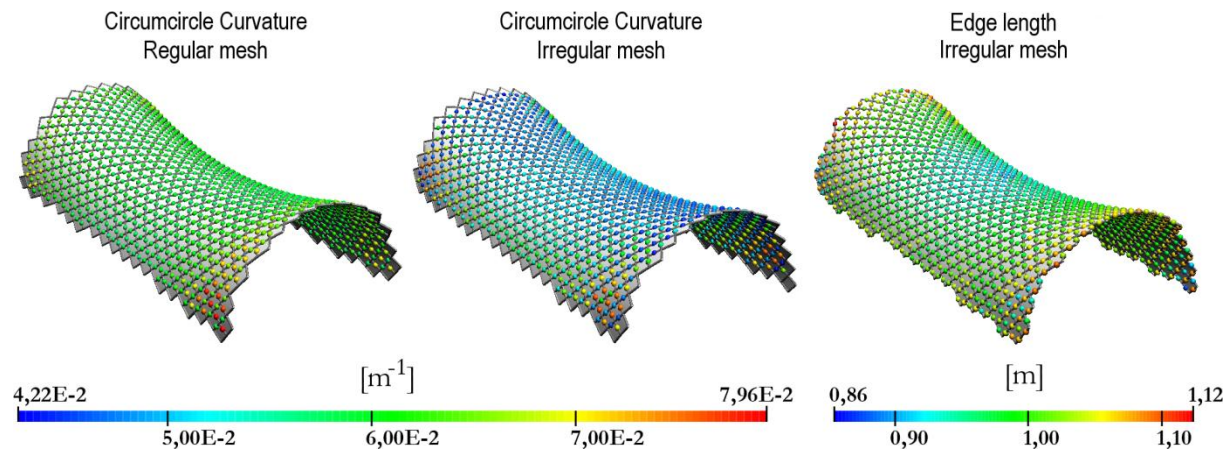


Figure 3-16: Comparison of the circumcircle curvature of the anticlastic surface with regular and irregular grids (left); segments' length of irregular anticlastic grid (right)

On the case of the synclastic surface, one can observe on Figure 3-17 that the most important curvature minimisation appears at the longitudinal sides (red to green/blue nodes) resulting from the diminution of the segment length in this area. The maximum and mean values of the profiles' curvature could be reduced to 85% - from 0.093 m^{-1} to 0.079 m^{-1} - and 68% - from 0.071 m^{-1} to

0.048 m⁻¹. The mesh size increases progressively from the bottom to the crown of the gridshell, going from 0.776 m to 1.254 m.

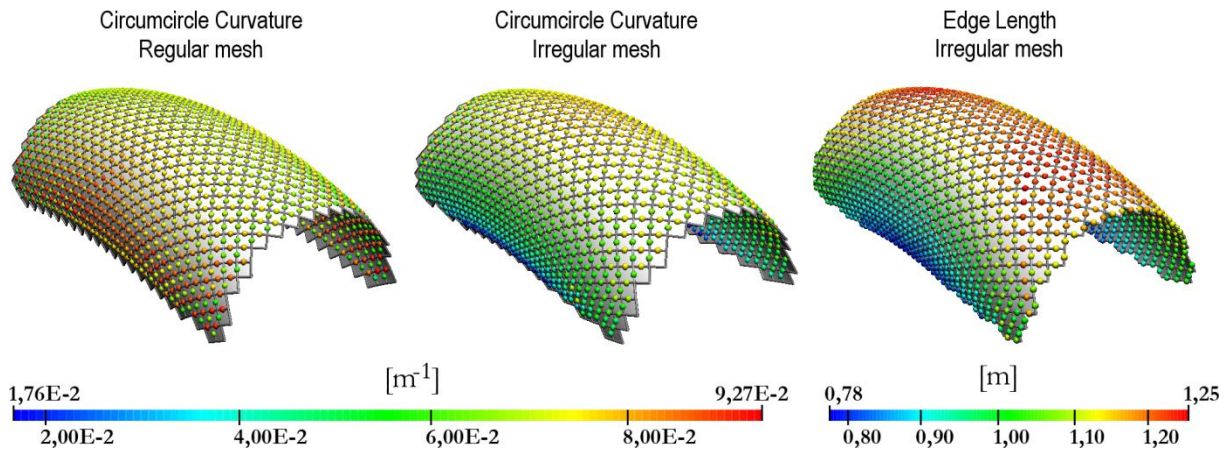


Figure 3-17: Comparison of the circumcircle curvature of the synclastic surface with regular and irregular grids (left); segments' length of irregular synclastic grid (right)

On the case of the surface with anti- and synclastic curvature, Figure 3-18 shows that the optimisation of the circumcircle curvature is more concentrated at the valleys (yellow/green to blue nodes), reducing its mean value to 77% - from 0.069 m⁻¹ to 0.053 m⁻¹. The maximum curvature values (red nodes) on the crowns could be hardly reduced. Concerning the mesh size distribution, the segment length increases from the valleys to the crowns of the surface, going from 0.789 m to 1.257 m.

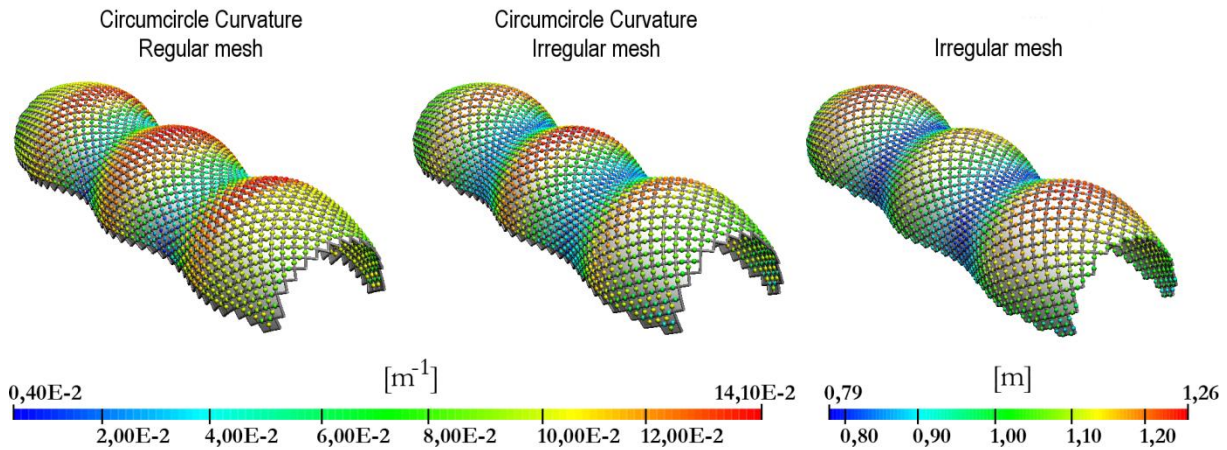


Figure 3-18: Comparison of the circumcircle curvature of the surface, with anti- and synclastic curvature, with regular and irregular grids (left); segments' length of irregular grid (right)

3.3.2 Further optimisation by allowing distance to reference surface

As formerly shown, with the variational method it is possible to calculate different grid patterns by modifying the weighting factors of the three penalising energies. In the previous section, the optimised meshes were constrained to keep a maximum distance to the reference surface lower than 1/500 of their span length. In the next optimisations, a higher distance to the target

geometry is allowed in order to further reduce the profiles' curvature. For it, the weighting factor of the reference surface energy λ_2 is reduced. During the optimisation of the three double-curved surfaces, the range of values for the weighting factors went from 2 to 3 for the reference surface energy, 4 to 12 for the edge length energy and 4 to 16 for the curvature energy.

In Figure 3-19, the resulting maximum and mean circumcircle curvature values (coloured) of the optimised irregular meshes are illustrated and compared with those obtained using the classic compass method [8] (grey) for regular grids, with an angle between guide curves of 90° . The colour of the columns represents the maximum distance between grids and target surface, which cannot exceed a value of 0.60 m. The curvature values have been calculated, using scripts developed with the 3D-modeling software Rhino. Again the mean curvature values could be generally stronger reduced than the maximum ones. The optimisation rates with respect to the regular meshes evolve in different ways for the three surfaces.

Compared to the optimised regular meshes, the highest reduction of curvature by the anticlastic surface is to be found by a distance to the reference surface up to 0.20 m: the maximum and mean curvature values decrease from 0.064 m^{-1} to 0.050 m^{-1} (77%) and from 0.052 m^{-1} to 0.028 m^{-1} (53%). On the case of the synclastic surface, the maximum and mean curvature values could be mostly reduced at maximum allowable distances to reference surface up to 0.40 and 0.50 m, respectively: to 73% - from 0.090 m^{-1} to 0.066 m^{-1} - and to 34% - from 0.057 m^{-1} to 0.019 m^{-1} . Finally, on the case of the surface with anti- and synclastic curvature, the highest minimisation of the maximum and mean values could be obtained at maximum allowable distances of 0.30 and 0.50 m: to 92% - from 0.134 m^{-1} to 0.123 m^{-1} - and 54% - from 0.047 m^{-1} to 0.026 m^{-1} .

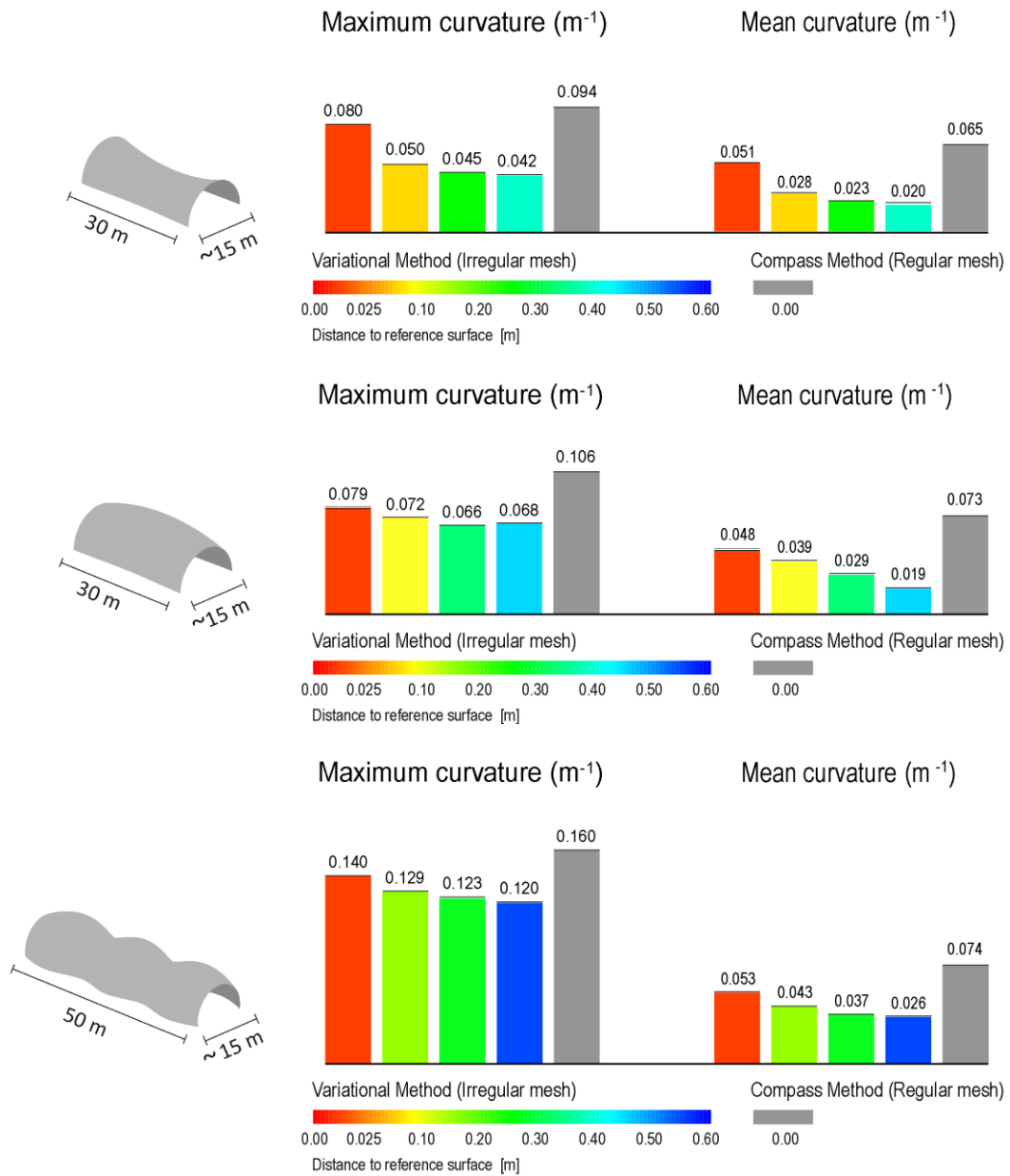


Figure 3-19: Comparison of the maximum and mean circumcircle curvature values for three double-curved grids, optimised as irregular meshes, obtained with the variational (coloured) and compass (grey) methods

3.4 Summary

The residual stresses generated in the grid profiles resulting from the shaping process of elastic gridshells are cause of important reductions of their bearing capacity under external loading. In this chapter, a methodology based on variational principles to determine regular and irregular meshes on or near a reference surface and with minimised profiles' curvature is proposed and applied to four double-curves surfaces. The following conclusions can be drawn from the chosen case studies.

3.4.1 Influence of initialisation mesh and weighting factors on the optimisation

In the proposed approach, the optimisation of the profiles' curvature evolves through an iterative process which is strongly influenced by the initialisation mesh and the values assigned to the weighting factors of the sub-energies to be minimised. To obtain a maximum reduction of the profiles' curvature, it is important to widely explore different initialisation meshes with varying shear angles and different combinations of weighting factors. Nevertheless, it is important to always prove, during the optimisation, that other relevant constructive and structural requirements are also fulfilled. The mapping technique used for the initialisation mesh in the proposed approach is based on conformal parameterisation, which allows almost constant angle between edges but usually presenting a great variety on the edge lengths. Further research could focus on the use of alternative mapping techniques for the determination of the initialisation mesh, e.g. the Wire Mesh Design approach which provides meshes with constant edge length.

3.4.2 Reduction of mean vs. maximum curvature values

As with the proposed variational principles approach the optimisation has an effect on the sum of the curvature values and not directly on the maximum curvature value, in most of the cases the mean curvature could be stronger reduced than the maximum one. Depending on the surface geometry, a diminution of the highest curvature values became difficult. By allowing more distance between grid and reference surface, the optimisation results could be improved.

The main objective of the grid optimisation is to minimise the material stresses to which the grids are subjected due to their bending process and increase its stresses reserves to be able to carry higher external loading. The need of stress reserves is distributed depending on the grid geometry and the nature of the external loads. By the optimisation of the grid, it would be optimal to reduce the profiles' curvature, there where the stresses are the highest under the most critical external load, which can coincide or not with the maximum stresses after the bending process. An optimisation of the grid pattern according to the distribution of the required stress reserves, depending on the structure geometry and loading case, could provide further structural advantages.

3.4.3 Construction of resulting geometry

It is essential to note that, to build the resulting optimised geometry, the grid must be firstly shaped into the optimised form, through external forces, and then be braced by a stiffening layer, which introduces in-plane shear stiffness in the gridshell, before removing the shaping forces. The bracing layer of elastic gridshells can consist in beam elements subjected to tension and compression (e.g. Weald and Downland Museum, England), diagonal cable elements resisting only tension (e.g. Multihalle Mannheim, Germany and Orangery Gridshell in Chiddingstone Castle, England) or structural surface panel elements (e.g. Savill Garden Gridshell, England), as

illustrated in Figure 3-20. In the case that elastically-bent beams are used as bracing elements, it would be optimal to also consider their curvature during the optimisation process. The examples presented in this chapter focused only on the optimisation of the grid. Nevertheless, with the variational method it would be also possible to take into account the curvature of a third diagonal layer, using for example triangular - instead of quadrilateral - meshes.



Figure 3-20: Different bracing elements on elastic gridshells

It is also important to remark, that, due to constructive reasons concerning e.g. the technical operability of the shaping forces or the connection properties of the grid, it can result difficult to exactly obtain the optimised grid geometry. Examples of connections at the grid nodes with varying stiffness or kinematic constraints are illustrated in Figure 3-21.



Figure 3-21: Different grid connections on elastic gridshells

3.4.4 Optimisation with irregular grids

Using the definition of the circumcircle curvature energy and allowing variation of the edge lengths, a further reduction of the profiles' curvature of previously optimised regular grids has been possible. Nevertheless, one should take into account the effects on the construction process and on the load-bearing behaviour of the resulting irregular gridshells. Modifying the mesh size and with it the material distribution of the grid, the local and global stability as well as the stiffness of the gridshell changes. Therefore it is important to estimate and previously restrict the maximum allowable edge length.

The transformation of a regular into an irregular grid also complicates the deployment and the shaping process of the grid from a completely flat position. By the construction of irregular gridshells, the grid profiles are usually bent independently from each other in an incremental process, generally more time-consuming than that of regular gridshells. Nevertheless, if the bending stiffness of the grid profiles is low enough, large deformations can be induced on the profiles and the gridshell can be also built by deploying the grid from a flat state. However, in contrast to regular gridshells, the profiles must be additionally bent on the ground to allow the plane configuration. The structure can be built as a grid only when the material stresses do not exceed the allowable ones during the construction process. The stresses, to which the grid profiles are subjected, can be controlled by means of numerical analyses. In order to reduce the initial stresses, the grid can be partially assembled in the start configuration and the resting border profiles and connections introduced after shaping the grid. This procedure was used for the construction process of an elastic hemisphere with irregular grid and 10 m diameter presented in Chapter 5.

4. Numerical Analysis

4 Numerical Analysis

The bending process and load-bearing behaviour of elastic gridshells can be modelled and analysed using finite element methods. During the shaping of the profiles, internal forces are induced on the structure, so that the final equilibrium shape of the gridshell will be attained once its edges have been fixed, the bracing elements have been assembled and the external shaping forces have been removed. The goal of the finite element modelling is to quantitatively analyse the geometry and material stresses resulting from the shaping process and the load-bearing capacity of the gridshell under external loading. With an enough accurate model, not only the material and cross-sectional properties of the profiles can be taken into account, but also different types of grid connections and supports can be considered.

The construction process and the bearing behaviour of elastic gridshells are strongly affected by the selected grid pattern. Grid patterns with constant mesh size - regular grids – allow, for example, an erection process where the grid is bent as a whole. On the contrary, profiles of grids with variable mesh size - irregular grids - are usually bent independently from each other, in an incremental process. The orientation and arrangement of the profiles have furthermore an essential influence on the residual stresses after erection process and on the distribution of forces and deformability of the gridshell under external loading. These effects are analysed in this chapter on a regular anticlastic gridshell with three different grid patterns. The grid patterns have been defined using the variational method described in Chapter 3, with initialisation meshes differing in their shear angle, and modelled as gridshell structure by means of finite element methods. The procedures of definition and calculation of the finite element models are as well explained.

The shell behaviour of a elastic gridshell is attained once the grid has been triangulated. Elastic gridshells are usually braced using an additional layer of profiles, crossing cables or restraining rigid panels. Their assembling is generally more time-consuming than that of the grid, as multiple elements must be individually handled, connected in the air to the already bent grid and, in case of using a third layer of profiles, bent into the gridshell's geometry. In order to optimise the construction process, in the second part of this chapter, it is proposed to use tensile membranes which assume the function of restraining and at the same time covering the grid. The effects of a restraining membrane on the bearing capacity of a hemispheric gridshell are studied and analysed by means of finite element methods.

4.1 Definition and Calculation of the Finite Element Model

4.1.1 Initial plane configuration

Before starting with the simulation of the bending process and bearing behaviour of the optimised grids, it is necessary to determine their **initial plane configuration**. Different procedures are used depending if the mesh owns regular or irregular mesh size. Both cases start

with the importation of the optimised polyhedral mesh into the CAD-software Rhino as *.obj*-file. Here, the edges of the polyhedral mesh are firstly transformed into lines. A Script has been written in order to assign the lines to different layers corresponding to the two crossing profiles' layers of the grid. The Visual Basic Scripting Edition (Rhino's VBScript) has been used. The edges of the chosen polyhedral meshes generally own different orientations according to the corresponding grid layers. Script I consists on calculating the difference of the x- and y-coordinates of the start and end points of the edges and multiplying them. The edges are classified on the grid layers according to the sign of the product. At last, the grid is trimmed according to the boundaries of the target surface. Figure 4-1 illustrates the example of a regular anticlastic surface of 5 and 7.5 m height, 14 and 15 m width, 30 m length and 1 m mesh size. On the left, the optimised polyhedral mesh, which has been imported from VaryLab into Rhino, and the corresponding grid composed of line elements are shown. The orientation of the lines are visualised with arrows in Rhino. On the right, the principle of Script I for the classification of the edges, into the crossing layers, is given for two different orientations of the mesh edges.

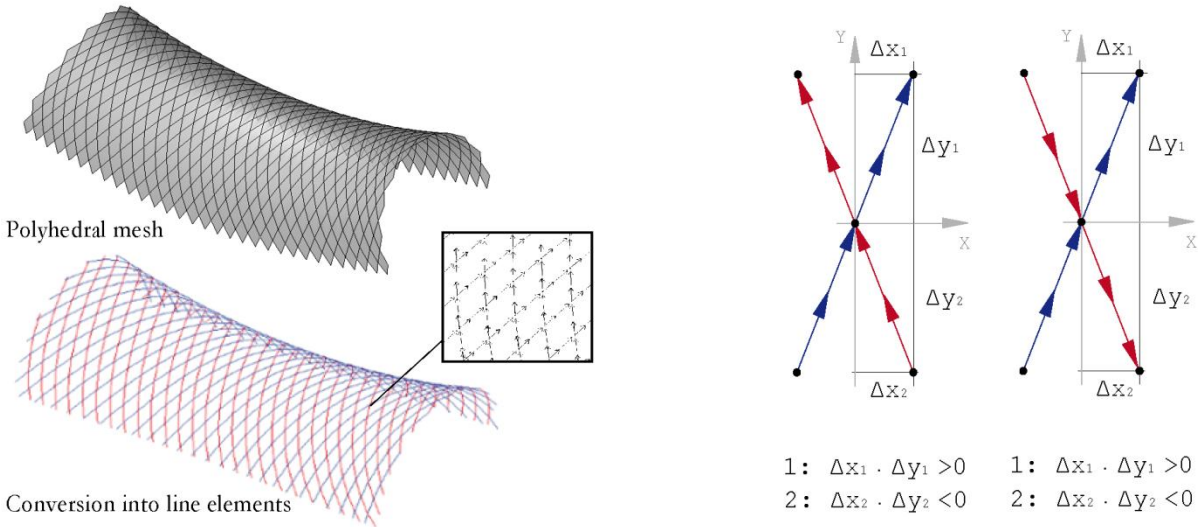


Figure 4-1: Illustration of polyhedral mesh and corresponding grid composed of line elements for an anticlastic surface (left) / Principle of Script I for the assignment of the mesh edges into the crossing grid's layers (right)

In the case of regular meshes, a second Script has been written in Rhino to trace the plane configuration of the grid. Firstly, Script II asks for a start grid's node, a shear angle between the crossing grid layers and the mesh size. From the start grid's node, the Script iteratively identifies the segments composing the grid profiles and their lengths. In each iteration, a new grid node is treated and its adjacent segments are founded by comparing node's coordinates with those of the start and end points of the grid segments. When the length of the considered segment is lower than the mesh size, the script identifies it as border segment and the corresponding length is drawn on the planar grid. On the left of Figure 4-2, the planar configuration of an anticlastic grid drawn in Rhino is illustrated.

In the case of irregular meshes, as the profiles are usually bent independently from each other, their orientation on the planar configuration is not relevant. The profiles, whose length can be taken from the bent grid's geometry, can be simply drawn as straight polylines on a same plane.

Besides the grid profiles, the bracing cables diagonalising the grid and the cladding elements on which the loads are applied on the finite element model have been also drawn in Rhino (see

Figure 4-2, middle). On the finite element model, the bending of the grid profiles is generated by shortening virtual cables which connect the grid nodes from their initial position on the planar configuration to their target position on the bent grid's geometry. The virtual cables own a minimal stiffness and are shortened by applying prestress forces. As illustrated on the right of Figure 4-2, the virtual cables are as well defined in Rhino. Finally, the model generated in Rhino is imported into the CAD-Interface of Sofistik – SofiPlus –, where the geometric elements are converted into finite elements with material and cross-sectional properties.

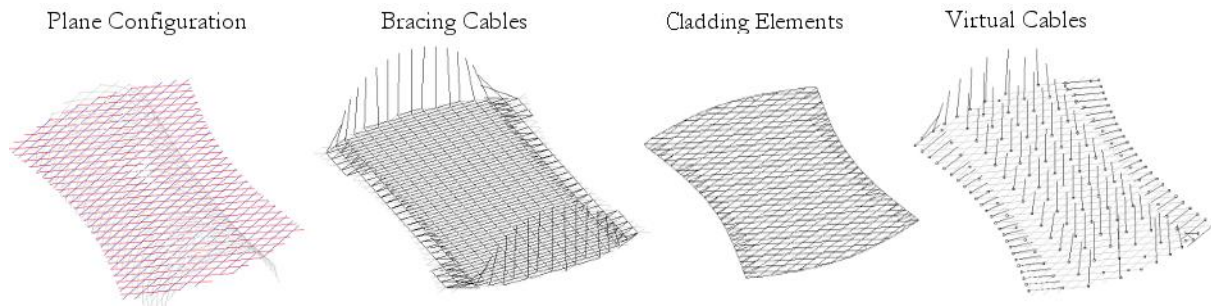


Figure 4-2: Plane configuration, bracing cables, cladding elements and shaping virtual cables defined in Rhino of an anticlastic gridshell

4.1.2 Finite element model

The finite element modelling in SofiPlus starts by assigning material and cross-sectional properties to all the structural elements of the gridshell. The grid profiles have been modelled as beam elements and assigned into two groups, corresponding to the crossing grid's layers. Depending on the bracing system, diagonal cable elements, which can only carry tensile forces, or a third layer of beam elements can be defined. Quad elements without stiffness have been modelled on the grid in order to apply surface loads.

This raw model is exported as text file and can be further refined with the Text Editor Teddy. Firstly, in order to obtain more accurate results, the beams are subdivided into smaller elements and the eccentricity between superposed grid profiles is introduced by modifying the z-coordinate of the second group of profiles. Then, the connection between superposed profiles, at the grid nodes, can be defined. As analysed in Chapter 5, this connection has a relevant influence on the bending process and bearing behaviour of the gridshell. In the practice, grid connections generally only allow rotation in the axis normal to the grid's surface and, with it, scissoring of the grid during the bending process. In the finite element models which have been analysed on this chapter, the connection elements have been defined with two coupling components: the first one consists on a hinged connection at the upper layer to a rigid node at the lower layer, the second one on a skewed kinematic constraint of rotations transverse to the axis defined by the two connected nodes. On the left of Figure 4-3, these coupling conditions have been illustrated.

In Chapter 5, the results obtained with numerical simulations are compared with those observed with physical prototypes. As the clamps used at the grid nodes of the built structures presented important imperfections, deformations of the physical gridshells were much higher than those of the numerical models. The influence of the stiffness of the connection elements on the structural

behaviour of gridshells is analysed in Chapter 5. Here, spring elements, axial and tangential to the direction defined by two connected grid nodes, and with variable stiffness coefficients, have been considered.

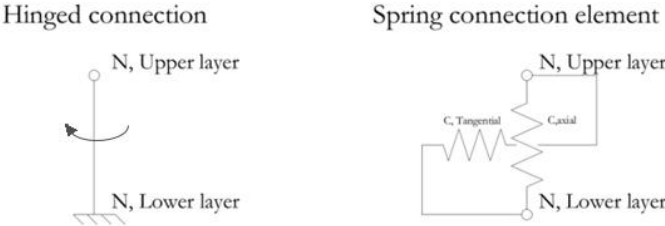


Figure 4-3: Modelling of grid connections with coupling and spring elements

Also on the text-based Editor Teddy, supports at the profiles' ends are introduced on the finite element model. During the shaping process, the displacements of the profiles' ends have been constrained in z-axis. Once the grid has been bent, the edges of the grid have been fixed, using hinged supports.

The equilibrium of the structure, at the shaping steps as well at its final state, has been calculated according to the third-order theory: material non-linearities and effects of the geometrical modification of the structure (e.g. variation of its stiffness under large deformations) are considered. Convergence problems commonly emerge on the simulation of the bending process, due to the high deformations and rotations to which the elements are subjected. In order to avoid them, the shaping process is modelled incrementally: profiles are progressively bent by applying increasing shaping forces on successive load cases. The load cases are consecutively considered as primary load cases on the calculation of the following ones, which means that, by the calculation of one load case, the stresses and displacements of the previous one are added.

There exists different ways to define the external forces inducing the shaping of the beam elements. By the structural analyses presented by Lafuente Hernández et al. in [6], the bending of the grids on the finite element models was generated by applying nodal displacements on predefined grid nodes. In 2011, Lienhard et al. [62] suggested a shaping methodology consisting on defining virtual cable elements, with reduced elastic stiffness, between the start and target positions of the profiles and shortening them through prestress forces. The advantage of this procedure is that the nodal displacements have not to be recalculated and redefined for each shaping load case and at each loaded node. A uniform prestress force can be applied to all cables independently from their lengths. By the simulations presented on the following sections, virtual shaping cables have been used. Nevertheless, it is important to notice that, the length of the virtual cables, after simulation of the shaping process, cannot be completely reduced to zero and that only a limited number of shaping forces can be practically applied on the grid. For these reasons, the bent grid does not perfectly acquire the target geometry.

Figure 4-4 illustrates the simulation of the bending process of a regular anticlastic gridshell. Here, the grid's bending has been induced trough nodal displacements. Once the grid has been shaped, the grid's edges are fixed with hinged supports and bracing cables are introduced to maintain the bent geometry and activate shear stiffness on the grid. Afterwards, the equilibrium of the structure is calculated without external shaping forces.

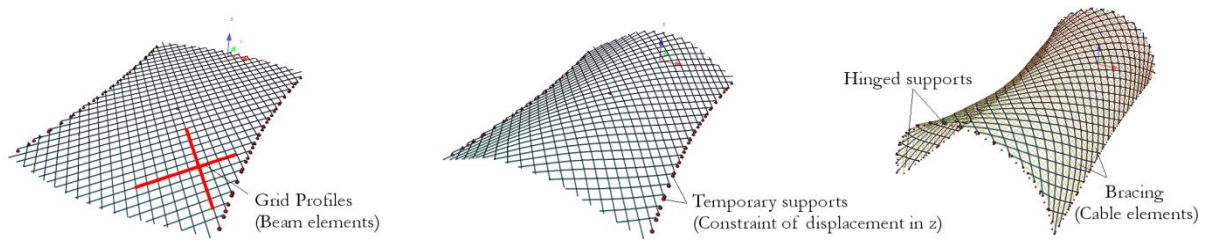


Figure 4-4: Modelling of bending process of regular anticlastic gridshell

In contrast to regular grids, the distortion and scissoring of grids with irregular mesh is restricted. Therefore, the profiles of irregular gridshells are generally not connected during the shaping process; they are bent independently from each other. Figure 4-5 shows the simulation of the bending process of the irregular Faraday Pavilion GFRP gridshell, investigated by Paul Nicholas, from the Centre For IT and Technology, and Ali Tabatai, from WEM3, in Copenhagen (Denmark) [63]. The radial profiles are firstly bent into their target geometry using virtual cables and afterwards fixed with temporary supports, applied along their length. Then, the transversal profiles are bent and connected to the radial ones. Finally, radial and transversal beams are fixed at their ends with hinged supports, the temporary supports of the radial elements and the shaping virtual cables are deactivated and the final equilibrium shape of the structure is calculated.

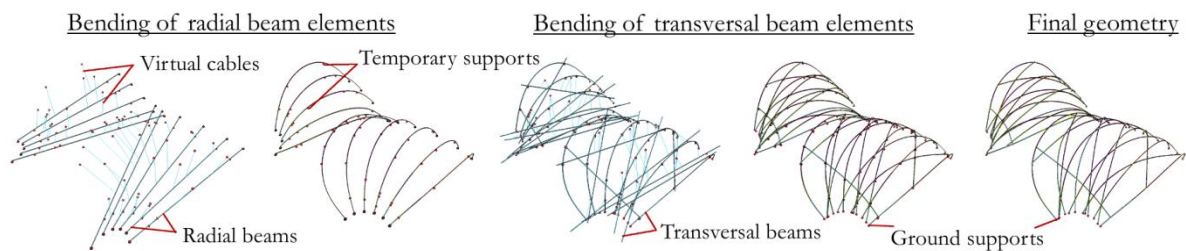


Figure 4-5: Modelling of bending process of irregular gridshell (Faraday Pavilion, 2012)

The equilibrium geometry that the structure adopts after the shaping process is strongly affected by the inner forces induced by bending the beam elements. These forces depend on the profiles' curvature and their material and cross-sectional properties. In Figure 4-6 the equilibrium geometry (*elastica curve*) of a 10 m long profile, which has been elastically bent by approaching its ends until a span length of 6 m, is compared to a 10 m long arch. The *elastica* curve has been simulated and calculated with Sofistik. Compared to the arch, the elastically bent profile deforms outwards on the middle and inwards at the sides. A similar deformability presents the unbraced anticlastic gridshell, with mainly transversally oriented profiles, after removing the external shaping forces. The middle of the grid deforms upwards while the lower part of the lateral sides inwards.

If it is wanted that the grid maintains the target - instead of the *bending induced* - geometry, bracing elements and, with it, shear stiffness have to be introduced before releasing the temporary supports or shaping forces. Shear stiffness is also necessary to enable shell behaviour of the structure under external loading. On the finite element model, bracing elements are deactivated

during the shaping process and activated when external loads are applied. If a third layer of profiles are used to triangulate the grid, their bending must be additionally simulated.

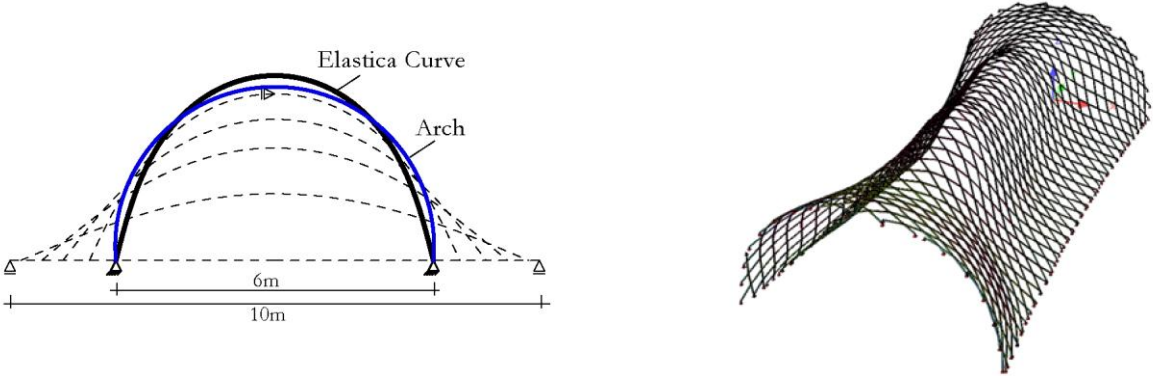


Figure 4-6: Comparison of elastica curve of a 10 m long profile with an arch of same length and span (left); Deformability of unbraced anticlastic grids after removing shaping forces - exaggerated by a factor of 5 (right)

In the following section, the load-bearing behaviour of three anticlastic regular gridshells with different grid pattern has been analysed. The gridshells are between 5 and 7.5 m high, 14 and 15 m wide and 30 m long. The deformation of the grids has been induced using virtual cables, whose residual length does not exceed the 2% of the structure’s span length.

4.2 Influence of the Grid Pattern on the Structural Behaviour

A target surface can be reproduced by multiple grid patterns. Nevertheless, due to structural and constructive limitations, not all patterns are buildable. The grid patterns basically differ from another in the orientation of the profiles and in their density - profiles’ length per surface unit. The orientation and density of the grid has an influence on the bending process of the structure and its load-bearing capacity. This effect has been analysed in this section for a regular anticlastic gridshell by means of finite element methods. Three grid patterns have been determined with the variational approach presented in Chapter 3. They differ on their shear angle, in transverse direction: 45°, 90° and 135°, as illustrated in Figure 4-7. The mesh size of the grid patterns has been defined so that the total length of the grid profiles remains the same: 1215 m ± 1%. The resulting mesh sizes of the grids are 1.39 (45°), 1.00 (90°) and 1.50 m (135°).

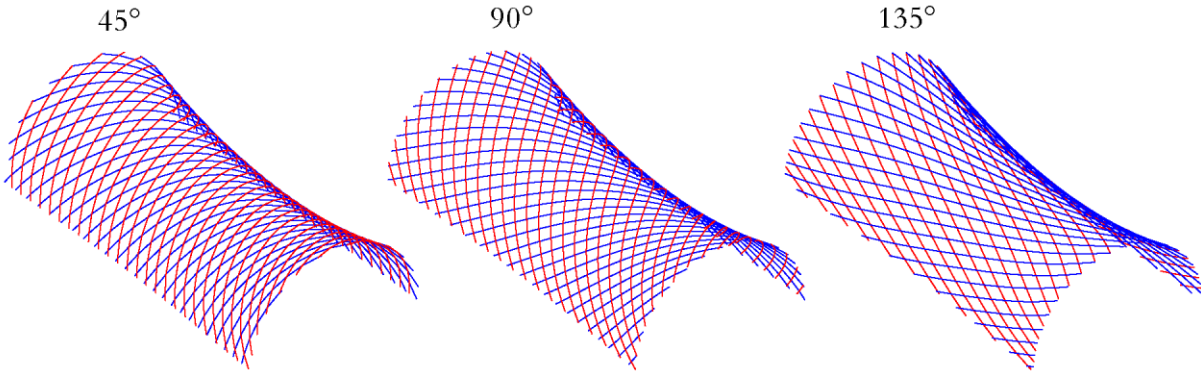


Figure 4-7: Anticlastic surface reproduced by three grid patterns with varying angle between profiles but same total profiles’ length

4.2.1 Bending process

The shaping process of the anticlastic gridshells has been modelled iteratively in four load cases with increasing shaping forces. The non-linear calculations have been performed according to the third-order theory and with an iteration tolerance for residual forces of 0.1 % of the maximum applied nodal load. The equation solvers “Iterative Equation Solver” (Conjugate Gradients) and “Direct Parallel Multifront Sparse Solver” of Sofistik have been used. The grids are composed of GFRP profiles with a modulus of elasticity equal to 25000 N/mm² and a tubular section of 50 mm diameter and 4 mm thickness. Virtual shaping cables have been defined on approximately every second grid node. The virtual cables possess a circular section of 6 mm diameter and a modulus of elasticity of 130000 N/mm², which has been reduced by a factor of 0.001 during the simulation of the bending process.

The shaping of the grid is induced by shortening the virtual cables applying prestress forces on them. The simulation of the shaping process ends when the lengths of the virtual cables cannot be further reduced due to convergence problems on the calculation. The length of the shaping cables cannot be absolutely reduced to zero but to a residual length. The mean and maximum residual lengths are 8, 10 and 10 cm and 20, 24 and 22 cm for the 45°, 90° and 135° grid patterns, respectively. The mean and maximum residual cable forces are 0.29, 0.14 and 0.14 kN and 0.91, 0.61 and 0.34 kN. The total number of prestressed virtual cables is 129, 180 and 127 for the 45°, 90° and 135° grids, respectively. Comparing the 45° and 135° grids, one can observe that, the higher the curvature and, with it, the bending moments on the profiles are, the higher the prestress forces on the cables must be to make the grid adopt the target geometry.

Due to the residual length and the limited number of virtual cables, the imposed grid’s geometry (*constrained grid*) obtained with Sofistik, before removing the shaping forces, differs from that defined with the variational approach. The mean and maximum distance between the grids shaped in Sofistik and the target surface are 9, 19 and 12 cm and 32, 22 and 22 cm for the 45°, 90° and 135° grid patterns, respectively. Only by the 45° grid, the grid node with the highest distance to the target surface is not connected to a shaping cable. As the distances have been calculated with the normal projection of the grid nodes onto the target surface, the maximum distance of the 90° grid is slightly lower than the maximum residual length of the virtual cables. In the following Table 4-1, the mean and maximum values of the residual forces and lengths of the virtual cables as well as the mean and maximum values of the distance to the target surface are resumed.

		45° (n=129)	90° (n=180)	135° (n=127)
Residual force of virtual cables [kN]	Mean	0.290	0.140	0.140
	Max	0.914	0.610	0.344
Residual length of virtual cables [m]	Mean	0.076	0.098	0.097
	Max	0.201	0.242	0.216
Distance to reference surface [m]	Mean	0.093	0.102	0.118
	Max	0.324	0.224	0.219

Table 4-1: Mean and maximum residual forces and lengths of virtual shaping cables and distance to reference surface

Differences on the bent geometry lead to variations on the profiles’ curvature. In addition to the differences due to the residual length and limited number of the virtual cables, the grid also

deforms when the external shaping forces are removed. On the studied cases, the grid has been braced before deactivation of the shaping forces (**braced grid**), so that the nodal displacements of the grid are minimal, partially due to elastic deformations of the structural elements: the maximum nodal displacements are 11 mm by the 45° grid, 11 mm by the 90° grid and 9 mm by the 135° grid. Deformations are much higher when releasing the grid without bracing elements (**unbraced grid**): 149 mm by the 45° grid, 136 mm by the 90° grid and 328 mm by the 135° grid. In the following

Figure 4-8, deformations at the longitudinal and transverse central axes, after removing the shaping virtual cables, are illustrated for the non-braced (grey) and braced (blue) grids, with an exaggeration factor of 10, and compared with the constrained geometry (green). The bracing elements consist in crossing stainless steel cables with a modulus of elasticity of 130000 N/mm² and 8 mm diameter.

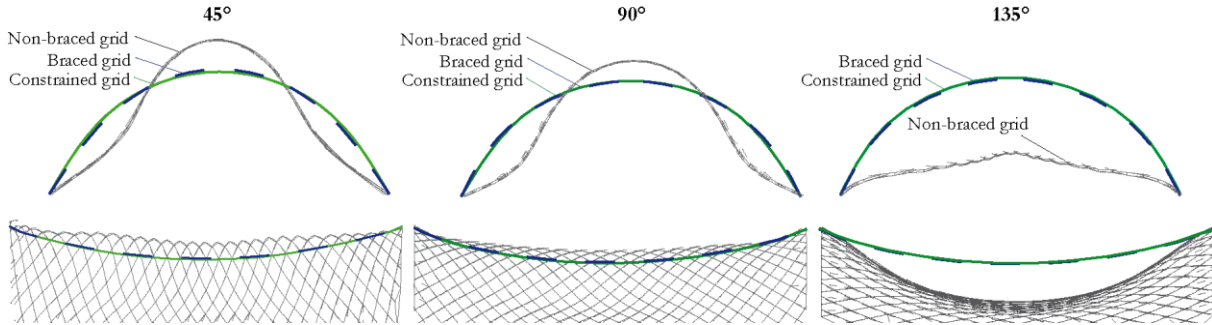


Figure 4-8: Grid deformations after removing shaping forces for non-braced (grey) and (blue) braced grids, exaggerated by a factor of 10

The orientation of the profiles – and consequently its curvature and resulting inner bending moments - strongly influences the deformability of the released unbraced grids. On the case of the 45° grid, as the profiles are basically transversally oriented, the grid deforms in a similar way than the elastically-bent profile acquiring the geometry of the *elastica* curve, as previously observed in Figure 4-6. The bottom sides of the grid deform inwards while the top outwards, inducing here higher curvature and stresses on the profiles. The deformation of the 90° grid is equivalent to the one of the 45° grid; nevertheless, the profiles’ curvature on the top of the 90° grid is lower and more homogeneous. In contrast to the 45° and 90° grid, the 135° grid strongly sinks overall and an important scissoring takes place on the middle. Figure 4-9 shows the three-dimensional deformation of the unbraced grids.

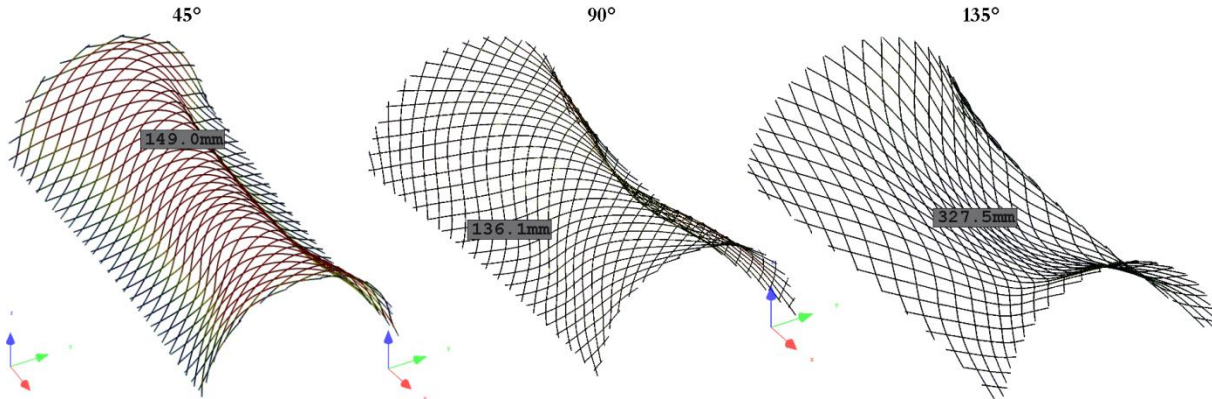


Figure 4-9: Deformations of unbraced grids after removing the shaping forces, exaggerated by a factor of 10

On the following figures, the curvature distributions of the grids obtained with the variational approach are compared with the equivalent stresses resulting from Sofistik. The geometry of the grids determined with the variational approach results from an optimisation of geometric aspects of the grid; the values on the figures correspond to the *Circumcircle Curvature* defined in Chapter 3. The *Equivalent Stresses* of Sofistik are obtained once the grid has been bent, fixed at its longitudinal and transverse edges, braced with crossing cables and released from the shaping forces. The grid's geometry obtained with Sofistik results from the calculation of an equilibrium of forces where the material and cross-sectional properties of the structural elements are considered. As the equivalent stresses are principally due to the bending moments, induced on the grid during the shaping process, they can be directly related to the profiles' curvature values.

In Figure 4-10 the values obtained for the 45° grid are shown. The circumcircle curvature distribution of VaryLab shows higher values (red/yellow) at the corners and lower values (green/blue) on the top. On the contrary, the highest stress values given by Sofistik are located on the middle of the structure. That is mainly due to the limited number of shaping cables on the model, especially at the corners and along the longitudinal edges, and their residual length. The lower the number of virtual cables is, the less the grid is constrained to the target positions and the stronger its geometry is influenced by the inner forces generated during the shaping process. Furthermore, the grid has been fixed with hinged supports so that, at the vicinity of the edges, it tends to relax (blue values).

Some similarities between both distributions can be however observed. Regarding the equivalent stresses along the longitudinal edge, the values at the corners result slightly higher (green/yellow) than at the middle (blue). Moreover, values on the centre of the top are slightly higher than at the sides. The minimum (dark blue), mean (pale blue) and maximum (red) values of the profiles' circumcircle curvatures are 0.132, 0.120 and 0.103 m⁻¹, which correspond to bending stresses of 64, 70 and 83 N/mm². These minimum and mean stress values, which are located on the top of the grid, are comparable but slightly lower than the equivalent stresses obtained with Sofistik on the top of the structure, which go from 67 to 89 N/mm² (yellow/red).

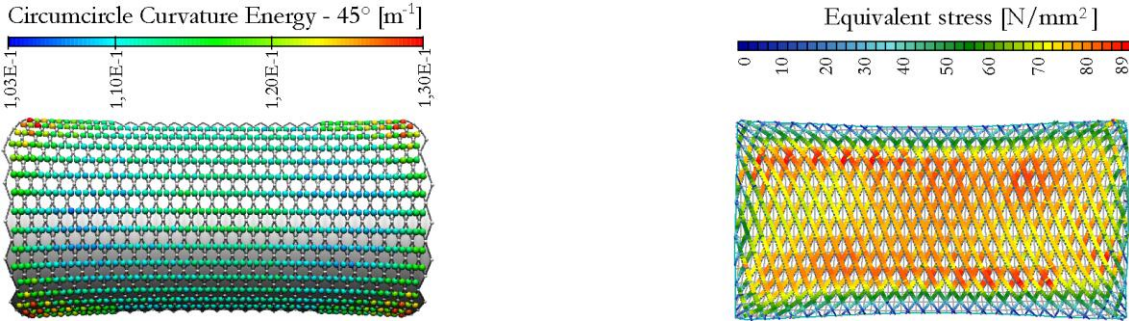


Figure 4-10: Profiles' circumcircle curvature on VaryLab (left) and equivalent stresses calculated in Sofistik (right) of the anticlastic gridshell with 45° grid pattern

In Figure 4-11 the circumcircle curvature and stress distributions of the 90° grid calculated with VaryLab and Sofistik are shown. The curvature distribution exhibits higher values (yellow/red) at the corners and lower (blue) on the middle of the grid. In a similar way, the equivalent stresses obtained with Sofistik are higher (yellow/red) at the corners and lower (blue) at the centre of the grid. Again, differences between the grid geometries resulting from VaryLab and Sofistik are

mainly due to the residual length and limited number of the shaping cables. Also here the relaxation of the grid at its edges (blue values) due to the hinged supports can be observed. The minimum (dark blue), mean (green) and maximum (red) circumcircle curvature values are 0.047, 0.061 and 0.092 m^{-1} , which correspond to bending stresses of 36, 40 and 57 N/mm^2 . These stress values are comparable to the ones obtained with Sofistik, which result on between 25 and 35 N/mm^2 on the centre and top of the front sides and between 45 and 63 N/mm^2 at the corners.

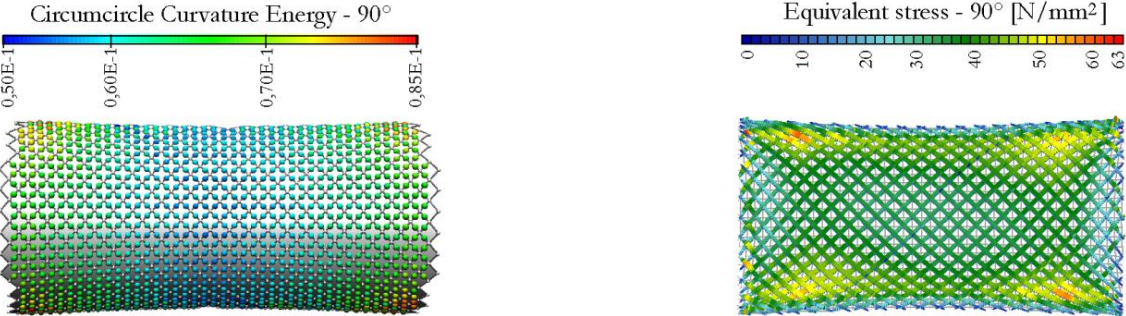


Figure 4-11: Profiles' circumcircle curvature on VaryLab (left) and equivalent stresses calculated in Sofistik (right) of the anticlastic grids shell with 90° grid pattern

Figure 4-12 illustrates the curvature and stress distributions of the 135° grid. The curvature distribution calculated with VaryLab exhibits values that progressively decrease from the front sides (orange/red) to the centre of the grid (dark blue). Similarly, but less gradually, the equivalent stresses calculated with Sofistik decrease from the transverse sides (red/yellow/green) to the middle of the grid (dark blue). Extreme values tend to be more concentrated on Sofistik than on VaryLab. The minimum (dark blue), mean (pale blue) and maximum (red) circumcircle curvature values results on 0.001, 0.015 and 0.042 m^{-1} , which correspond to mean and maximum bending stresses of 9 and 26 N/mm^2 . Despite the extreme equivalent stresses of Sofistik on the corners (red), which are equal to 39 N/mm^2 , these values are comparable to the equivalent stresses at the frontal sides, between 15 and 30 N/mm^2 (green/pale blue) and at the centre of the grid, between 3 and 15 N/mm^2 .

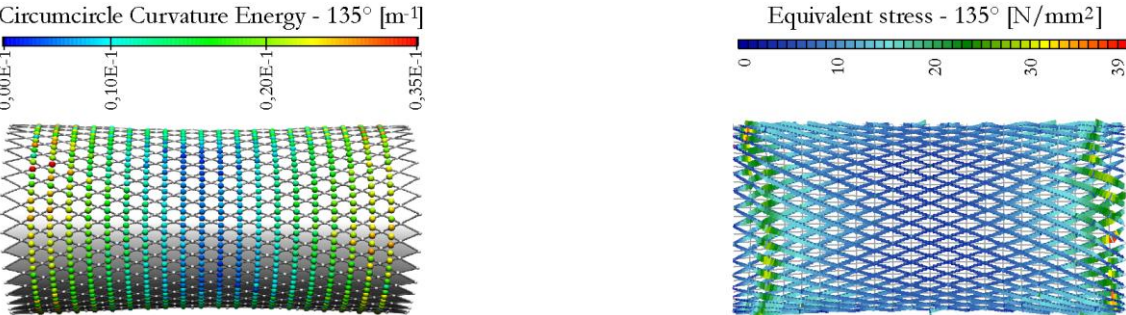


Figure 4-12: Profiles' circumcircle curvature on VaryLab (left) and equivalent stresses calculated in Sofistik (right) of the anticlastic grids shell with 135° grid pattern

4.2.2 External loading

The distribution of the section forces, on the profiles and cables, equivalent stresses and deformability of the three anticlastic gridshells under permanent and live loading are analysed in this section. The permanent load consists on the dead load of the structure and the inner forces generated by bending the grid. The live load corresponds to a uniformly distributed load of 0.80 kN/m^2 . Three distributions of this load have been studied: symmetric over the whole surface, asymmetric over one longitudinal half and asymmetric over one transverse half, as illustrated in Figure 4-13.

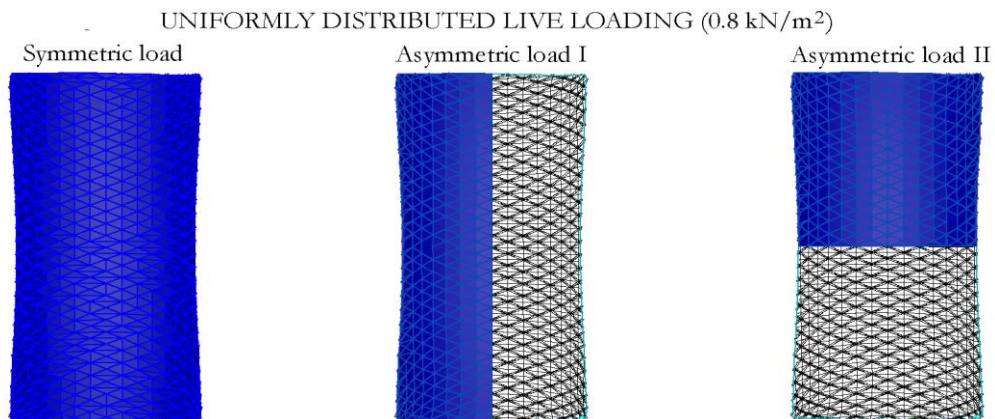


Figure 4-13: Uniformly distributed live load cases

4.2.2.1 Section forces

Depending on the orientation and arrangement of the grid profiles, different distributions of the section forces under permanent and external loading are obtained. Four load combinations have been considered: permanent load (I), permanent load + symmetric live load (II), permanent load + longitudinally asymmetric live load (III) and permanent load + transversally asymmetric live load (IV). In the following figures the resulting distributions of the bending moments in y- and z-axis and axial forces on the profiles as well as of the tensile forces on the cables are analysed and compared between the three gridshells.

Figure 4-14 to Figure 4-16 show the absolute values of the bending moments in y-axis. Comparing the load cases without and with live loads, bending moments on the gridshells are mostly generated by the shaping process. Consequently, and according to the curvature and stress distributions observed in the last section, the highest bending moments under permanent and live loads correspond to the 45° grid and the lowest to the 135° grid. Under external loading, the increment of bending moments by the 45° grid is mainly concentrated at the longitudinal sides and, similarly, by the 90° at the lateral sides and the middle of the grid. The increment of bending moments by the 135° is principally concentrated at the corners.

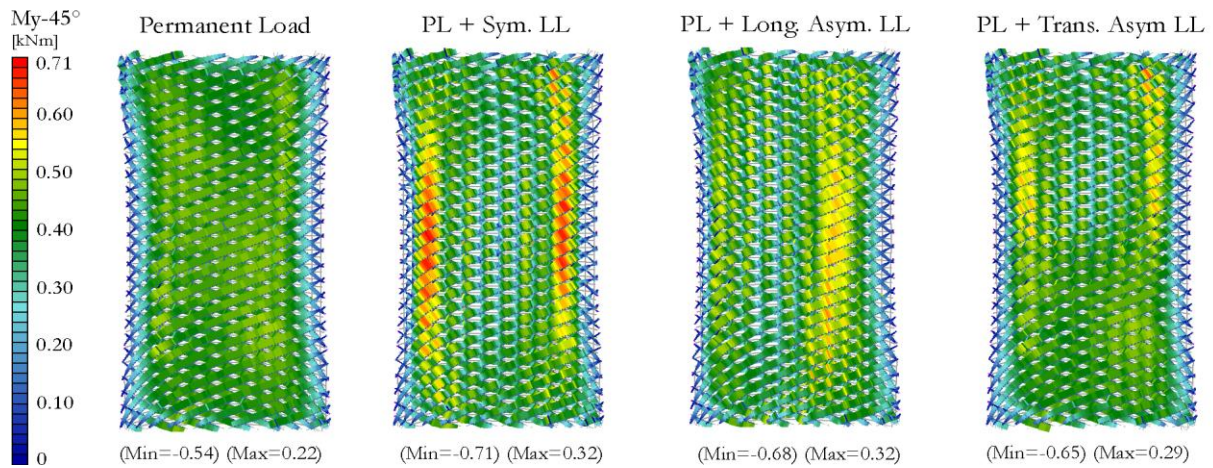


Figure 4-14: Bending moments in y-axis on grid profiles of 45° grids

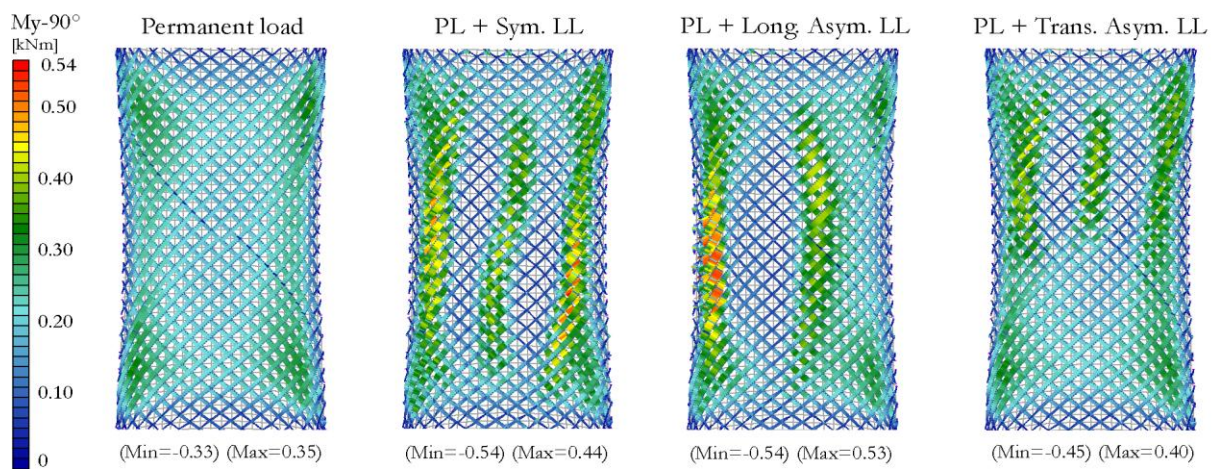


Figure 4-15: Bending moments in y-axis on grid profiles of 90° grids

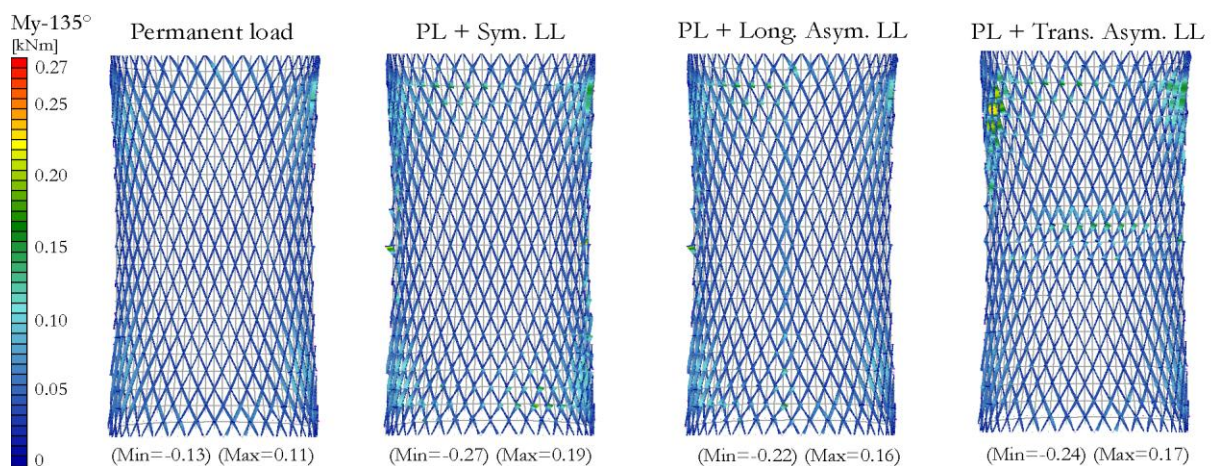


Figure 4-16: Bending moments in y-axis of grid profiles on 135° grids

Compared to the bending moments in y-axis, the maximum bending moments in z-axis (Figure 4-17 to Figure 4-19) of the three gridshells are more similar. Their distribution is less uniform and generally concentrated at the transverse sides. In addition, the increment of the maximum moments due to live loads is much lower. It is important to note that the distribution of the bending moments in y- and z-axis depends on the properties of the grid connections. As

described in the first chapter's section, two kinematic constraints have been given to the grid connections of the analysed structures: the first one consists on a displacement constraint with a rigid connection at the lower layer and a hinged connection at the upper layer, the second one on a skewed constraint of rotations transverse to the axis defined by the two connected nodes.

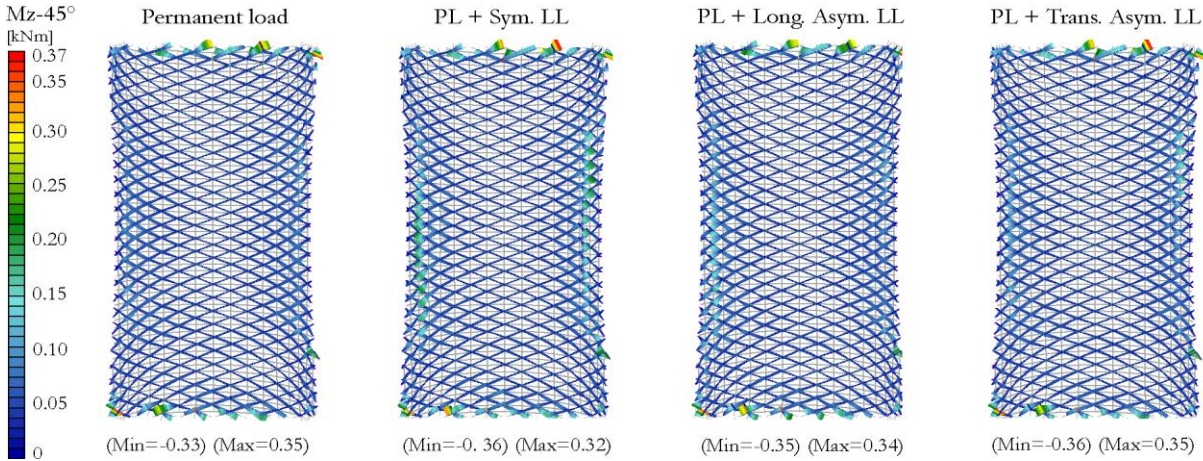


Figure 4-17: Bending moments in z -axis of grid profiles on 45° gridsbell

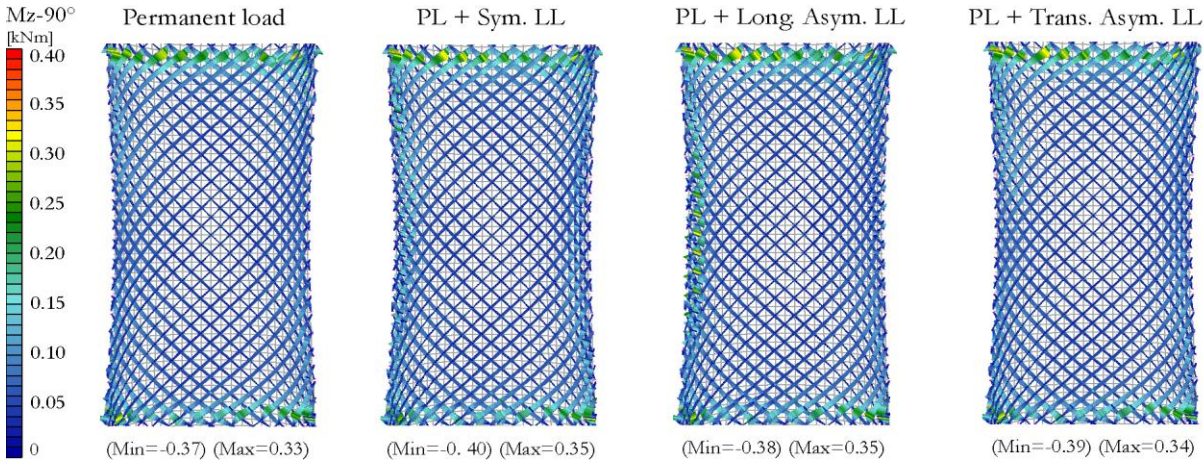


Figure 4-18: Bending moments in z -axis of grid profiles on 90° gridsbell

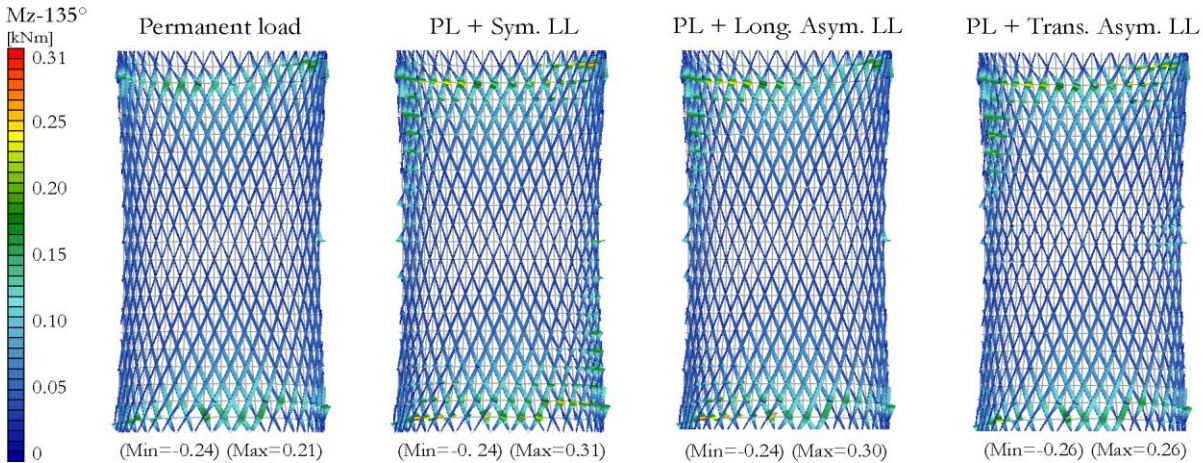


Figure 4-19: Bending moments in z -axis of grid profiles on 135° gridsbell

Regarding the axial forces carried by the profiles of the gridshells, J. Graf analyses in [64] the force distribution of two steel-glass gridshells with different grid patterns: the quadratic and Zollinger barrel gridshells, with respectively parallel and diagonally oriented profiles, according to the longitudinal and transverse axes of the structures. Both gridshells consist in short barrel shells with parabolic section and supported at its four corners. The transverse and longitudinal edge beams are modelled as weightless HEB 800 profiles; their stiffer axis is oriented perpendicularly to the shells' surface. Displacements of the transverse edges are constrained in longitudinal direction so that the analysed gridshells correspond to middle fields between binders of a continuous barrel shell. Diagonal steel cables are used to brace the gridshells. The structural analyses demonstrate the influence of the profiles' orientation on the beam and cable forces and on the deformability of the structures. Under uniformly distributed loading, on the Zollinger gridshell, the tensile membrane forces acting on the longitudinal edges are transferred to the transverse binders directly through the diagonally oriented profiles. In contrast, on the quadratic gridshell, the transfer of the edge membrane forces must be mostly carried by the less stiff diagonal cables. This results on a higher stiffness of the Zollinger barrel shell compared to the quadratic one. Under a uniformly distributed load of 2 kN/m^2 , the tensile forces on the profiles of the Zollinger barrel shell are about 2.5 times higher than the cable forces on the quadratic one; however, the highest cable force of the quadratic barrel shell is 3.5 times higher than that of the Zollinger shell.

Figure 4-20 to Figure 4-22 illustrate the axial forces on the grid profiles of the anticlastic elastic gridshells. In contrast to the bending moments, the difference of axial forces between the load cases without and with live loads is higher. One can observe that, the more transversally the profiles are oriented, the stronger the membrane forces are transversally transferred to the longitudinal edges (smallest span length) and, due to the positive curvature in this direction, through compression forces. On the other hand, when the profiles are more longitudinally oriented, the structure stiffness on transverse direction is significantly diminished so that only a reduced level of compression membrane forces can be carried in this direction. Once the structure cannot carry further compression forces on the transverse direction, the grid starts to buckle in this direction, the middle of the structure strongly deforms downwards and loads start to be carried in longitudinal direction; given the negative curvature in this direction, through tensile forces. Despite the differences with the steel-glass gridshells analysed by J. Graf in terms of geometry, materiality as well as connection and support conditions, the distribution of forces under uniformly distributed loads presents some similarities at the corners of the gridshells. The transfer of forces at the intersections between longitudinal and transverse edges is generally more intensive than on the rest of the structure and takes place through tensile forces, on the profiles spanned between the edges, and through compression forces, on the profiles oriented toward the corners.

The load behaviours under asymmetric loading are equivalent to those of the symmetric loadings, but concentrated on the respectively loaded areas of the grids. The maximum axial forces remain similar, except from the 135° gridshell under transversally asymmetric live load, where the compression forces of the profiles oriented toward the grid corners significantly increase.

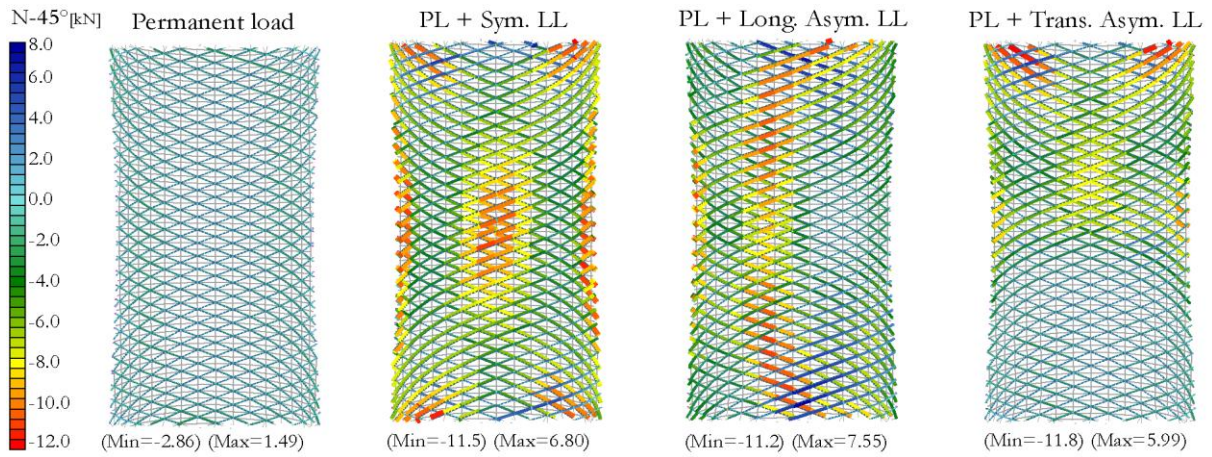


Figure 4-20: Axial forces on grid profiles of 45° gridsbell

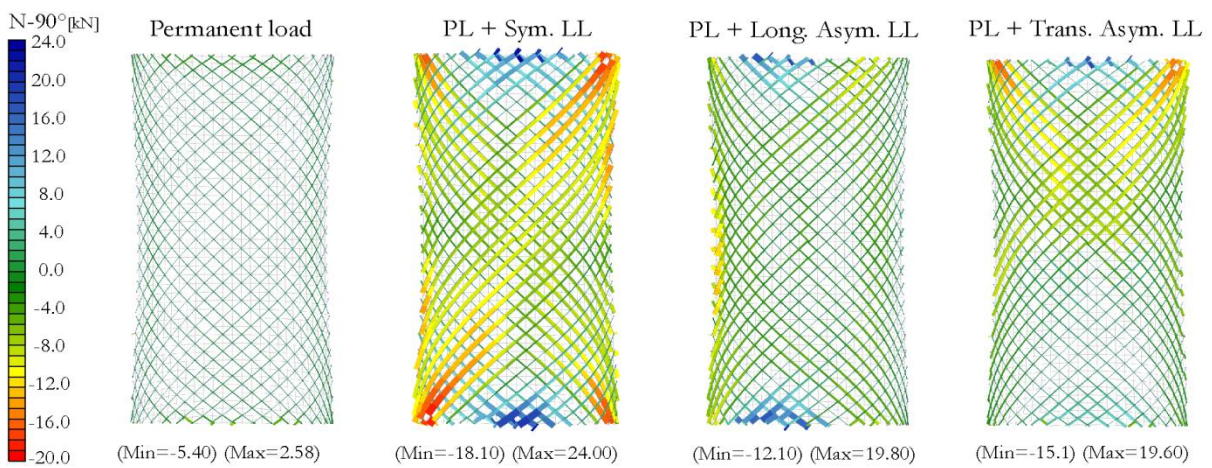


Figure 4-21: Axial forces of grid profiles on 90° gridsbell

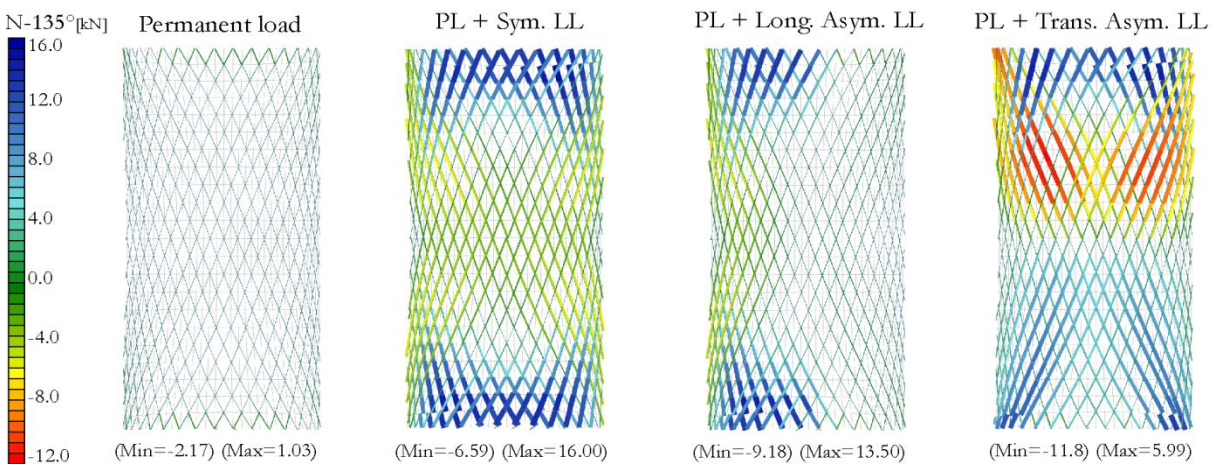


Figure 4-22: Axial forces of grid profiles on 135° gridsbell

Figure 4-23 to Figure 4-25 illustrate the distribution of tensile forces on the bracing cables. As by the axial forces on the grid profiles, tension on the cables is minimal under permanent loading and becomes notable under external loading. It is also confirmed that the more longitudinally the profiles are oriented, the stronger the forces are longitudinally transfer and, due to the anticlastic

surface, the higher the bracing cables in longitudinal direction are subjected to tension. One can also observe that tensile forces on the cables are higher there where axial forces on the profiles are lower: at the top of the transverse sides by the 45° and 90° gridshells but on the centre by the 135° gridshell. The maximum cable forces of the three gridshells are similar.

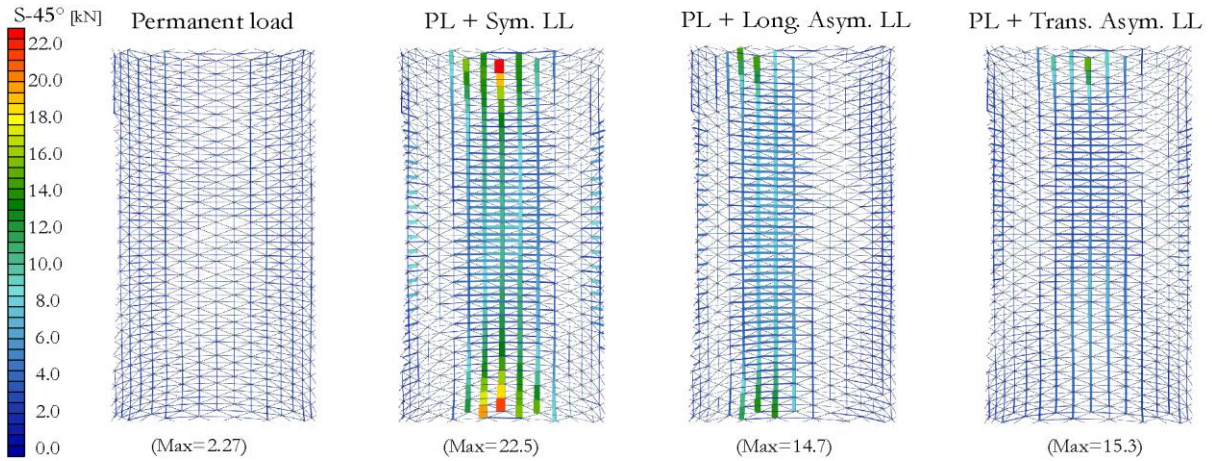


Figure 4-23: Cable forces on 45° gridshell

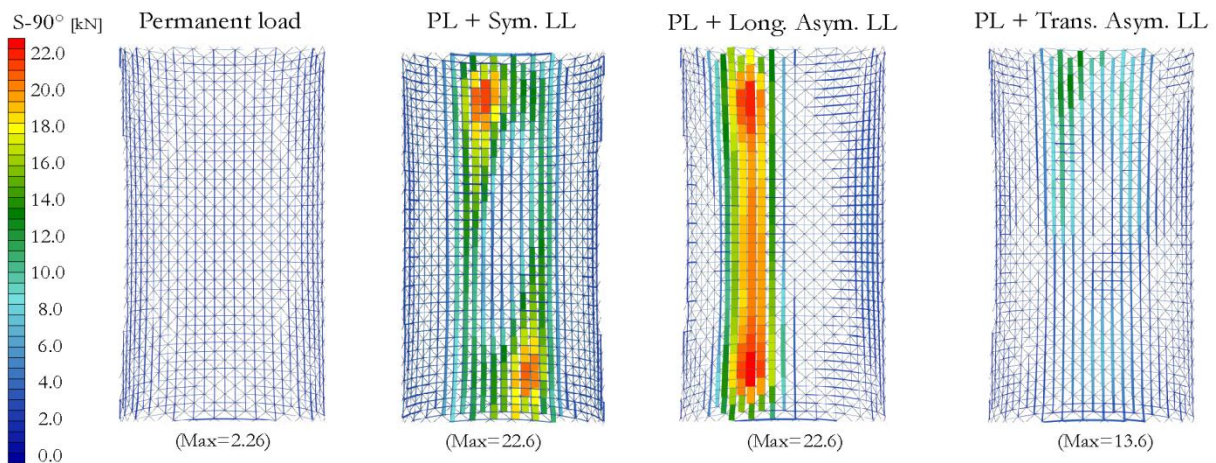


Figure 4-24: Cable forces on 90° gridshell

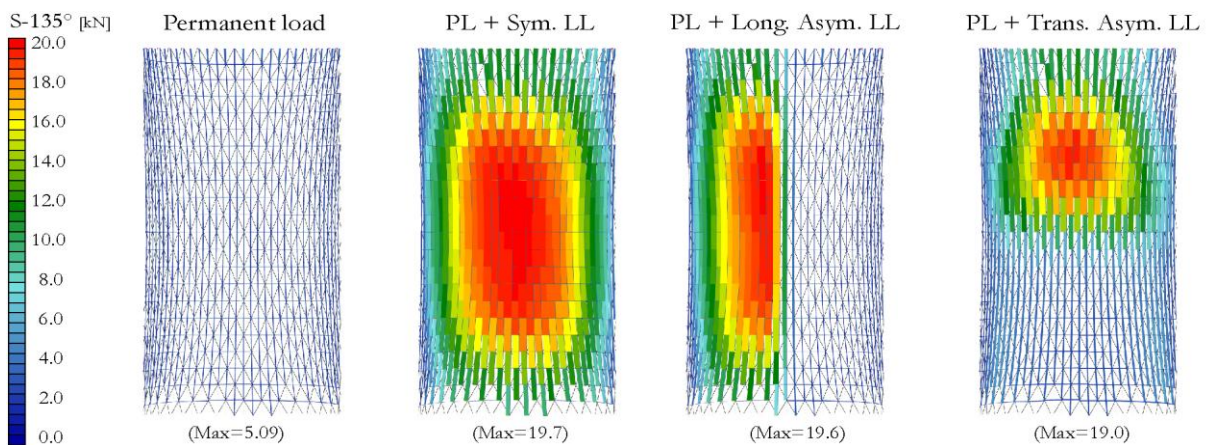


Figure 4-25: Cable forces on 135° gridshell

4.2.2.2 Equivalent stresses

As demonstrated in the first section, depending on the orientation of the profiles, different curvature values and consequently residual stresses result from the bending process. It has also been shown that the highest equivalent stresses after grid's shaping are to be found on the 45° and the lowest on the 135° gridshells. In Figure 4-26 to Figure 4-28 the increment of the equivalent stresses under external loading is analysed. One can observe that the stress distributions are equivalent to those of the bending moments in y-axis. On the 45° gridshell, the equivalent stresses mostly increase at the longitudinal sides. Similarly, on the 90° gridshell, the stress increment is mainly concentrated at the lateral sides and additionally at the middle of the grid. The equivalent stresses of the 135° gridshell increase more locally, on the transverse sides. For all the gridshells, equivalent stresses are mostly due to the grid's bending and the maximum values of the symmetric live load case are comparable to those of the asymmetric live load cases.

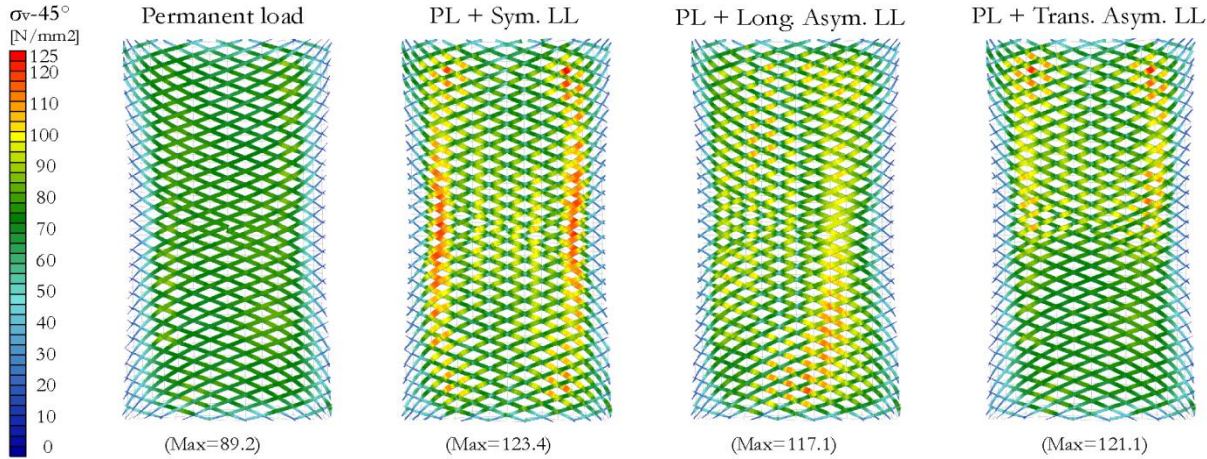


Figure 4-26: Equivalent stresses on 45° gridshell

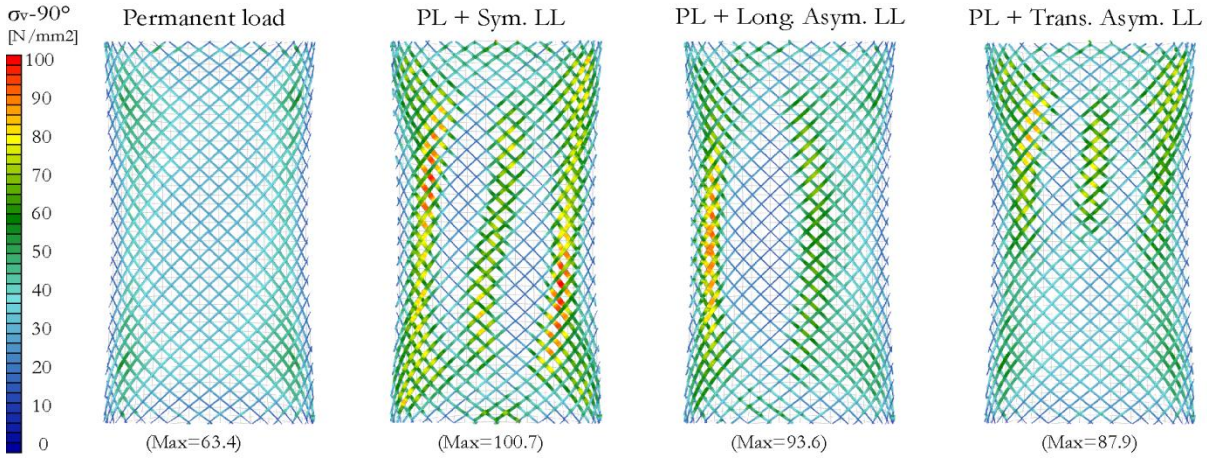


Figure 4-27: Equivalent stresses on 90° gridshell

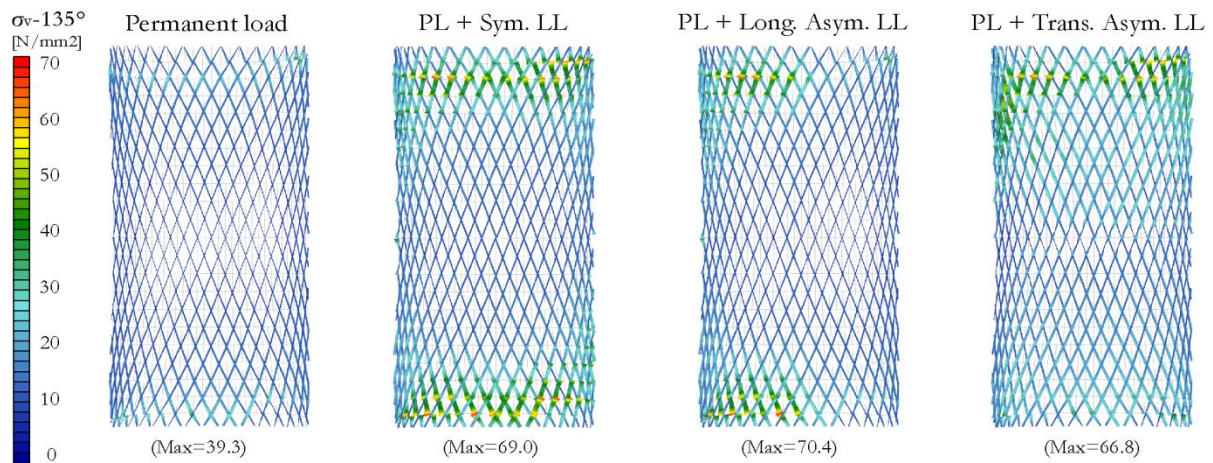


Figure 4-28: Equivalent stresses on 135° grids

4.2.2.3 Deformations

Besides the transfer of forces and distribution of material stresses, the orientation of the grid also affects the stiffness and deformability of the gridshells. Figure 4-29 shows the deformation under symmetric load of the gridshells at their longitudinal and transverse axes, exaggerated by a factor of 10. By the transverse section of the 45° gridshell, the middle of the structure deforms downwards while the sides deform outwards. The 90° gridshell deforms in a similar way until a live load of approximately 0.6 kN/m². By higher loads, the middle of the gridshell buckles and starts to deform upwards generating a waved section in transverse direction. The deformation of the 135° gridshell is characterised by a global abatement of the structure. The maximum nodal displacements are higher on the 90° gridshell - 225 mm – and similar between the 45° and 135° gridshells - 165 and 167 mm, respectively.

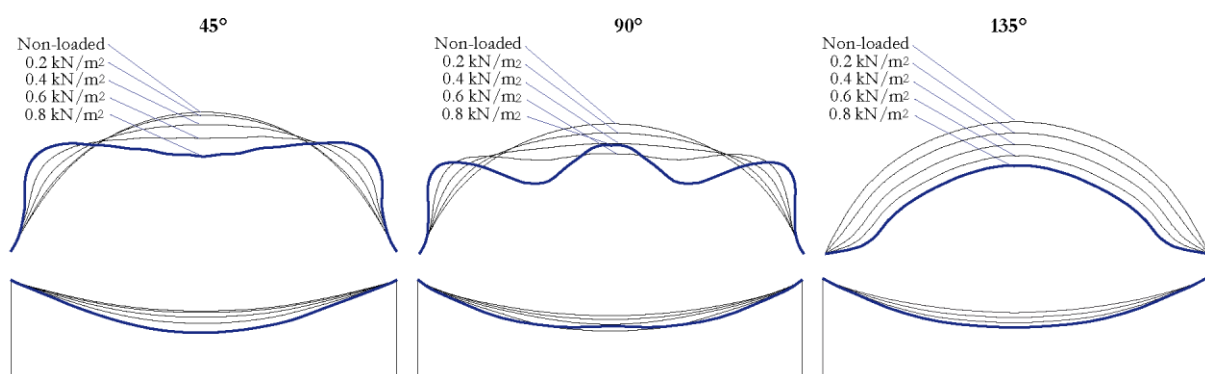


Figure 4-29: Progressive deformation of anticlastic gridshells under symmetric loading, exaggerated by a factor of 10

Deformations under asymmetrical loading are equivalent to those under symmetrical loading but concentrated on the respectively loaded areas of the gridshell. Nevertheless, the nodal displacements under asymmetrical loads are higher or lower than under symmetrical loads depending on the orientation of the grid. On the case of the 45° gridshell, the maximum nodal displacements are lower when the gridshell is loaded asymmetrical while, on the 90° gridshell,

they augment under longitudinally asymmetric loading and shrink under transversally asymmetric loading. On the case of the 135° gridshell, the nodal displacements slightly increase when loaded asymmetrically. In Figure 4-30 to Figure 4-32, the deformed gridshells are illustrated, with an exaggeration factor of 10.

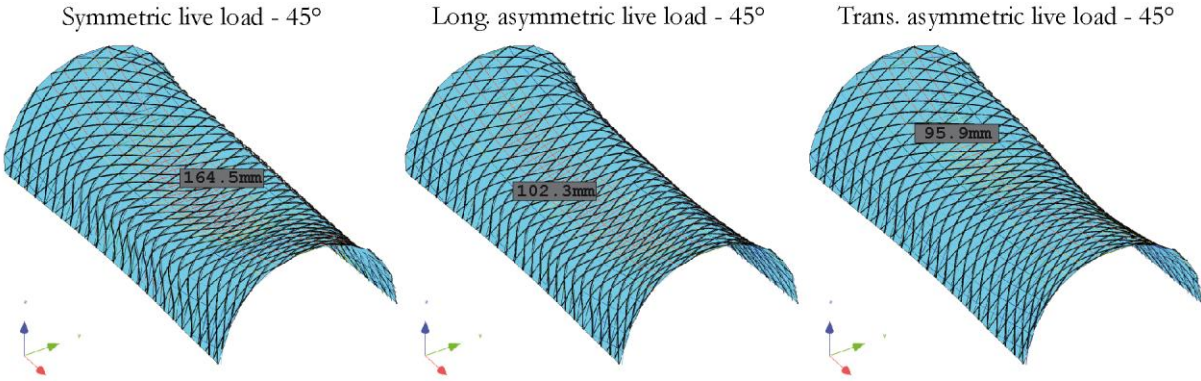


Figure 4-30: Deformation of 45° gridshell under symmetric and asymmetric loading, exaggerated by a factor of 10

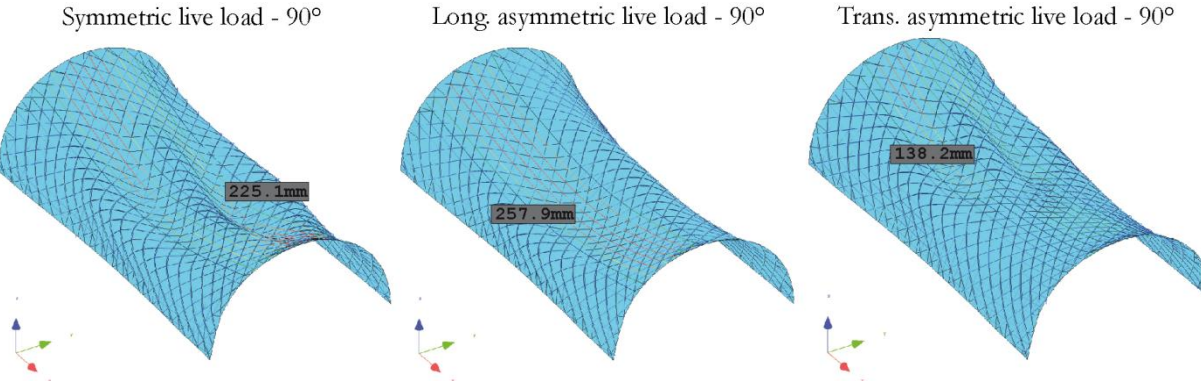


Figure 4-31: Deformation of 90° gridshell under symmetric and asymmetric loading, exaggerated by a factor of 10

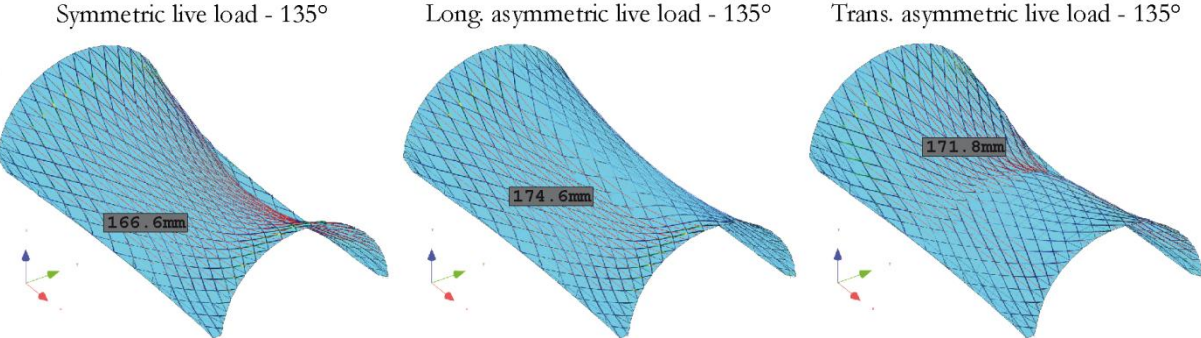


Figure 4-32: Deformation of 135° gridshell under symmetric and asymmetric loading - exaggerated by a factor of 10

Burkhardt et al. in [2] differentiated and qualitatively compared in a load-deformation graphic (see Figure 4-33) the load-bearing behaviour of continuum shells, non-strained and elastic gridshells and cable nets. The bearing capacity of compression-loaded shells under increasing loading is characterised by a progressive, slight diminution of the structure’s stiffness until achieving a

collapse point, principally due to stability problems. Generally, due to their non-interrupted transfer of membrane forces, continuum shells are more efficient and own higher stiffness than gridshells. Contrary to the shells, tension-loaded cable nets are distinguished by a firstly low but rapidly increasing stiffness under growing loading.

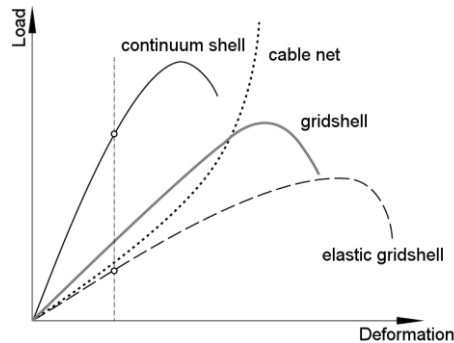


Figure 4-33: Load-deformation curves of continuum shells, non-strained and elastic gridshells and cables nets [2]

The deformability of the three anticlastic gridshells under increasing live loading has been analysed. In Figure 4-34 the maximum nodal displacements in function of the applied load intensity are presented and compared for the symmetric and asymmetric load cases. Generally, one can observe that the load-bearing behaviour of the 45° gridshell – with a transfer of forces dominated by compression forces in transverse direction - resembles that of the shell structures on Figure 4-33; while the 135° gridshell – with a transfer of forces dominated by tensile forces in longitudinal direction - tends to behave similarly to tensile structures. The 90° gridshell exhibits buckling problems under symmetric and transversally asymmetric loading. On this gridshell, lower loads are transversally transferred to the longitudinal edges through compression forces. By higher loads, the grid starts to buckle and loads begin to be carried in longitudinal direction through tensile forces.

Under symmetric loading, the maximum nodal displacements of the three gridshells are similar until a load of about 0.60 kN/m². At this point, the curves of the 45° and 135° intersect and the 90° gridshell buckles. Under higher loads, the highest maximum nodal displacements correspond to the 90° and the lowest to the 135° gridshells. On the case of longitudinally asymmetric loading, differences between the gridshells are stronger. The curves of the 45° and 135° gridshells intersect later, at a load of approximately 1.3 kN/m². The 90° gridshell exhibits the lowest stiffness from the beginning. Under transversally asymmetric loading, the curves of the 45° and 135° gridshells would intersect at a load of approximately 1.2 kN/m² but convergence problems appear by the calculation of the 135° gridshell. The maximum nodal displacements of the 90° gridshell are similar to the 45° gridshell until a load of about 0.60 kN/m², then buckling problems appear and the 90° gridshell starts to strongly deform.

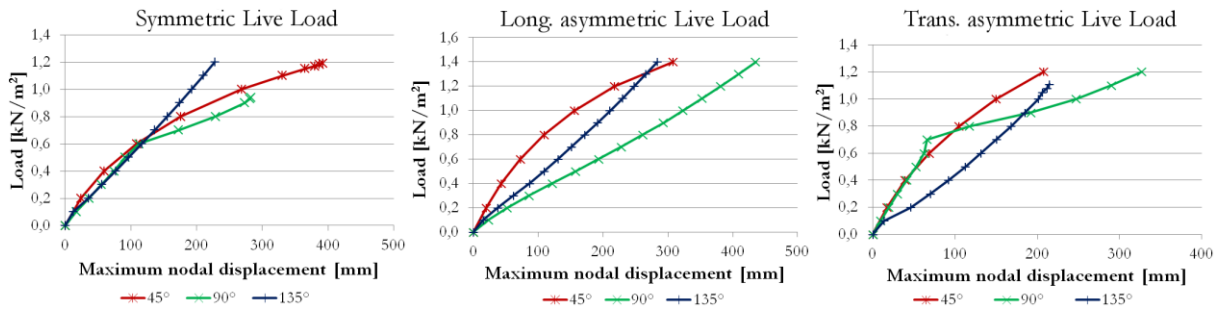


Figure 4-34: Maximum nodal displacements under increasing symmetric, longitudinally asymmetric and transversally asymmetric live loads

Figure 4-35 shows the corresponding maximum equivalent stresses on the gridshells in function of the applied loads. One can see that the equivalent stresses resulting from the bending process are decisive. The increment of the maximum equivalent stresses of the 45° and 135° gridshells is similar for all three load cases. The curves of the 90° gridshell, under symmetric and transversally asymmetric loading, exhibit kink points there where stability problems appear. Moreover, the maximum equivalent stresses of the 90° gridshell increase more rapidly than by the other two gridshells, under growing loading.

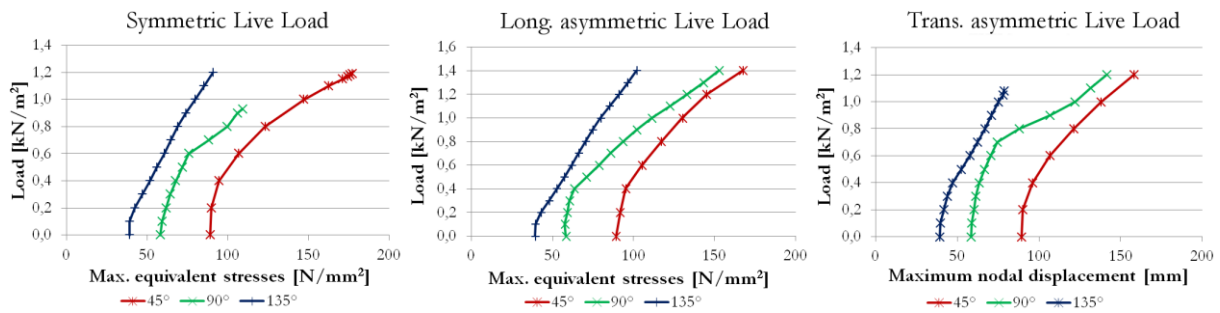


Figure 4-35: Maximum equivalent stresses under increasing symmetric, longitudinally asymmetric and transversally asymmetric loads

4.2.3 Summary

The structural behaviour of three anticlastic regular gridshells with varying grid pattern has been analysed. The grid patterns differ on the shear angle of the initialisation meshes: 45°, 90° and 135° in respect of the transverse axis of the structures. For all the gridshells, it could be confirmed that:

- By removing the external shaping forces, once the grid has been bent and its edges fixed, the grid deforms and acquires a new equilibrium shape. By bracing the grid before deactivation of the shaping forces (**braced grid**), the nodal displacements of the grid are minimal and the target surface can be maintained. Deformations are much higher when the shaping forces are removed before introducing the bracing elements into the grid (**unbraced grid**).

- The **residual** bending moments and material stresses induced on the grids during the shaping process are dominant, as they are significantly higher than those exclusively caused by external loads.

The comparison of the structural behaviours of the three different anticlastic gridshells evidence that:

- The orientation of the grid profiles has an important effect on the **residual stresses**, to which the structure is subjected after its bending process: the maximum profiles' curvature, and with it the maximum bending stresses, are to be found on the 45° grid and the lowest on the 135° grid.
- The orientation of the grid profiles affects also significantly the **distribution of the section forces** on profiles and cables under external loading: the more transversally the profiles are oriented, the stronger the membrane forces are transversally transferred to the longitudinal edges (smallest span length) and, due to the positive curvature in this direction, through compression forces. Inversely, when the profiles are more longitudinally oriented, the structure stiffness on transverse direction is significantly diminished so that only a reduced level of compression membrane forces can be carried in this direction. Once this level is achieved, the grid starts to buckle in transverse direction, its middle deforms downwards and loads start to be carried in longitudinal direction; given the negative curvature in this direction, through tensile forces Tensile forces on bracing cables are higher there where axial forces on the profiles are lower.
- Furthermore, the **load-deformation behaviour** of the gridshells under increasing external loading also depends on the orientation of the profiles. Gridshells with more transversally oriented profiles are more subjected to compression forces and exhibit therefore a shell bearing behaviour. The transfer of forces of gridshells with more longitudinally oriented profiles is dominated by tensile forces and their bearing behaviour resembles that of tensile structures.

4.3 Membrane as Bracing Element

Elastic gridshells are distinguished by its rapid construction process. The use of continuous profiles, which can be elastically bent into a specific shape, saves times and costs given that a less number of elements has to be handled on site and fewer connection have to be assembled. Moreover, in the case of developable gridshells, the grid can be comfortably assembled on its flat position and afterwards bent as a whole. Nevertheless, after the bending process, the grid must be additionally braced in order to provide the structure with in-plane stiffness. Usually the bracing members consist of a third outer layer of diagonal profiles, tensile cables or rigid panels. Their assembling is generally more time-consuming than that of the grid, as the multiple bracing elements must be individually handled, connected in the air to the grid nodes and, in case of using diagonal profiles, bent into the gridshell's geometry. In this manner, one of the great advantages of elastic gridshells is clearly reduced.

In order to optimise the construction process of elastic gridshells, in this chapter it is proposed to employ a membrane surface to cover and at the same time to restrain the grid. Thus, a single membrane surface has to be assembled so that less time is needed for the construction process and material savings are achieved. The use of tensile membranes as restraining element has been already investigated in hybrid arch structures by Alpermann et al. in [65][66][67]. Here, with the introduction of tensile membranes, deformations of the hybrid structures could be efficiently reduced. Their restraining effect strongly depended on the stiffness, prestress and orientation of the membrane as well as on the stiffness of the arch profiles. In the following sections, the potential and limitations of using tensile bracing membranes on elastic gridshells are investigated. A 4-field planar grid and a hemispheric gridshell of 5 m diameter have been considered as application case studies.

4.3.1 Membrane braced 4-field grid

The restraining effect of tensile membranes and its dependence on the membrane properties - orientation, stiffness and prestress - have been firstly studied on a 2 m x 2 m planar 4-field grid. The shear stiffness of the 4-field grid has been analysed by means of finite element methods using the FEA-software Sofistik. The 4-field grid has been punctually loaded by applying a horizontal force on its upper corner: Point A in Figure 4-36. The resulting deformations have been studied.

The 2 m x 2 m 4-field grid is composed of two superposed crossing layers; each layer consists in three parallel continuous profiles. The intersections between the layers take place every 1 m. The profiles own the properties of glass fibre reinforced plastics, with a modulus of elasticity of 25000 N/mm² and have a tubular section, with a diameter of 20 mm and a thickness of 3 mm. The connections between superposed profiles allow scissoring - variation of the angle between profiles - of the grid fields.

The restraining effect of the tensile membrane has been compared with that of plywood panels, diagonal steel cables and GFRP profiles. The corresponding finite element models are illustrated in Figure 4-36. All the bracing elements are connected punctually to the grid nodes. The membrane and plywood panels have been modelled as plane elements, the cables as tensile elements and the profiles as beam elements. In the case of the membrane and plywood panels, the perpendicular contact between panels and grid has been modelled using stiff axial spring elements, which only are activated under compression forces.

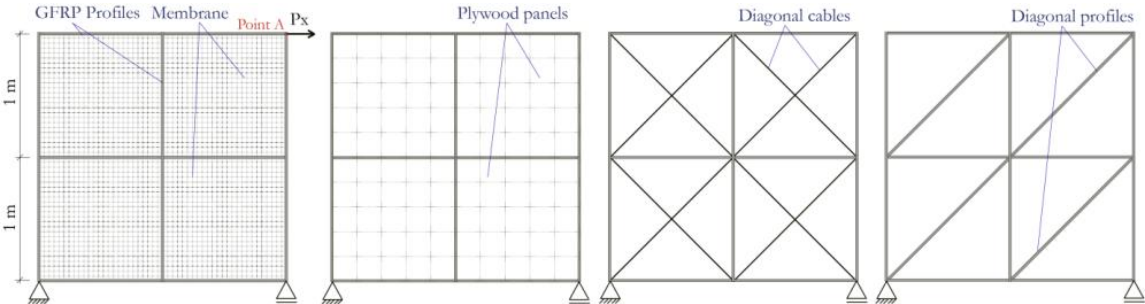


Figure 4-36: Structural system of the 4-field grid with different bracing elements

4.3.1.1 Influence of membrane's orientation

Tensile membranes are usually strongly elastically anisotropic. The influence of the membrane's orientation - orientation of yarn's fibres warp and weft - has been analysed by comparing the shear stiffness of two grids braced with membranes whose yarns are diagonally and longitudinally oriented. Table 4-2 resumes the properties of the membranes used in the finite element models.

Bracing element	Material	Warp/weft orientation
1.a Membrane	Polyester cloth, PVC/PVDF coating Type III, thickness = 1.02 mm Prestress $warp/weft = 0.1 \text{ kN/m}$ $E_{warp/weft} = 1000 \text{ N/mm}^2$ (1020 kN/m)	Diagonal
1.b Membrane	Shear modulus $G = 30 \text{ N/mm}^2$ (30 kN/m) Poisson's ratio $\nu = 0.25$	Longitudinal

Table 4-2: Membrane properties on the models analysing the influence of membrane's orientation

In Figure 4-37 the nodal displacements at Point A by increasing horizontal load can be observed. One can notice that the diagonally oriented membrane provides much higher shear stiffness to the grid than the longitudinally oriented: the nodal displacement at Point A under 0.55 kN is reduced from 175 to 18 mm.

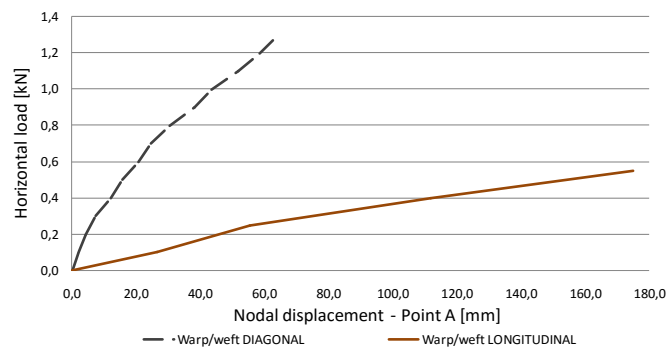


Figure 4-37: Nodal displacements by increasing horizontal load at Point A with membranes with diagonal (blue) and longitudinal (red) orientation of the warp/weft yarns

Figure 4-38 illustrates the distribution of the principal membrane forces on the membrane, which is consequently more effective by the diagonal orientation, and the grid deformation under a horizontal load at Point A of 0.55 kN.

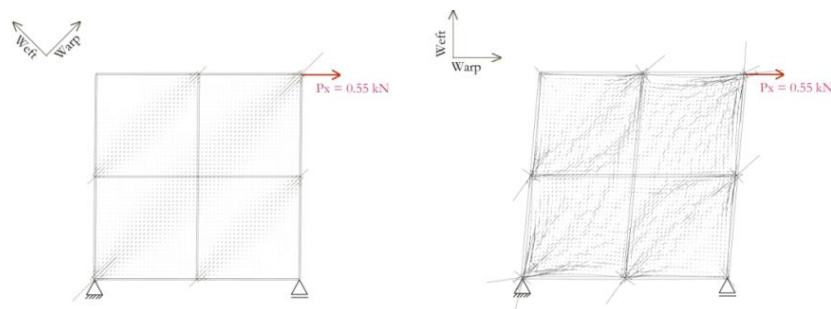


Figure 4-38: Distribution of principal membrane forces and deformation under horizontal load of 0.55 kN at Point A with membranes with diagonal (left) and longitudinal (right) orientation of warp/weft yarns

4.3.1.2 Influence of membrane's stiffness

Membranes dispose of lower axial stiffness than diagonal cables, bars or rigid panels and can only carry in-plane forces, so that they improve principally the shear stiffness of the grid. The mechanical properties of tensile membranes strongly vary depending on the nature of their components - yarn and coating. In order to investigate the influence of the membrane's stiffness on the bearing capacity of the 4-field grid, membranes with varying values of modulus of elasticity have been modelled and their restraining effect has been compared with that of bracing diagonal cables, beams and rigid plane elements. Table 4-3 resumes the properties of the membranes used in the finite element models.

<i>Bracing element</i>	<i>Material</i>	<i>Stiffness</i>
2.a Membrane	Polyester cloth, PVC/PVDF coating, Typ III, $t = 1.02 \text{ mm}$	$E_{\text{warp/weft}} = 500 \text{ N/mm}^2 \text{ (510kN/m)}$
2.b Membrane	Prestress $_{\text{warp/weft}} = 0.1 \text{ kN/m}$	$E_{\text{warp/weft}} = 1000 \text{ N/mm}^2 \text{ (1020kN/m)}$
2.c Membrane	$G = 30 \text{ N/mm}^2 \text{ (30 kN/m)}$	$E_{\text{warp/weft}} = 1500 \text{ N/mm}^2 \text{ (1530kN/m)}$
2.d Membrane	Poisson's ratio $\nu = 0.25$	$E_{\text{warp/weft}} = 2000 \text{ N/mm}^2 \text{ (2040kN/m)}$
2.e Cables	Stainless steel, $d = 6 \text{ mm}$	$E = 130.10^3 \text{ N/mm}^2$
2.f Profiles	GFRP, $d = 20\text{mm}$, $t = 3 \text{ mm}$	$E = 25.10^3 \text{ N/mm}^2$
2.g Panel	Plywood F40/40 E60/40, $t = 4\text{mm}$	$E_{\parallel} = 4400 \text{ N/mm}^2$, $E_{\perp} = 4700 \text{ N/mm}^2$

Table 4-3: Element properties of the models analysing the influence of membrane's stiffness

On the following graphic Figure 4-39, the nodal displacements at Point A of the grids under increasing horizontal load are illustrated and compared to that of grids braced with diagonal steel cables, diagonal GFRP-tubes and F40/40-plywood panels. One can observe that the membrane's stiffness has a strong influence on the deformation of the grid. By a horizontal load of 1.15 kN, the nodal displacement at Point A corresponds to 113 mm, 55 mm, 39 mm and 28 mm for the membranes with moduli of elasticity of 500 N/mm^2 , 1000 N/mm^2 , 1500 N/mm^2 and 2000 N/mm^2 , respectively. Nevertheless, the restraining effect of all the tensile membranes remains significantly lower than that of conventional bracing elements.

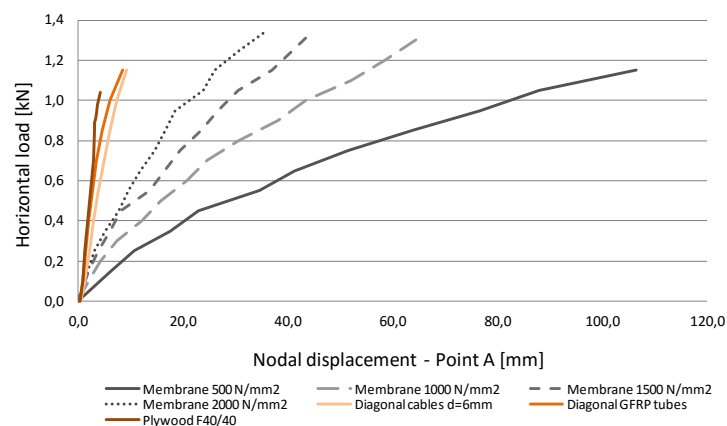


Figure 4-39: Comparison of restraining effect of tensile membranes of different stiffness with diagonal cables, diagonal GFRP tubes and plywood panels by the deformation of the 4-field grid under increasing horizontal point load

The final choice of the membrane's stiffness should however consider its constructive consequences. The higher the stiffness is, the more complex its confection and handling on site will be. Figure 4-40 illustrates the deformation of the 4-field grid under a horizontal point load of 1.15 kN, braced with membranes with moduli of elasticity of 500 N/mm² and 2000 N/mm² - exaggerated by a factor of 2 - and with diagonal cables, bars and plywood panels - exaggerated by a factor of 5.

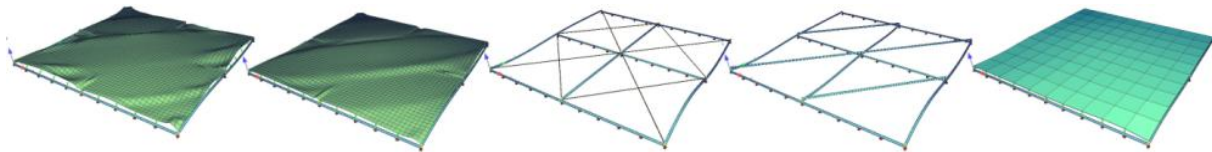


Figure 4-40: Deformation of 4-field grid braced with membranes with $E = 500 \text{ N/mm}^2$ and $E = 2000 \text{ N/mm}^2$ - exaggerated by a factor of 2 -, diagonal cables, bars and plywood panels - exaggerated by a factor of 5 - under a horizontal load of 1.15 kN at Point A

4.3.1.3 Influence of membrane's prestress

Membranes are light structural elements as they are supposed to carry principally tensile forces and are therefore not subjected to stability problems. If compression acts on the membrane, it can lose its stress and wrinkles can appear. In order to avoid this and to increase the structure's stiffness, prestress is induced on the membrane. In the case of the 4-field grid, four models with different prestress levels have been defined and the distribution of the principal membrane forces as well as the shear stiffness of the grid have been analysed.

Bracing element	Material	Prestress
3.a Membrane	Polyester cloth, PVC/PVDF coating	$v_{warp,weft} = 0.1 \text{ kN/m}$
3.b Membrane	Typ III, thickness = 1.02 mm Prestress warp/weft = 0.1 kN/m	$v_{warp,weft} = 1.0 \text{ kN/m}$
3.c Membrane	Ewarp/weft = 1000 N/mm ² (1020 kN/m) Shear modulus $G = 30 \text{ N/mm}^2$ (30 kN/m)	$v_{warp,weft} = 1.5 \text{ kN/m}$
3.d Membrane	Poisson's ratio $\nu = 0.25$	$v_{warp,weft} = 2.0 \text{ kN/m}$

Table 4-4: Element properties of the models analysing the influence of membrane's prestress

The following Figure 4-41 illustrates the nodal displacement of the 4-field grid braced with membranes with varying prestress level ($v_{warp/weft} = 0.1, 1.0, 1.5$ and 2.0 kN/m) under increasing horizontal loads. For prestress levels of 1.0, 1.5 and 2.0 kN/m, one can notice a kink on the curves at horizontal loads of 0.5, 0.7 and 0.9 kN, respectively. This kink corresponds to the loss of tensile stress on the diagonal receiving compression forces. Inducing higher prestress on the membrane, this kink appears later and the deviations at Point A can be considerably reduced: for example, from 64 mm to 40 mm with prestresses of 0.1 and 2.0 kN/m, under a horizontal load of 1.3 kN.

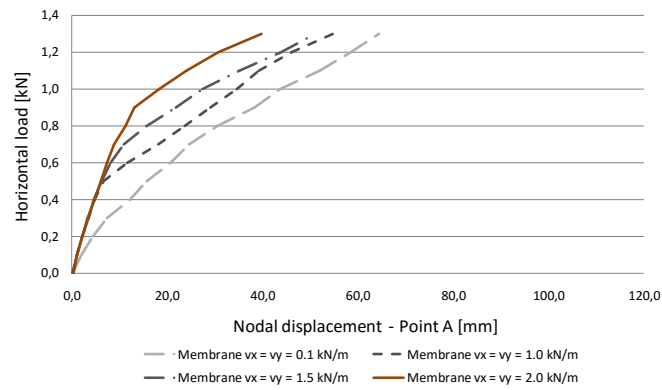


Figure 4-41: Nodal displacements by increasing horizontal loads at Point A in grids braced with membranes with prestress levels in warp and weft of 0.1, 1.0, 1.5 and 2.0 kN/m

Figure 4-42 shows the principal membrane forces of the restraining membranes with 0.1 and 2.0 kN/m prestress by horizontal loads of 0.2, 0.8 and 1.3 kN. One can observe that, with a higher prestress level, the membrane carries forces on the diagonal subjected to compression until the tensile stresses are consumed on this direction.

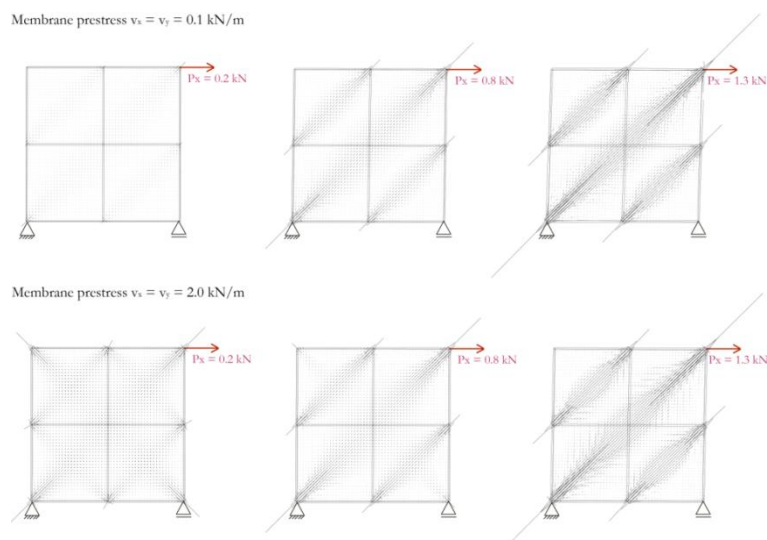


Figure 4-42: Principal membrane forces of restraining membranes with 0.1 (top) and 2.0 kN/m (bottom) prestress for horizontal loads of 0.2, 0.8 and 1.3 kN

4.3.2 Membrane braced gridshell – Hybrid Hemisphere

The aim of this section is to investigate the restraining effect of tensile membranes on a doubly-curved elastic gridshell. A hemispheric regular gridshell of 5 m diameter and 0.74 m mesh size has been considered as example. The analyses focus on the influence of the connection conditions between grid and membrane: with and without connection at the grid nodes. The structural analysis has been performed using finite element methods using the FEA-package of SOFISTIK. The structure has been calculated according to the third-order theory: material non-linearities (e.g. on the spring elements defined along the profiles and connected to the membrane, which

are used to simulate contact between them and are able to carry only compression) and effects of the geometrical modification of the structure (e.g. variation of the structure's stiffness under large deformations) are considered.

4.3.2.1 Description of Finite Element Model

The grid profiles own the properties of glass fibre reinforced plastic, with a modulus of elasticity of 25000 N/mm^2 , and have a tubular section of 2 mm diameter and 3 mm thickness. The membrane corresponds to a Ferrari Précontraint 1302 S2 with polyester cloth and PVC/PVDF coating ($E_{\text{warp/weft}} = 1500/1200 \text{ N/mm}^2$, $t = 1.02 \text{ mm}$) and the warp and weft yarns are oriented in meridian and radial directions. The connections between the superposed grid layers have been modelled as coupling elements: a hinged connection at the upper layer to a rigid node at the lower layer.

For the connection between grid and membrane, two types of stiff spring elements have been used. The first type corresponds to springs with only axial stiffness, modelling the perpendicular contact of the membrane over the grid. They are defined along all the beam elements, their direction is approximately normal to the membrane surface, they can only carry compression forces and they own a stiffness coefficient of 10^3 kN/m . The second type corresponds to the connection of the membrane at the grid nodes. They are defined only at the grid nodes and their direction is also normal to the membrane's surface. They have axial and lateral stiffness with coefficients of 10^3 kN/m .

Hinged supports have been defined at the profiles' ends. The edge supports of the membrane are also modelled using spring elements with axial and transversal coefficients of 1 kN/m . These spring coefficients have been defined after benchmarking the finite element model with the prototype described in Chapter 5.

The numerical modelling consists of two parts. Firstly, the bending process of the grid is simulated using 129 virtual shaping cables. As the grid is regular, the profiles of the superposed layers are connected on the initial flat position of the grid and this is bent as a whole. It is this bent geometry, with still activated shaping forces, which has been considered to define the membrane's geometry: the coordinates of the membrane have been calculated by projecting the coordinates of the bent grid in radial direction, by a distance of the radius of the GFRP tubes – along the upper profiles' layer – or 1.5 times the diameter of the GFRP tubes – along the lower profiles' layer. The shaping forces are removed, once the grid has been already fixed at its edges and the membrane and the corresponding connection elements have been introduced. Afterwards, the external loads have been applied at the grid nodes as point loads.

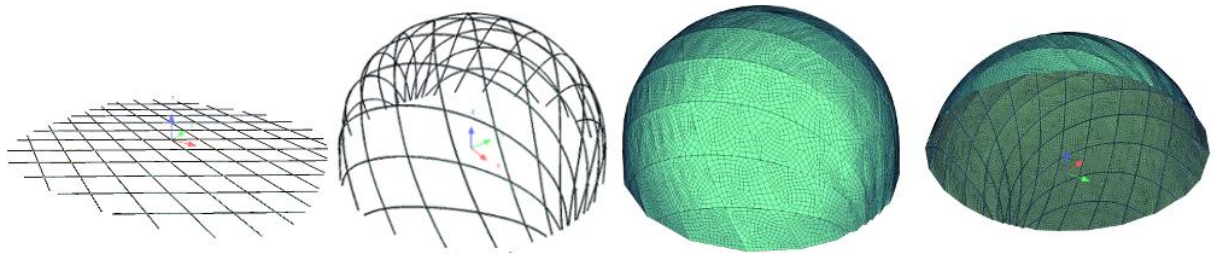


Figure 4-43: Finite Element Model of hybrid elastic gridshell: planar geometry, bent geometry with shaping forces and bent geometry after removing shaping forces with membrane, from the outside and the inside

4.3.2.2 Study of the influence of connection between grid and membrane

The joining of the membrane to the grid nodes is time-consuming and requires the design and manufacture of adequate constructive details. Therefore, it is important to estimate its structural effects on the gridshell. In this chapter, the bearing behaviour of the grid under permanent and asymmetric external loading has been calculated and compared for three systems: grid without membrane, grid with membrane without joining at the grid nodes and grid with membrane with joining to the grid nodes. The permanent load consists on the dead load of the structure and the inner forces induced by bending the grid. The external load corresponds to vertical point loads, which have been applied over one half of the grid.

4.3.2.3 Permanent loads

Once the grid has been bent in a specific geometry and fixed at its edges, when the external shaping forces are removed, the grid searches and adopts a new equilibrium's geometry. This new geometry varies depending on if the grid has been braced or not before removing the shaping forces. Figure 4-44 illustrates the nodal displacements of the three grid configurations, once the shaping forces are deactivated. Compared to the unbraced grid, one can see that, using the membrane as bracing element without joining at the grid nodes, the upward deformation at the top and the outwards deformation at the sides (sides without singularity points on the grid), are reduced: the maximum nodal displacements decrease from 36 mm to 6 mm at the top and from 92 to 25 mm at the sides. The inward deformations at the sides (with singularities or higher concentration of profiles) could be also, but in less measure, optimised: from 98 to 42 mm. By joining the membrane at the grid nodes, its restraining effect is more efficient: deformations could be reduced over the whole grid to a maximum value of the nodal displacements of 32 mm.

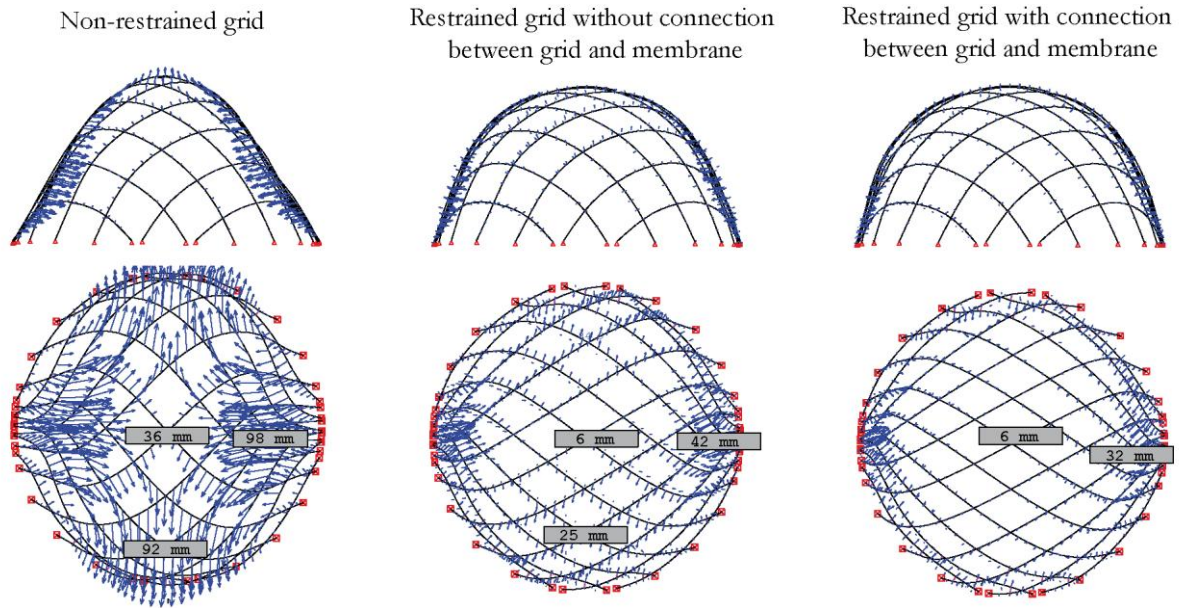


Figure 4-44: Nodal displacements and deformation - exaggerated by a factor of 5 - of the grids by removing external shaping forces

4.3.2.4 Asymmetric load

The restraining effect of the membrane and the influence of the connection to the grid are more evident under the action of external forces, as here a higher shear stiffness of the structure is necessary. Half of the hemispheric grid has been loaded with vertical loads of 0.2 kN at 47 grid nodes (Total load = 9.4 kN, Projected area = 9.8 m²), as illustrated in Figure 4-45.

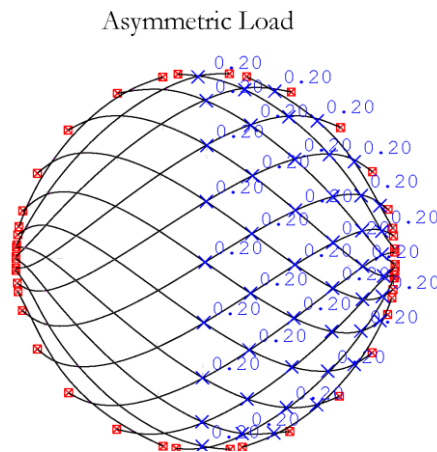


Figure 4-45: Loaded grid nodes

Figure 4-46 shows the grid deformations and nodal displacements of the three grid configurations. The restraining effect of membrane achieves to reduce the maximum nodal displacements of the grid from 264 mm to 95 and 63 mm, without and with joining at grid nodes.

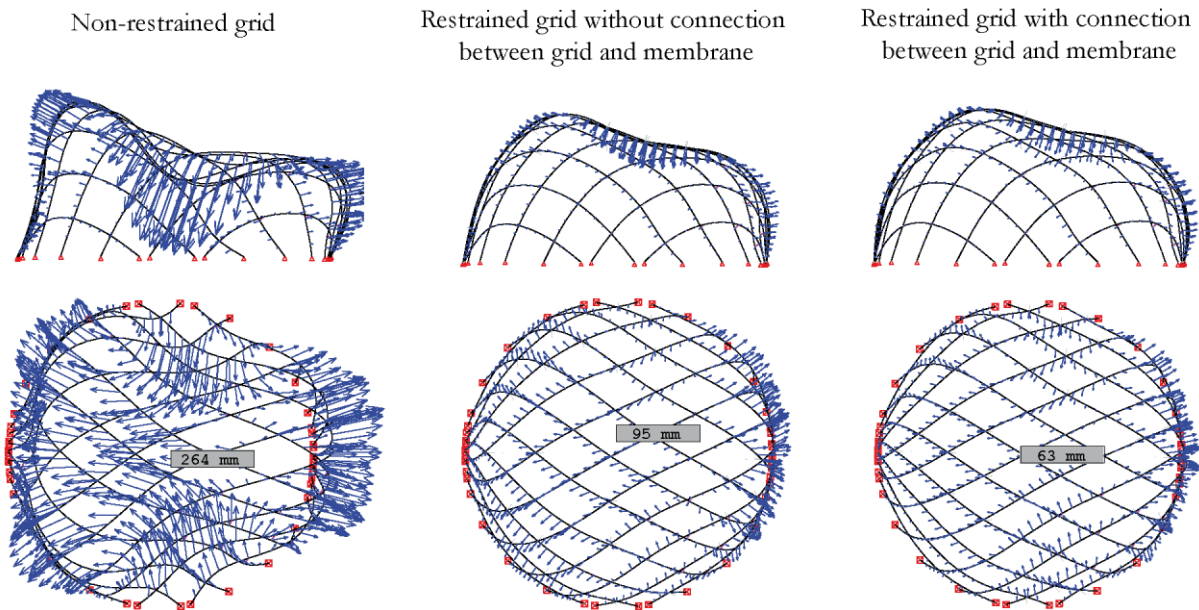


Figure 4-46: Nodal displacements and deformation - exaggerated by a factor of 5 - under asymmetric load

4.3.2.5 Equivalent stresses

The introduction of shear stiffness on the grid has an influence not only on the deformability of the structure but also on the material stresses resulting on the grid profiles. Figure 4-47 shows the equivalent stresses before and after applying asymmetric external loads. One can observe that, with the membrane, maximum residual stresses on the bent grids, which are located on the sides with outward deformations, could be minimally reduced: from 166 to 160 (without joining to grid) and 159 N/mm² (with joining to grid). A higher optimisation is achieved when loading the grid with external forces. On the unbraced grid, stresses mostly increase at the non-loaded half of the top of the grid, attaining a maximum value of 185 N/mm²; on the other half stresses decrease, as the curvature of the profiles gets here lower when loading them vertically. Changes on the maximum stresses of the membrane-restrained grids, before and after external loading, are minimal: maximum equivalent stresses of 158 and 164 N/mm² are obtained under asymmetric load.

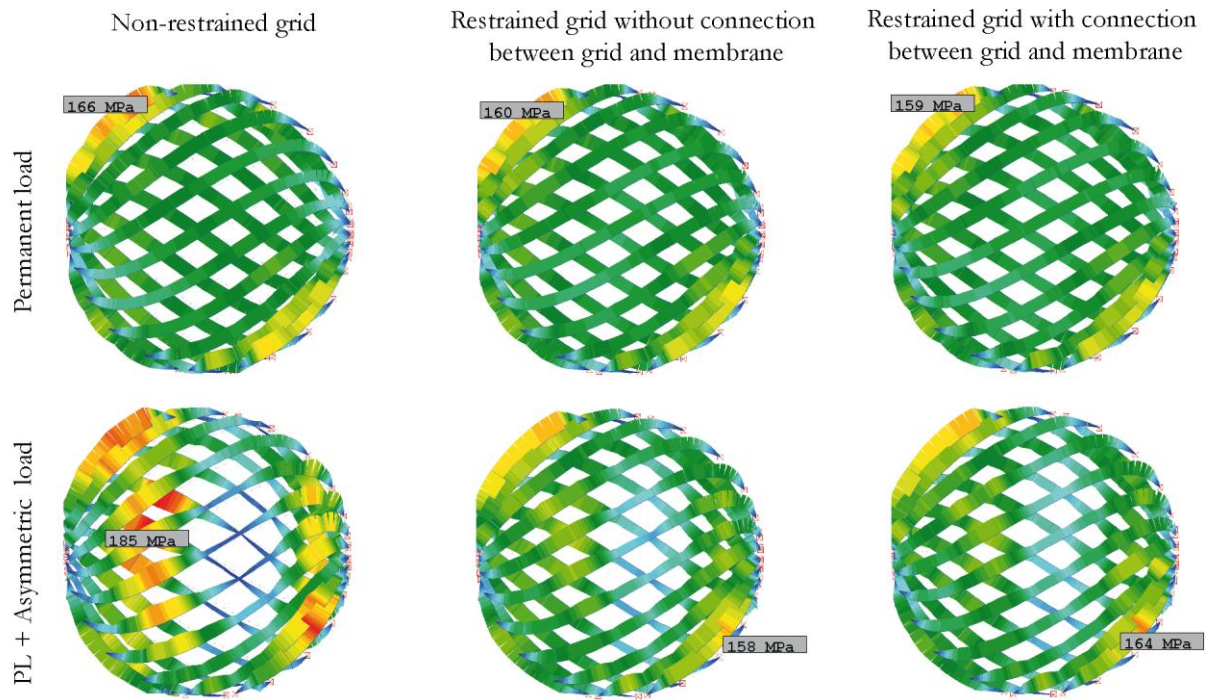


Figure 4-47: Equivalent stresses under permanent loads, without (up) and with (bottom) asymmetric load

4.3.3 Summary

The restraining effect of tensile membranes on a planar grid has been studied. The results confirmed that:

- Membranes with diagonally oriented yarns afford much higher shear stiffness to the grid that membranes with parallel oriented yarns.
- Membranes with higher stiffness offer a stronger reduction of the grid's deformations. Compared to conventional bracing elements as crossing cables and a diagonal profiles, the restraining effect of the tensile membrane remains nevertheless moderate.
- Inducing prestress on the membrane, it can carry a certain level of forces in the diagonal receiving compression, thus deformations are more strongly reduced.

The restraining effect of a tensile membrane on a hemispheric grid has been also studied. The analyses focus on the influence of the connection conditions between grid and membrane: with and without joining at the grid nodes. The results evidence that:

- By using a restraining membrane without joining to the grid, deformations of the bent grid after removing the shaping forces are reduced, there where the grid deforms upwards and outwards. By connecting the membrane to the grid nodes, its restraining effect can be optimised and deformations decrease over the whole grid.

- Similar consequences appear when loading the grid with asymmetric external loads. The nodal displacements of the non-braced grid can be strongly reduced introducing shear stiffness through the tensile membrane; particularly when joining the membrane to the grid nodes.
- The residual stresses due to the bending process of the grid are dominant for all the structures. Differences on the equivalent stresses between non-braced and braced grids under permanent loads are minimal; they become a bit more significant under external loading.

The bracing effect of tensile membranes on elastic gridshells strongly depends on constructive aspects like the connections at the grid nodes or the achievement of wrinkle-free surfaces. In order to benchmark the finite element model, a physical prototype has been built and its bearing capacity has been compared to that of the numerical simulation. The results of the comparative analyses are presented in Chapter 5.

5. Experimental Validation

5 Experimental Validation

Numerical techniques are commonly used for the calculation of stress distributions and displacements of complex indeterminate bearing structures. Nevertheless, to model the elements they are composed of and the connection properties between them, simplifications and approximations are done. The purpose of this chapter is to analyse the influence of these simplifications on the results of the simulation and thereby recalibrate and benchmark the numerical models with physical prototypes.

5.1 Construction of a Developable Irregular Elastic Gridshell

As shown in Chapter 3, allowing the mesh size of a grid vary during its optimisation (*irregular mesh*), a higher reduction of the profiles' curvature can be achieved. However, it is important to consider the consequences of using a grid with variable edge length on the load-bearing behaviour and construction process of elastic gridshells. Modifying the mesh size and with it the material distribution of the grid, the local and global stability as well as the stiffness of the gridshell changes. An evaluation and restriction of a maximum allowable edge length during optimisation is therefore advantageous.

The transformation of a regular into an irregular grid also complicates the shaping process of the grid from a completely flat position, as the grid loses its degree of freedom on scissoring. Therefore, by the construction of irregular gridshells, the grid profiles are usually bent independently from each other in an incremental process, generally more time-consuming than that of regular gridshells. Nevertheless, if the bending stiffness of the profiles is low enough, large deformations can be induced on them and, in some cases, the irregular grid can be developed into a flat configuration. However, to permit the flat configuration, the profiles must be here already bent, instead of being straight as on the regular grids. The degree of deformability of the grid depends on the surface geometry and pattern of the structure.

By designing elastic gridshells, it is important to control that the material stresses on the profiles do not exceed the allowable ones during the construction process. The stresses to which the grid profiles are subjected can be controlled for example using numerical simulation. In the case of irregular gridshells, in order to reduce the bending stresses during the shaping process, the grid can be partially assembled in the start configuration and the resting border profiles and connections introduced after bending the grid.

This erection method has been used for the construction of an elastic hemisphere with irregular grid and 10 m diameter. This section focuses on its design, construction and the comparison of the geometry and bearing behaviour of the prototype with those obtained by the numerical simulation.

5.1.1 Grid design

The investigated gridshell was originally planned for a digital all-dome projection system with spherical screen of 10 m diameter, as illustrated in Figure 5-1. The construction consists on a lightweight hybrid structure composed of an irregular elastic gridshell and a double layer vacuum PVC polyester membrane. The vacuum between the two membranes - the one lying over and the other under the grid - sucks the outer membrane to the grid, generating constant radial forces on the gridshell, and holds the inner membrane in place at a distance of 100 mm. As the surface geometry of the structure - a sphere - was already predefined due to functional reasons, investigations concentrate on the grid optimisation and construction process.

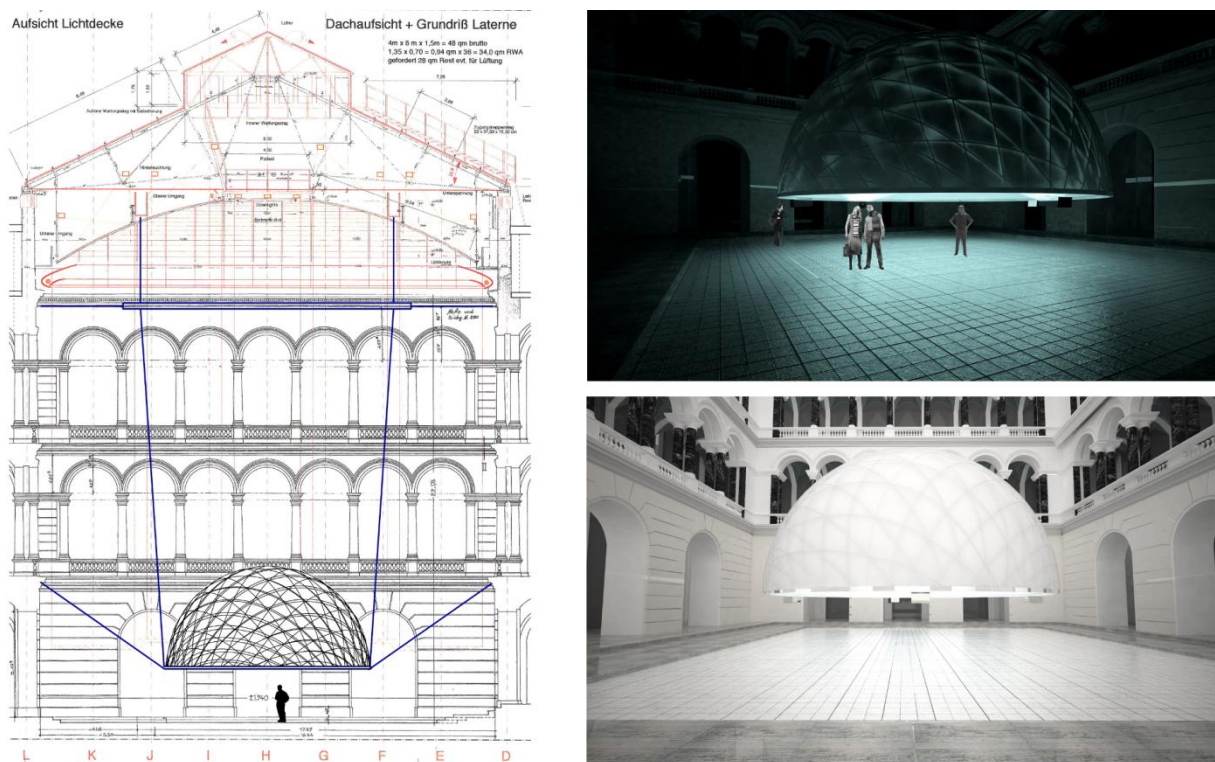


Figure 5-1: Design of the all-dome projection system with an elastic gridshell as bearing structure

The grid pattern has been determined using the design approach, based on variational principles, described in Chapter 3. Firstly, the target geometry of a sphere with 10 m diameter has been defined as NURBS-surface and afterwards converted into a polyhedral mesh with the 3D-modeling software Rhino. Secondly, the polyhedral mesh has been conformally remeshed with an initialisation angle between edges of 45° and this mesh has been optimised in terms of profile's curvature by means of variational principles with the modular software of VaryLab. The optimisation of the initialisation mesh has been performed as regular and as irregular meshes. For the edge length energy, a target value of 1 m has been assigned for the regular mesh and a range between 0.5 m and 1.5 m for the irregular mesh. The weighting factors for the reference surface, segment length and curvature energies corresponded to 4, 6-8 and 4-6 for the regular mesh. By the irregular mesh, they varied from 6-10, 4-8 and 8-14. The maximum and average resulting distance to the 10 m diameter reference sphere were 8.5 cm and 1.9 cm for the regular grid and 6.3 cm and 3.1 cm for the irregular. The edge length of the irregular mesh varies from 0.66 m to

1.20 m. However, it is important to remark that, the length of the profiles for the real structure, is not directly taken from the edges' length but from interpolated curves, passing through the mesh's vertices, which have been traced in Rhino.

In the following Figure 5-2 the resulting grid patterns with regular mesh (middle) and irregular mesh (right) are compared with that defined with the compass method (left). One can observe that the segments of the grid with regular mesh tend to follow an S-curve orientation and to concentrate in two opposite singularity points. By the irregular mesh the singularities disperse. The segment length here increases from the lower edge to the crown of the hemisphere, in part influenced by the configuration of the initial conformal mesh, which has a similar distribution.

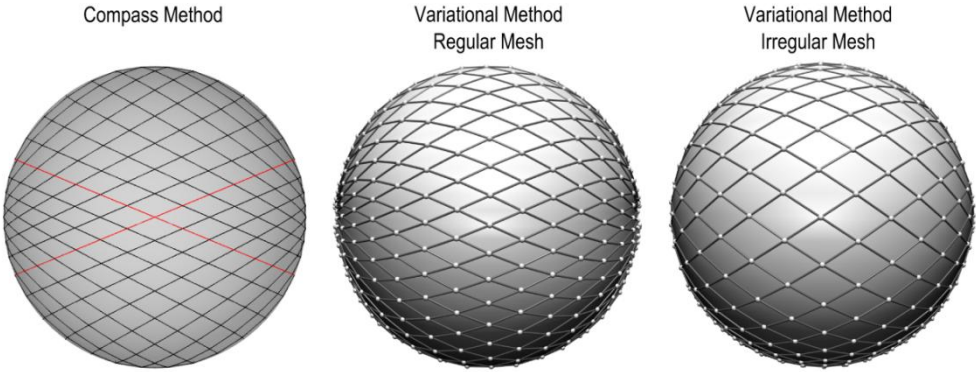


Figure 5-2: Comparison of grid patterns determined with the compass method (left) and the variational approach with regular (middle) and irregular (right) meshes

The grid pattern defined with the compass method presents a maximum profiles' curvature of 0.355 m^{-1} . After optimisation using the variational method with regular and irregular meshes, the maximum curvature could be respectively reduced to 0.311 and 0.281 m^{-1} . A curvature of 0.340 m^{-1} was found by Bouhaya et al. in [10] by means of genetic algorithms. A further optimisation was not carried on to avoid too high concentrations of profiles. Nevertheless, it would be possible to further reduce the profiles' curvature, by exploring different initialisation meshes and modifying the energies' weighting factors during the optimisation [11]. Before construction, the distribution and orientation of the grid profiles was studied in a 1:10 physical model, shown in Figure 5-3.



Figure 5-3: Physical 1:10 modelling of the irregular hemisphere

As the structure was initially planned for indoor spaces and the loading coming from the vacuum between the outer and inner membranes, equivalent to 0.05 kN/m^2 with a security factor of 5, was relatively low, bracing could be simplified by triangulating the grid every two meshes with an outer third layer of profiles, which reduced the number of elements to be bent and assembled to the already shaped grid.

5.1.2 Numerical simulation

The objective of the numerical simulation is, on the one hand, to evaluate the geometry resulting from the bending process, which becomes important when calculating the stability of the structure or planning the cladding's geometry; on the other hand to control that the material stresses do not exceed the allowable ones during the construction process and under external loading.

The bending process and load-bearing behaviour of the irregular hemisphere have been modelled and analysed with a non-linear three-dimensional finite element model, defined with the FEA-package of Sofistik. The bending of the grid has been generated using the simulation methodology suggested by Lienhard et al. in 2011 [62], in which 498 virtual cables with minimal stiffness are defined between the start and target geometries of the elements to be bent and their shaping is induced by prestressing these cables and, consequently, reducing at maximum their lengths. Further details of the calculation of actively-bent structures using finite element models have been given in Chapter 4.

The modelled GFRP grid is composed of beam elements with a tubular section of 20 mm diameter and 3 mm thickness and an elasticity modulus of 25 GPa. The profiles' ends have been fixed with hinged supports. The connections between the superposed layers have been modelled with varying rigidity to analyse their influence on the structural behaviour of the gridshell. In the first model they are defined as coupling elements: hinged connection at upper layer to a rigid node at the lower layer. In the second and third models, they have been simulated as spring elements with axial and transversal coefficients of 100 and 10 kN/m and 10 and 5 kN/m, respectively. Different values for the stiffness coefficients have been tested; the chosen values provide deformations which are similar to those of the prototype. The spring elements have been oriented in radial direction. The eccentricities between superposed layers are considered so that moments generated by transverse forces are transferred to the grid nodes. Both simulations have been illustrated in the following figure.

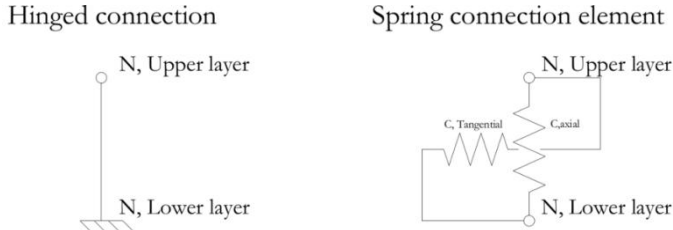


Figure 5-4: Grid connections modelled as hinged coupling and spring elements

Contrary to regular meshes, the start flat geometry of irregular grids is not evident: as scissoring of the grid is restricted, the profiles cannot be straight in the flat geometry but they must be bent to allow it, which induces material stresses from the very beginning of the erection process. In order to control the stresses generated in the plane position of the grid and during its shaping process, the deployment of the grid has been simulated. This simulation consists of two phases. Firstly, the grid profiles of the first and second layers have been bent, independently from each other, into the predefined configuration geometry. Then, both layers have been connected at the intersection points through hinged coupling or spring elements and the profiles' ends have been fixed with hinged supports. Afterwards, the shaping forces on the grid and the supports have been incrementally removed so that the grid relaxes and adapts new equilibrium positions, in which it has been controlled that the stresses on the profiles don't exceed their bending strength. The contact to the ground has been modelled using stiff spring elements at the grid nodes, with the property of being able to carry forces only after their deformation exceeds a certain gap - the distance from the grid nodes to the ground -, which corresponds to the moment where the grid lies on the ground. Because of the large deformations during the deployment of the grid, the process had to be gradually modelled in seven steps; after each step the definition of the spring gaps is actualised. In Figure 5-5 the grid geometry is illustrated for five different deployment stages: from left to right, the supports on the profiles' ends are incrementally released. During the erection process of the gridshell, to minimise the bending stresses on the grid, the profiles carrying the highest bending moments - the 12 shortest profiles located at the grid sides without singularity points - were not installed on the flat configuration but added afterwards on the bent grid. The grid has a total of 38 profiles. In the same way, these border profiles were not introduced on the simulation of the deployment process of the grid.

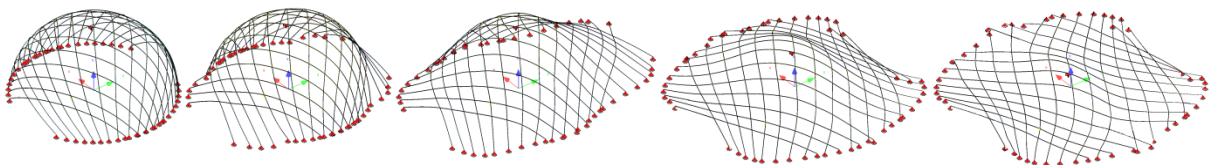


Figure 5-5: Numerical simulation of the deployment of the grid to analyse the material stresses at its starting flat position and during construction process

The profiles of the bracing third layer have been bent in the numerical model in the same way than for the first two layers and have connected to the grid with the same coupling and spring elements. Figure 5-6 shows the modelled grid before and after adding the bracing layer. With the partial triangulation of the grid, the shell capacity of the structure is activated and external loads can be applied. Point loads, which represent the sand bags with which the physical model has been loaded, have been defined at the grid nodes.

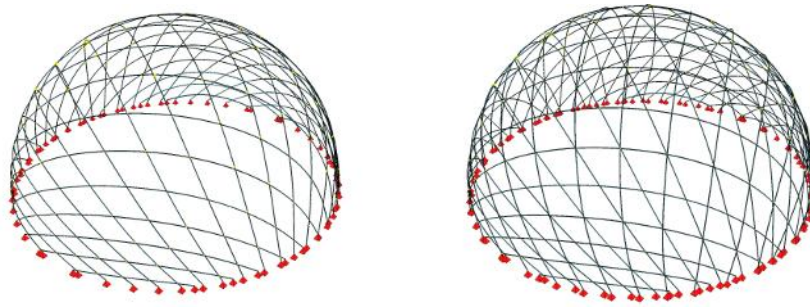


Figure 5-6: Modelling of grid without and with bracing layer of profiles

The resulting maximum equivalent stress of the shaped grid after bracing corresponds to 72.9 MPa, which represents a material utilisation of approximately 52%, considering load and material safety factors of 1.5 and 1.2 as recommended in [68] and a bending strength of the GFRP tubes (Co. Fibrolux GmbH) of 250 MPa. The maximum curvature values of the profiles in y- and z-axes are similar, which results on comparable bending moments in both axes. The choice of a rotationally symmetric section is therefore optimal. In Figure 5-7 the bending moments in y- and z-axes of the final grid have been illustrated. While the maximum bending moments in y-axis are located on the sides with stronger concentration of profiles, the maximum bending moments in z-axis are to be found on the opposite side. Compared to the bending moments, axial forces do not imply, initially, significant material stresses. The maximum equivalent stress of the third layer of profiles represents 86.2 MPa. As mentioned in Chapter 3, future research should concentrate on integrating the bracing layer, if this one is also elastically bent, in the optimisation process. The prototype has been tested under incremental external point loads until achieving stability problems on the grid. Maximum equivalent stresses of 174 MPa have been obtained with the numerical simulation.

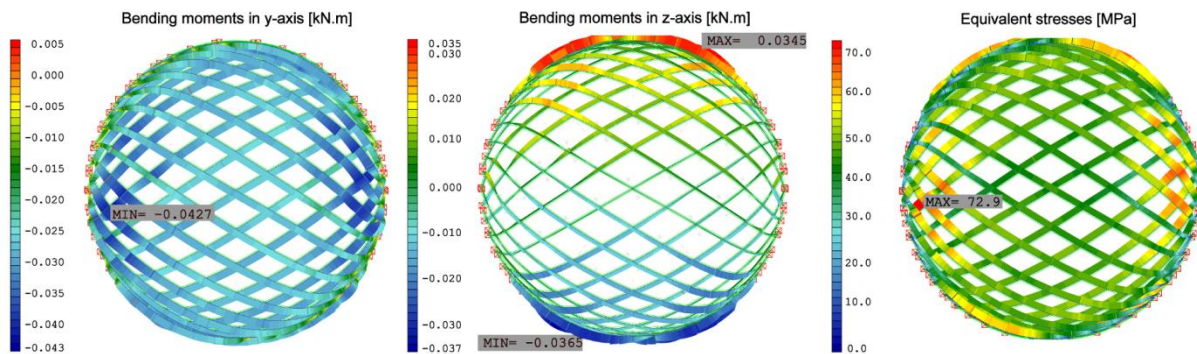


Figure 5-7: Resulting moments in y- and z-axes and maximum equivalent stress on the bent grid after bracing

5.1.3 Construction

The gridshell is composed of GFRP profiles of 20 mm diameter and 3 mm wall thickness. Aluminium tubes, with an inner diameter of 20 mm, were used to prolong the profiles, as the highest deliverable length of the GFRP rods was 6 m. Tests were done to observe the influence of the connection's length on the profile's curvature. Two GFRP rods of 6 m were connected

with aluminium tubes of 40, 80 and 120 mm. The prolonged rods of 12 m were bent by approaching their ends to a span of 6 m. In Figure 5-8 the curvature of the rods at the connected point has been compared with that of the *elastica* curve. While the rods with the 80 and 120 mm long connections shown similar curvatures, the rod with the 40 mm long connection exhibited a notable kink at the joining point and higher differences to the *elastica* curve. A length of 80 mm was finally chosen because of economic reasons.

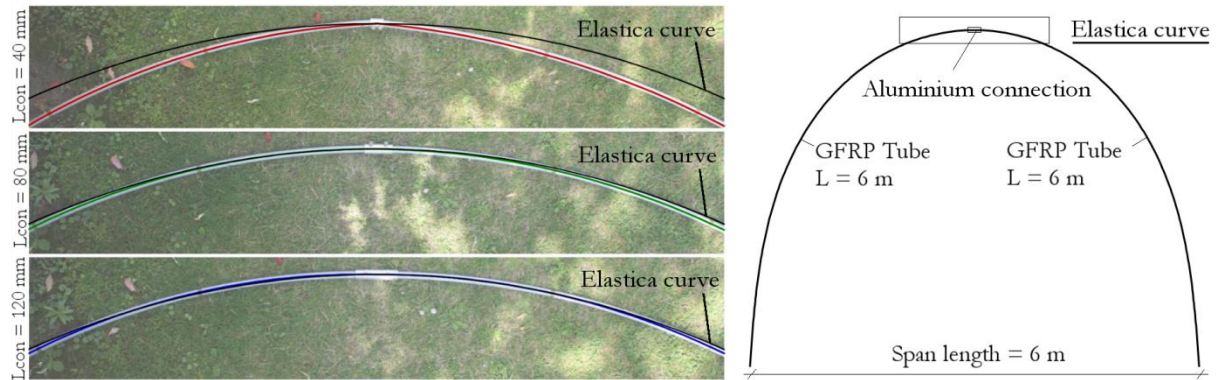


Figure 5-8: Influence of the length of the aluminium connection tube on the curvature of the prolonged profiles

In Figure 5-9 the aluminium connection tubes at the prolongation points and the connection clamps between superposed layers at the grid nodes are illustrated. To fix the profiles into the aluminium tubes, two hexagon sockets have been used, which can be screwed into the aluminium tubes until reaching contact to the GFRP tubes. For the interlayer connections, double and triple swivelling pipe clamps with inner rubber walls have been chosen. Single pipe clamps with screwed threaded pins have been used for the connections of the tubes to the edge ring, made of OSB-plates. The length of the pins could be adapted according to the distance between grid layers and ring. The weight of the grid structure - profiles and connections - and that of the edge timber ring were 211 and 175 kg, respectively.



Figure 5-9: Aluminium tubes with contact hexagon sockets (left) were used to prolong the rods, double and triple (left, middle) swivelling pipe connections to connect the grid layers and single pipe clamps with screwed threaded pins to connect the rods to the edge timber ring

In order to simplify the construction of the hemisphere and reduce the use of scaffoldings, it was planned to bend the structure as a whole grid. Figure 5-10 illustrates four stages of the construction process of the hemispheric gridshell. At the top-left corner one can see the flat grid being assembling on the ground. As the grid owns an irregular mesh, the profiles are already bent at the initial plane configuration. To reduce the bending stresses, the border profiles, which were subjected to critical bending moments, were not installed at the grid's initial flat state but after

being bent. On the top-right corner, the bending of the grid is induced by pushing it upwards using four bars and bringing the profiles' edges simultaneously into their final position on the edge ring. After fixing the grid on the edge ring, the rest of the profiles were included. On the bottom-left corner, the bracing outer layer is installed using one scaffolding tower on the interior of the structure. The hemisphere was built over eight podiums, in order to be able to transport the scaffolding system from the outside to the interior of the structure and vice versa. The complete gridshell is finally to be observed on the bottom-right corner.

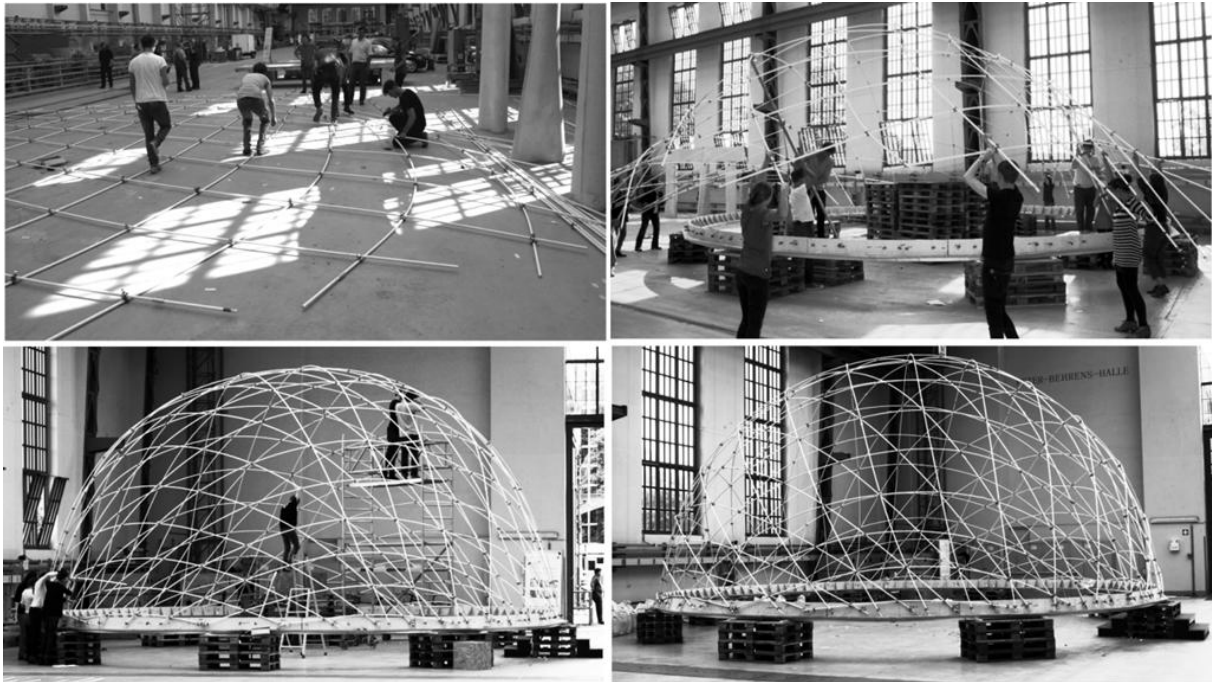


Figure 5-10: Construction process of the irregular elastic hemisphere

Before starting with the erection process, the positions of the grid intersection points were marked on the three layers. Once the grid was bent and fixed to the edge ring and the shaping forces removed, it adopted a relaxed geometry influenced by the inner forces induced during the bending process. By installing the third layer and connecting it to the grid at the intersection points, the structure should acquire the designed geometry (*shaping function* of bracing elements). That was performed with only manpower as the grid stiffness was relatively low. Nevertheless, due to the residual forces to be overcome at some points and due to sliding in some pipe clamps, the exact position of the connection points could not always be assured.

After bracing the grid with the third layer of profiles, the structure was loaded quasi-symmetrically and asymmetrically with hanging sandbags in order to analyse its bearing capacity and compare it with that of the numerical model. With a three-dimensional laser scanner (FARO® Laser Scanner Focus^{3D}) the coordinates of 38 intersection points, which were pre-marked with black and white identification labels, could be registered during the loading tests. Figure 5-11 shows the loaded structure and the scanner device.



Figure 5-11: Hemispheric gridshell during loading tests and registration of the resulting deformations using a three-dimensional laser scanner

In Figure 5-12 the designation of the registered points and the position of the hanging sandbags are given. The points' designation follows the orientation of the third layer so that points with the same first digital number belong to the same bracing profile. Two quasi-symmetric load cases were applied, where weights of 20 or 30 kg were hung at 34 intersection points. On the two first asymmetric load cases, the structure carried weights of 20 and 30 kg at 19 intersection points. On a third asymmetric load case, where weights at 18 intersection points were increased from 30 to 40 kg, local stability problems were attained and large deformations could be observed at the top of the structure.

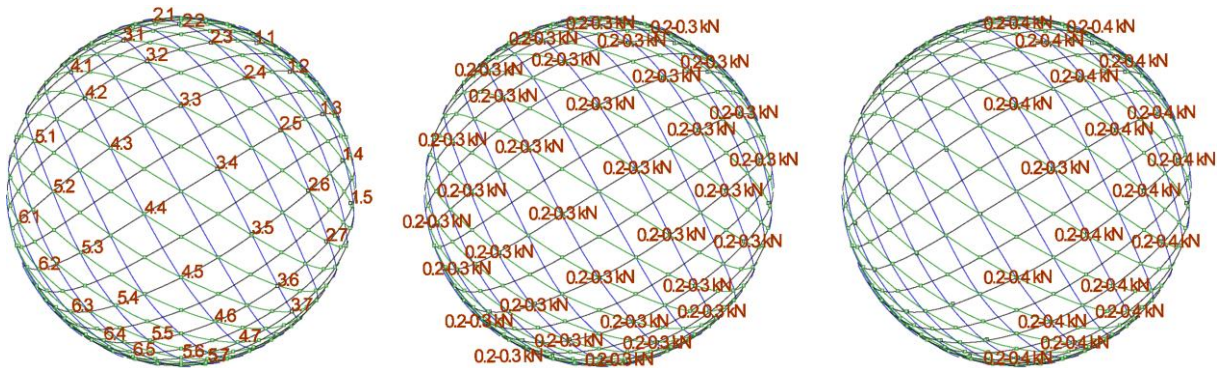


Figure 5-12: Designation of the nodes whose coordinates were registered during the loading tests using laser scanner and position of the 34 and 19 loaded nodes on the quasi-symmetric and asymmetric load cases

5.1.4 Comparison between numerical and physical models

5.1.4.1 Gridshell's geometry

The grid's geometries of the physical and numerical models before and after adding the bracing layer have been compared. Figure 5-13 shows the deviation of the non-braced grid from the target hemispheric grid at each registered point for the prototype and numerical models (with

coupling and springs elements as interlayer connections). On the vertical axis the distances between the grid nodes and the target hemispheric grid are given in mm. On the horizontal axis the designation of the considered nodes is specified. The magnitude of the maximum deviations is similar for all the models. Maximum values are always to be found on the Node 3.2 and correspond to 177 mm for the prototype, 165 mm for the finite element model with coupling elements and about 173 mm for the two finite element models with spring elements. The influence of the properties of the connection at the grid nodes on the unbraced geometry is low. The maximum differences between physical and numerical models can be observed on the Node 2.1, which is located at the bottom of the structure, and correspond to approximately 94 mm for all the models.

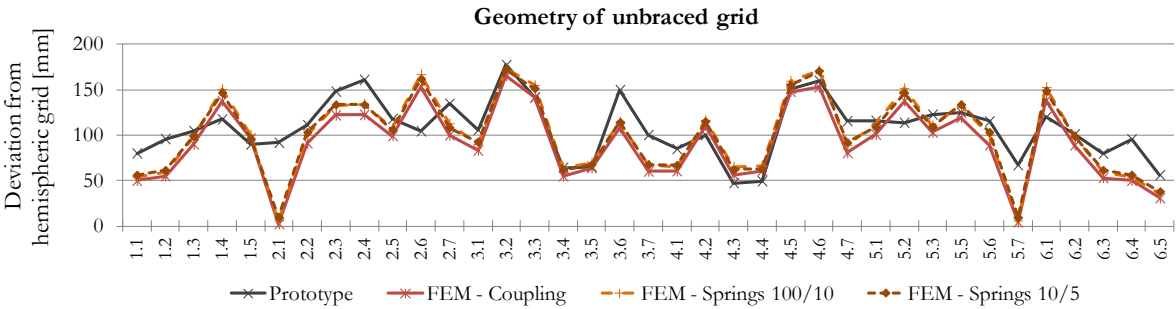


Figure 5-13: Deviation of unbraced grid's geometry, from target hemispheric grid, of physical and numerical models

Figure 5-14 shows the deviation of the grids, after being braced, from the target hemispheric grid for the prototype and numerical models. As in the previous figure, on the vertical axis, the distances from the nodes of the physical and numerical braced grids to the target hemispheric grid are given in mm and, on the horizontal axis, the designation of the considered nodes is specified. As expected, one can observe that connecting the third layer to the designated intersection points of the grid, deviations from the target hemispheric geometry are reduced on all the models. This reduction is slightly higher on the numerical models than on the prototype. Maximum deviations result on 90 mm for the physical model (Node 2.1), 46 mm for the numerical model with coupling elements (Node 2.5), 51 mm for the numerical model with spring elements with higher rigidity (Node 3.2) and 55 mm for the one with spring elements with lower rigidity (Node 3.2). The influence of the modelling of the interlayer connection on the braced geometry is also here low. The maximum difference between physical and numerical models can be again observed on the Node 2.1 and correspond to 94, 96 and 98 mm when using coupling and more rigid and less rigid spring elements, respectively.

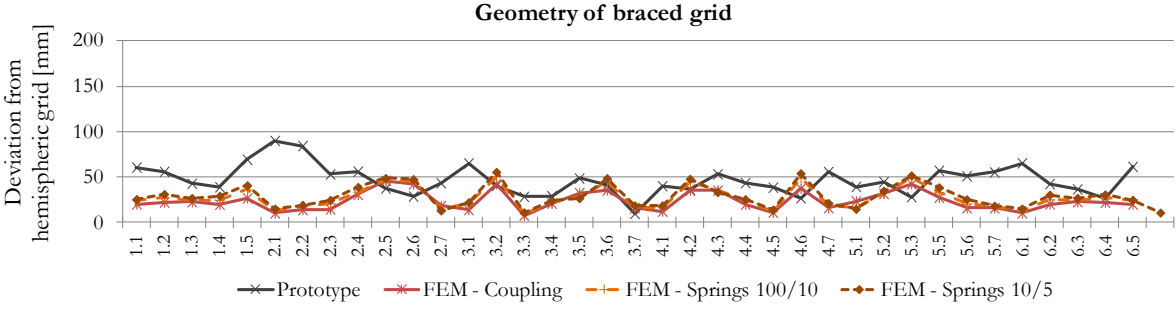


Figure 5-14: Deviation of braced grid's geometry, from target hemispheric grid, of physical and numerical models

5.1.4.2 Loading bearing behaviour

The quasi-symmetric and asymmetric load cases that were applied on the prototype have been simulated on the finite element models and the resulting deformations have been compared. In the two first following figures the bearing behaviour of the structures under symmetric loading can be observed. Figure 5-15 illustrates the nodal displacements at each registered point for the prototype and numerical models under the first symmetric load. Here, 34 grid nodes have been loaded with 0.20 kN. On the vertical and horizontal axes, the nodal displacements in mm and the designation of the considered nodes are respectively defined. Generally, the outlines of the curves and the positions of the maximum deformations are similar. Nevertheless, the magnitude of the nodal displacements highly differs between the models. Deformations on the prototype are significantly higher than those on the model with coupling elements as grid connections. The models with spring elements exhibit lower deviations from the results obtained with the prototype – their deformations are slightly lower and higher when more and less rigid springs are used. In all the models, except for the one with coupling elements, the maximum nodal displacements are to be found on the top of the middle profiles 3 and 4: Nodes 3.4 and 4.4. Their highest values correspond to 80 mm for the prototype, 56 mm for the finite element model with more rigid spring elements and 94 mm for the finite element model with less rigid spring elements.

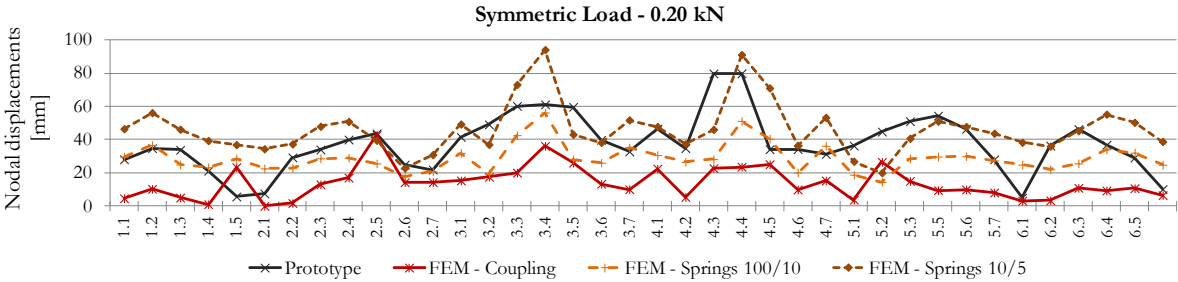


Figure 5-15: Nodal displacements under first symmetric load of physical and numerical models

In Figure 5-16 the nodal displacements can be observed for the second symmetric load, where 34 grid nodes were loaded with 0.30 kN. As previously, the outlines of the curves and the positions of the maximum deformations are in general similar but again the magnitude of the nodal displacements considerably differs. Deformations on the prototype are higher than those resulting from the numerical simulations. The maximum values are to be found again on the top of the middle profiles 3 and 4. The highest nodal displacements correspond to 246 mm for the prototype, 67 mm for the finite element model with coupling elements, 102 mm for the finite element model with more rigid spring elements and 178 mm for the finite element model with less rigid spring elements.

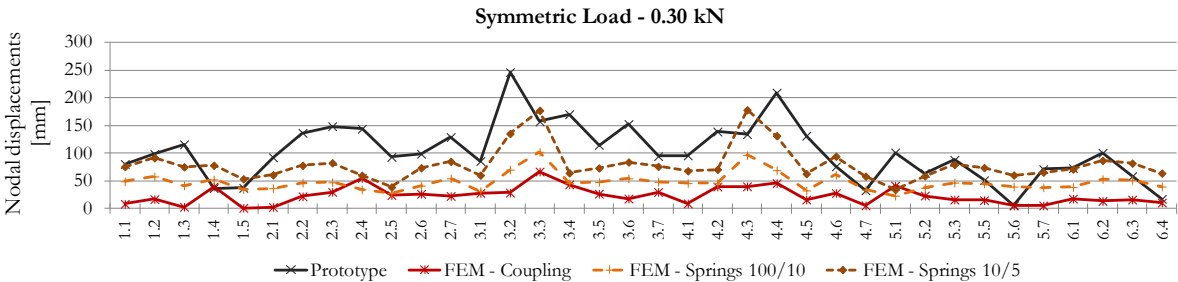


Figure 5-16: Nodal displacements under second symmetric load of physical and numerical models

In the three following figures, deformations under increasing asymmetric loading are shown. Figure 5-17 gives the nodal displacements when the structure is asymmetrically loaded in 19 grid nodes with 0.20 kN. Again, similarities can be noticed on the contour of the curves and on the location of the maximum values. The highest nodal displacements are to be found in all the models – except for the numerical model with coupling elements – on the Node 3.4 and result on 105 mm for the prototype, 96 mm for the finite model with more rigid spring elements and 147 mm for the finite element model with less rigid spring elements.

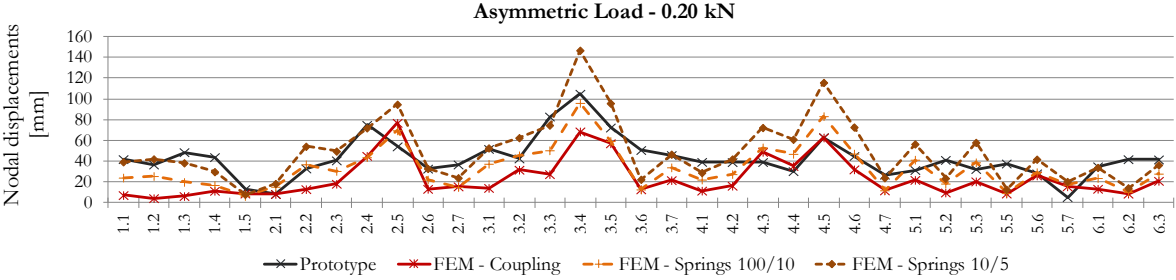


Figure 5-17: Nodal displacements under first asymmetric load (point loads of 0.2 kN) of physical and numerical models

Figure 5-18 shows the nodal displacements after increasing the point loads from 0.20 to 0.30 kN. The models exhibit an increment of the deformations in similar proportion. The highest values coincide on Node 3.4 and result on 190 mm for the prototype, 118 mm for the finite element model with coupling elements, 167 mm for the finite element model with more rigid spring elements and 259 mm for the finite element model with less rigid spring elements.

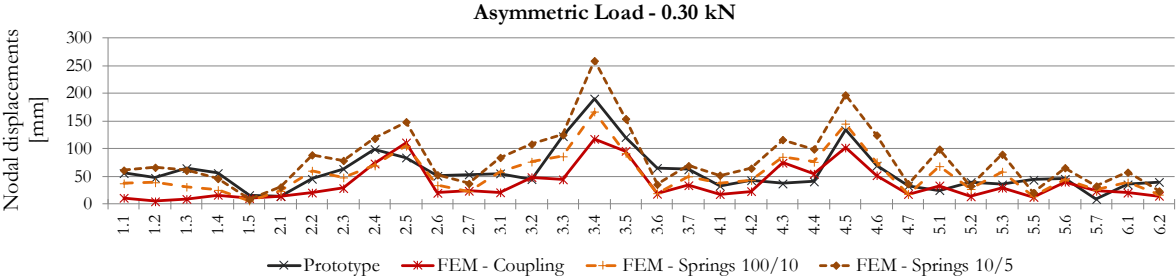


Figure 5-18: Nodal displacements under second asymmetric load (point loads of 0.3 kN) of physical and numerical models

When augmenting the point loads to 0.40 kg, local stability problems and consequently concentrated large deformations could be observed on the physical model. The profiles of the outer bracing layer, with higher distances between connections than on the other two grid layers, started to buckle. This effect was reproduced in lower measure by the numerical models with spring elements but not with the one with coupling elements. The Node 4.5 exhibits the greatest nodal displacement with a value of 558 mm for the prototype, 287 mm for the finite element model with more rigid spring elements and 361 mm for the finite element model with less rigid spring elements.

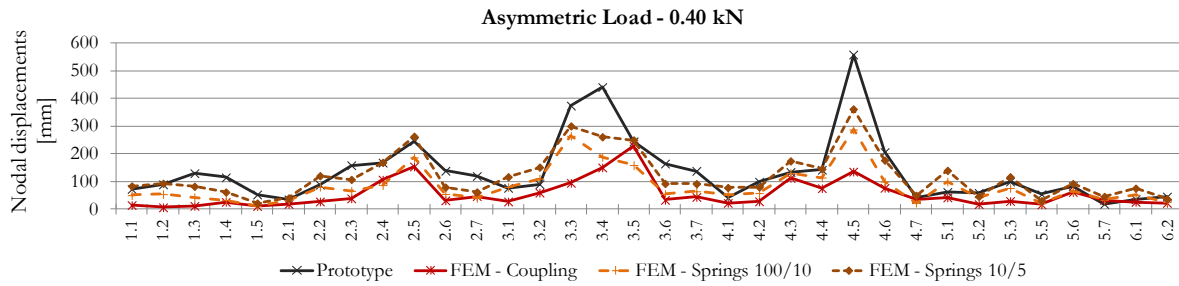


Figure 5-19: Nodal displacements under third asymmetric load (point loads of 0.4 kN) of physical and numerical models

The deformations of the gridshell, under the highest asymmetric load, which have been obtained with the prototype and with the numerical model (with the less rigid spring elements), are illustrated in Figure 5-20. One can detect, in both models, the buckling of the profiles of the outer bracing layer on the top of the structure.

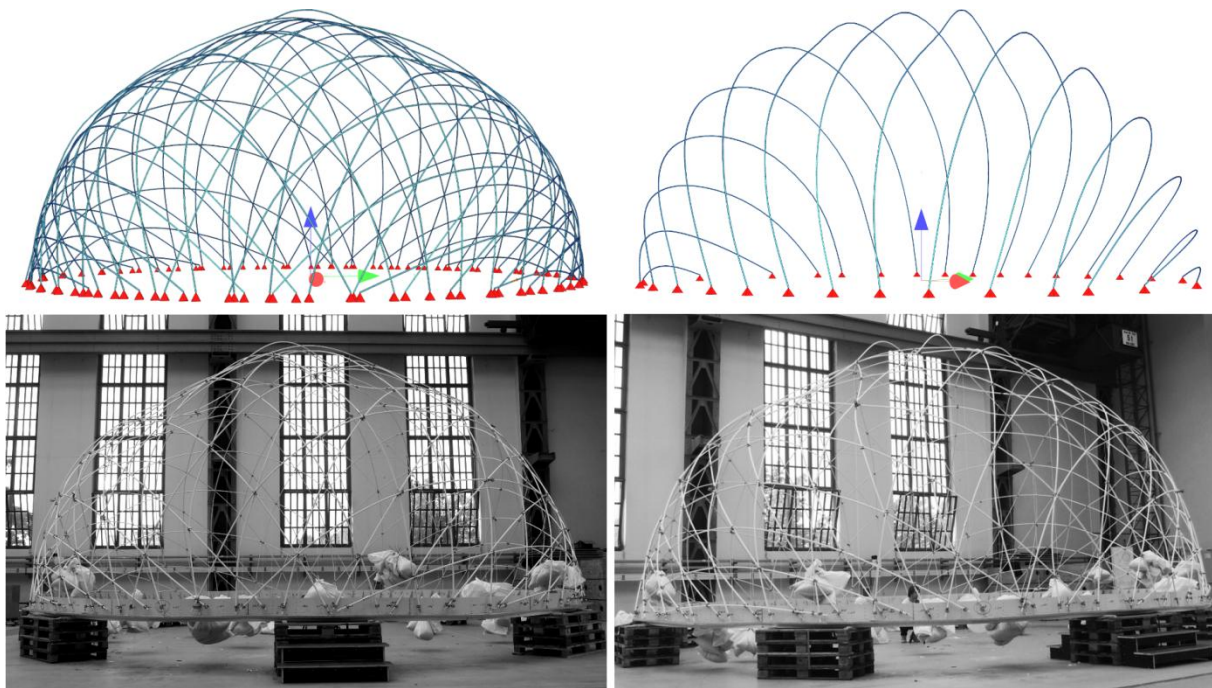


Figure 5-20: Deformation of the gridshell under asymmetric loading with 0.40 kN point loads

The differences between real and simulated structures can be due to imperfections induced during the construction of the structure – e.g. by sawing the tubes or marking the intersection points on the profiles – or to differences on the properties of the connections and supports. On the built gridshell, the transversal spring elements which were used to model, together with the axial springs, the connections between superposed layers, own a constant spring coefficient independently of the direction of the forces acting tangentially to the hemisphere's surface. On the real model, deformations on the connection clamps are different if the transversal forces act longitudinally or transversally to the profiles' axis.

On the other hand, due to the large imperfections of the structure under the second and third asymmetric load cases, the tolerance limit for the non-linear analysis had to be raised. The tolerance limit for the residual forces has been defined as a fraction of the maximum load acting on the nodes. The tolerance for the symmetric and the first asymmetric load cases is 0.001 while

for the second and the third asymmetric load cases are 0.01 and 0.1, respectively. The accuracy of the results obtained using higher tolerance limits is thus lower.

Some of the structural aspects observed in the GFRP gridshell built by Douthe et al. in 2006 [14] could be also stated during the construction of the hemisphere:

- The low bending stiffness of the GFRP profiles allowed a rapid erection process of the grid and the assembling of the outer bracing layer using only manpower.
- Despite the only partial bracing of the gridshell, the increment of the structure's stiffness after installation of the third layer of profiles was notable. By loading the gridshell symmetrically with more than 3 times the weight of the grid, the resulting maximum deformations were lower than 1% of its span length.

5.2 Construction of a Membrane Braced Regular Elastic Gridshell

Figure 5-21 shows some moments of the installation of the outer bracing layer on the irregular hemispheric grid presented on the previous section. To overcome the residual forces at some grid nodes and to connect the outer layer at the right positions, the force of multiple students were sometimes needed. In order to optimise the construction process of elastic gridshells, we study the potential of employing tensile membranes to cover and at the same time to restrain the grid. Consequently, as fewer elements must be assembled and handled on site, time and material are saved.



Figure 5-21: *Assembling of bracing layer on the irregular hemisphere*

The bracing capacity of tensile membranes on elastic gridshells has been tested on a prototype: a regular elastic hemisphere of 5 m diameter. This chapter focuses on its design and erection processes and compares the bearing capacity of the prototype with that of the numerical simulation.

5.2.1 Grid design

The hybrid gridshell is composed of a regular hemispheric grid of 5 m diameter and a covering tensile membrane. The pattern of the grid, which has been defined using the variational approach described in Chapter 3, is shown in Figure 5-22.

The optimisation of the grid has been performed as regular mesh with an initialisation angle between edges of 67.5° . As on the previous prototype, whose mesh was optimised with an initialisation angle of 45° , the segments of the mesh follow an S-orientation and concentrate in two opposite points. The optimisation of the mesh has been so performed that the concentrations of the profiles remained constructively buildable. The mesh size of the grid corresponds to 0.74 m. As the optimisation with the variational method provides meshes that do not perfectly stay on the reference surface, the resulting optimised grid has been projected to a sphere of 5 m diameter. The maximum and mean curvature values of the profiles are 0.67 and 0.46 m^{-1} . To determine the length of the profiles to be taken for the grid's construction, the mesh segments have been not considered but interpolated curves passing through the mesh's vertices.

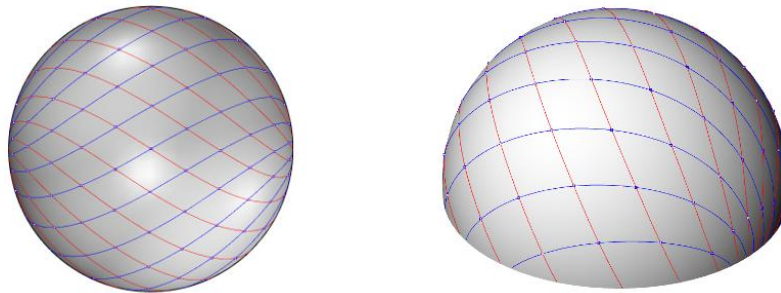


Figure 5-22: Optimised grid pattern of hybrid hemisphere

5.2.2 Numerical simulation

The bending process and load-bearing behaviour of the hybrid hemisphere have been modelled and analysed with a non-linear three-dimensional finite element model, using the FEA-package of Sofistik. The simulation consists of two parts. Firstly, the shaping process of the grid has been modelled. As in the previous prototype, the bending of the beam elements has been generated using the simulation methodology suggested by Lienhard et al. in 2011 [62], in which virtual cables with minimal stiffness are defined between the start and target geometries of the elements to be bent and their shaping is induced by prestressing these cables and consequently reducing at maximum their lengths. Once the grid has been bent, the profiles' ends have been fixed with hinged supports. The second part consists in the activation of the membrane and the application of external loads on the structure.

The numerical analysis focuses on the influence of the properties of the interlayer connections on the bearing behaviour of the structure. As by the irregular gridshell, the connections between superposed grid layers have been modelled as coupling and as spring elements (see Figure 5-4). The coupling elements represent a hinged connection at the upper layer to a rigid node at the lower layer. Two models using spring elements with varying stiffness coefficients have been defined: in the first one, the axial and transversal coefficients are 10 and 5 kN/m and, in the second one, 2 and 2 kN/m. Different values for the stiffness coefficients have been tested; the chosen values provide deformations which are similar to those of the prototype. The spring elements are oriented in radial direction. The eccentricities between superposed layers are considered so that moments generated by transverse forces are transferred to the grid nodes.

The contact between membrane and grid has been modelled using stiff springs which are oriented in radial direction (normal to the membrane's surface), have only axial stiffness and are only able to carry compression forces. They are defined along all the beam elements and their stiffness coefficient is 10^3 kN/m. In Chapter 4, the structural effect of the connection of the membrane to the grid at the grid nodes has been studied. In the same manner, on the following structural analysis, different models have been considered: with and without additional spring elements at the grid nodes. These additional springs are only defined at the intersection of the grid layers and have axial and lateral stiffness coefficients of 10^3 kN/m. The connection of the border of the membrane to the edge ring has been modelled with springs of reduced axial and transversal stiffness of 1 kN/m. Further details of the finite element model have been given in Chapter 4. In Figure 5-23, the finite element model is illustrated without and with the membrane's quad elements.

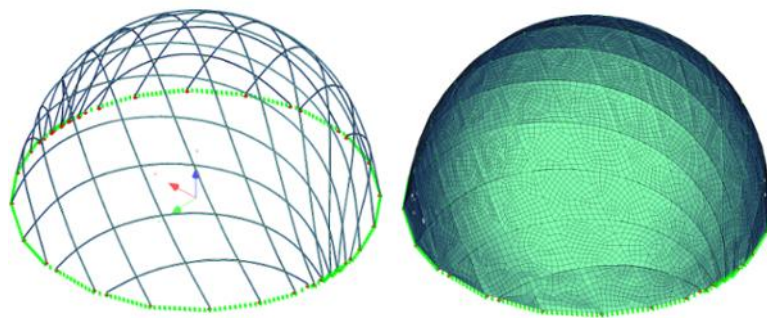


Figure 5-23: Modelling of grid without and with restraining membrane

The geometry of the membrane on the finite element model has been determined depending on the activation or not of the connection between membrane and grid. In the first case (with membrane's connection at the grid nodes), its initial geometry corresponds to that of the grid, constrained through shaping forces. In the second case (without connection at the grid nodes) the membrane's geometry corresponds to that of the grid, after being bent, fixed and released of external shaping forces. In both cases, the coordinates of the membrane have been calculated by projecting the coordinates of the respective grid profiles in radial direction, by a distance of the radius of the GFRP tubes along the upper profiles' layer and 1.5 times the diameter of the GFRP tubes along the lower profiles' layer.

5.2.3 Construction

The hybrid gridshell is composed of a GFRP grid structure and a tensile membrane Ferrari Précontraint 1302 S2. Due to economic reasons, it was decided to use the same profiles as those chosen for the first prototype: tubes of 20 mm diameter and 3 mm wall thickness. It was controlled, with the numerical analysis, that the maximum equivalent stresses, after bending the grid and under external loads, do not exceed the bending strength of the material reduced by a material safety factor of 1.2 ($\sigma_d = 208$ MPa). The resulting equivalent stresses in all finite element models, before and after applying the nodal forces, were similar and maximum values of about 171 MPa appeared. The highest deliverable length of the profiles was 6 m and, to prolong them,

aluminium tubes of 80 mm length were used. Double swivelling clamps with inner rubber walls were employed to connect the superposed grid layers. The grid was fixed on a ring made of OSB-plates using single clamps.

The restraining and covering membrane owns polyester cloth and PVC/PVDF coating and its mechanical properties correspond to a Type III, according to the European Design Guide for Tensile Surface Structures [7]. The choice of the membrane resides on the analyses of the influence of the membrane's stiffness on its restraining effect presented in Chapter 4. The stiffness of the membrane should be high to optimise its stiffening action but not too high to keep its handling on site and assembling on the already bent grid practicable. The geometry of the membrane's surface corresponds to a hemisphere. The warp and weft yarns are oriented in meridian and radial direction. To fix the membrane on the timber ring, a PVC-tube was introduced through the ring's stiffening ribs and a rope was laced and spanned through it and the edge eyelets of the membrane. In Figure 5-24 outer and inner views of the finished hybrid gridshell as well as details of the connections are presented.

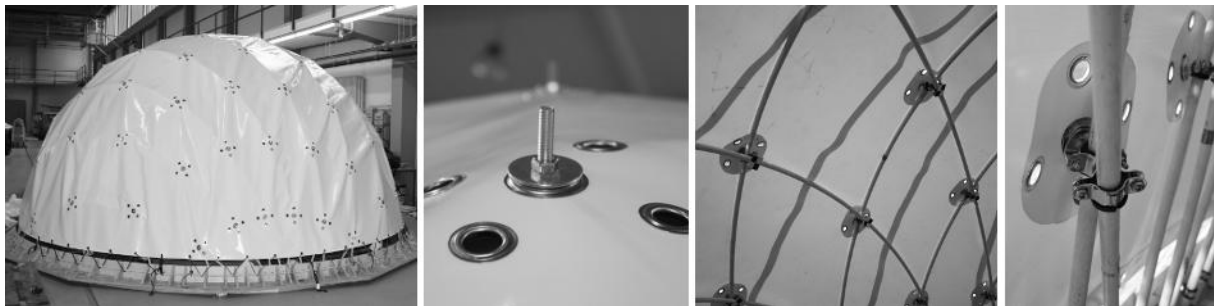


Figure 5-24: Outer and inner views and connection details of the hybrid hemisphere, with joining between membrane and grid

The erection process of the hybrid gridshell started with the assembling of the initially plane grid, which was afterwards bent by pushing it upwards on the centre of the grid and next connected to the edge ring. Then, the membrane was progressively spread over the grid and finally tensed and fixed to the ring. Only manpower was needed. Figure 5-25 shows some stages of the erection process.

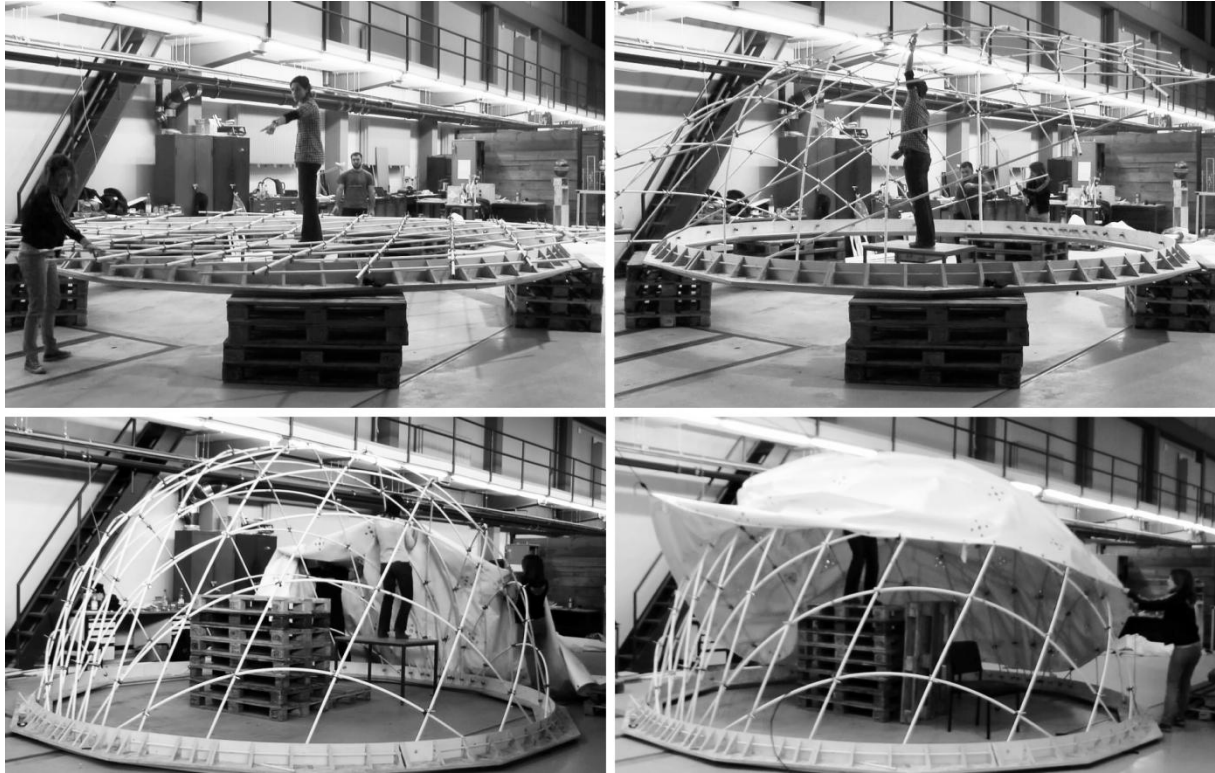


Figure 5-25: Shaping process of grid and installation of bracing membrane

The prototype has been tested with and without connection between membrane and grid at the grid nodes. On the first case, this connection was provided by threaded pins screwed on nuts welded on the upper clamps of the grid nodes, as illustrated in Figure 5-24. For it, the membrane was perforated at 85 positions, corresponding to the grid intersection nodes, with eyelets of 25 mm hole diameter. On these positions, the membrane was reinforced with disks of 180 mm diameter of the same textile material. The positions of the eyelets on the membrane were determined with a three-dimensional geometric model. An alternative connection was planned – but not needed to be used - in case that the grid’s stiffness would have been too high or the geometric imperfections too important to fit the threaded pins into the membrane’s eyelets. This alternative connection consisted in four additional eyelets at the grid nodes, to tie the membrane to the grid with two crossing buckle straps.

Once the grid has been fixed on the ring and no further shaping forces are applied, the grid adopts a released geometry, induced by the inner forces resulting from the bending process. This geometry is characterised by an upward deformation on the top of the grid, an inward deformation at the sides where the singularity points are located and an outward deformation at the opposite sides (see Figure 5-26). With the connection of the membrane at the grid nodes, it was intended to approach the released grid’s geometry to the target hemispheric surface - *shaping function* - by pushing and fitting the grid’s nodes into the membrane’s eyelets, as done using the outer bracing layer on the first prototype. All the eyelets could be met, except for two nodes at the bottom of the grid, where the distance between nodes and corresponding eyelets were too high. Furthermore, wrinkles appeared on the membrane, possibly due to inwards deformations on the released geometry and to constructive imperfections, as sliding of the profiles at the grid nodes or deformation of the clamps.

In the case without connections between grid and membrane at the grid nodes, the threaded pins and clamping washers were removed. Here, the released geometry of the grid was manipulated by tightening the edge rope at the support ring and introducing a small prestress into the membrane. In Figure 5-27 the generated offsets between eyelets and grid nodes can be identified.

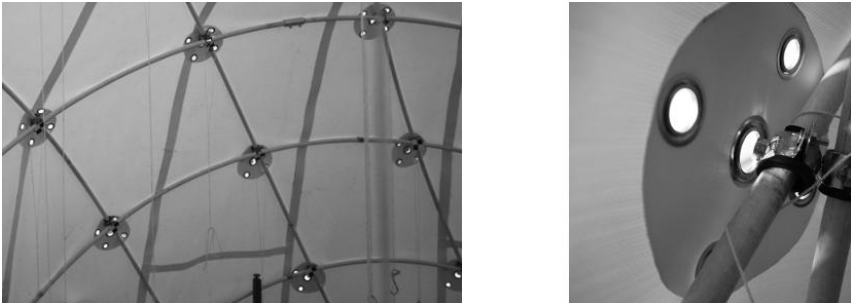


Figure 5-27: Inner views and connection details of the hybrid hemisphere without joining between membrane and grid

After installing the membrane, the hybrid gridshell was asymmetrically loaded with 17 weight loads of 0.10 – 0.29 kN which were applied at the grid nodes. The resulting deformations were registered at 76 grid nodes using a three-dimensional laser scanner (FARO® Laser Scanner Focus^{3D}). In Figure 5-28 the designation of the analysed nodes and the position of the weights on the structure are indicated.

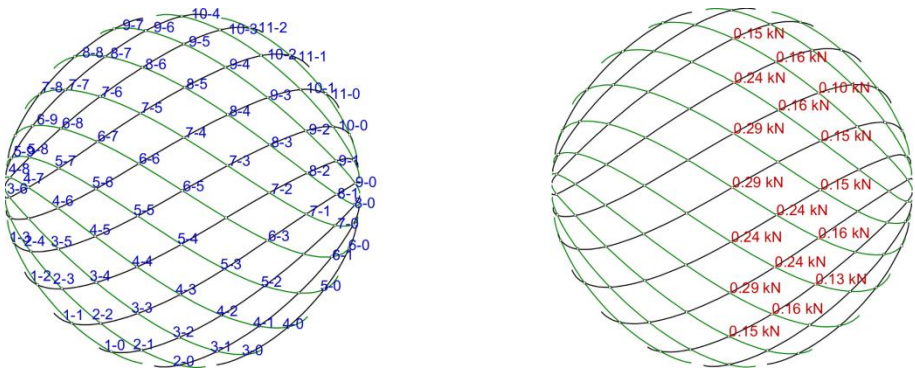


Figure 5-28: Designation of registered grid nodes (left) and position of weight loads (right)

5.2.4 Comparison between numerical and physical models

The function of the restraining membrane is to introduce shear stiffness on the grid and thereby to reduce its deformation, on the one hand, after removing the shaping forces – when a predefined geometry is to be maintained (*shaping function*) – and, on the other hand, under external loading. These both structural effects have been numerically analysed and compared with those observed on the prototype.

5.2.4.1 Gridshell’s geometry

The following graphics illustrate the deviation of the grid’s geometry of the physical and numerical models from the target hemispheric grid, for the cases where the grid is not restrained, the grid is restrained but not connected to the membrane and the grid is restrained and

connected to the membrane at the grid nodes. All three numerical models have been calculated with three different grid's interlayer connections: with coupling elements, with spring elements with axial and transversal coefficients of 10 and 5 kN/m and with spring elements with axial and transversal coefficients of 2 and 2 kN/m.

On the vertical axis of Figure 5-29, the distances between the nodes of the non-restrained grids and the target hemispheric grid are given in mm. On the horizontal axis the designation of the considered nodes is specified. One can see that the physical model presents higher deviations at the border profiles 1, 2 and 10, 11, while the peaks of the curves of the numerical models are more distributed. The maximum deviation corresponds to 138 mm at Node 2.3 for the prototype and 116 (Node 8.1), 98 (Node 9.0) and 91 mm (Node 9.0) for the numerical models with coupling elements, more rigid springs and less rigid springs as interlayer connections. Their maximum deviations from the physical model are to be found at Node 2.3 and respectively result on 131, 124 and 96 mm. The important differences observed on the prototype at the border profiles, can probably be related to the deformations on the connection clamps. These border profiles own the highest curvature on the grid and, consequently, the highest inner forces, which resulted on declamping of some grid connections.

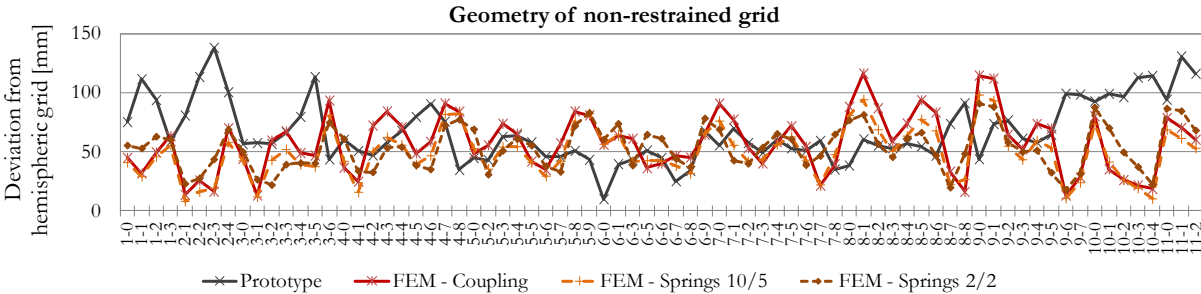


Figure 5-29: Deviation of non-restrained grid's geometry from target hemispheric grid of physical and numerical models

Figure 5-30 illustrates the deviations of the physical and numerical grids with restraining membrane, but without connection between membrane and grid at the grid nodes, from the target hemispheric grid. On the prototype, the membrane was installed over the bent grid which had already acquired the released geometry: equilibrium shape after bending the grid, fixing it at the edge ring and removing all the shaping forces. Similarly, on the numerical model, the membrane has been activated on the released grid. In order to simulate the prestress on the membrane through tensioning of the edge rope at the support ring, the membrane has been slightly prestressed with a force of 0.01 kN/m in radial direction. In general, but in low measure, deviations are smaller and the grid's geometry is slightly nearer to the hemisphere. The maximum deviations result on 124 mm for the prototype and 109, 94 and 88 mm for the numerical models, with coupling elements, more rigid springs and less rigid springs as interlayer connections. Their deviation from the physical model remains similar with maximum values of 123, 110 and 101 mm, respectively.

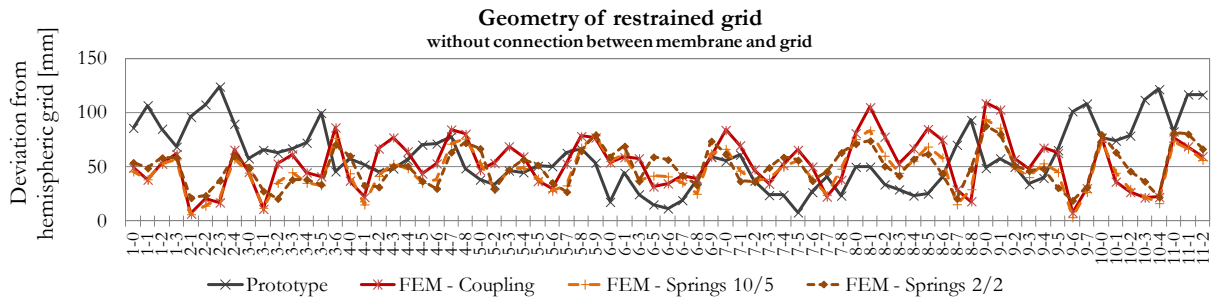


Figure 5-30: Deviation of restrained grid's geometry – without connection between membrane and grid nodes - from target hemispheric grid of physical and numerical models

The geometries obtained by connecting the restraining membrane to the grid nodes are given in Figure 5-31. The physical and the numerical models exhibit a slightly higher reduction of the deviations from the hemispheric grid. The maximum deviations result on 116 mm for the prototype and 83, 68 and 85 mm for the numerical models with coupling elements, more rigid springs and less rigid springs as interlayer connections. The differences between the numerical models and the prototype are a bit reduced and the maximum values correspond to 89, 89 and 85 mm.

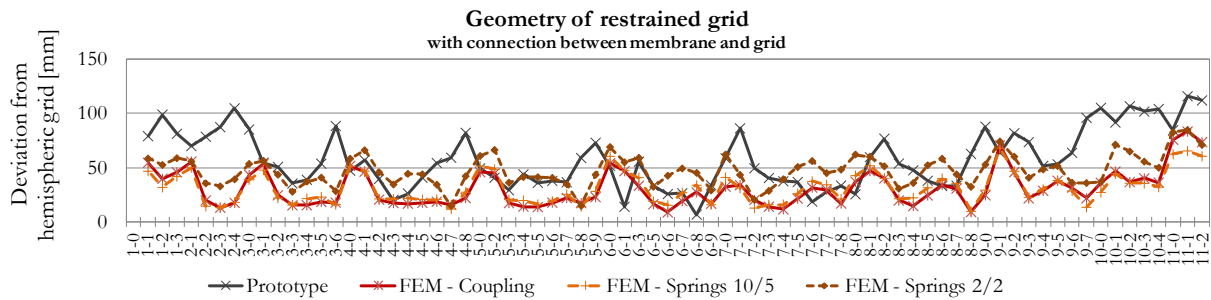


Figure 5-31: Deviation of restrained grid's geometry – with connection between membrane and grid nodes - from hemispheric grid of physical and numerical models

5.2.4.2 Load bearing behaviour

Comparisons of the load-bearing capacity of the physical and numerical structures under asymmetric loading have been performed and illustrated in the following graphics. Half of the structure was loaded with 17 weight loads of 0.10 – 0.29 kN applied at the grid nodes. In Figure 5-32, the resulting deformations are shown for the models without connection between membrane and grid. On the vertical and horizontal axes, the nodal displacements in mm and the designation of the considered registered nodes are respectively specified. The outline of the deformation curves mainly correspond to each other. However, as by the first prototype, the measure of the nodal displacements differs depending on the properties of the grid connections. Deformations on the prototype are significantly higher than those on the model with coupling elements as interlayer connections. The deformations resulting from the models with spring elements are more similar to those obtained with the prototype, particularly with the model with less rigid springs. In all the cases, the maximum nodal displacement is to be found on the top of the middle profile 6 at the Node 6.5 and corresponds to 149 mm on the prototype, 84 mm on

the finite element model with coupling elements, 100 mm on the finite element model with more rigid elements and 141 mm on the finite element model with less rigid spring elements.

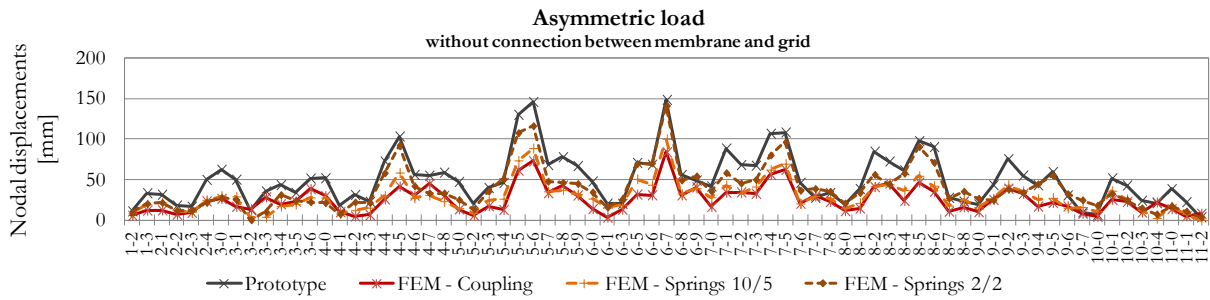


Figure 5-32: Nodal displacements under asymmetric loading of physical and numerical models, without connection between membrane and grid nodes

On the case where the membrane was joined to the grid nodes, important wrinkles could be observed on the prototype. This was probably due to the deviations of the released grid's geometry from the actual hemispheric surface of the membrane, specially there were the grid tends to deform inwards. Another reason can be the imperfections occurring at the interlayer connections, where sliding of the rubbers or deformation of the clamps happened. The effect of the membrane on the prototype was not the one attained with the numerical calculations: the maximum nodal displacement with connection at the grid nodes results higher than without connection. Nevertheless, in all the cases, the maximum nodal displacement is to be found on the top of the middle profile 6 at the Node 6.5 and corresponds to 205 mm on the prototype, 72 mm on the finite element model with coupling elements, 90 mm on the finite element model with more rigid elements and 135 mm on the finite element model with less rigid spring elements.

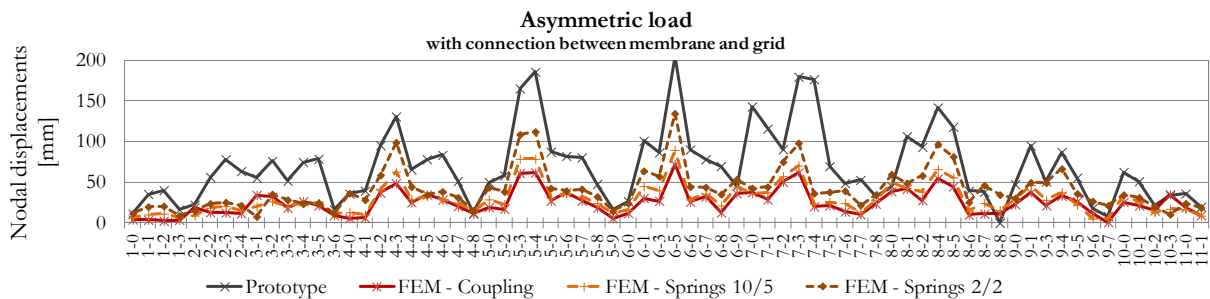


Figure 5-33: Nodal displacements under asymmetric loading of physical and numerical models, with connection between membrane and grid nodes

In the following Figure 5-34, the stiffness of numerical membrane-braced grids, with and without connection between grid nodes and membrane, is compared with that of non-braced and cable-braced grids. As interlayer connection, the spring elements with lower stiffness coefficients have been used. The asymmetric load has been applied with a factor of 0.5, as with higher loads the non-braced grid presents convergence problems. The effect of the restraining membrane is notable; the maximum nodal displacements on the non-braced grid could be reduced from 244 mm to 69 mm (without connection at grid nodes) and 61 mm (with connection at grid nodes). Nevertheless, the restraining effect of the cable elements is much higher: maximum nodal displacements on the cable-restrained grid results on 13 mm.

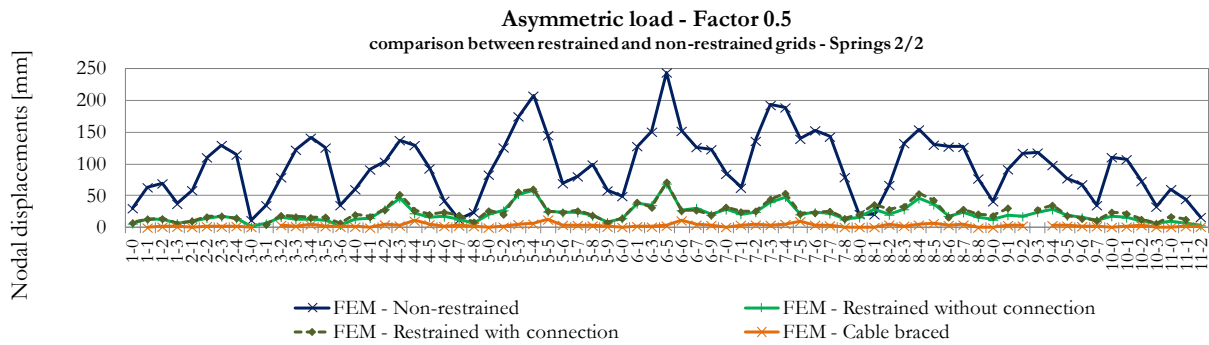


Figure 5-34: Comparison of nodal displacements under asymmetric loading between membrane- and cable braced grids

Figure 5-35 illustrates the distribution of the principal membrane forces, which shows the predominance of meridian and ring forces on the membrane, which was in part visualised by the orientation of the wrinkles that appeared on the prototype.

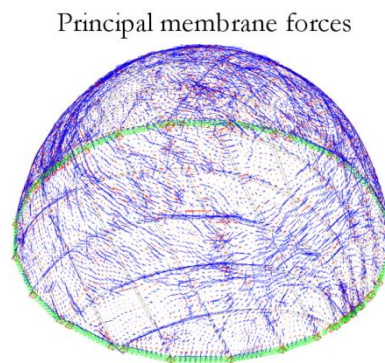


Figure 5-35: Deformation and distribution of principal membrane forces on numerical model

In Figure 5-36 the prototype under external asymmetric loading, with connection between grid nodes and membrane, and the distribution of the generated wrinkles can be observed. Wrinkles marked with rot arrows correspond to the meridian forces similar to those observed with the finite element model. The large wrinkles marked with the green arrows, which resulted from the great downward deformations at the top of the structure, could not be totally reproduced by the numerical simulation. Further research could prove the improvement of the model's accuracy, by reducing the size of the membrane's finite elements. The biggest quad element of the investigated models owns a surface of 91 cm².

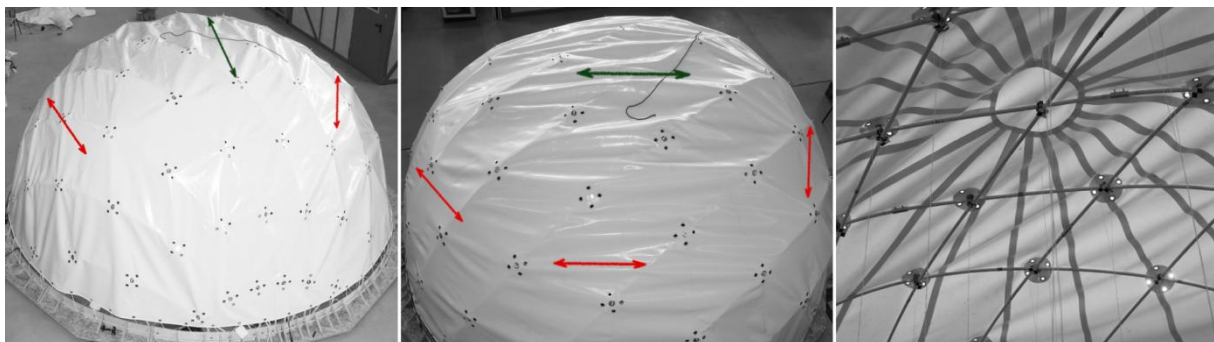


Figure 5-36: Formation of wrinkles on asymmetrically loaded prototype

5.3 Summary

In this chapter the design and construction of two prototypes of elastic gridshells have been described and their bearing behaviour studied with the aim of benchmarking the numerical models used for the structural analysis. The first prototype represents a elastic gridshell with irregular mesh and partially braced with a third layer of profiles. The second prototype concerns a regular gridshell braced with a tensile membrane.

5.3.1 Developable irregular gridshell

Elastic gridshells with irregular meshes offer a diverse variety of advantages: for example, a higher minimisation of the profiles' curvatures, an optimised profiles' distribution and mesh size according to local structural requirements or new aesthetic possibilities for architectural purposes. Nevertheless, the use of irregular meshes complicates the bending process of the grids from a completely flat position, as the grid loses its degree of freedom on scissoring. By the construction of the irregular hemisphere of 10 m diameter, it could be demonstrated that, if the bending stiffness of the grid is low enough, large deformations can be induced on them and, by an adequate profiles' distribution, the irregular grid can be developed into a flat configuration, which allows a rapid erection process. However, to permit the initial flat configuration, the profiles must be here already bent, instead of being straight as on the regular grids. By means of non-linear finite element models, it could be proved that the material stresses during the construction process do not exceed the allowable ones. In order to reduce these stresses, the grid was during the erection process only partially assembled (26 profiles) and the resting 12 border profiles were introduced after shaping the grid. Despite the only partial bracing of the gridshell, the increment of the structure's stiffness after installation of the third layer of profiles was relevant. By loading the gridshell symmetrically with more than 3 times the weight of the grid, the resulting maximum deformations were lower than 1% of its span length.

The structural behaviour of the irregular prototype has been compared to those of three numerical models, which differ on the definition of the interlayer connections (coupling elements, spring elements with higher stiffness and spring elements with lower stiffness). The following results have been evidenced:

- For all the numerical models, similar deviations from the physical model have been observed on the resulting grid's geometry, before and after being braced. The prototype's geometry could be relatively well reproduced by the simulation, particularly on the unbraced situation. The maximum deviations resulted on 94 - 98 mm.
- In contrast, under external loading, important differences have been found between numerical and physical models, especially when using coupling elements, hinged connection at the upper layer to a rigid node at the lower layers. The use of spring elements with reduced stiffness allows more similar results. Nevertheless, the influence of the properties of the interlayer connections on the structure's deformability depends on

the nature and intensity of the applied loading. Considering the maximum nodal displacements, with the spring elements with axial and transversal coefficients of 100 and 10 kN/m, more similar values have been obtained for asymmetric load cases with 0.20 and 0.30 kN point loads. With the spring elements with axial and transversal coefficients of 10 and 5 kN/m, more similar values have been obtained for symmetric load cases, with 0.20 and 0.30 kN point loads and the asymmetric load case with 0.40 kN point loads. In general, the increment of the grid's deformations under increasing loading is faster on the prototype than on the numerical models.

- Differences between real and simulated structures are mainly due to imperfections on the interlayer connections, as sliding and deformation of the clamps at the grid nodes could be observed. Improvements on the construction, and the consequent simulation, of interlayer connections for tubular sections are to be further investigated.

5.3.2 Membrane braced gridshell

With the use of tensile membranes as bracing and at the same time cladding elements, time and costs during the erection process of elastic gridshells can be optimised. By the construction and testing of the hybrid prototype, the restraining effect of the membrane could be firstly noticed on the reduction of the grid's deviations from the target grid's geometry, after removal of the shaping forces. The restraining effect of the membrane, under external loading, could be also physically noticed by the formation of wrinkles in the bracing directions.

In addition, the comparison between the physical and numerical models allowed determining the influence of the properties of the interlayer connections on the bearing behaviour of the hybrid structure. Three numerical models with the same elements for the interlayer connections as on the irregular gridshell have been investigated:

- In contrast to the irregular gridshell, differences between the numerical models are already notable by comparing the resulting grid's geometry, before and after adding the membrane. The maximum deviations of the simulations from the prototype are to be found on the non-restrained grid's geometry with maximum values of 131, 124 and 96 mm, for the models with coupling elements, spring elements with higher stiffness and spring elements with lower stiffness.
- Under external asymmetric loading, differences between the numerical models are higher. The use of spring elements with reduced stiffness allows more similar results than those obtained with the coupling elements and spring elements with higher stiffness. Differences between numerical and physical prototypes depend on the activation or not of the connection between membrane and grid. The grid's deformation under asymmetric loading could be much better reproduced without than with connection at the grid nodes. The effect of the connection between membrane and grid nodes on the prototype was not the one attained with the numerical calculations, as the maximum nodal displacement with connection at the grid nodes resulted higher than without connection. This was again probably due to the imperfections observed at the interlayer connections of the

prototype, where strong sliding of the rubbers or deformation of the clamps happened. Improvements could be done on the construction of more appropriate connections between grid layers.

6. Conclusion and Perspectives

6 Conclusion and Perspectives

Scope of work

The aim of the present thesis is to explore the structural criteria to be considered on the design and construction of elastic gridshells. Besides a review and classification of existing design procedures and construction materials for elastic gridshells, this work proposes an optimisation method based on variational principles to determine grids with reduced profiles' curvature, on a constrained or reference surface geometry, for regular and irregular meshes.

Furthermore, investigations of the influence of the grid pattern on the load-bearing behaviour of elastic gridshells are provided. The structural analyses have been performed using non-linear three-dimensional finite element models and calculations according to the third-order theory. Two physical prototypes have been as well built in order to explore their construction process and compare their structural behaviour with that of the numerical simulations.

Design principles

In Chapter 2, the main structural and constructive aspects to be considered on the design of elastic gridshells have been presented. Three design criteria have been identified:

- *Gridshell's geometry.* The gridshell's geometry should fulfil the required building's function, specific surrounding conditions as well as the aesthetic expectation. Furthermore, the geometry, and specially the curvature, of the gridshell play an important role on its structural performance and behaviour as shell structure. Different design approaches to determine the geometry and convenient grid pattern of elastic gridshells have been presented and classified according to the use or not of form-finding methods.
- *Post-bending residual stress.* The profiles reproducing the intended curved geometries and patterns are subjected to strong bending stresses, which have to be compensated with appropriate material and sectional properties. These residual stresses, which are generally higher than those generated exclusively from external loads, should be low enough to provide the structure with sufficient stress reserves.
- *Gridshell's stiffness.* By the choice of the profiles' axial and bending stiffness, two contradictory constructive and structural aspects have to be respected: the stiffness of the grid should be low enough to be technically able to be bent and to prevent extreme shaping and support forces; at the same time, it should be high enough to provide the grid with enough out-of-plane stiffness and avoid stability problems.

The final design of elastic gridshells results from an iterative process where the surface geometry and the grid's pattern and stiffness are modified and adapted until obtaining a structurally efficient and architecturally satisfactory gridshell.

The required axial and bending stiffness for the grid profiles can be obtained with materials appropriate for *elastically-bent* structures, which are materials with high limit strain. A low ratio of modulus of elasticity to strength allows high curvature on the profiles and provides them with more stress reserves after bending. Furthermore, materials with high moduli of elasticity can better supply the gridshell with the needed stiffness. Here, it is important to remark that the stiffness of the profiles do not only depend on the materials' mechanical properties but also on their manufacture possibilities regarding the definition of the cross-section. Another important aspect of the materials is their creep-relaxation behaviour, in order to anticipate the long-term deflection of the gridshell and its actual stress reserve by the time live loads are applied. Recent creep tests, performed with glass fibre reinforced composites under bending loads, show that the creep factors of GFRP are significantly lower than those of timber and NFRP.

The mechanical properties - flexural strength, modulus of elasticity, allowable minimum radius of curvature and specific strength - of materials suitable for elastic gridshells have been specified and compared. Considering the minimum radii of curvature and the modulus of elasticity of the materials, CFRP allow the smallest radii of curvature - together with GFRP - while offering much higher stiffness than the rest of materials. Nevertheless, due to their high production costs, the use of CFRP in construction engineering is relatively reduced. GFRP offer similar allowable curvature values than CFRP but relatively lower stiffness. The next smallest radii of curvature are provided by bamboo and NFRP, both owning lower stiffness values than CFRP and GFRP. The elasticity modulus of timber is comparable to that of NFRP and bamboo; but its allowable radius of curvature is higher. At last, paper exhibits low radii of curvature but extreme low stiffness while aluminium exhibits high stiffness but higher allowable radii of curvature. Application examples of these materials on the construction of elastic gridshells have been presented and illustrated.

Grid finding and optimisation

In Chapter 3, a methodology based on variational principles to determine regular and irregular meshes on or near a reference surface and with optimisation of the profiles' curvature is proposed and applied to three double-curved surfaces. Compared to regular grid patterns determined with the "compass method", the maximum profiles' curvature could be reduced to around 82-88%, in the case where the grids were forced to stay on the reference surface. By allowing a distance to the reference surface up to 0.60 m, the maximum profiles' curvature could be reduced to 45-79%.

The following conclusions have been drawn:

- *Influence of initialisation mesh and weighting factors on the optimisation.* In the proposed approach, the optimisation of the profiles' curvature evolves through an iterative process which is strongly influenced by the initialisation mesh and the values assigned to the weighting factors of the sub-energies to be minimised. To obtain a maximum reduction of the profiles' curvature, it is important to widely explore different initialisation meshes with varying shear angle and different combinations of weighting factors. The mapping technique used in the proposed approach to define the initialisation mesh is based on

conformal parameterisation, which allows almost constant angle between edges. Further research could focus on the use of alternative mapping techniques for the determination of the initialisation mesh, e.g. the Wire Mesh Design which provides meshes with constant edge length. However, it is also important to prove, during the optimisation, that other relevant constructive and structural requirements are also fulfilled.

- *Optimisation with irregular grids.* Using the definition of the circumcircle curvature energy as well as target mean and range length values for the edge length energy, optimisations with irregular meshes have been performed and a further reduction of the profiles' curvature of previously optimised regular grids has been possible. Compared to the optimised regular grids, the mean profiles' curvature could be additionally reduced to 68-85%. Nevertheless, one should take into account the effects on the construction process and on the load-bearing behaviour of the resulting irregular gridshells. Modifying the mesh size of the grid, the local and global stability and stiffness of the gridshell changes and the shaping of the grid from a completely flat position becomes difficult, as the grid loses its degree of freedom on scissoring.
- *Reduction of mean vs. maximum curvature values.* As with the proposed variational method the optimisation has an effect on the sum of the curvature values, the mean curvature values are generally stronger reduced than the maximum ones, particularly by the optimisation of irregular grids. Depending on the surface geometry, a diminution of the highest curvature values can become difficult. The main objective of the grid optimisation is to minimise the material stresses to which the grids are subjected due to their bending process and increase its stresses reserves to be able to carry the design external loads. The need of stress reserves is distributed depending on the grid geometry and the nature and intensity of the external loads. By the optimisation of the grid, it would be optimal to reduce the profiles' curvature, there where the stresses are the highest under the most critical external load, which can coincide or not with the maximum stresses after the bending process. An optimisation of the grid pattern according to the distribution of the required stress reserves, depending on the structure geometry and loading case, could provide further structural advantages.
- *Construction of resulting geometry.* The bracing layer of elastic gridshells can consist in beam elements subjected to tension and compression, diagonal cable elements resisting only tension or structural surface panel elements. In the case that elastically-bent beams are used as bracing elements, it would be optimal to also consider their curvature during the optimisation process. The optimisation examples presented in this work focus only on the optimisation of the grid. Nevertheless, with the variational method it would be also possible to take into account the curvature of a third diagonal layer, using for example triangular - instead of quadrilateral - meshes.

Numerical Analysis

The orientation and distribution of the profiles on the grid pattern affects not only the profiles' curvature but also the structural behaviour of the gridshell. In Chapter 4, the structural behaviour of three anticlastic regular gridshells with varying grid pattern has been analysed. The gridshells are between 5 and 7.5 m high, 14 and 15 m wide and 30 m long. The grid patterns differ on the shear angle of the initialisation meshes: 45° , 90° and 135° in respect of the transverse axis of the structures. For all the gridshells, it could be confirmed that:

- By removing the external shaping forces, once the grid has been bent and its edges fixed, the grid deforms and acquires a new equilibrium shape. By bracing the grid before deactivation of the shaping forces - *braced grid* -, the nodal displacements of the grid are minimal and the target surface can be maintained. Deformations are much higher when the shaping forces are removed before introducing the bracing elements into the grid - *unbraced grid*.
- The residual bending moments and material stresses induced on the grids during the shaping process are dominant, as they are significantly higher than those exclusively caused by external loads.

The comparison of the structural behaviours of the three different anticlastic gridshells evidence that:

- The orientation of the grid profiles has an important effect on the geometry of the released (without external shaping forces) unbraced grid as well as on the residual stresses, to which the structure is subjected after its bending process: the maximum profiles' curvature, and with it the maximum bending stresses, are to be found on the 45° grid and the lowest on the 135° grid.
- The orientation of the grid profiles also significantly affects the distribution of the section forces on profiles and cables under external loading: the more transversally the profiles are oriented, the stronger the membrane forces are transversally transferred to the longitudinal edges through compression forces on the profiles (due to the positive curvature in transverse direction). Inversely, when the profiles are more longitudinally oriented, the structure stiffness on transverse direction is significantly diminished so that only a reduced level of compression membrane forces can be carried in this direction. Once this level is achieved, the grid starts to buckle in transverse direction and loads start to be carried in longitudinal direction through tensile forces (due to the negative curvature in longitudinal direction). Tensile forces on bracing cables are higher there where axial forces on the profiles are lower.
- Furthermore, the load-deformation behaviour of the gridshells under increasing external distributed loading also depends on the profiles' arrangement. Gridshells with more transversally oriented profiles are more subjected to compression forces and exhibit therefore a shell bearing behaviour. The transfer of forces of gridshells with more longitudinally oriented profiles is dominated by tensile forces and their bearing behaviour resembles that of tensile structures.

Also in this chapter, the bracing effect of tensile membranes on elastic gridshells has been studied. In order to optimise the construction process of elastic gridshells, it is proposed to employ a membrane surface to cover and at the same time to restrain the grid. Thus, a single membrane surface has to be assembled so that less time is needed for the construction process and material savings are achieved. In this work, the shear stiffness of a membrane restrained 4-field planar grid and hemispheric gridshell of 5 m diameter have been analysed. The results confirmed that:

- *Planar grid.* Membranes with diagonally oriented yarns afford much higher shear stiffness to the grid than membranes with parallel oriented yarns. Furthermore, membranes with higher stiffness offer a significantly stronger reduction of the grid's deformations. Nevertheless, compared to conventional bracing elements as crossing cables and diagonal profiles, the restraining effect of the tensile membrane remains moderate. Moreover, inducing prestress on the membrane, it can carry a certain level of forces in the diagonal receiving compression, thus deformations are more strongly reduced.
- *Hemispheric gridshell.* The analyses focus on the influence of the connection conditions between grid and membrane: with and without joining at the grid nodes. By using a restraining membrane without joining to the grid nodes, deformations of the bent grid after removing the shaping forces are reduced, there where the grid deforms upwards and outwards. By connecting the membrane to the grid nodes, its restraining effect can be optimised and deformations decrease over the whole grid. Similar consequences appear when loading the grid with asymmetric external loads. The nodal displacements of the non-braced grid can be strongly reduced introducing shear stiffness through the tensile membrane; particularly when joining the membrane to the grid nodes. The residual stresses due to the bending process of the grid are dominant for all the structures. Differences on the equivalent stresses between non-braced and braced grids under permanent loads are minimal; they become a bit more significant under external loading.

On the presented structural analyses, geometric imperfections on the gridshells have not been considered. Further research could focus on the definition of these imperfections and their influence on the load-bearing behaviour and stability of elastic gridshells.

Experimental validation

The structural behaviour of elastic gridshells strongly depends on constructive aspects as the connections at the grid nodes or the real properties of the supports. In order to benchmark the finite element models, two physical prototypes have been built and, in the last chapter of the thesis, their load-bearing capacity has been compared to that of the numerical simulations. The first prototype represents a elastic gridshell with irregular mesh and partially braced with a third layer of profiles. The second prototype concerns a regular gridshell restrained with a tensile membrane. The analyses focus on the influence of the properties of the connections between superposed grid layers on the load-bearing behaviour. Three types of connection elements have been considered: coupling elements - hinged connection at the upper layer to rigid node at the

lower layer- and two spring elements with higher and lower axial and transversal stiffness coefficients.

By the construction of the irregular hemisphere of 10 m diameter, it has been demonstrated that, if the bending stiffness of the grid is low enough, large deformations can be induced on them and, by an adequate profiles' distribution, the irregular grid can be shaped from a flat configuration, which allows a rapid erection process. However, to permit the flat configuration, the profiles must be here already bent, instead of being straight as on the regular grids. By means of non-linear finite element models, it has been proved that the material stresses during the construction process do not exceed the allowable ones. In order to reduce these stresses, the grid has been initially only partially assembled and the resting border profiles, which would had been subjected to too high stresses, have been introduced after shaping the grid. Despite the only partial bracing of the gridshell (the grid has been triangulated every two meshes), the increment of the structure's stiffness after installation of the third layer of profiles is relevant. By loading the gridshell symmetrically with more than 3 times the weight of the grid, the resulting maximum deformations result to be lower than 1% of its span length.

The comparison of the structural behaviour of the irregular prototype with that of the numerical models evidences that:

- The prototype's geometry could be relatively well reproduced by the simulation, particularly for the unbraced situation. The properties of the interlayer connections on the numerical models have not a relevant influence on the resulting geometries.
- In contrast, under external loading, important differences have been found between numerical and physical models, especially when using coupling elements. The use of spring elements with reduced stiffness allows more similar results. In general, the increment of the grid's deformations under increasing loading is faster on the prototype than on the numerical models.
- Differences between real and simulated structures are mainly due to imperfections on the interlayer connections, as sliding and deformation of the clamps at the grid nodes could be observed. Improvements on the construction, and the consequent simulation, of interlayer connections for tubular sections are to be further investigated.

Regarding the construction of the hybrid hemisphere of 5 m diameter, the analyses of the prototype's geometry have demonstrated the activation of the shaping function of the membrane, as the grid's geometry could be approximated, in a moderate measure, to the target hemisphere after assembling the membrane to the structure. The restraining effect of the membrane under external loading could be physically noticed by the formation of wrinkles in the bracing directions.

By the comparison between the physical and numerical hybrid models, it could be observed that:

- In contrast to the irregular gridshell, the properties of the interlayer connections on the numerical models have a notable influence on the resulting grid's geometry, before and

after adding the membrane. Indeed, due to the smaller diameter and with it higher profiles' curvature of the hybrid hemisphere, the interlayer connections are subjected to higher forces and deformations. The maximum deviations between the numerical simulations and prototype are to be found on the non-restrained grid's geometry.

- Under external loading, differences between the numerical models are higher. The use of spring elements with reduced stiffness allows more similar results than those obtained with the coupling elements and spring elements with higher stiffness. The grid's deformation under asymmetric loading has been able to be much better reproduced without than with connection at the grid nodes. The effect of the connection of the membrane to the grid nodes on the prototype was not the one attained with the numerical calculations. This was again probably due to the imperfections observed at the interlayer connections of the prototype.

Future research

The multidisciplinary and ingenious character of lightweight elastic gridshells - from the numerical analysis for the determination of the gridshell's geometry to the design and manufacture of the grid connections - keeps attracting the interest of many engineers and architects. Since the construction of the pioneering timber gridshells, a wide research on design methods and suitable materials for elastic gridshells has been performed.

Fiber-reinforced materials as GFRP, with a high modulus of elasticity and bending strength, have been successfully used in the last decade for the construction of small and middle span temporary gridshells. Future research is needed on the study of the long-term creep-relaxation behaviour of already established and emerging fibre-reinforced materials and on the definition of corresponding design standards and guidelines.

The grid optimisation proposed in this thesis focuses on the reduction of the curvature of the grid profiles. Concerning the optimisation of irregular grids, future studies could investigate the optimisation of the profiles' distribution and grid's mesh size according to local and global structural requirements.

Regarding the presented influence of the grid pattern on the load-bearing behaviour of anticlastic gridshells, future research could explore further surface geometries. In the same manner, the analyses of the restraining effect of tensile membranes on the hemispheric gridshell could be extended to different surface geometries. Here, it would be also interesting to develop a form-finding method, to find the optimal membrane's geometry, which forces the grid to adopt a target shape, without acquiring wrinkles. Improvements are also needed on the assembling details between membrane and grid nodes.

Bibliography

- [1] J. Schlaich, R. Bergermann, A. Bögle, P. Cachola Schmal and I. Flagge, leicht weit = Light Structures : Jörg Schlaich, Rudolf Bergermann, München; Berlin; London; New York: Prestel, 2003.
- [2] M. Bächer and B. Burkhardt, Multihalle Mannheim - Dokumentation über die Planungs- und Ausführungsarbeiten an der Multihalle Mannheim, Stuttgart: Krämer, 1978.
- [3] F. Otto, E. Schauer, J. Hennicke and T. Hasegawa, IL 10 Gitterschalen / Grid Shells: Bericht über das japanisch-deutsche Forschungsprojekt STI, durchgeführt von Mai 1971 bis Mai 1973 am Institut für Leichte Flächentragwerke, Stuttgart: Seibu Construction Company / Institut für leichte Flächentragwerke / Krämer, 1974.
- [4] S. Adriaenssens, P. Block, D. Veenendaal and C. Williams, Shell Structures for Architecture: Form Finding and Optimization, Routledge, 2014.
- [5] J. Lienhard, H. Alpermann, C. Gengnagel and J. Knippers, "Active Bending, a Review on structures where bending is used as a self formation process," in *Proceedings of the International Association for Shell and Spatial Structures (LASS) Symposium*, Seoul, Korea.
- [6] E. Lafuente Hernández, C. Gengnagel, S. Sechelmann and T. Rörig, "On the Materiality and Structural Behaviour of highly-elastic Gridshell Structures," in *Computational Design Modelling. Proceedings of the Design Modelling Symposium Berlin 2011*, Springer Berlin Heidelberg, 2011, pp. 123-135.
- [7] B. Forster and M. Mollaert, "Engineered fabric architecture," in *European Design Guide for Tensile Surface Structures*, Brüssel, 2004, pp. 25-42.
- [8] J. Hennicke and K. Matsushita, Gitterschalen Gridshells, Stuttgart: Krämer, 1974.
- [9] L. Du Peloux, O. Baverel, J.-F. Caron and A. F. Tayeb, "From shape to shell: a design tool to materialize freeform shapes using gridshell structures," in *Rethinking Prototyping. Proceedings of the Design Modelling Symposium Berlin 2013*, Berlin, 2013.
- [10] L. Bouhaya, B. O. and C. J.F., "Optimisation structurelle des gridshells," in *Proceedings of the 10ème Colloque National en Calcul des Structures Association Symposium (CSMA 2011)* , Presqu'île de Giens, 2011.
- [11] E. Lafuente Hernández, C. Gengnagel, S. Sechelmann and T. Rörig, "Topology Optimisation of Regular and Irregular Elastic Gridshells by Means of a Non-linear Variational Method," in *Advances in Architectural Geometry 2012*, Springer Vienna, 2012, pp. 147-160.

- [12] E. Lafuente Hernández, O. Baverel and C. Gengnagel, “On the Design and Construction of Elastic Gridshells with Irregular Meshes,” *International Journal of Space Structures. Special Issue "Active-Bending"*, 2013.
- [13] R. Harris, J. Romer, O. Kelly and S. Johnson, "Design and construction of the Downland Gridshell," *Building Research & Information*, vol. 31, no. 6, p. 427–454, November-December 2003.
- [14] C. Douthe, C. Jean-Francois and B. Olivier, “Gridshell structures in glass fibre reinforced polymers,” *Construction and Building Materials*, vol. 24, p. 1580–1589, 2010.
- [15] A. Day, “An introduction to dynamic relaxation,” *The Engineer*, p. 219, 1965.
- [16] M. R. Barnes, “Form-finding and Analysis of Tension Structures by Dynamic Relaxation,” *International Journal of Space Structure*, vol. 14, no. 2, pp. 89-104, Januar 1999.
- [17] M. Barnes and D. Wakefield, “Dynamic Relaxation applied to interactive form finding and analysis of air-supported structures,” in *Proceeding of Conference on the Design of Airsupported Structures*, 1984.
- [18] M. Kuijvenhoven, “A design method for timber grid shells,” Delft, 2009.
- [19] M. Kuijvenhoven and P. Hoogenboom, “Particle-spring Method for Form Finding Grid Shell Structures Consisting of Flexible Members,” *Journal of International Association for Shell and Spatial Structures*, vol. 53, no. 1, pp. 31-38, March 2012.
- [20] L. Bouhaya, O. Baverel and J. Caron, “Mapping two-way continuous elastic grid on an imposed surface: Application to grid shells,” in *Proceedings of the International Association for Shell and Spatial Structures (IASS) Symposium*, Valencia, 2009.
- [21] J. Li and J. Knippers, “Designing Regular and Irregular Elastic Gridshells by Six DOF Dynamic Relaxation,” in *Proceedings of Design Modelling Symposium*, Berlin, 2013.
- [22] V. Hara, March 2011. [Online]. Available: <http://www.architectural.com/avanto-architects-ville-hara-and-anu-puustinen-kupla-helsinki-zoo-lookout-tower/>.
- [23] C. Pirazzi and Y. Weinand, “Geodesic Lines on Free-Form Surfaces - Optimized Grids for Timber Rib Shells,” in *World Conference in Timber Engineering WCTE*, Portland, 2006.
- [24] P. Nicholas, E. Lafuente Hernández and C. Gengnagel, “The Faraday Pavilion: activating bending in the design and analysis of an elastic gridshell,” in *Proceedings of Simulation for Architecture and Urban Design Symposium (SimAUD)*, San Diego, 2013.
- [25] N. Kotelnikova-Weilera, C. Douthe, E. Lafuente Hernandez and O. Baverel, “Materials for Actively-Bent Structures,” *International Journal of Space Structures*, vol. 28, no. 3&4, 2013.
- [26] J. Graf, "Entwurf und Konstruktion von Translationsnetzschalen," Grauer, 2002.

- [27] A. Darby, T. Ibell and M. Evernden, “Innovative Use and Characterization of Polymers for Timber-Related Construction,” *Materials*, vol. 3, no. 2, pp. 1104-1124, 2010.
- [28] P. Gressel, “Kriechverhalten von Holz und Holzwerkstoffen - Auswirkungen auf den Formänderungsnachweis,” in *Ingenieurholzbau in Forschung und Praxis*, J. Ehlbeck and G. Steck, Eds., Karlsruhe, Bruderverlag, 1982, pp. 55-66.
- [29] J. Caron and Q. Son, “Creep of pultruded composite pipes under permanent bending,” in *Proceeding of the 3rd international conference on durability and field applications of fibre reinforced polymer composites for construction (CDCC 2007)*, Quebec, 2007.
- [30] N. Kotelnikova-Weiler, C. Douthe, E. Lafuente Hernandez, O. Baverel and C. Gengnagel, “Materials for Actively-Bent Structures,” *International Journal of Space Structures*, vol. 28, no. 3 & 4, 2013.
- [31] C. Gengnagel, E. Lafuente Hernández and R. Bäumer, “Natural-fibre-reinforced plastics in actively-bent structures,” *Construction Materials*, vol. 166, no. CM16, p. 365–377, December 2013.
- [32] “EN 1995 1-1 (Eurocode 5): Bemessung und Konstruktion von Holzbauten; Teil1-1: Allgemeines; Allgemeine Regeln und Regeln für den Hochbau,” 2004.
- [33] X. Li, “Physical, Chemical, and Mechanical Properties of Bamboo and Its Utilization Potential for Fiberboard Manufacturing,” Louisiana, 2004.
- [34] M. McQuaid, Shigeru Ban, London: Phaidon Press Limited, 2003, pp. 60-67.
- [35] S. Gaß and K. Dunkelberg, *Bambus = Bamboo. Mitteilungen des Instituts für Leichte Flächentragwerke (IL-31)*, Stuttgart: Krämer, 1985.
- [36] L. Navier. [Online]. Available: <http://navier.enpc.fr/Composites-et-construction?lang=fr>.
- [37] P. Wambua and J. I. Ignaas Verpoest, “Natural fibres: can they replace glass in fibre reinforced plastics?,” *Composites Science and Technology*, vol. 63, p. 1259–1264, 2003.
- [38] S. Joshia, L. Drzal, A. Mohanty and A. S., “Are natural fiber composites environmentally superior to glass fiber reinforced composites?,” *Composites: Part A*, vol. 35, p. 371–376, 2004.
- [39] C. Aktas, “Impact of product lifetime on life cycle assessment results,” University of Pittsburgh, 2011.
- [40] M. Dweib, B. Hu, A. O'Donnell, S. H.W. and R. Wool, “All natural composite sandwich beams for structural applications,” *Composite Structures*, vol. 63, p. 147–157, 2004.
- [41] A. O'Donnell, M. Dweib and R. Wool, “Natural fiber composites with plant oil-based resin,” *Composites Science and Technology*, vol. 64, p. 1135–1145, 2004.

- [42] R. Burgueño, M. J. Quagliata, A. K. Mohanty, G. Mehta, L. T. Drzal and M. Misra, “Load-bearing natural fiber composite cellular beams and panels,” *Composites: Part A*, vol. 35, p. 645–656, 2004.
- [43] C. Gensewich and U. Riedel, “Pultrusion von Konstruktionswerkstoffen aus nachwachsenden Rohstoffen,” *Die Angewandte Makromolekulare Chemie*, vol. 272, pp. 11-16, 1999.
- [44] K. Van de Velde and P. Kiekens, “Effect of material and process parameters on the mechanical properties of unidirectional and multidirectional flax/polypropylene composites,” *Composite Structures*, vol. 62, pp. 443-448, 2003.
- [45] I. Angelov, S. Wiedmer, M. Evstatiev, K. Friedrich and G. Mennig, “Pultrusion of a flax/polypropylene yarn,” *Composites: Part A*, vol. 38, p. 1431–1438, 2007.
- [46] X. Peng, M. Fan, J. Hartley and M. Al-Zubaidy, “Properties of natural fiber composites made by pultrusion process,” *Journal of Composite Materials*, vol. 46, pp. 237-246, 2012.
- [47] O. Faruk, A. K. Bledzki, H. P. Fink and M. Sain, “Biocomposites reinforced with natural fibers: 2000–2010,” *Progress in Polymer Science*, vol. 37, p. 1552–1596, 2012.
- [48] R. Bäumer, C. Gengnagel and E. Lafuente Hernández, 2012. [Online]. Available: <http://biopolymernetzwerk.fnr.de/biobasierte-werkstoffe/werkstoffe/naturfaser-verstaerkte-kunststoffe-nfk/>.
- [49] L. C. Bank, *Composites for Construction: Structural Design with FRP Materials*, New Jersey: John Wiley & Sons, 2006.
- [50] “EN 1999-1-1 (Eurocode 9): Design of aluminium structures - Part 1-1: General structural rules,” 2007.
- [51] A. I. Bobenko and Y. B. Suris, *Discrete Differential Geometry: Integrable Structure*, vol. 98 of Graduate Studies in Mathematics, American Mathematical Society, Providence, RI, 2008.
- [52] S. Sechelmann, T. Rörig and A. Bobenko, “Quasiisothermic Mesh Layout,” in *Advances in Architectural Geometry 2012*, Wien, Springer Vienna, 2012, pp. 243-258.
- [53] Y. Liu, H. Pottmann, J. Wallner, Y.-L. Yang and W. Wang, “Geometric Modeling with Conical Meshes and Developable Surfaces,” *ACM Transactions on Graphics (TOG)*, vol. 25, no. 3, pp. 681-689, 2006.
- [54] H. Pottmann, A. Schiftner, P. Bo, H. Schmiedhofer, W. Wang, N. Baldassini and J. Wallner, “Freeform surfaces from single curved panels,” *ACM Transactions on Graphics (TOG)*, vol. 27, no. 3, p. 76, 2008.
- [55] [Online]. Available: <http://www.varylab.com>

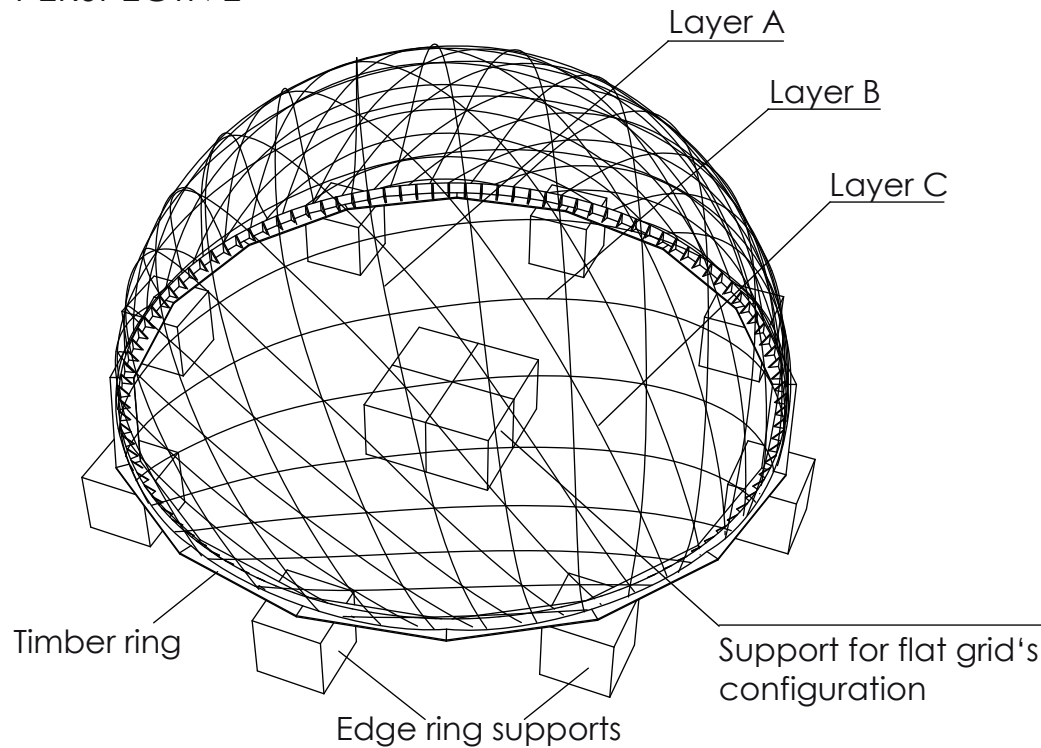
- [56] B. Springborn, A. Schröder and U. Pinkall, “Conformal equivalence of triangle meshes,” *ACM Transactions on Graphics (TOG)*, vol. 27, no. 3, 2008.
- [57] S. Adriaenssens, M. Barnes and C. Williams, “A new analytical and numerical basis for the form-finding and analysis of spline and gridshell structures,” in *Computing device in civil and structural engineering*, Edinburgh, Civil Comp. Press, 1999, p. 83–90.
- [58] C. Douthe, O. Baverel and C. J.F., “Form-finding of a gridshell in composite materials,” *Journal of the International Association for Shell and Spatial Structures*, vol. 47, no. 1, pp. 53-62, April 2006.
- [59] S. B. J. Balay, K. Buschelman, W. Gropp, D. Kaushik and al., 2011. [Online]. Available: <http://www.mcs.anl.gov/petsc>.
- [60] S. Benson, L. C. McInnes, J. Mor'e, T. Munson and J. Sarich, 2007. [Online]. Available: <http://www.mcs.anl.gov/tao>.
- [61] H. Sommer, 2010. [Online]. Available: <http://jpetsctao.zwoggel.net/>.
- [62] J. Lienhard, S. Schleicher and J. Knippers, “Bending-active Structures – Research Pavilion ICD/ITKE,” in *Proceedings of the International Symposium of the LABSE-IASS Symposium: Taller Longer Lighter*, London, UK, 2011.
- [63] P. Nicholas, E. Lafuente Hernandez and C. Gengnagel, “The Faraday Pavilion: activating bending in the design and analysis of an elastic gridshell,” in *SimAUD 2013*, San Diego, CA, United States.
- [64] J. Graf, “Entwurf und Konstruktion von Translationsnetzschaalen,” 2002.
- [65] H. Alpermann and C. Gengnagel, “Hybrid membrane structures,” in *Proceedings of the International Association for Shell and Spatial Structures (IASS) Symposium*, Shanghai, 2010.
- [66] H. Alpermann and C. Gengnagel, “Shaping actively-bent elements by restraining systems, Proceedings,” in *Proceedings of the International Association for Shell and Spatial Structures (IASS) Symposium*, Seoul, 2012.
- [67] H. Alpermann and C. Gengnagel, “Restraining actively-bent structures by membranes,” in *Proceeding of the VI International Conference on Textile Composites and Inflatable Structures, Structural Membranes*, Munich, 2013.
- [68] “BÜV-Empfehlung : Tragende Kunststoffbauteile im Bauwesen - Entwurf, Bemessung und Konstruktion,” Stand 2010-08.

APPENDIX

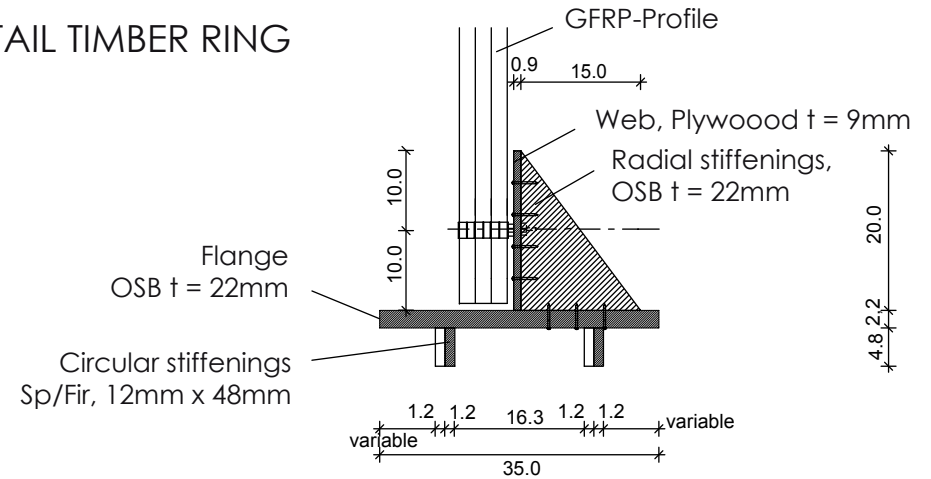
**Construction Plans of Developable
Irregular Elastic Gridshell**

Workshop TWL II - FLYING DOME - University of the Arts Berlin

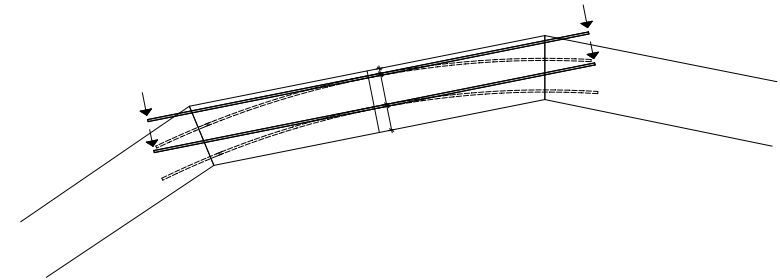
PERSPECTIVE



DETAIL TIMBER RING

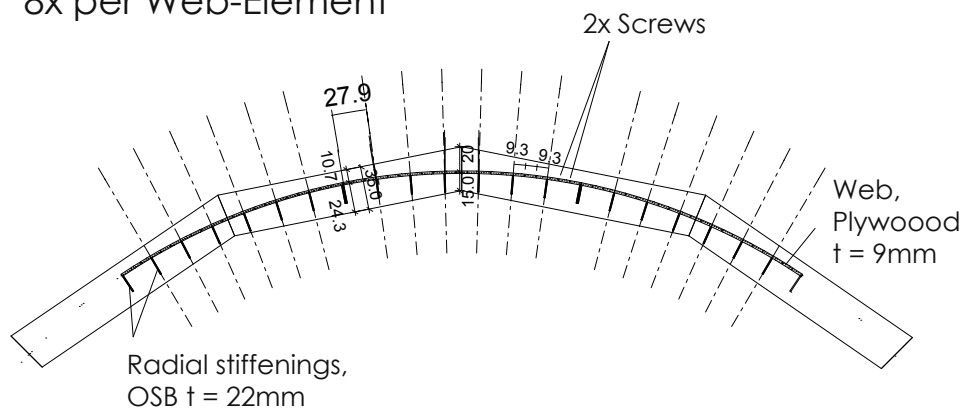


ELASTICALLY-BENT FEET AND WEB OF TIMBER RING



POSITION OF RADIAL STEFFINGS

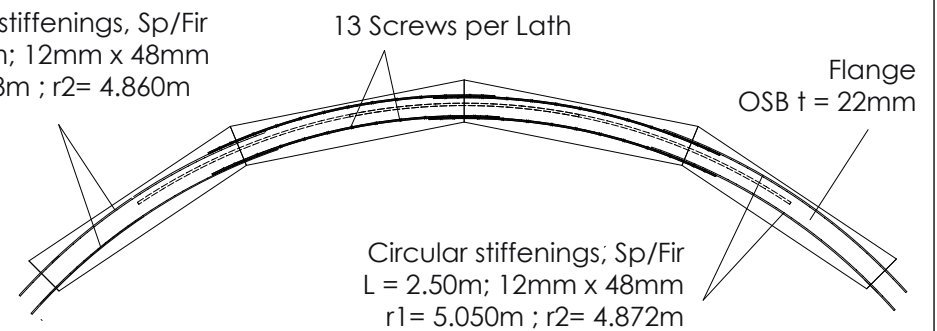
8x per Web-Element



POSITION OF CIRCULAR STIFFEINGS

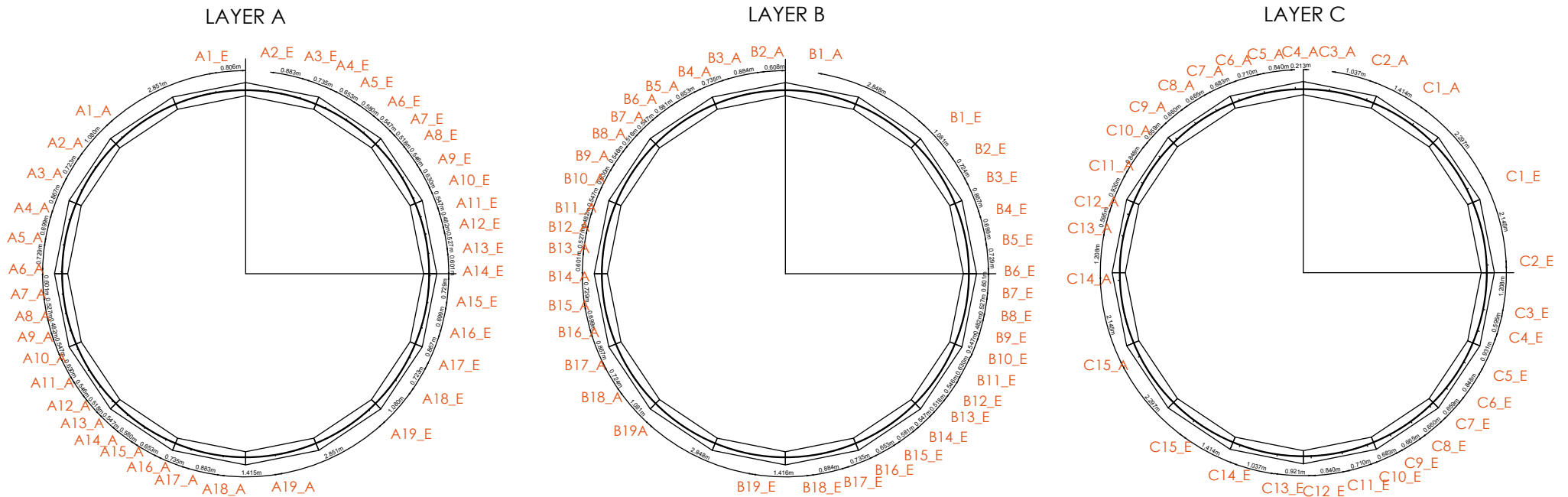
2x per Flange-Element

Circular stiffenings, Sp/Fir
 $L = 2.50\text{m}$; 12mm x 48mm
 $r1 = 5.038\text{m}$; $r2 = 4.860\text{m}$



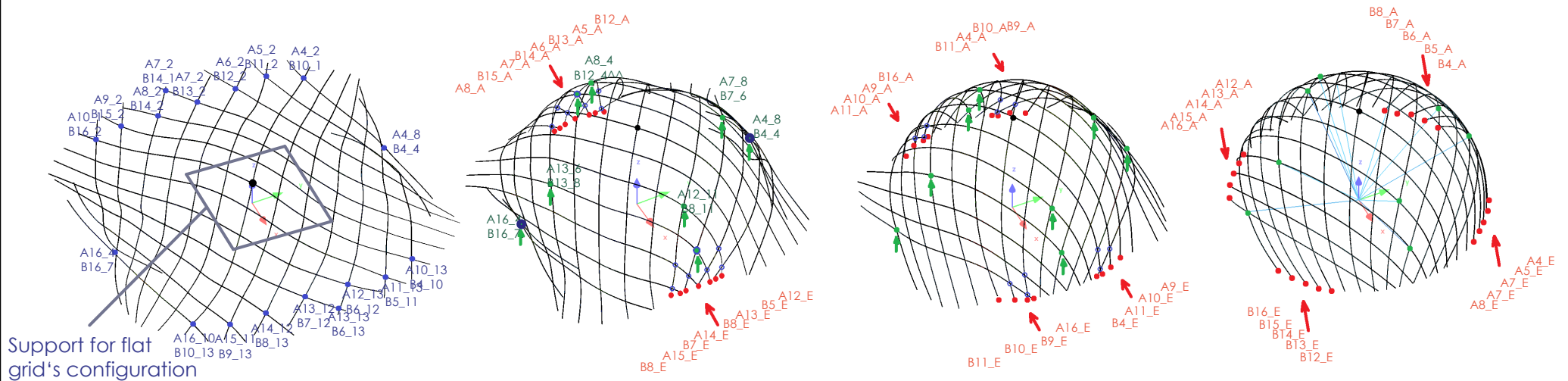
Workshop TWL II - FLYING DOME - University of the Arts Berlin

POSITION OF BOREHOLES AT RING'S WEB



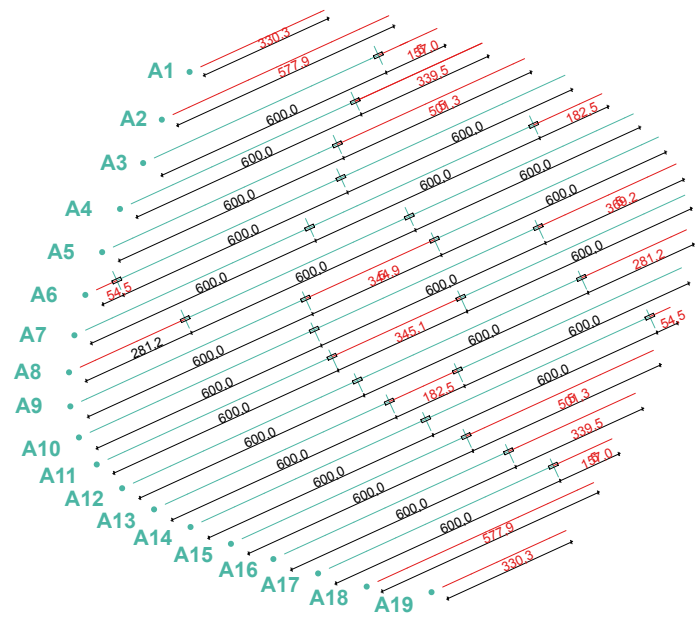
SHAPING PROCESS

● WITHOUT CONNECTION ● SUPPORT TO BE MOVED AND FIXED ● CONNECTION TO BE ASSEMBLED ● TEMPORARY SUPPORTS

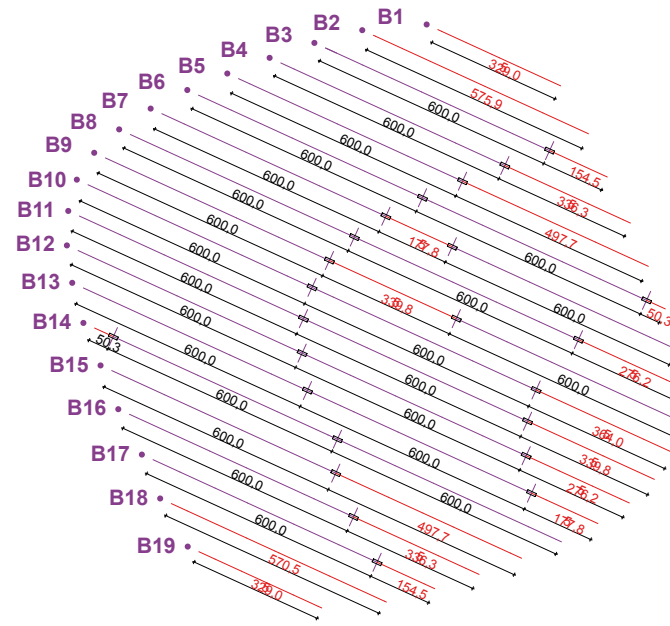


Workshop TWL II - FLYING DOME - University of the Arts Berlin

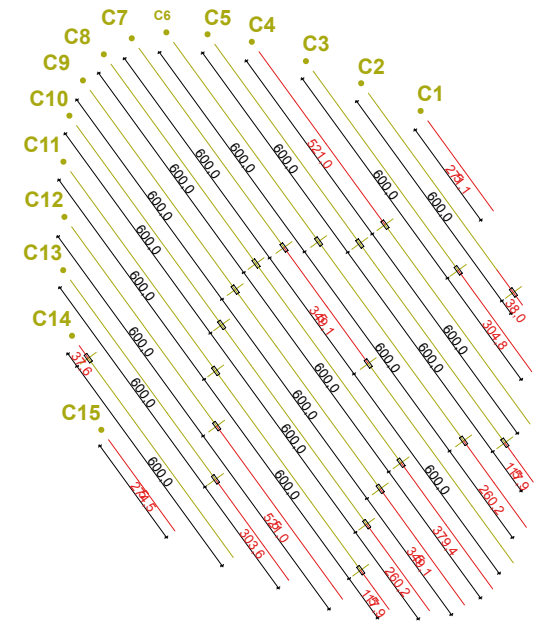
POSITION OF PROLONGING CONNECTION



Layer A



Layer B

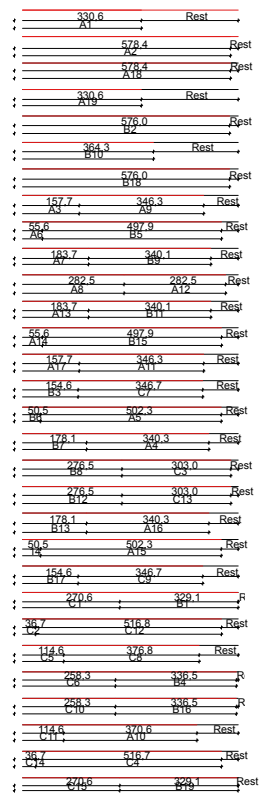


Layer C = Bracing

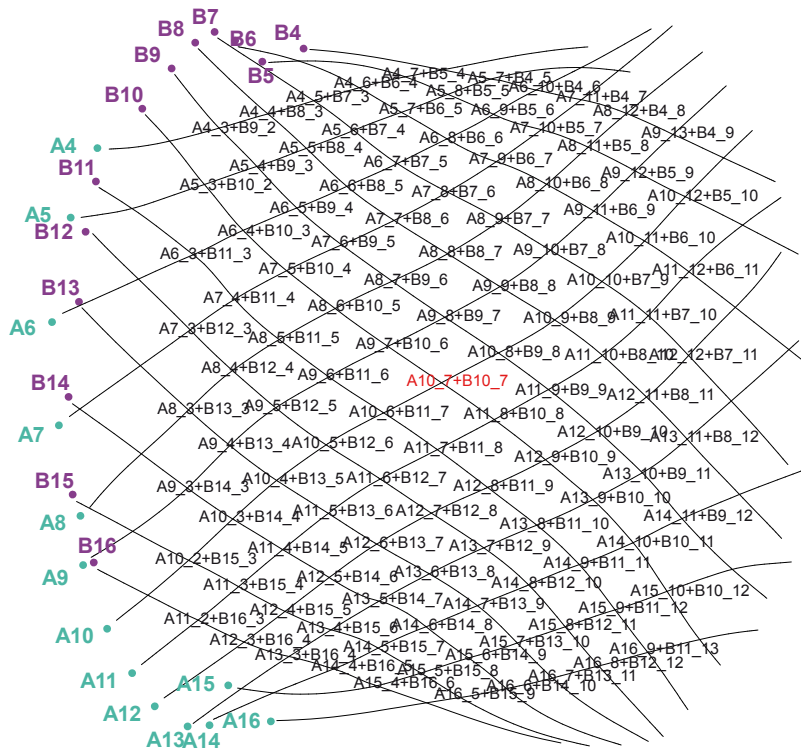
● Profiles' start

Workshop TWL II - FLYING DOME - University of the Arts Berlin

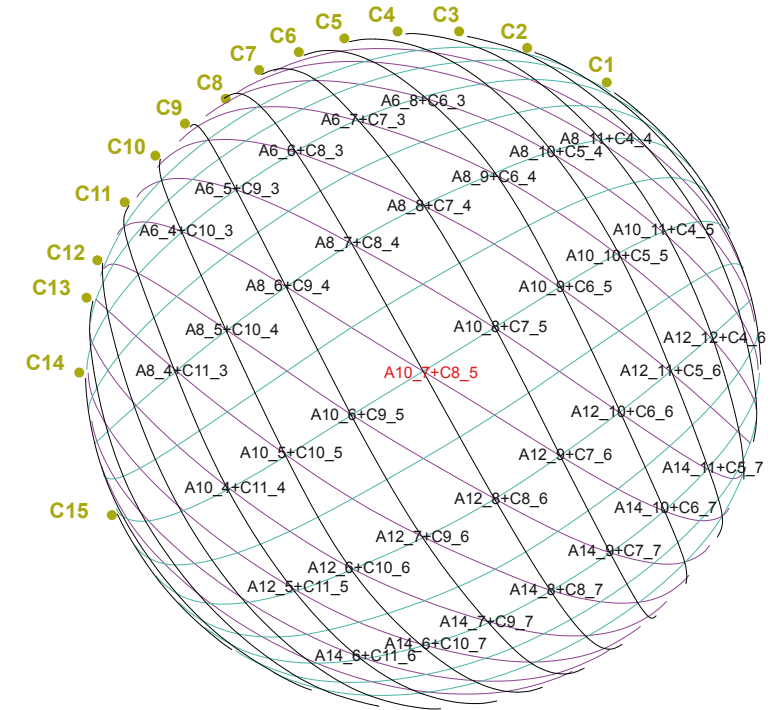
CUTTING LAYOUT



INTERSECTIONS BETWEEN LAYERS A + B



INTERSECTIONS BETWEEN LAYERS A + B + C



Workshop TWL II - FLYING DOME - University of the Arts Berlin

POSITION OF INTERSECTION BETWEEN LAYERS

